VARIATION OF MANNING'S COEFFICIENT WITH CHANNEL STAGE

by

Ta Wei Soong and Perry Michael DePue II

June 1996

VARIATION OF MANNING'S COEFFICIENT WITH CHANNEL STAGE

by

Ta Wei Soong and Perry Michael DePue II

This final report has been submitted to the
Water Resources Center
University of Illinois at Urbana-Champaign
in partial fulfillment of project requirements

June 1996

ABSTRACT

Although Manning's roughness coefficient is known to vary with river stage, information on this aspect is limited, and practitioners have to resort to trial-and-error approaches or rely on their judgment to quantify the variation. This research was aimed at investigating the variation patterns of Manning's roughness coefficient over depth. Investigators conducted an extensive laboratory experiment using a fairly long and large channel, in the shape of half of a compound cross section, to simulate natural rivers. This experimental channel allowed a comprehensive investigation of both uniform and composite roughness elements along the channel's wetted perimeter. Data were taken from both cases: when flow was restricted in the main channel (to simulated a prismatic channel) and when it covered the floodplain. In addition, the investigators converted data from other researchers to verify factors not covered in this study.

The researchers found that while geometry and roughness patterns can both affect the magnitude of Manning's coefficient over depth, the effects vary in prismatic and floodplain channels. Experimental data were used to identify the variation patterns of Manning's roughness in the floodplain channel as well as the effects of varying roughness distribution in the main channel and floodplains.

Investigators also made a number of recommendations regarding the equations that should be used to quantify the variation of the overall Manning's n value for a channel section. Suggestions were made as to the specific use of these equations, including the number of subareas within the channel to be considered, the type of division lines between the subareas, and the ranges of applicability of the equations.

Key Words:

Manning's Roughness Coefficient, Compound Channel, Composite Channel, Floodplain, Open Channel Flow, Flow Resistance, Composite Roughness, Predictive Equation.

ACKNOWLEDGMENTS

This research was supported by a grant from the Water Resources Center at the University of Illinois at Urbana-Champaign (UIUC). The M.S. thesis of the second author, Mr. Michael DePue II, formed the basis of this report. The authors would like to thank Professor B.C. Yen, UIUC, for his advice and assistance throughout the project. Special thanks are extended to Dr. John Braden, Director of the Water Resources Center, for his administrative guidance on the progress of this research. Douglas Anderson, an undergraduate student in the former Theoretical and Mechanical (TAM) Department at UIUC, worked extensively on laboratory experiments. Mr. Anderson conducted initial research for this project and won a paper contest in the TAM Department. His hard work and diligent attitude are highly appreciated. The authors are also grateful to the UIUC Department of Civil Engineering for use of the experimental facilities at the Hydrosystems Laboratory and to the Illinois State Water Survey where the senior author works. Several Water Survey personnel assisted in the project: Dr. Renjie Xia participated in laboratory tasks, and Mr. Tim Mahannah constructed the channel sections and gave technical assistance. Ms. Sarah Hibbeler reviewed a preliminary draft of the manuscript, and Ms. Lacie Jeffers revised the manuscript.

TABLE OF CONTENTS

LIST OF TABLES

List of Figures

1. INTRODUCTION

The Manning equation is one of the most widely used formulas for open-channel problems. Engineers use it to estimate flow velocity and discharge for a wide range of hydraulic designs and practices, such as flood routing, urban runoff, and irrigation, or for inferring erosion and sedimentation potential, evaluating nutrient transport, and in many other studies. The equation is easy to use and employs parameters that can readily be determined for specific problems.

The Manning equation has the well-known form:

$$V = \frac{k_n}{n} R^{\frac{2}{3}} S^{\frac{1}{2}} \qquad (1.1)$$

where V is the mean velocity, k_n is a constant equal to 1 $m^{1/2}$/sec or 1.486 $ft^{1/2}$/sec, R is the hydraulic radius, S is the channel slope, and n is the roughness coefficient. Manning's equation is applicable to uniform, fully developed turbulent flow conditions. R can be obtained by dividing the total cross-sectional area, A, by the wetted perimeter, P; and S, which is generally less vigorous in differentiating among bed, surface, energy, and momentum slopes, can be estimated for the given reach. Determination of n, however, relies more on empirical approaches.

Theoretically, the coefficient n represents the resistance to flow that originates with uneven boundary surfaces. Represented in terms of boundary roughness height, k, Manning's coefficient can be expressed as (Chow, 1959):

$$n = f(\frac{R}{k}) k^{\frac{1}{6}} \qquad (1.2)$$

where f represents a function, and the reverses of f is the definition for relative roughness. Chow concluded that for a wide range of R/k, variation in $f(R/k)$ is small, and may be assumed constant and equal to an average value. On the basis of actual observations, Strickler (1923) derived an equation similar to 1.2, using mean diameter for k. Others have arrived at similar equations by substituting representative bed material diameters for k. Examples are:

$n = 0.031\ d_{75}^{\ 1/6}$ (Henderson, 1966)
$n = 0.034\ d_{50}^{\ 1/6}$ (Strickler, 1923)

Using the mean diameter of the sand grains to represent k (Nikuradse, 1932) is now known specifically as Nikuradse sand roughness, or k_s.

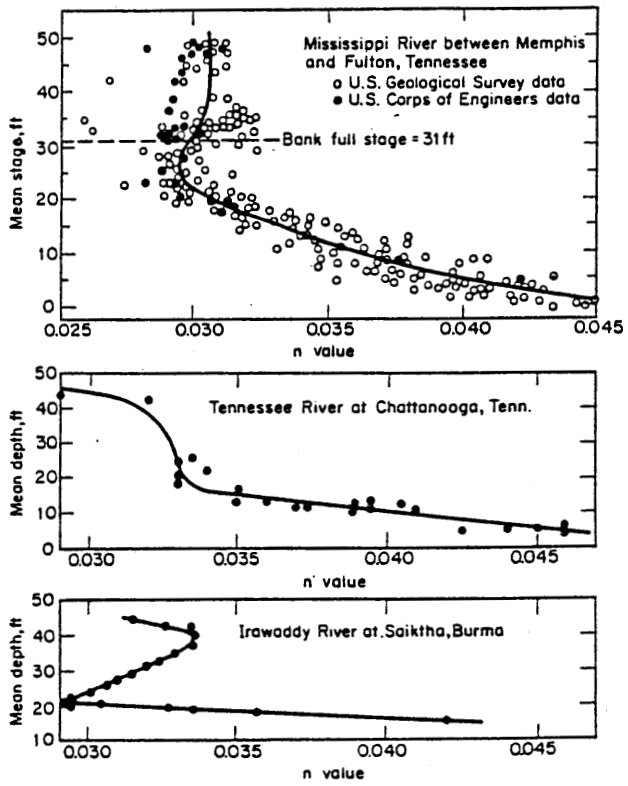

Figure 1.1. Variation of n with mean stage or depth (material reproduced with permission of the McGraw Hill Companies from *Open Channel Hydraulics*, by Ven Te Chou, 1959)

different at shallow depths. Many investigators have indicated that a momentum transfer between the main channel and floodplains causes the discrepancy and have outlined methods of subdividing the cross sections to correct the application procedures. However, none of these methods have proven to be comprehensive or practical.

The changes of n with stage can cause errors in estimating velocities or discharges in prismatic channels. In compound channels, determination of discharge using the whole cross section is still practical; otherwise, more complicated two-dimensional models have to be used. This approach of varying Manning's coefficient with stage will perhaps simplify the discharge computation for compound channels. However, no information is as yet available to engineers. For computer programs such as HEC6 (U.S. Army Corps of Engineers, USACOE, 1981) it is recommended that the n versus Q relationship be determined in the calibration procedures. If the available field data do not exist or are insufficient, applications may be hampered. Therefore, determining the rational-based n versus stage relationship can have great significance for practical applications

1.1. Problem Statement

When applying equation 1.1 to natural channels, Manning's n actually represents the total resistance to the flow. Rouse (1965) pointed out that Manning's n can be affected by many factors, from the fluid properties, flow characteristics, cross-sectional geometry, and the geomorphology of the reach, to the sediment content. The coefficient so determined by local roughness usually is not sufficiently representative of the overall resistance. Hence in practice, n values are determined by referencing recommendations given in text books such as Chow (1959), Barnes (1967), and Arcement and Schneider (1989). As many practitioners may have experienced, the selected n value commonly is not correct the first time it is calculated and must be arrived at through a trial-and-error approach. Such an approach employs no physical reasoning, but is accepted as the only way to determine n, because tabulations and illustrations cannot cover all types of channels. On many occasions, experience alone has led to the determination of the n value (Barnes, 1967).

Given measured data, engineers can get a sense of n values at a site. Applying the determined n value still involves uncertainty especially at depths outside of the range from which it was determined. The n value generally is assumed to be invariant over depth (Henderson, 1966; Yen and Overton, 1973), which may be valid in simple channels of uniform roughness. In natural channels, however, it is common to have materials of different roughness along the cross-sectional boundary. Therefore, assuming invariant n may be risky.

Figure 1.1 (Lane, 1951, with figures from Chow, 1959, p. 105) illustrates calculated n values at different stages of three rivers. The variation is not only obvious, but also significant. Other researchers such as Fread (1989) also have conceptually demonstrated how Manning's n varies with depth for smooth and rough channel scenarios. No investigation has specifically focused on the n versus depth relationship, perhaps because the open-channel issue has drawn most of the attention.

The figure not only illustrates that n varies with depth, but also shows a dramatic change in n when the river's depth passes the bankfull stage. Natural channels generally have a main channel, which may overflow to floodplains on one or both sides. Such a channel system is called the compound channel. A compound channel is more efficient in carrying flows than a rectangular channel with the same area (Myers, 1991). Occasionally, a drainage channel is designed as a compound channel so that low flows will be concentrated and can carry away silt and debris (Posey, 1967). Evaluating discharge for compound channels is difficult, however. When the river stage passes the bankfull stage, the cross-sectional geometry experiences an abrupt change (figure 1.2). Using the whole cross section, as in equation 1.1, has led to underestimation of discharge in shallow floodplain depths by nearly 26~30 percent (Myers, 1987). Hydraulic characteristics, such as velocity and discharge in the main channel and floodplain subsections, are quite

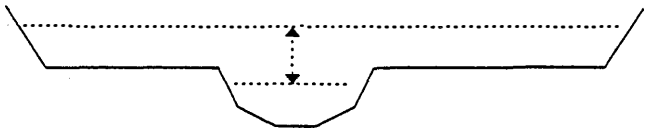

Figure 1.2. Natural compound channel

1.2. Objectives

Determining how n varies with depth can significantly affect the use of Manning's formula and may have some practical applications. Although many factors can affect the n value in natural channels, it is understood that the two major variables causing n to change with depth are the different roughness of materials along the wetted perimeter and changes in geometry. Because information for a systematic evaluation of the n versus depth relationship is not available, the objectives of this research are to:

1. investigate the n versus depth relationship under controlled experiments,
2. systematically evaluate existing equations for composite n values and their applicability to changing depths, and
3. recommend a method for evaluating n versus depth for compound channels that resemble natural channels.

1.3. Approaches

A channel having more than one roughness along the wetted perimeter is called a composite channel. Several methods have been proposed for the determination of composite n values, but they have not been evaluated systematically, and their results differ even for a simple trapezoidal channel, as shown by Yen (1992a). Considering that changing river stages are a process of adding or deleting roughness to the channel cross section, these existing formulas provide a starting point to investigate the problem.

In order to validate these equations, a compound channel experiment focusing on varying roughness has been conducted. Realizing that the current knowledge about

Manning's n is limited to a special case of steady, uniform, sediment-free flow in prismatic channels with constant slope, without lateral flow, and of impervious rigid boundaries with densely distributed, statistically homogeneous roughness elements (Yen, 1992a), the experiments were conducted under steady uniform flow conditions. For these given simplifications, the functional relationship between Manning's n and contributing variables can be expressed as (Yen, 1992a):

$$n = f(\mathbf{R}, \mathbf{F}, \eta, \frac{k_s}{h}, G_c) \tag{1.3}$$

where f represents a function, $\mathbf{R}$ is the Reynolds number, $\mathbf{F}$ is the Froude number, η is a nondimensional representation of cross-sectional shape, k_S is the Nikuradse equivalent sand roughness (to represent the wall roughness effect), h is a representative depth, and G_C is a nondimensional parameter representing the lateral variation of the sediment diameter or wall roughness size along the wetted perimeter of the cross section. The controlled experiment was intended to analyze the method for determining the base Manning's n value and subsequently the variation of this coefficient with river stages. The final formula(s) could be of the same general form employed by Yen (1992a):

$$n_c = \sum w_j n_j \tag{1.4}$$

in which division of the whole cross section into subsections is implied. In this equation, n_c is the cross-sectional n value, w_j is the weighting function of the j^{th} subarea to be investigated, and n_j is j^{th} subarea's roughness.

2. LITERATURE REVIEW

Articles concerning the Manning's equation are abundant. Recently, Yen (1992a) conducted an in-depth review of Manning's coefficient in which contributions by many investigators were discussed. The thesis of this report will focus on how to compute composite roughness and information pertaining to the effects of geometry and roughness on open channel flows.

2.1. Existing Methodologies

Currently there are ten equations available for computing the equivalent roughness for a cross section given different roughness of materials along the wetted perimeter. The ten equations, together with the basic assumptions (Yen, 1992a), are given in table 2.1.

Table 2.1 Existing Equations for Computing Composite Roughness, Yen (1992)

Equation	*Reference*	*Basic assumption*	*Eq. no.*
$n_c = \frac{PR^{5/3}}{\sum \frac{P_i R_i^{5/3}}{n_i}}$	Lotter (1933)	Total discharge is sum of subarea discharge, slope $S = S_j$	(2.1)
$n_c = \frac{\sum (n_i P_i R_i^{1/3})}{PR^{1/3}}$		Total shear force, $P\sqrt{(\gamma RS)}$, is sum of subarea shear forces; $S = S_j$ and $V_j / V = (R_j/R)^{1/2}$	(2.2)
$n_c = \frac{\sum (n_i P_i / R_i^{1/6})}{P / R^{1/6}}$		Same as above except velocity $V_j/V = 1$	(2.3)
$n_c = [\frac{1}{P}\sum (n_i^2 P_i)]^{1/2}$	Pavlovskii (1931) Einstein & Banks (1950)	Total resistance force, F, is sum of resistance force. Also $S = Sj$, and $V^2/R^{1/3} = V_j^2/R_j^{1/3}$	(2.4)
$n_c = [\frac{1}{P}\sum (n_i^{3/2} P_i)]^{2/3}$	Horton (1933) Einstein (1934)	$V = V_j$, $S = S_j$, and $A = \sum A_j$	(2.5)
$n_c = \frac{P}{\sum (P_i / n_i)}$	Felkel (1960)	Note special case of Eq. 2.1 with $R_j / R = 1$	(2.6)
$n_c = \frac{\sum (n_i P_i)}{P}$		Contribution of component roughness is linearly proportional to wetted perimeter	(2.7)
$n_c = \exp[\frac{\sum P_i h_i^{3/2} \ln n_i}{\sum P_i h_i^{3/2}}]$	Krishnamurthy & Christensen (1972)	Logarithmic velocity distribution over depth h for wide channel, $S = S_j$, $Q = \sum Q_i$, $n = 0.0342k$	(2.8)

Table 2.1 Concluded

Equation	*Reference*	*Basic assumption*	*Eq. No.*
$n_c = \frac{\sum n_i A_i}{A}$	USACOE (1968) Cox (1973)		(2.9)
$n_c = [\frac{\sum (n_i^{3/2} A_i)}{A}]^{2/3}$	Colebatch (1941)	Same as Eq. 2.5, but with an error in derivation.	(2.10)

Note: n_c is the composite roughness, P is the total wetted perimeter, R is the overall hydraulic radius, h is the depth, A is the total area, and subscript j implies the corresponding parameters for that subsection.

2.2. Assumptions in Existing Methodologies

In application, these equations divide the channel cross section into subsections so that hydraulic properties in each subsection can be treated as uniform. Then one hydraulic property is identified so that its value for the whole cross section is equivalent to the sum of contributions from each subsection. Assumptions are imposed to enable or simplify the summation process. A summary of these assumptions is presented as follows.

1. *Each subsection has the same mean velocity, which is also equal to the mean velocity of the whole cross section.* Examples are equations 2.3 (Lotter, 1933), 2.5 (Horton, 1933; Einstein, 1934), and 2.10 (Colebatch, 1941). The Manning equation is a uniform flow equation, hence the assumption fits the equation. However, channel flows have lateral distribution, and rapid changes occur when the depth varies greatly between subsections.
2. *The total resisting force equals the sum of the forces developed in each subarea.* An example is equation 2.4 (Pavlovskii, 1931; Muhlhofer, 1933; Einstein and Banks, 1950).
3. *The total shear force is the sum of subarea shear forces.* Examples are equations 2.2 and 2.3 (Lotter, 1933). Christensen (1992) indicated that it is the bed shear-stress distribution that affects the total conveyance. A comparison of total conveyance as calculated by the whole cross-sectional approach and the summation approach indicates that the summation approach, which employs the bed shear-stress distribution, actually should give a better approximation than the whole cross-sectional approach. This is quite an interesting conclusion. In any case, the difference

between these two equations is that equation 2.2 uses $V_j/V = (R_j/R)^{1/2}$, which is based on conveyances, while equation 2.3 assumes that $V_j/V = 1$.

4. *The total discharge of the flow equals the sum of the discharge of the subdivided areas.* Examples are equations 2.1 (Lotter, 1933) and 2.8 (Krishnamurthy and Christensen, 1972). This assumption should be applicable to rectangular or wide-shallow channels. The methods for dividing compound channels can affect the results of these equations, as appreciable errors have been noted when applying this assumption to shallow floodplain depths in compound channels.

5. *Weighting coefficients are assigned according to the ratio of the wetted perimeter or subarea to the whole cross section's wetted perimeter or area.* Examples are equation 2.6 (Felkel, 1960) and equation 2.9 (Cox, 1973), respectively.

6. *The slope in each subsection is equal to the total slope.* Most of the equations employ this assumption which may be valid for water surface slopes but not for momentum or energy slopes (Yen, 1992).

In the context of approximating total conveyance of natural channel sections as a linear summation over subsections, the summation approach was examined by Garbrecht and Brown (1991), who concluded that it leads to overestimation of total conveyance for sections with a width to depth ratio smaller than 10. However, Christensen (1992) noted that the summation approach should lead to better estimates of total conveyance than the conventional single channel approach, which is an approximation. Hence, the summation approach for determining the overall n value should lead to better representation of n. The discussions of both Garbrecht and Brown (1991) and Christensen (1992) applied to simple concave channels.

2.3. Application to Prismatic Channels

These equations were derived from data based on prismatic channels. As with their counterpart, compound channels, the method of dividing the cross section into subsections can affect results. In prismatic channels, it is reasonable to apply dividing lines at locations where there are breaks in roughness or geometry along the wetted perimeter. The division method can be either vertical (dividing lines parallel to depth direction) or bisectional (dividing the angle at a corner). Unlike compound channels for which the dividing line between the main channel and floodplain has been associated with a momentum transfer mechanism and treated in the form of apparent shear stresses (e.g., Wormleaton et al., 1981), the magnitudes of imbalance between subsections in prismatic channels have seldom been quantified. Some researchers consider the shear stress at such

artificial interfaces as created by both methods to be small and insignificant (e.g., Christensen, 1992).

Yen (1992a), on the other hand, noted that the composite n value as calculated by these ten equations was quite different even for a simple trapezoidal channel. He compared the equations' results at one depth in a trapezoidal channel with different roughness along its sidewalls and bottom and a cross section that was divided into three subareas with both vertical and bisectional division methods. This example is used here to compare a range of depths with different roughness distribution and different geometry (figure 2.1). The intent is to compare:

1. the differences among these equations, and
2. the effects of geometry and roughness distribution.

Several figures were derived for a trapezoidal channel with a bottom width of 1.33 feet, maximum depth of 0.66 feet, and sidewalls of 45° inclination. Subdivision lines are located at the two corners in accordance with the vertical division method. Figure 2.2 illustrates the results for the case of a rough channel bottom (n = 0.018) and smooth sidewalls (n = 0.013), figure 2.3 for uniform roughness (n = 0.013), and figure 2.4 for rough sidewalls (n = 0.018) and a smooth channel bed (n = 0.013). In addition to differences in results, other observations include:

- The prediction pattern for most equations is sensitive to roughness distribution. Figure 2.2 shows that all equations predict decreasing n values with increasing depth, due to the effect of smooth sidewalls. However, figure 2.3 shows that equations 2.4 - 2.10 predict constant n values given uniform roughness while equation 2.3 predicts increasing n over depth. Also, the degree of difference between equations 2.1 and 2.2 increases. Figure 2.4 shows that all equations, except for equation 2.1, predict increasing n values, apparently due to greater roughness on sidewalls.
- Equation 2.1 always predicts the lowest n value.

The effects of channel geometry are illustrated in figures 2.5 and 2.6 for two additional geometries, triangular and rectangular channels (see sketches, figure 2.1). Only the bisectional division method can be used for these two geometries. Although the examples are arbitrary, the depth and area of all these cross sections are kept equivalent. The uniform roughness case is compared with n = 0.013. Following are some observations:

- Equations 2.1, 2.2, and 2.3 respond to geometry changes.
- The n versus depth curve varies the least in a rectangular channel. The degrees of variation for triangular and trapezoidal channels are similar.

Figure 2.7 shows additional test results, assuming that there are two segments of roughness on the inclined walls (n = 0.013 and n = 0.018, divided halfway). Results indicate the following:

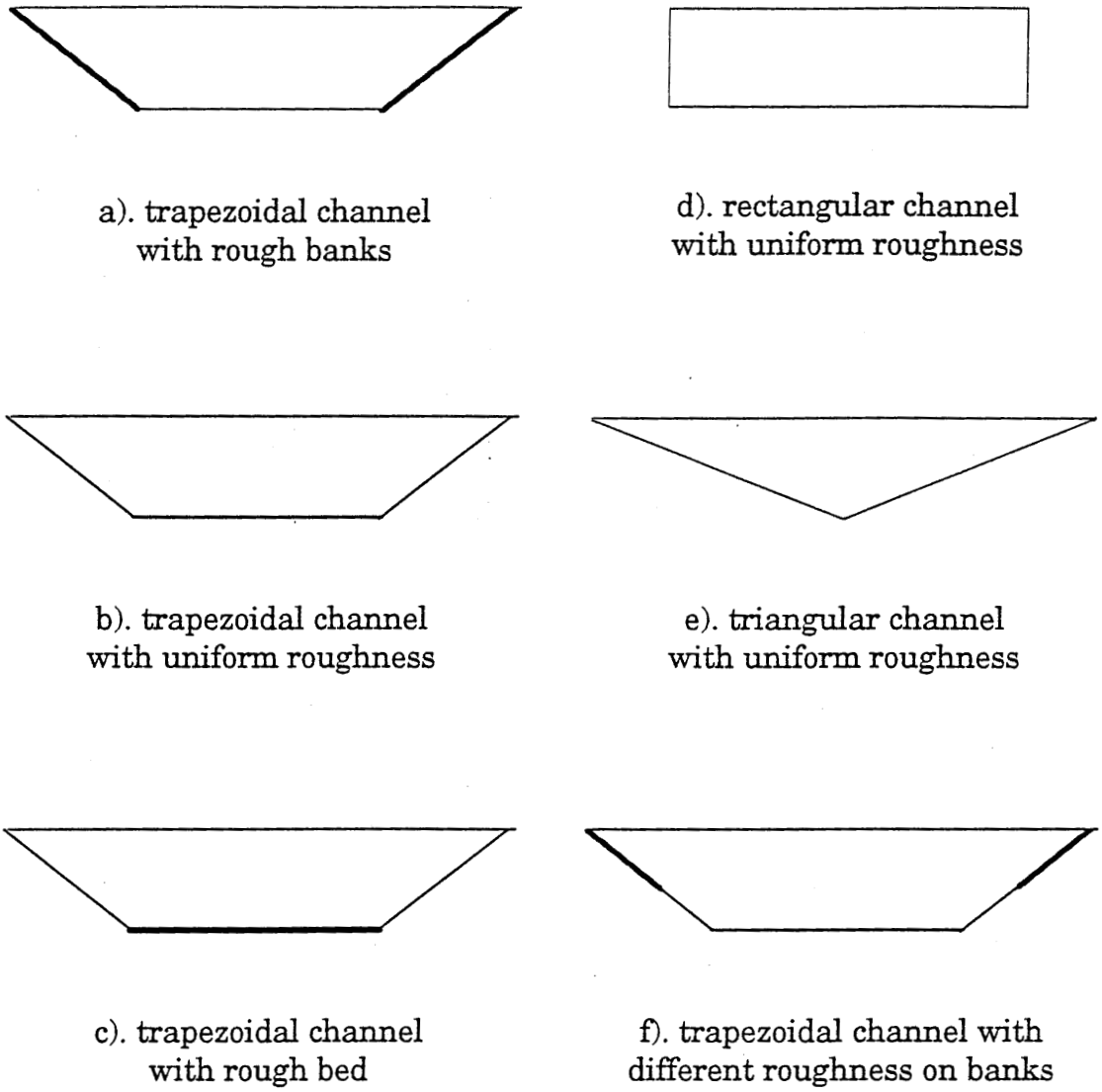

Figure 2.1. Schematics of idealized channels tested for equations

- Given an additional roughness change along the perimeter, the general n versus depth pattern also changes after the point at which roughness changes.
- All equations show increasing n after the rough section on sidewalls, except for equation 2.1, which shows decreasing n after the break.

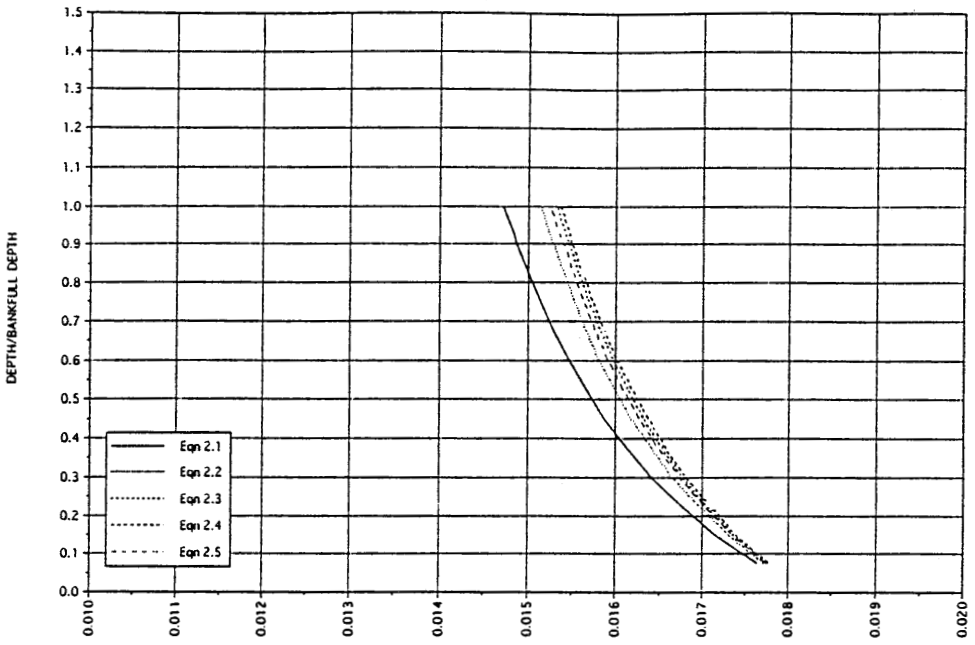

Figure 2.2a **Performance of equations 2.1 to 2.5 for a trapezoidal channel with rough bed and smooth sidewalls**

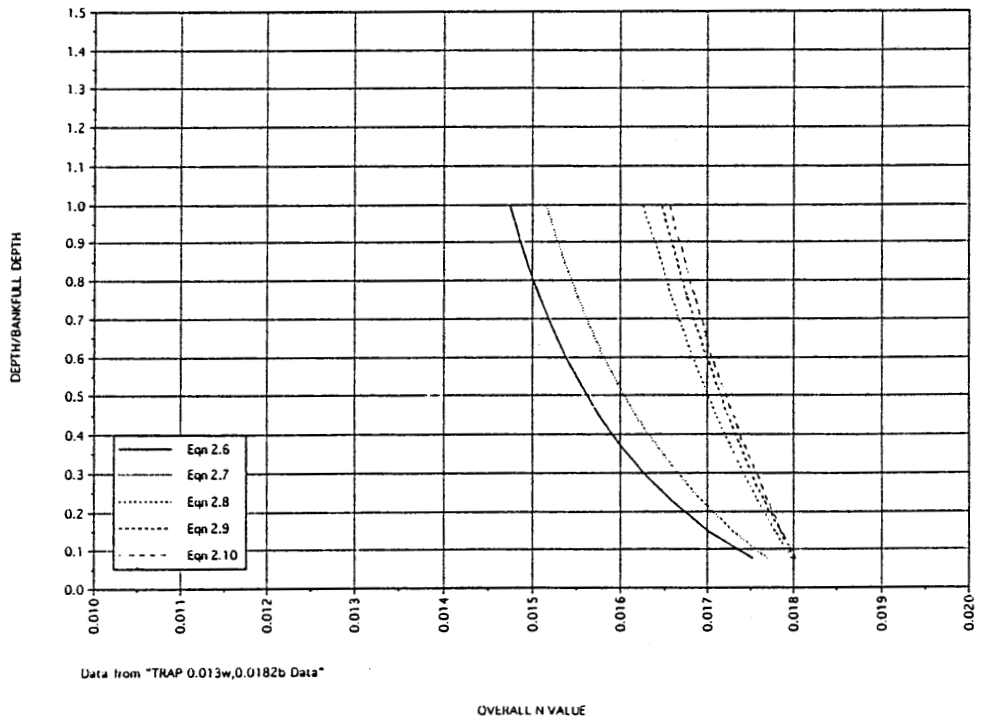

Figure 2.2b **Performance of equations 2.6 to 2.10 for a trapezoidal channel with rough bed and smooth sidewalls**

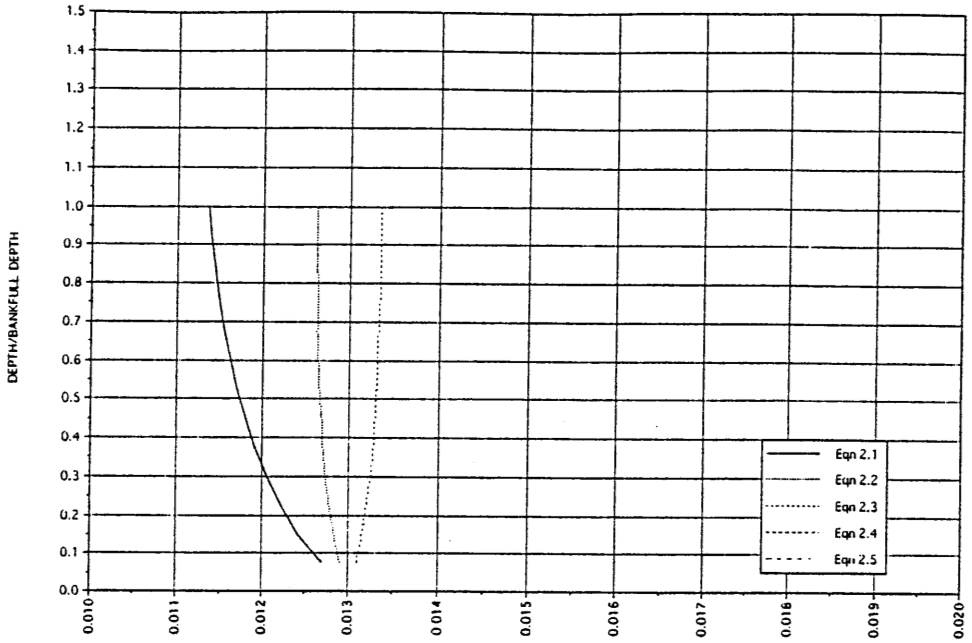

Figure 2.3a Performance of equations 2.1 to 2.5 for a trapezoidal channel with uniform roughness

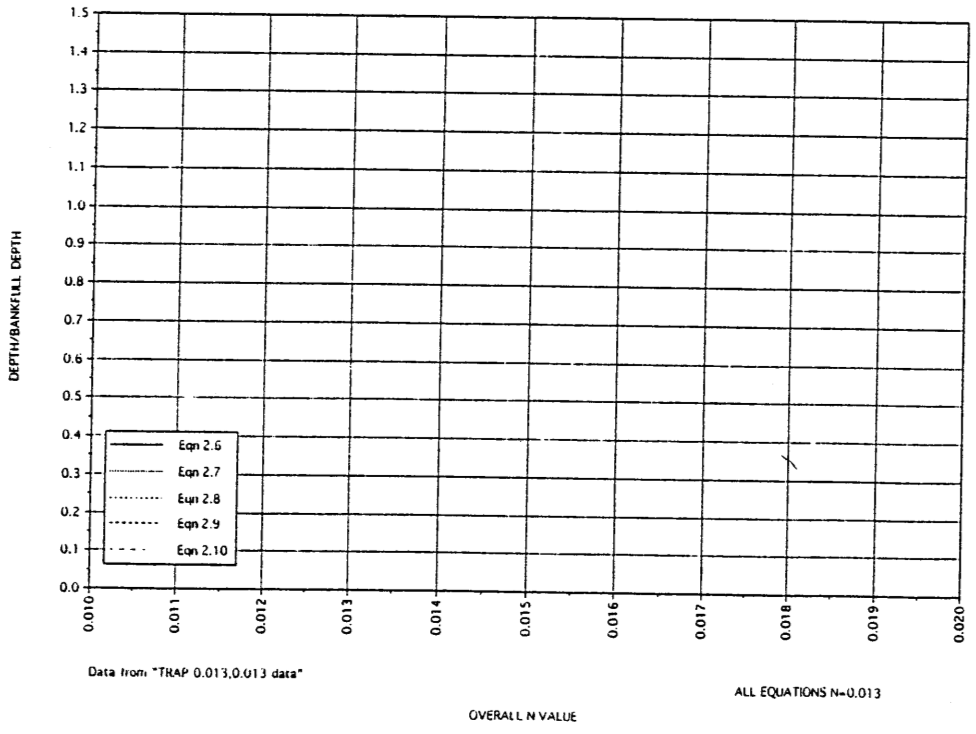

Figure 2.3b Performance of equations 2.6 to 2.10 for a trapezoidal channel with uniform roughness

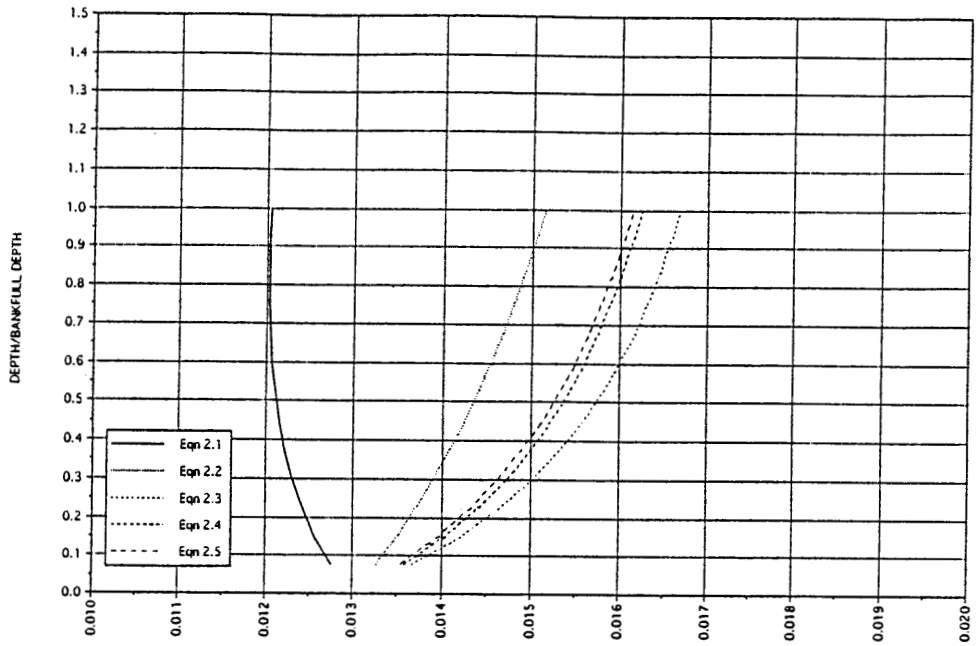

Figure 2.4a Performance of equations 2.1 to 2.5 for a trapezoidal channel with rough wall and smooth bed

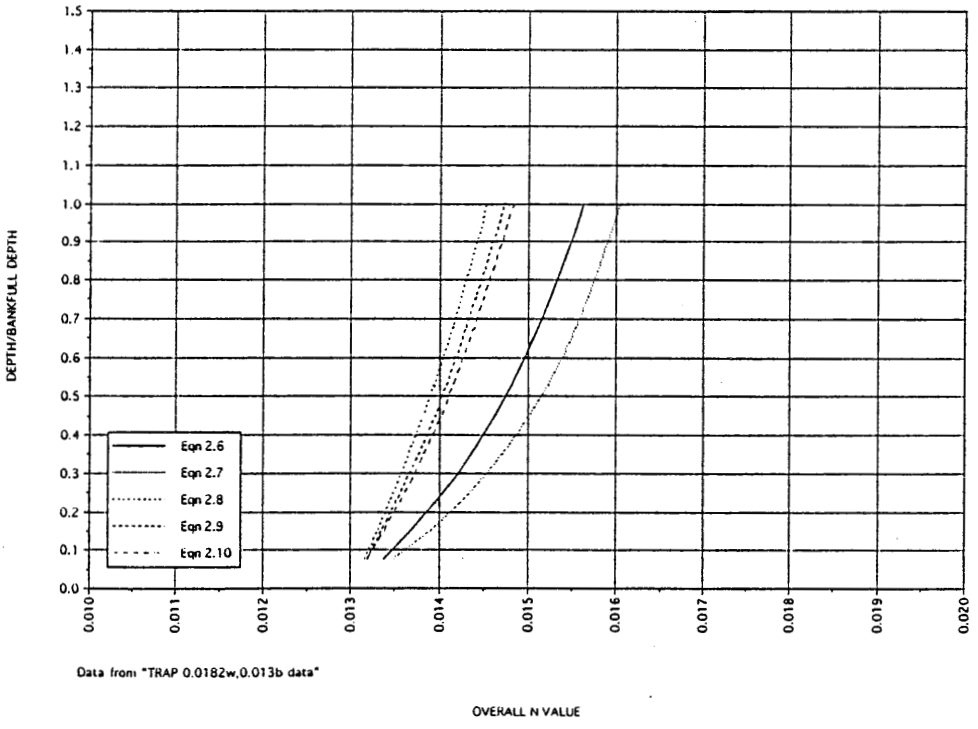

Figure 2.4b Performance of equations 2.6 to 2.10 for a trapezoidal channel with rough wall and smooth bed

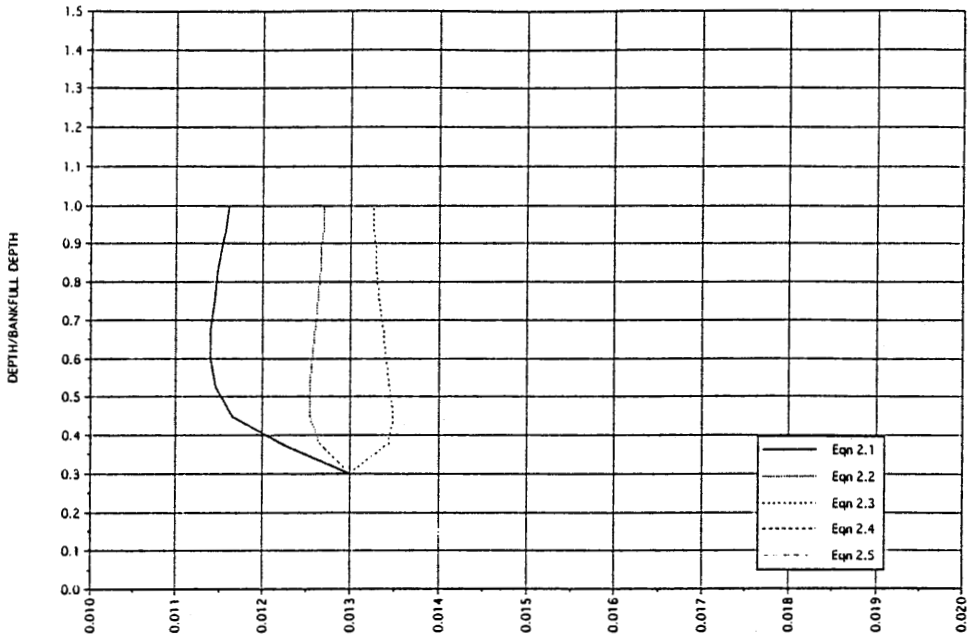

Figure 2.5a Performance of equations 2.1 to 2.5 for a triangular channel with uniform roughness

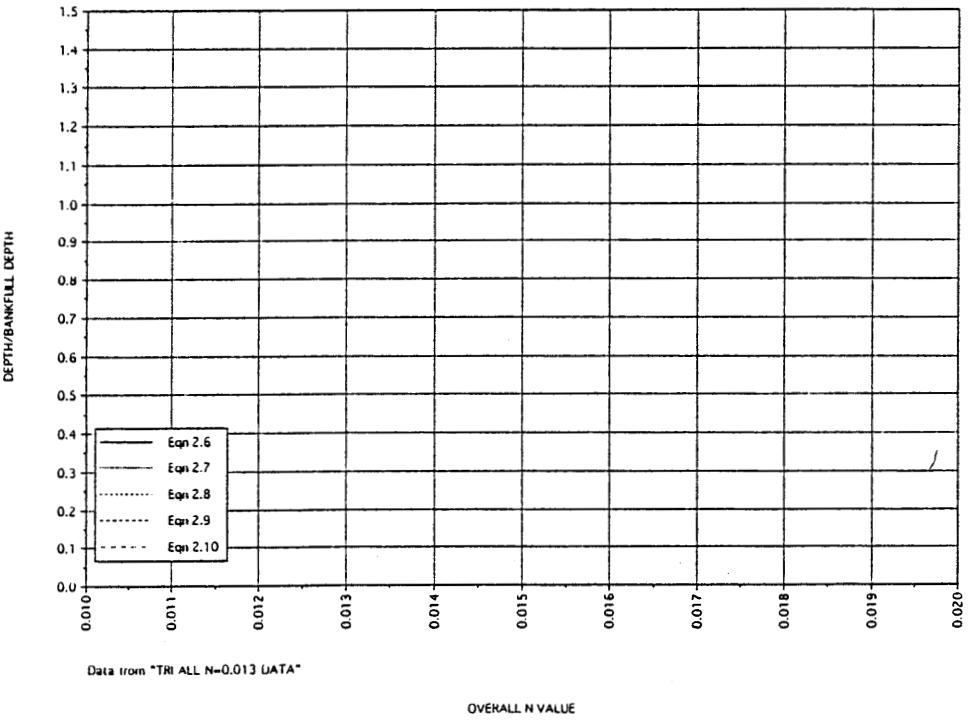

Figure 2.5b Performance of equations 2.6 to 2.10 for a triangular channel with uniform roughness

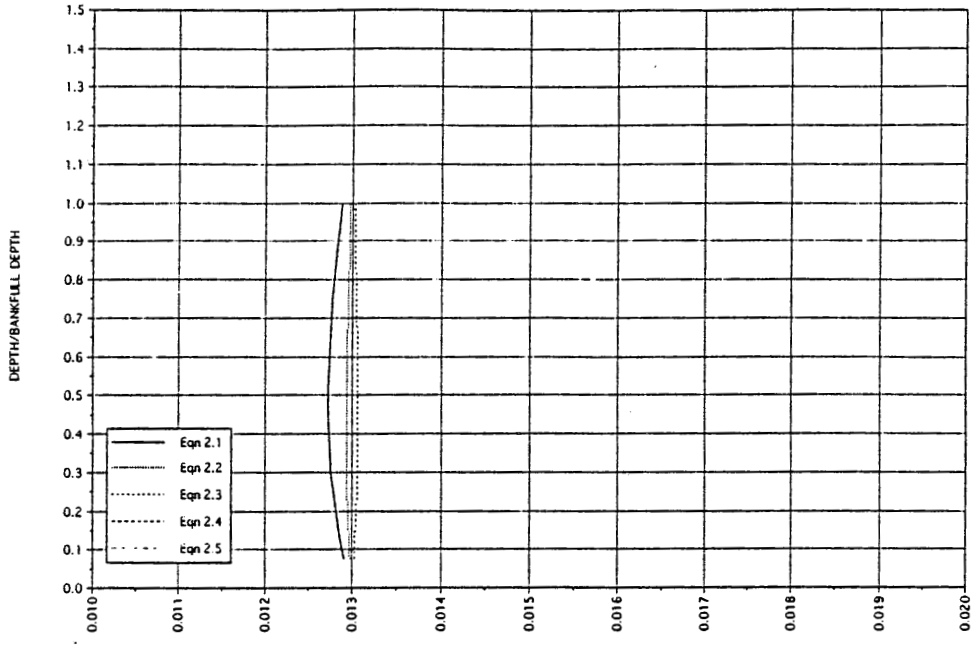

Figure 2.6a Performance of equations 2.1 to 2.5 for a rectangular channel with uniform roughness

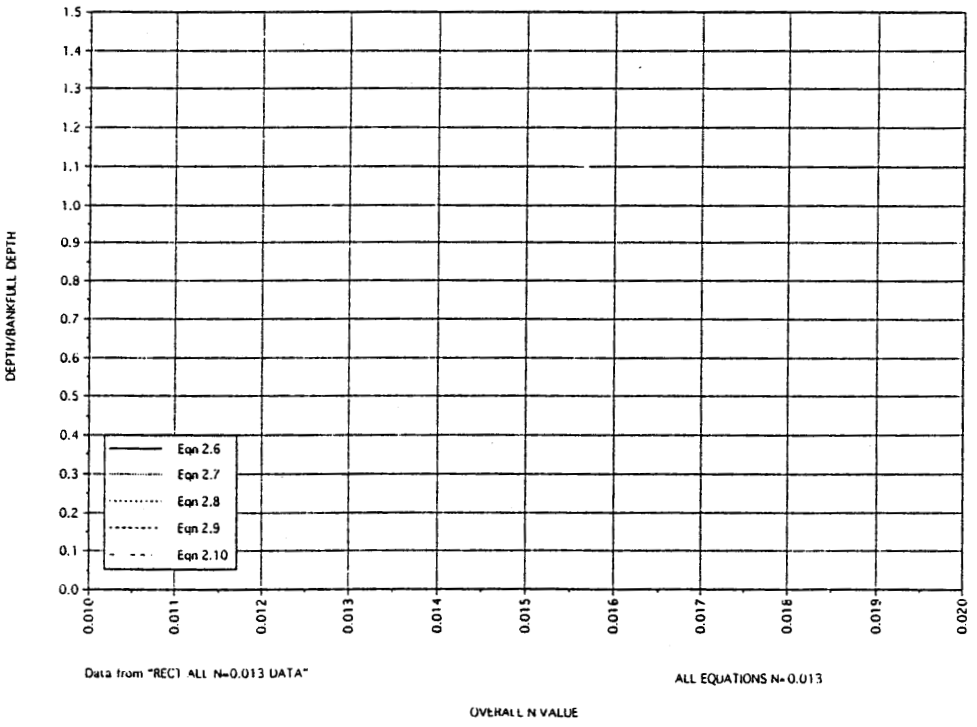

Figure 2.6b Performance of equations 2.6 to 2.10 for a rectangular channel with uniform roughness

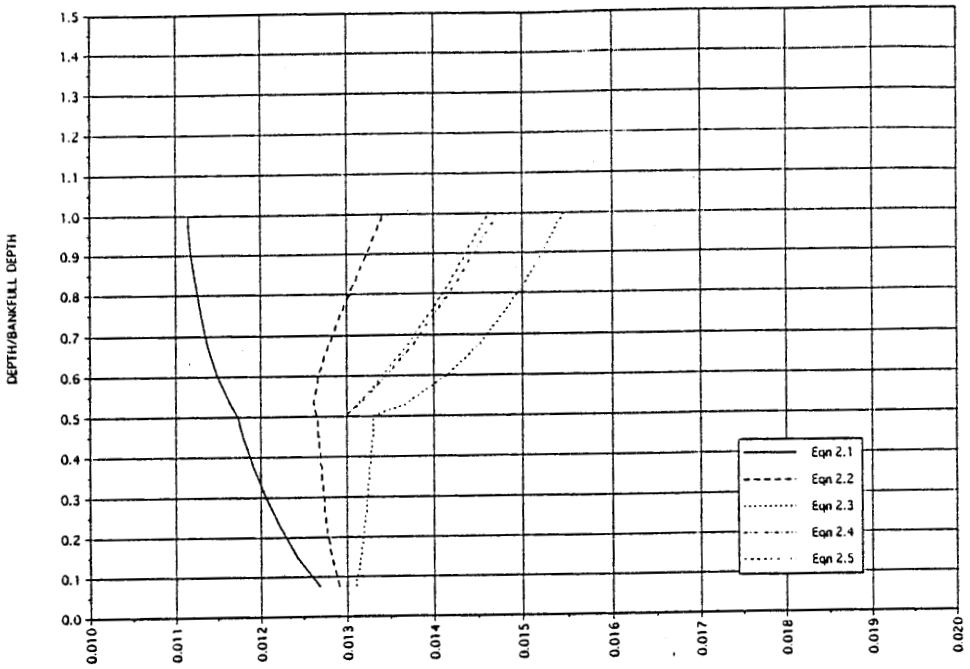

Figure 2.7a Performance of equations 2.1 to 2.5 for a trapezoidal channel with varying roughness on sidewalls

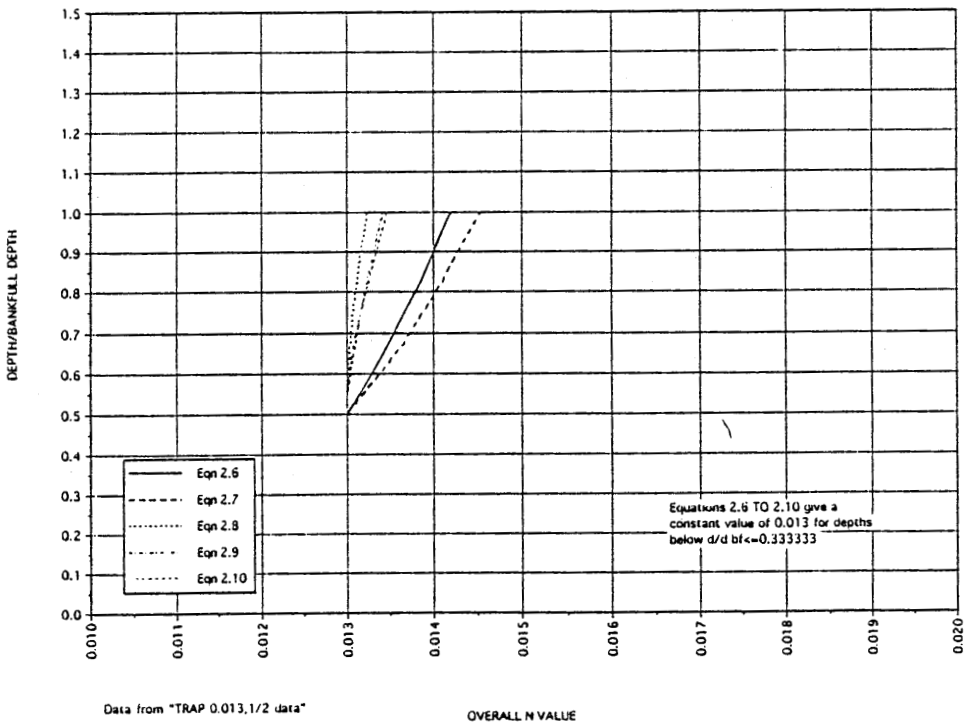

Figure 2.7b Performance of equations 2.6 to 2.10 for a trapezoidal channel with varying roughness on sidewalls

2.3.1. Cross-Sectional Shape

Cross-sectional shape is important because it governs the pattern of velocity distribution, boundary shear stress, and secondary circulation in the channel (Myers, 1991). The development of secondary flows accounts for energy losses and increases in resistance. Secondary flow is apparently more pronounced in rectangular channels than in, say, triangular channels; therefore, rectangular channels should have higher channel resistance than triangular channels. It is believed that when the degree of roughness is constant, the friction factor decreases generally in the order of rectangular, triangular, trapezoidal, and circular channels (Chow, 1959).

The state of flow also directs how the channel shape affects the friction factor. Chow (1959) indicated that for smooth channels the shape of the channel does not have an important influence on friction in turbulent flow as it does in laminar flow. For rough channels, on the other hand, the channel shape has a pronounced effect on the friction factor in the turbulent region. At the complete turbulent state, the friction factor is independent of Reynolds number and depends solely on roughness, hydraulic radius, and channel shape.

In the above examples of uniform boundary roughness, the overall n values at full depth as predicted by these equations are very close, hence the influence of shape cannot be evaluated by these equations. Moreover, only equation 2.3 predicts increasing overall n at higher depths, which is consistent with the development of secondary circulation flow. Overall, it is clear that in prismatic channels the n versus depth curve responds to changes in roughness and geometry. In order to evaluate systematically which equation is most capable of incorporating these conditions, data from a controlled environment are needed. Following are previous studies from which data can be adopted for the purpose of this research.

2.3.2. Data from Previous Studies

Cox (1973) analyzed the effect of roughness on Manning's n value in a simple rectangular channel, allowing bed roughness to differ from that of banks. Because of the cross-sectional shape, he used diagonal division lines at the corners to obtain subareas. Cox's analyses were based upon experimental data by Pillai (1962) and USACOE (1968). Pillai investigated the effects of different roughness patterns in simple rectangular and trapezoidal channels, using three types of roughness. Among the three equations he tested, 2.5, 2.9, and 2.10, Cox concluded that equations 2.9 and 2.10 performed best overall for rectangular channels of composite roughness.

Knight and MacDonald (1979) conducted experiments aimed at clarifying the distribution of shear stress in channels of varying roughness. Their work concentrated on the effect of channel bed roughness on the overall shear stress patterns. Experiments were

conducted in a rectangular flume 1.51 feet wide and 1.25 feet deep. The bed roughness was provided by rectangular strips attached to the bed. Knight, and MacDonald reached two major conclusions based on their data. First, the percentage of shear force carried by the channel walls is lowest at maximum bed roughness, and this value increases with increasing depth in the channel. Second, the standard sidewall correction procedure (used later in this report) appears to give relatively accurate results, even though cross-channel transfer of momentum is present.

The data of Knight and MacDonald, while thorough, are not easily adapted to the form used in this report, and thus is not used to check the performance of the ten equations.

Motayed and Krishnamurthy (1979) conducted a field investigation into the effects of varying roughness along the perimeter of a channel. They reviewed the performance of four of the equations investigated later in this report, 2.1, 2.4, 2.5, and 2.8, using data from 36 streams in the eastern United States. The data appear to be confined to flows lower than bankfull depths. Motayed and Krishnamurthy concluded that equation 2.1 produces the best results in providing an overall section n value.

2.4. Application to Compound Channels

Applying the concept of composite roughness to compound channels produces another problem in addition to roughness differences: the change in geometry between the main channel and floodplains. When water flows onto the floodplain, the wetted perimeter increases at a rate much faster than the total area. Hence, using the one-dimensional equation for the whole compound channel would result in underestimation of average velocity or total discharge for given depths or overestimation of depths at given discharges (e.g., James and Brown, 1977). Posey (1967) also illustrated that underestimation occurs most obviously at shallow floodplain depths.

It is clear that at shallow depths, the velocity in the main channel can be much higher than that in the floodplains. The velocity difference inevitably results in a lateral transfer of momentum from the fast-moving main channel to the floodplain (Wormleaton et al., 1981). Sellin (1964) confirmed with laboratory data the presence of lateral transfer of momentum, and presented photographic evidence of a series of vortices that caused energy losses at the interface. Myers (1978) proposed an apparent shear force -- a force due to the momentum transfer -- as a measure of the net effect of momentum transfer on the floodplain.

2.4.1. Division Method

The existence of apparent shear stress at the main channel and floodplain interface prompted engineers to seek different means to compute discharges. The most common approach adopted has been to treat the channel and floodplain separately. Several division methods have been proposed (e.g., Nalluri and Judy, 1985; Baird and Ervine, 1984; Knight and Demetriou, 1983, Wormleaton et al., 1981; Daugherty and Franzini, 1977; Yen and Overton, 1973; Posey, 1967; and Chow, 1959). In general there are vertical, diagonal, and horizontal division methods, as well as zero shear stress lines, as proposed by Yen and Overton (1973). The location and hydraulic characteristics of the interface are the subject of these methods. For example, Posey (1967) found that at low floodplain depths the most accurate results were obtained if the imaginary vertical boundary was included in the main channel wetted perimeter and omitted for the floodplain calculation. The discharges for each subdivision are calculated individually and summed to give the overall discharge. When the momentum transfer is ignored (that is, the imaginary interface is not counted as part of the wetted perimeter), these methods either overestimate the discharge at given depths or underestimate the depth for a known discharge.

Yen and Overton reviewed the general methods but found that the shear stress on the surface along the division lines was not zero. In such cases, they argued, the division lines should be included in the calculation of the wetted perimeter to more accurately balance the weight component. On the other hand, if the division lines are included in the wetted perimeter calculation, the shear stress on the division lines should be known. It would be most difficult, if not impossible, to determine shear stress on such arbitrary division lines for each and every case of floodplain channel flow. Hence, they proposed zero shear subdivision lines and gave inclination angles -- a function of floodplain depth and channel geometry -- to be used in practice. Hadjipanos (1980) noted that zero shear stress lines are actually curves that are difficult to define without detailed information.

Vertical, diagonal, and horizontal division lines are generally easier to apply. Wormleaton et al. (1981) reviewed the effect of these methods on discharge calculation in compound channels on the basis of experimental data from a rectangular compound channel. Combining their conclusions with those of Wormleaton and Hadjipanos (1985), the following few points can be observed:

- Vertical interface methods tend to overestimate the discharge in the main channel subdivision. The degree of overestimation increases with floodplain roughness and is also higher at low floodplain depths.
- When vertical subdivisions are used, the magnitude of the shear stress at the interface is strongly related to the velocity difference between the adjacent subdivisions, the depth ratio (total depth/bankfull depth, y/D), and width ratio (floodplain/main channel).

- At low floodplain depths, the apparent shear stresses across the vertical interface planes are much higher than the main channel boundary shear stresses. They also increase with greater floodplain roughness.
- Method VE (interface not included in computation) overestimates main channel flow to the greater extent. Both methods, VE and VI (interface included in computation), give the same errors for floodplains since they make the same assumptions.
- In general, it is clear that at higher floodplain depths, the vertical interface methods give more accurate total discharge values than the horizontal methods. However, errors in the individual subsections are generally smaller with the horizontal interface.
- Results for the diagonal and horizontal interface methods show similar characteristics.

Since vertical subdivision is the easiest method to set up in the laboratory and the method most likely to be used in engineering practices, conclusions on vertical interfaces need to be emphasized. However, Yen (1992a) notes that bisectional (diagonal) subdivision lines generally approximate zero shear lines more accurately than the vertical subdivision method. Therefore they should give more consistent overall n values with depth. Still, several of the division methods encounter difficulties in determining an average friction factor for the whole channel in their applications. Our research, seeking to determine the variation of overall roughness with depth, provides another approach for calculating discharge in compound channels.

2.4.2. Cross-Sectional Geometry

According to Yen (1992a), changes in geometry when water rises from the main channel to the floodplains are the most significant influence on the overall resistance coefficient. He noted that equation 2.1 is commonly considered the best equation to represent this effect. James and Brown (1977) showed that the overall n value apparently decreases in value at depths just above the bankfull stage as a compensation for the increase in the wetted perimeter. They concluded that the Manning equation does not accurately predict the stage-discharge relationship in a compound channel for shallow floodplain depths ($1.0<y/D<1.4$), and suggested a correction factor, equal to the total n value divided by the overall n value at the bankfull stage, to the hydraulic radius to obtain a correct stage-discharge curve for a given cross section. The effect of geometry seems to disappear at high stages, i.e., $y/D>1.4$, and the correction factor is no longer necessary. James and Brown considered that equation 2.9 performed well in channels of composite shape. They extended the use of this equation to compound channels of composite roughness and obtained acceptable results. Yen et al. (1985), however, found that equation 2.1 produced reasonable results for compound channel tests.

Similar to prismatic channels, the effects of main channel and floodplain geometry are associated with the presence of secondary circulation. Yen and Overton (1973) noted

that secondary flows that influence the overall cross section resistance coefficient are generally caused by the presence of corners within the geometry of the section. Apparently, the rectangular-shaped channel produces higher secondary circulation at the right angles. On the other hand, Sellin (1967) found that channel shape (from rectangular to trapezoidal) has no significant effect on the momentum transfer mechanism.

In rectangular and rectangular two-step compound channel experiments, Myers (1991) found that a wide rectangular section (width 750 mm) can carry as much as 80 percent less than a narrow channel (width 200 mm) and 25 percent less than a compound section (width 750 mm) at the same cross-sectional area. He then focused on channel widths and found that friction factors in wide rectangular sections are as much as 45 percent greater than in narrow sections and as much as 25 percent greater than in compound sections of the same overall width. The narrow channels tended to have a higher capacity than wider channels because the point of maximum velocity was below the water surface, and thus more of the flow was at maximum velocity. Myers emphasized that the shape of a channel affects flow in the channel because of secondary circulation patterns.

Channel geometry also includes floodplain widths. Many studies, such as the one by Ghosh and Mehta (1974), have shown that channel geometry influences the distribution of boundary shear stress and the location of its maximum and minimum values. By summarizing many researchers' data, Hadjipanos (1980) concluded that y/D ratios and floodplain roughness affect the distribution of shear stress, and that the ratio of floodplain width to main channel width can cause a shift in the location of the maximum values.

Whether the floodplain was symmetric or asymmetric seemed to have little effect upon the correction factor proposed by James and Brown (1977). Roughening of the floodplain shifted the n behavior to a larger magnitude. Cokljat and Younis (1995) compared results from their turbulence model with experimental data from a rectangular two-step compound channel. Some of their results follow.

- Rectangular symmetrical two-step flume (base model): the contours of longitudinal velocity were mostly symmetrical with the maximum velocity occurring near the centerline; steeper contour lines appeared at the main-channel and floodplain interface.
- Asymmetrical rectangular compound channel (one floodplain only): the magnitude of longitudinal velocity did not change, but the center of maximum velocity moved away from the original centerline toward the main channel; higher velocity occurred on the floodplain.
- Asymmetrical rectangular compound channel with roughened floodplain: higher longitudinal velocity occurred in the main channel, with pockets of high velocity on the floodplain and denser velocity contours at boundaries.
- Symmetrical compound channel with uniform roughness, rectangular floodplain, and main channel walls inclined at 45°: the longitudinal velocity did not differ from the base model, contour lines have steeper gradients near the boundary.

2.4.3. Data from Previous Studies

Sellin (1964) investigated the interaction between the flow in the main channel and the flow in the floodplain, including limited investigation of the effects of variation in roughness along the wetted perimeter. His tests contained scenarios in which the entire channel had the same roughness, and the entire floodplain had slightly higher roughness than the main channel. Although not enough information was provided about the base n values of the roughness materials used, approximate values were given. The experiment was conducted in a symmetrical compound channel 18 inches in width. The main channel was 4.5 inches wide and 1.75 inches deep. The small size of the channel and low Reynolds numbers used in the tests may have affected the n value. Table 2.2 gives some of the significant flow variable ranges of Sellin's data and data from other studies discussed in this section.

James and Brown's investigation (1977) was on the effects of geometry on floodplain flow. Three of their many test series are used later in this report to test against the ten equations in predicting the overall n value in asymmetrical floodplain channels.

Hadzipanos (1980) conducted an experiment on compound channels with varying roughness, concentrating on the effects of momentum transfer between the sections. The laboratory channel was a symmetrical compound channel 3.96 feet wide, with a main channel 0.94 feet wide and 0.39 feet deep. The main channel had one roughness, and the floodplains had four different roughness materials. All test cases were conducted under steady uniform flows. Hadzipanos' data require reprocessing and are therefore not included in this report. Pertinent information on the range of variable values considered in his tests is given in Table 2.2. The experimental data of Wormleaton et al. (1982) appear to be the same data published earlier in Hadzipanos' 1980 thesis.

The work of Blalock and Sturm (1981) gives insight into the fluid mechanics of flow in compound channels. They provided a procedure for determining the minimum specific energy in a compound channel. The need for a more precise definition of the Froude number in compound channels has been observed in studies cited later in this report. The method used by Blalock and Sturm is one step toward providing a more accurate description. While relatively simple to use, their procedure is not used in this study because of the large quantity of data to be analyzed and the problem of accurately correlating all the data in a similar manner. As already mentioned, the limitations of the more traditional approach will become apparent later in this report, most notably in the data of Myers and Brennan (1990).

Using data from a large-scale compound channel experiment, Myers and Brennan (1990) examined the fluid mechanics of flow resistance in these channels. They conducted tests in symmetrical and asymmetrical channels roughened by the same material, and noted that the momentum transfer mechanism increases the value of the main channel resistance coefficient and decreases the value of the floodplain resistance coefficient when these

Table 2.2. Summary of Pertinent Information from Selected Studies for Comparing Roughness Variation in Channel Flow

Reference	*Channel geometry*	*Variable roughness*	*Range of R*	*Range of F*
Sellin (1964)	Rectangular Compound	Yes	~4.600E+03 - ~7.438E+03	n/a
Cox (1970)	Rectangular	Yes	~6.975E+04	n/a
James & Brown (1977)	Trapezoidal, Symm & Asym Floodplain	Yes	2.296E+03 - 2.850E+04	n/a
Pillai (1962)	Rectangular and Trapezoidal	Yes	2.734E+04 - 9.256E+04	0.4410 - 0.7872
Yen and Overton (1973)	Rectangular Compound	Yes	~1.888E+05 - ~1.674E+05	~1.126** ~1.000**
Knight & MacDonald (1979)	Rectangular with Strip Roughness	Yes, bed only	0.212E+05 - 3.711E+05	n/a
Motayed & Krishnamurthy (1980)	Natural Channel	Yes	n/a	n/a
Hadzipanois (1980) and Wormleaton, Allen & Hadzipanos (1982)	Rectangular; Simple and Compound Channels	Yes, floodplain only	5.381E+03 - 2.437E+04	0.2099 0.7646
Myers & Brennan (1990)	Trapezoidal: Simple & Compnd Channels	No	1.526E+04 - 8.718E+05	0.5552 9.7395
Myers (1991)	Rectangular: Simple & Compnd Channels	No	2.974E+03 - 2.337E+04	0.3104 - 0.6471

Notes: * Because ranges for Froude and Reynolds numbers were rarely given, they were computed using the best information available.

** Excessively high Froude numbers are probably due to inadequate definition of Froude numbers for compound channels. See the literature review for a discussion of Blalock and Sturm (1981).

values are calculated independently. They also showed that the effect of the momentum transfer mechanism increases with increasing floodplain width.

The maximum width of their experimental channel, including floodplains, was 32.71 feet. The main channel was 4.92 feet wide at the base, with 45° sloping sidewalls. The main channel depth was 0.49 feet. Although they lacked variation in roughness, Myers and Brennan provided sufficient information to calculate the variation of the overall

cross-sectional n value with depth in their compound channel. Five of the tests they conducted are examined in more detail later in this report.

2.5. Summary

The ten composite equations exhibited very different results in prismatic channels. Their differences become even more evident given changing roughness along the wetted perimeter. It has been shown that the effects of changing roughness on the n versus depth curve are greater than the effects of channel geometry in prismatic channels. Based on the previous discussion of the development of secondary circulation, it seems that equation 2.3 best reflects this process. However, data are needed to verify this concept and the effects of changing roughness.

At the same time, geometric changes in shallow floodplains are more significant in compound channels. The range of shallow floodplain depths can be approximately defined as from $1.0 < y/D < 1.4$. The n value decreases rapidly at depths just above bankfull stage, but gradually recovers at higher floodplain depths. The effects of varying roughness and other geometric factors on the n versus depth relationship have not been studied closely. Defining an n versus depth curve for a given channel reach provides both a better way to estimate n for different water depths in engineering practices, and an easier way compared to division methods to calculate discharge in compound channels.

3. EXPERIMENTAL INVESTIGATION

In order to validate the composite roughness equations and to investigate how overall n changes with depth, a controlled laboratory experiment was conducted in the Hydrosystems Laboratory at the University of Illinois at Urbana-Champaign.

3.1. Channel Design and Construction

An experimental channel system, including a water-supply system, head tank, compound channel, tail tanks, and measurement, system was built within a main tilting flume. The tilting flume was much larger than the original proposed flumes; however, it was the only flume available during the project period. Therefore, it was decided to build a larger channel and fully utilize the available size so that errors relating to low Reynolds numbers could be avoided. The experimental work produced very good results, but it also occupied a major portion of the project period. The design of the experiment and construction of the flume are explained as follows.

3.1.1. Tilting Flume

The entire compound channel resided in a large tilting flume in the Hydrosystems Laboratory. The flume was 161 feet long, 6 feet wide, and 4 feet deep, and was supported on a center pin with a hydraulic jack at the end for slope adjustment. The flume slope varied between 0 and 2.5%.

3.1.2. Water-Supply System

Flow for the experiment was supplied by a constant head tank housed at the top of a water tower. Pumps 3, 4, 5, and 6 in a separate pump room supplied an 18-inch-diameter manifold to the head tank. With all four pumps in operation, the maximum supply to the head tank was approximately 13.4 cubic feet per second (cfs). During the experiments, pumps 3 and 6 were used either separately or in conjunction. These pumps had rated discharges of 4.45 and 2.23 cfs, respectively, at a head of 87 feet. The static differential head difference between the maximum water surface in the sump and the crest of the head tank skimming weirs was 54 feet, and 10 1/8 inches (Maxwell, 1972).

For this experiment, a water-supply line connection was installed from the existing water-supply pipes to a head tank. In order to deliver sufficient discharge to the channel, approximately 85 feet of 6-inch-diameter PVC pipes were used. Flow was controlled by two 8-inch valves in the existing supply pipe just before the PVC water-supply line. One valve controlled the discharge while the other was used to completely shut off the water

without changing the flow rate once the water was restarted. When pump 3 was in operation, the maximum discharge to the channel was approximately 2.9 cfs. The deliverable flow probably was limited by the 6-inch pipe. In general, however, this flow rate satisfied most of the runs conducted during the experiment. The rate of flow delivered to the channel was always checked with the volumetric tank.

3.1.3. Head Tank

A head tank was designed and constructed to regulate flows into the channel. The head tank was 5 feet long and equal in width to the channel. A series of honeycomb baffles were built at the bottom of the top half of the head tank for energy dissipation purposes. Inflow from the PVC pipes was dumped directly on the baffles. A vertical adjustable gate at the center of the head tank further dampened the waves caused by the water supply. Before water entered the channel, three layers of screen and mesh and a layer of rubberized hair were placed in the flow path to dampen any waves in the surface.

3.1.4. Experimental Channel

At the time this experiment began, one-half of the total length of the tilting flume was occupied for another experiment. Therefore, the head tank started halfway in the flume. The channel model was assembled on the floor into segments before it was placed into the flume. A full channel segment was 8 feet long, made of 5/8-inch-thick plywood. Supports made of 2-by-4 wooden studs were then screwed into the underside of the channel. The span between each wooden support was less than 2 feet. The channel segment defined one-half of a trapezoidal channel, which included three subareas (figure 3.1). The first subsection, the Main Channel (MC), was 8 inches wide, followed by the second subsection, the Main Channel Border (MCB), also 8 inches wide. The incline wall was raised 45° to meet the final section, the Floodplain (FP), which was 30 inches wide. The centerline of the channel, located at the wall of the main tilting flume, was Plexiglas, and all its joints were smoothed so that it could be used as a non-roughened edge of the channel. The floodplain section ended with a vertical wall made of plywood coated with plastic.

Segments were then moved into the flume and placed on concrete blocks for assembly. They were connected by splicing the joints with 2-by-4 studs screwed into the underside of the channel. Additional wooden boards were attached to the underside of the channel sections to brace any areas determined to be at risk of deflection.

The whole channel consisted of eight full-length segments and one half-length segment for a total length of 68 feet. Weather stripping was attached to the edge closest to the Plexiglas wall and the sections were forced against the wall. Multiple layers of

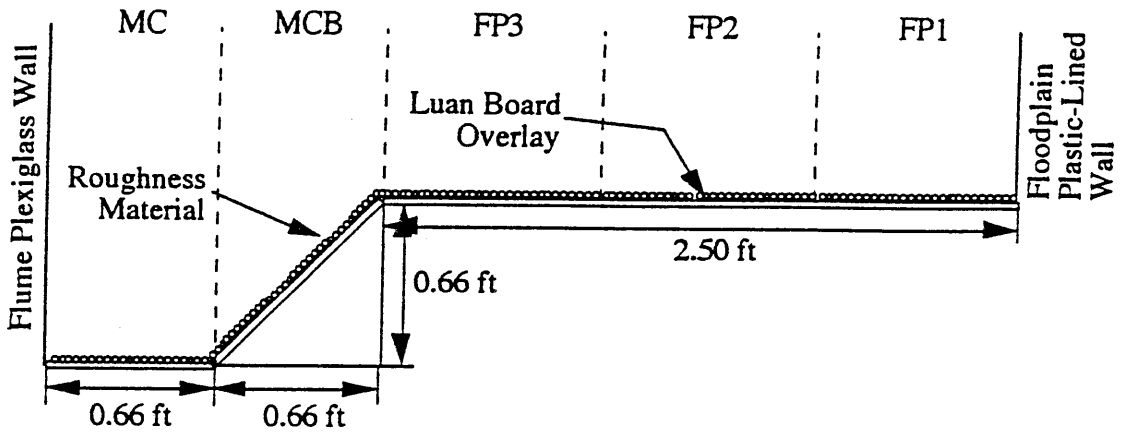

Dimensions are exterior dimensions. Area and Wetted Perimeter Based on interior dimensions measured at luan board surface. Flow direction is into page.

Figure 3.1. Experimental channel

silicone caulking were applied to each joint in the section, and the wood portions were sealed using deck water sealer and polyurethane varnish. Finally, the entire length of the flume was lined with 6-mil plastic sheeting glued in place to prevent leakage.

The concrete blocks were 18 inches (0.46 meters, m) above the floor of the flume. This allowed working space under the channel and enabled water to run down when an upstream experiment was in operation. Once all of the sections were in place, the entire flume was measured to assure a uniform bed slope along the length. If necessary, commercially available shims were inserted between the concrete blocks and wooden supports to adjust the height of the channel so that a deviation of no more than 1/8 inch was achieved.

3.1.5. Tailgates and Measuring Tanks

The downstream structure consisted of a flow separation device, three tailgates, and three measuring tanks. Between the last channel segment and the tailgates was a 4-foot non-roughened channel section. Vertical Plexiglas dividers were set up between the MC and MCB and between the MCB and FP areas. These dividers extended to the

tailgates designed for each channel portion so that the discharge in each portion could be found.

The gates were designed for each flow portion. Each gate consisted of two layers, one fixed and one movable (figure 3.2). Both fixed and adjustable gates had multiple slot openings. The openings were horizontal on the MC and FP gates, and tilted 45° on the MCB gates. This design aligned the opening with the expected velocity gradient to minimize distortion to the profile of the approaching velocity. In order to establish uniform flows, the movable gate was attached to a threaded metal rod, allowing adjustment of the tailgate positions to within approximately 0.005 feet.

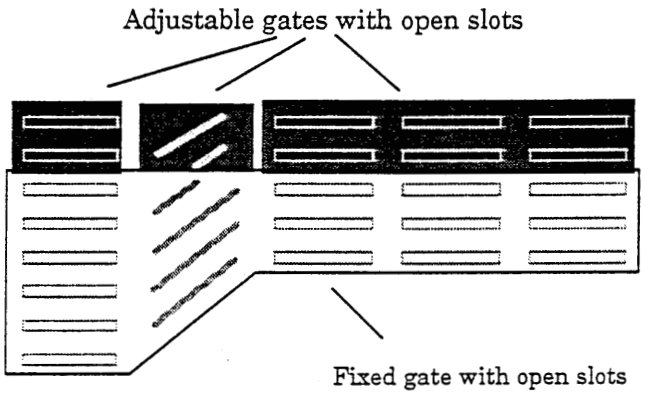

Figure 3.2. Tailgate design

After passing through the tailgates, water dropped into three separate tanks, one for each portion of the channel. Baffles were used to reduce the energy of the flow before three weir measurements. Three sharp-crested triangular weirs at the downstream end of the tanks all had the same design, with 30° openings. Water depths in each tank behind the outflow weir were measured with a point gage measurement device. A three-way valve system allowed water from each tank to be transmitted to the point gage. The weirs were then calibrated so that discharge in each tank could be determined. From the weirs, water then passed to a volumetric tank where discharge for the entire channel was measured again. A plan view of the entire channel system is presented in figure 3.3.

3.2. Design and Construction of Roughness Elements

The channel boundary was roughened by fitting roughness elements (roughened luan boards) across the cross section (see figure 3.1). Five elements could be placed

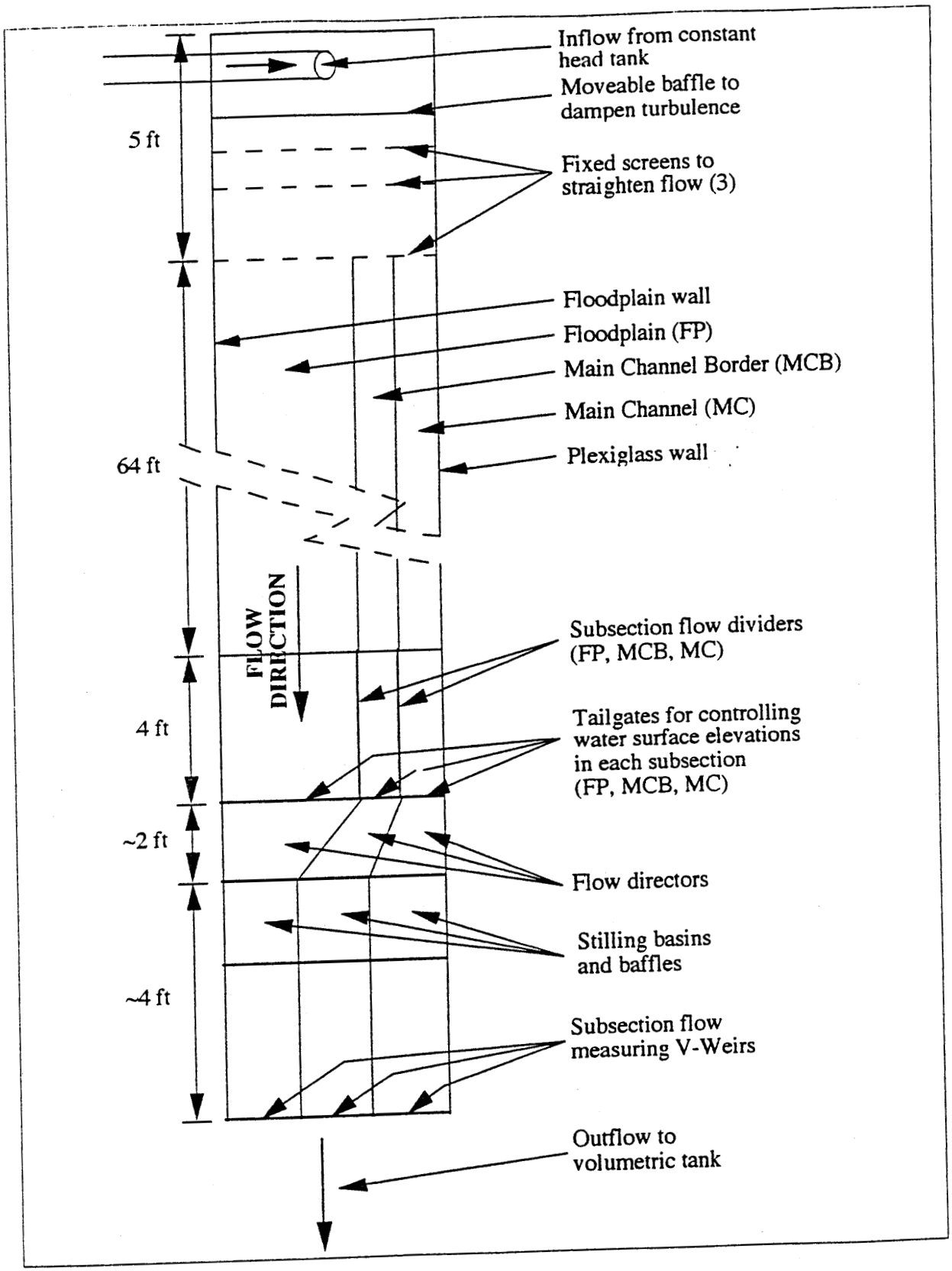

Figure 3.3 Plan view of experimental channel

laterally across the channel at all sections. Multiple roughness elements were designed at the MC, MCB, FP3, FP2, and FP1 locations so that roughness patterns could be developed by placing different roughness elements at the MC, MCB, and FPs. Additionally, the roughness within the floodplain was expected to vary among the FP3, FP2, and FP1 sections. The elements were held in place by galvanized deck screws placed at approximately 1.5 feet on center.

Roughness materials were pea gravel, black magnum sandblasting grit, and a fine-grained laboratory sand. Before constructing the roughness elements, the pea gravel was sorted using a mechanical sieve to provide a high degree of uniformity in particle size. The sand and black magnum were considered quite uniform and were not sorted. Figure 3.4 gives the percent finer ranges for each of the materials. Table 3.1 gives the coefficient of gradation (C_G) and the uniformity coefficient (C_U) for each of the materials. Table 3.2 gives the equivalent sand roughness values (d_{50}) for each of the materials. C_G and C_U are defined as follows:

$$C_G = \frac{d_{30}^2}{d_{60} \times d_{10}} \qquad \text{and} \qquad C_U = \frac{d_{60}}{d_{10}}$$

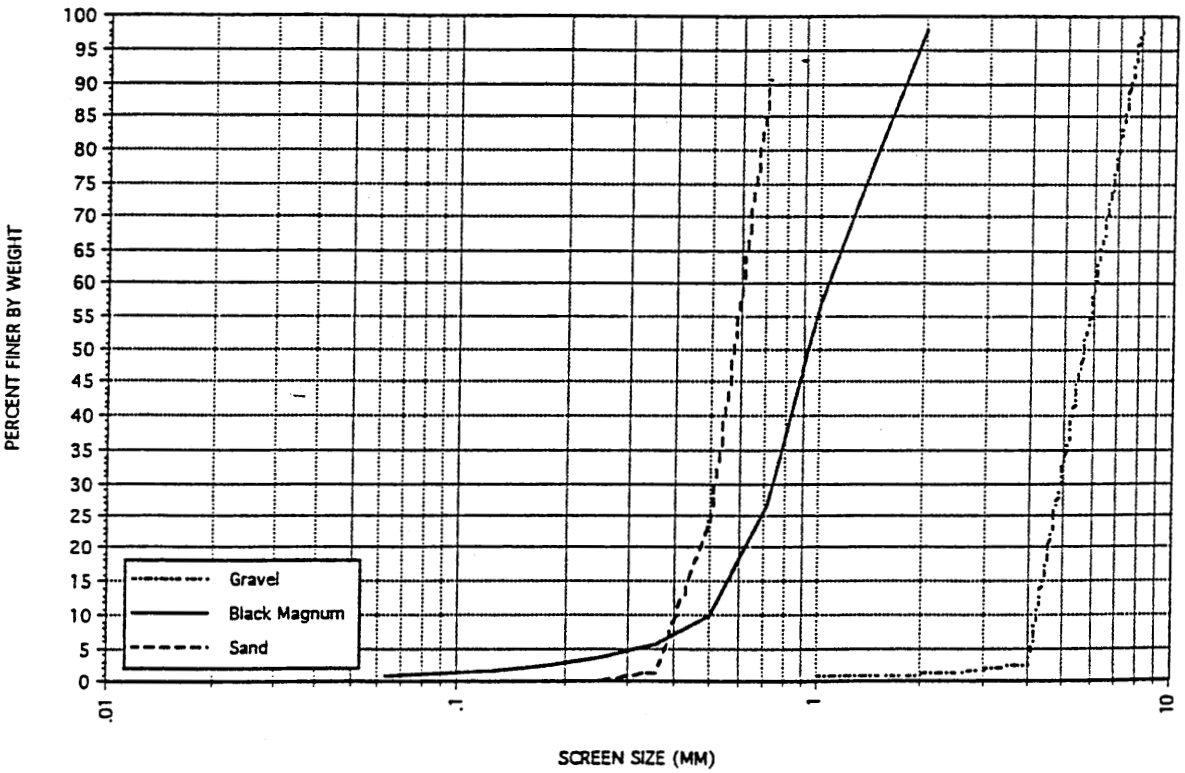

Figure 3.4. Grain size distributions for roughness element materials

After dozens of trials, generic oil-based exterior paint was selected as the adhesive for the roughness material. Oil paint was uniformly applied to the luan board, and the roughness materials were then sprinkled over the wet paint as uniformly as possible. This element was then left to dry on the lab floor. Any roughness material inadvertently brushed off during installation was replaced prior to the experiments. Any wearing of the roughness material during the experiments was similarly replaced. Every attempt was made to maintain these roughness elements for each test.

Table 3.1. Gradation and Uniformity Coefficient for Selected Roughness Materials

Material	*Uniformity coef*	*Coef of gradation*
Gravel	1.484	0.960
Black magnum	2.144	1.030
Sand	1.491	1.065

Table 3.2: Equivalent Sand Roughness Values for Roughness Materials

Material	*ks (ft)*	*ks (mm)*
Gravel	1.968E-02	6.00
Black magnum	3.051E-03	0.93
Sand	1.903E-03	0.58

3.3. Determining Base n Values

Figures 2.2, 2.3, and 2.4 illustrated that base n values can shift the predicted values. An improperly assigned base n value can therefore render an incorrect estimation of the n value at higher depths using the ten equations. A direct way to assess the base n value is to conduct the uniform roughness test in a wide rectangular channel.

Base roughness tests were conducted twice throughout the experiment, once before and once after. Both the black magnum and the gravel elements were tested before and after the experiment, while sand elements were tested prior to the experiment only. (Sand elements were the least-used elements. Results from the first base roughness test for sand were conclusive enough to produce a sufficiently accurate base roughness value.) The data judged to be of the best quality from each of the measurement sets were used in computing a base roughness value for each element type.

A wide rectangular channel was constructed by building a temporary vertical wall at the junction between the main channel border and floodplain. The wall was constructed using 3/8-inch plastic-lined plywood of the same height as the permanent floodplain wall. Three floodplain elements, FP1, FP2, and FP3, of the same roughness were then placed in

the temporary rectangular channel for testing. Figure 3.5 shows how this temporary channel was constructed.

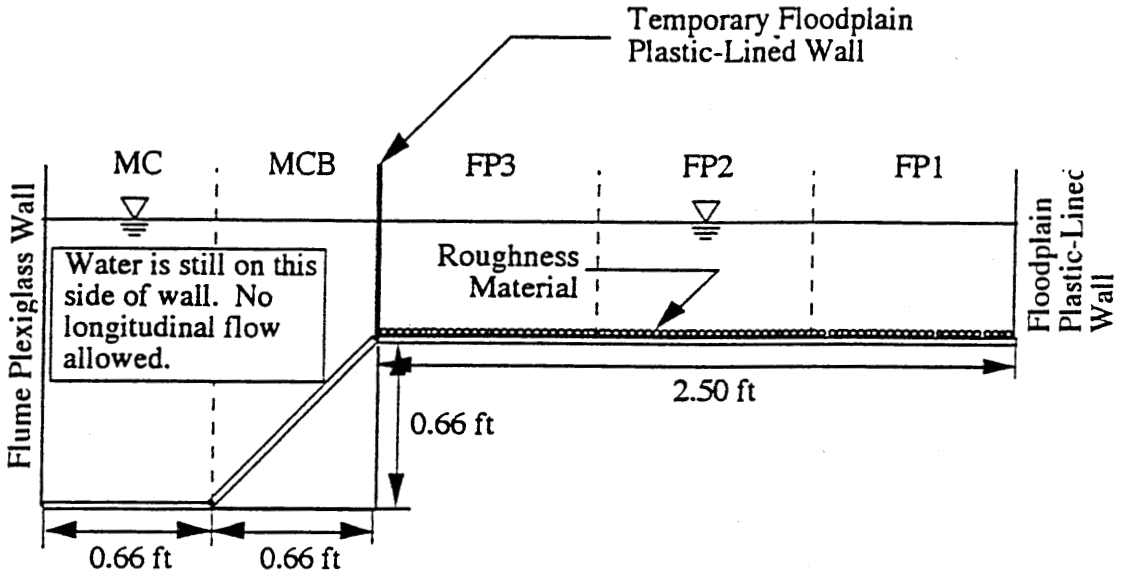

Dimensions are exterior dimensions. Area and Wetted Perimeter
Based on interior dimensions measured at luan board surface.
Flow direction is into page.

Figure 3.5. Temporary rectangular channel for determination of base roughness

The conduct of the base roughness tests was essentially identical to the conduct of the overall tests except that portions of the main channel and main channel border areas were not used. The floodplain tailgate was adjusted to derive steady uniform flow in the temporary rectangular channel.

A series of runs, for at least eight depths, was conducted for each roughness type. The data were processed in a manner identical to that used for the overall tests (to be discussed later). The base roughness values for the materials used in this report are detailed in table 3.3.

The range of base n values found from the materials was slightly lower than expected. Several equations relating the grain size to the local n value were consulted. The predicted values for each material based are shown in table 3.4.

Table 3.3. Base Manning n Values for Roughness Materials

Material	*Base n value*
Gravel	0.0182
Black magnum	0.0130
Sand	0.0120

Table 3.4. Base Manning n Values for Roughness Materials as Predicted by Empirical Equations

		Roughness material		
Source	*Equation*	*Gravel*	*Black magnum*	*Sand*
Measured data	----	.0182	.0130	0.0120
Bray (1979)	$n = 0.048\ d_{50}^{0.179}$	.0238	.0170	0.0156
Stickler (1923)	$n = 0.034\ d_{50}^{1/6}$	.0176	.0129	0.0120
Henderson (1966)	$n = 0.031\ d_{75}^{1/6}$	.0167	.0127	0.0111

Overall, the base roughness n values fell within the range of predictions. Moreover, it appears that the equation by Strickler (1923) performed the best, especially for finer materials.

3.4. Apparatus Verification

Parameters to be measured during the experiment were: discharge, water surface slope, submerged cross sections, velocity, and temperature. For the purpose of quality control in measurements, the apparatus was verified as follows before the experiment.

1. For each run, the flow rate was set with the number of turns of the main supply valve. A relation chart between the number of fractions of a turn (i.e., 1/6, 2/6, 3/6 turns and so on) of the valve and the flow rate was derived. As shown in figure 3.6, the flow rate varied almost linearly with the number of turns at low discharge. In addition, a volumetric tank was always used for the determination of discharge.
2. The discharge for each run was obtained using a main flume volumetric tank designed for weight measurement. When the outflow from the channel became constant, generally a few minutes after the water had run through the channel, the outflow was diverted into the volumetric tank. A U-shaped mercury manometer recorded head differentials before and after the water entered the tank. The calibration chart for the volumetric tank is presented in figure 3.7. A timer was used to record the time required to make a given weight change. During the experiment, the calibration curve for the volumetric tank was independently verified in the laboratory using two large capacity weighing tanks. Using the change in weight of water, the time of the flow measurement, and the temperature of the water, the flow rate in cfs was found by dividing the weight by the time and specific weight of the water.

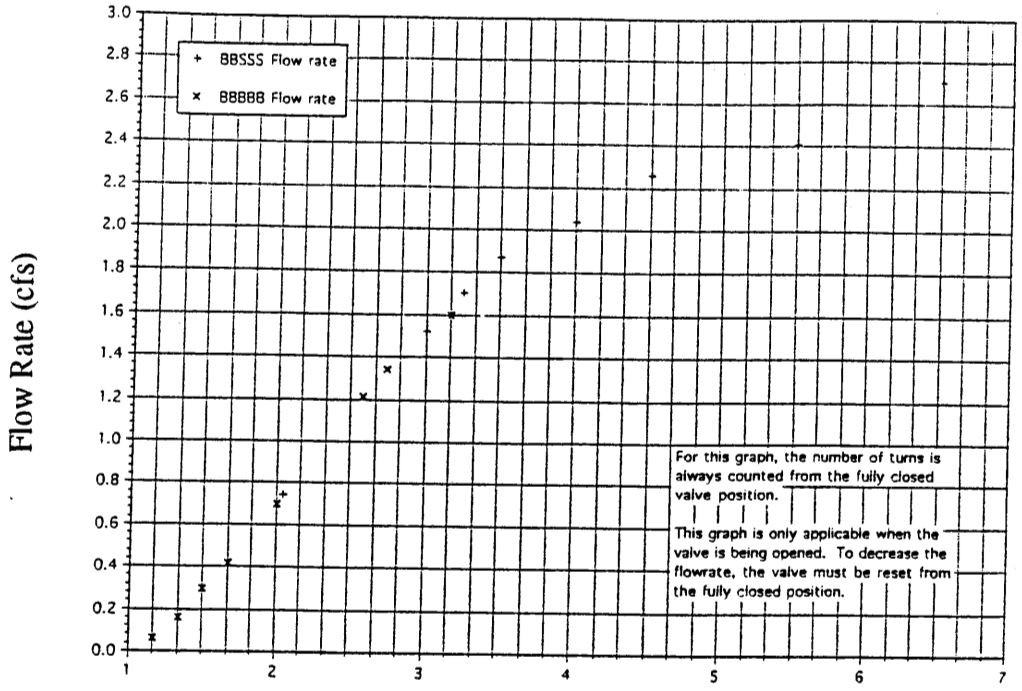

Figure 3.6 Relationship between flow rate and number of valve turns

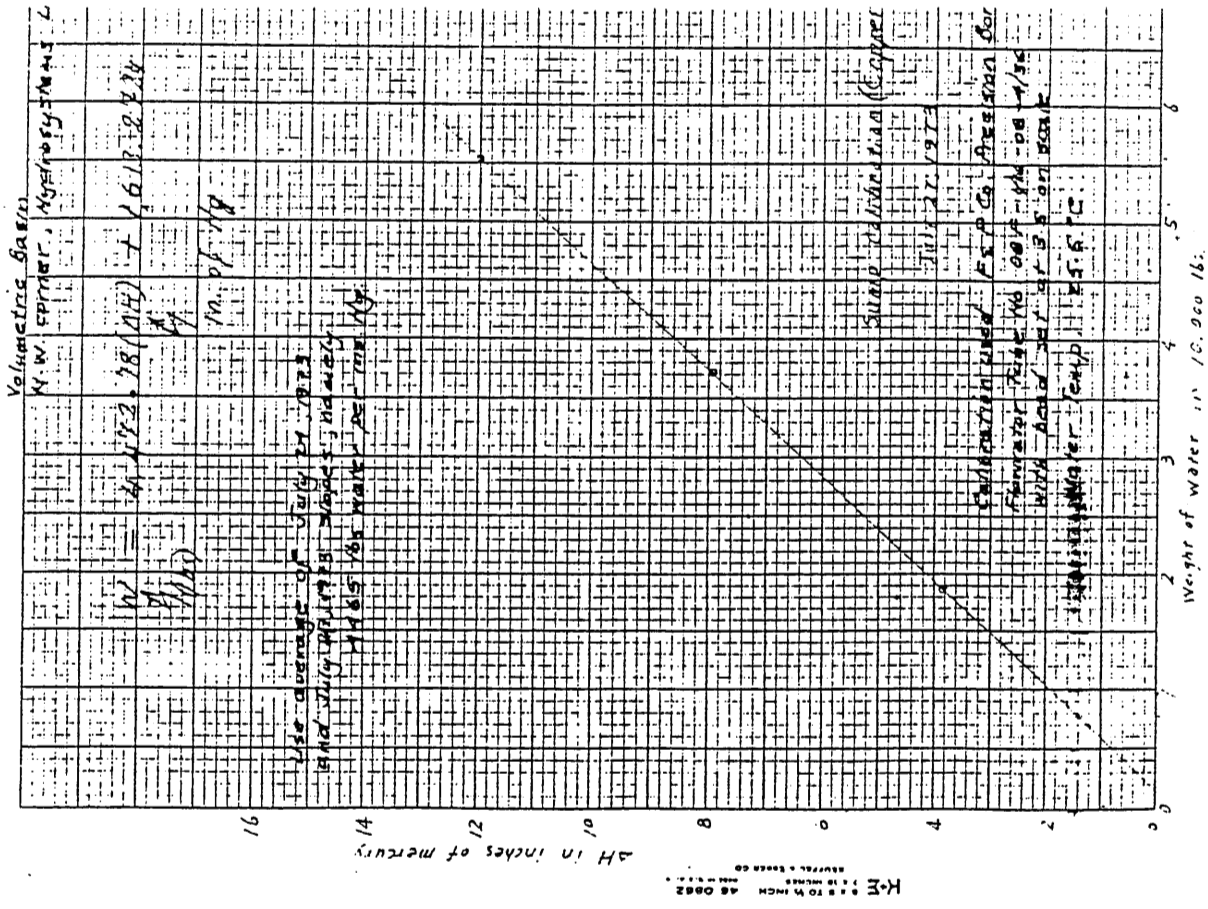

Figure 3.7 Calibration chart for the volumetric tank (after Maxwell, 1972)

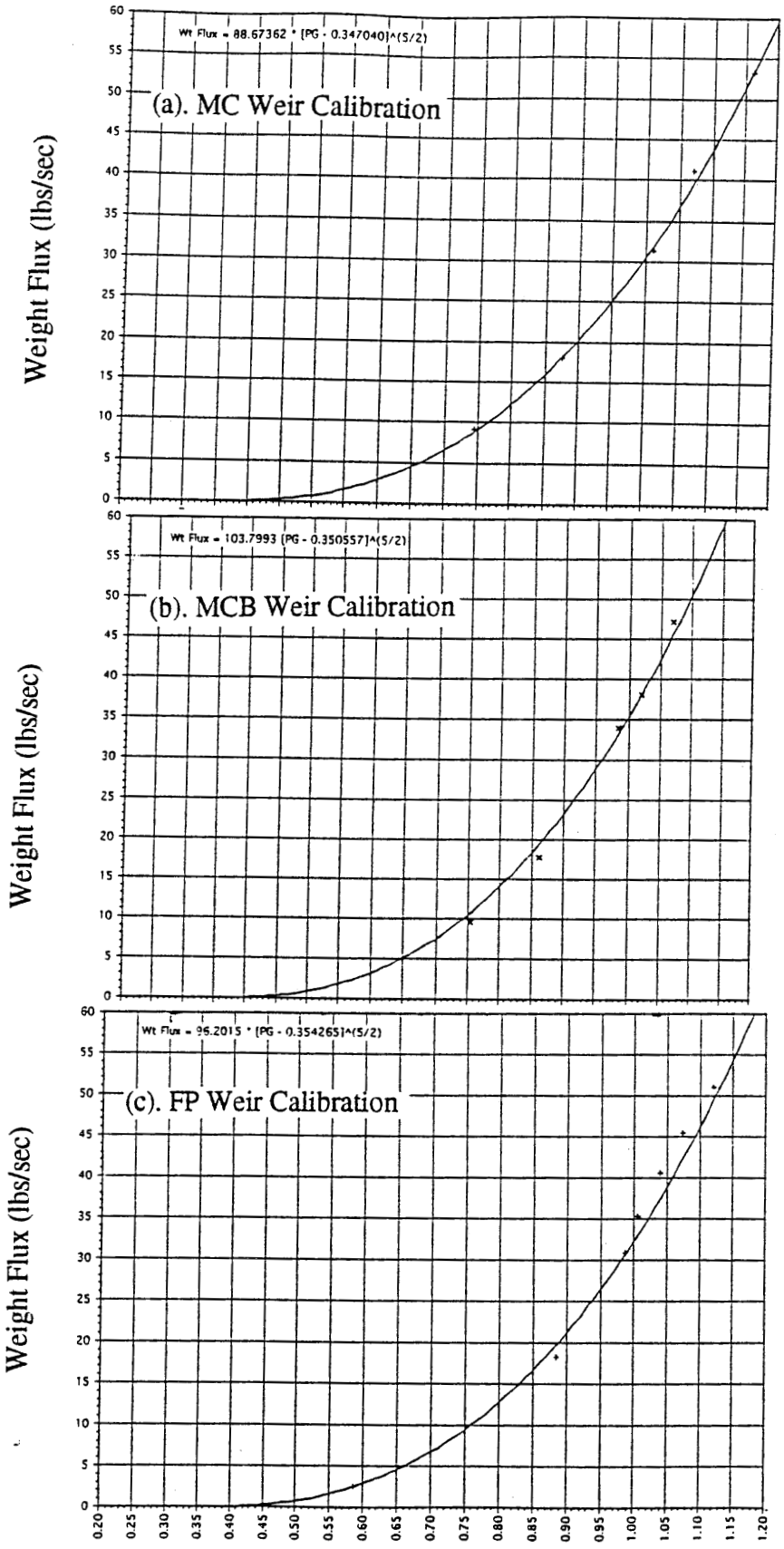

Figure 3.8 Calibration curves for three downstream weirs

3. Flows in each of the channel sections (MC, MCB, and FP) were determined by three sharp-crested triangular weirs at the downstream end of the end-tanks. All had the same design with a 30° opening, and were calibrated twice before their use in the tanks (see figures 3.8 a-c).
4. Water surface elevation, water depth, and cross-sectional geometry were measured with a Lory Type-A point gage mounted on a transverses carriage. The carriage was designed so that the gage could be moved across the channel on a transverses frame, and the whole carriage could slide on two rails on the top of the flume's two sidewalls. A tape readable to 0.2 cm (0.0066 feet) was mounted on the transverses frame. In the longitudinal direction, a tape readable to 1/8 inches (0.0104 feet) was mounted on top of the two sidewalls. The gage had a precision readable to 0.001 feet.
5. Water temperature was determined to the nearest 0.1° C.

One crucial piece of information determined during the test was water depth or slope of the water surface. This was measured using the point gage in the carriage that slide along the two rails on top of the flume's two sidewalls. The railings were assumed to be straight and parallel to the flume bed as well as the channel bed. Slight deflections would yield inaccurate results. To verify this assumption and to determine the true bed slope, level water tests were used. The procedures were to seal both ends of the channel and fill it with water. Time was allowed for the water to become still. The distance from the benchmark elevation, defined as the railing of the flume superstructure, to the water surface was measured at a large number of longitudinal locations using the point gage. The still water surface was to be horizontal and the railing's readings equal to the slope of the flume and the channel bed so that any minor deflections on the railings could be detected and corrections assigned. Because of the extreme importance of these correction values, multiple tests were conducted on different days and at different times to insure that other factors, such as the effect of temperatures on the metal flume superstructure, were not causing excessive error.

3.5. Experiment Procedures

Given the large channel dimensions, the experiments could be conducted with sufficient flow rates to remain in a relatively high Reynolds numbers range. The experiments were conducted under steady uniform flow conditions.

To insure that steady uniform flow was established, the following procedures were used.

1. A given flow rate was set.

2. Tailgates were kept in the fully open position. The inflow would first establish either an M1 or M2 (mostly M2) surface profile.
3. Water surface elevation and flow depth 65 feet upstream of the tailgate were measured with the Lory Type-A point gage. This point was far away from the influence of downstream gates. It was tested and verified that a constant depth would exist approximately 50 feet away from the tailgates after flow was established
4. The point gage was then moved downstream to a point approximately 15 feet upstream of the tailgates. The constant depth obtained from the upstream end was then set at this location by adjusting the tailgates. Because the dividers were transparent, it was able to check if water surface elevations in all three compartments were equal.
5. Once the downstream elevation was set, the upstream elevation was rechecked to insure it had not changed. The tailgates were used to make slight adjustments to the water surface if necessary.
6. Additional measurements were taken approximately 25 feet upstream of the tailgates to confirm the constant depth. Variations within 0.003 feet of the exact values were accepted due to the presence of variable roughness patches, small waves, and minor variations in the benchmark elevations for each longitudinal location.

Other measurements were taken after a steady uniform flow was achieved, including:

1. Water temperature for determining the density and viscosity of the fluid.
2. Flows over each component of the channel (i.e., MC, MCB, and FP).
3. Cross-sectional geometry using the point gage and the tape mounted on the transverse carriage to record the area and wetted perimeter.
4. Overall discharge of the experimental run.

All of the data were recorded on a standard project data sheet. Figure 3.9 is an example of one such sheet filled out during the experiment.

3.6. Raw Data Processing

A processing program was written in Microsoft Quick BASIC for Macintosh to process the experimental data for the project. The program took the following factors into consideration.

MANNING N FOR COMPOSITE / COMPOUND CHANNELS EXPERIMENTAL TRIALS

Filename: GGGGG 11 (A)

RAW DATA WORKSHEET SPRING 1995

Page 1/2

Date: 6-22-95 Time: 8:10 pm Temperature (°C): 24.7

Experiment Operators: Michael Turns of Valve: ~~5~~ 2 5

ROUGHNESS SEQUENCE

MC	MCB	FP3	FP2	FP1
G	G	G	G	G

(VIEW SEQUENCE LOOKING DOWNSTREAM)

TOTAL FLOW DEPTH (IN): _____

APPROX FP DEPTH (IN): _____

LONGITUDINAL WATER SURFACE MEASUREMENTS:

Longit Locn (ft-in)	53		22		34					
Low PG Reading (ft)	2.293				2.295					
High PG Reading (ft)	2.302		2.2975		2.307					
(A)	2.2975		Approx							

VELOCITY MEASUREMENTS: Longitudinal Location (ft-in): 42-3"

Transv Locn (cm)	6	12	18	6	12	18	26	6	12	18
Vert PG Reading (ft)	0.100	0.1	0.1	0.35	0.35	0.35	0.350	0.600	0.6	0.6
Left Pitot PG (ft)	0.973	0.974	0.967	0.948 0.950	0.907	0.893 0.904	0.913 0.921	0.909	0.888	0.875
Right Pitot PG (ft)	1.087	1.082 1.092	1.094	1.114 1.123	~~1.138~~ 1.152	1.161 1.168	1.148	1.151 1.157	1.170	1.184 1.192
Transv Locn (cm)	26	32	6	12	18	26	32	40	48	64
Vert PG Reading (ft)	0.6	0.6	0.85	0.85						
Left Pitot PG (ft)	0.881	0.903 0.912	0.896	0.884	0.868	0.875	0.857	0.899 0.908	0.918	0.924
Right Pitot PG (ft)	1.178 1.185	1.152	1.158 1.168	1.178	1.190	1.184	1.173	1.157	1.144	1.139

CROSS SECTION GEOMETRY MEASUREMENTS: Longitudinal Location (ft-in): _____ Reading Point: _____

Transv Locn (ft-in)			21.7	40.4	117.8					
PG Reading (ft)			1.364	2.028	Wall					

PIPE BEND MANOMETER MEASUREMENTS:

	Left (+)	Right (-)
Valve Closed (in)		
Valve Open (in)		

DOWNSTREAM WEIR MEASUREMENTS:

	MC	MCS	FP	
Low PG Reading (ft)	1.174	1.045	1.116	Overflowing Slightly
High PG Reading (ft)	1.205	1.060	~~1.135~~	1.135

WEIGHING TANK MEASUREMENTS:

	Left (+)	Right (-)
WT Start (in)	0.99	1.02
WT End (in)	4.61	4.68

Time (sec): 216.0

Figure 3.9 Example data sheet

3.6.1. Coordinate System

A left-hand Cartesian coordinate system was used. The positive coordinate of x pointed into the flow, y was vertical from the channel bed, and z was perpendicular to the x-y plane to the right when facing downstream. The coordinate system used in taking the raw data satisfied this requirement because the instrument cart slid parallel to the channel bed and the point gage projected perpendicularly from the cart.

3.6.2. Discharge

The program determined the total channel flow rate using the readings from the volumetric tank manometer. The calibration curve for the volumetric tank (figure 3.8) was digitized in the program. Using the changes in manometer readings, the time interval, and the temperature of the water, the flow rate in cfs was found by dividing the weight by the time and specific weight of the water. The specific weight of the water was taken from standard textbooks such as Rouse (1978) once water temperature was known. A gravitational constant of 32.174 feet per square second (ft/sec^2) was used to find the specific weight of water.

3.6.3. Cross-Sectional Area and Wetted Perimeter

The wetted perimeter and cross-sectional area for each run were measured from the luan board to the water surface. Strictly speaking, the area and wetted perimeter should be measured from some base reference point in the roughness material overlay (Yen and Overton, 1973). This reference point would need to be determined individually for each case, making it impractical for this experiment given the many combinations of roughness elements in MC, MCB, and FPs. A calculation showed that the error introduced was small and acceptable: the maximum roughness particle diameter was 0.0197 feet, the maximum error introduced with and without the roughness overlay for the wetted perimeter was 0.039 feet, with the maximum wetted perimeter of 4.164 feet (note that the sidewall was not roughened). For the submerged area, the maximum error was about 0.08 square feet (ft^2) with the maximum submerged area of 1.92 ft^2.

3.6.4. Reynolds and Froude Numbers

The Reynolds and Froude numbers were calculated for error analysis, which is discussed later. They were computed using the general formulas for open channel flow, i.e., using average velocity and the whole composite section. The Reynolds number was defined as $Re=VR/\nu$. Inserting the relations $Q=V/A$ and $R=A/P$, it can be simplified to $Re=Q/P\nu$. In the program, P was the entire wetted perimeter including the plastic

sidewalls; Q was the overall flow rate determined earlier; and ν, the kinematic viscosity, was interpolated from tables in Rouse (1978) relating water temperature to water viscosity. The Froude number was computed as $Fe=V/(gd)^{0.5}$. Researchers such as Blalock and Sturm (1981) have discussed modified methods for computing cross-sectional Reynolds and Froude numbers; however, because of the large amount of data produced in this experiment and our desire to compare these data with the data of other researchers, it was decided that the simplest methods should be employed.

3.6.5. Correction for the Plexiglas Wall

After the composite Manning n value was found based on all of the wetted perimeter, including the non-roughened Plexiglas walls, it was then corrected for the slight roughness of the walls using the procedure outlined in Vanoni (1975). Essentially, this procedure converted the determined roughness value for the entire section to a roughness value for the roughened bed material, using the areas of influence of each section and a correction based on the smooth pipe friction factor relationship. Researchers such as Knight and MacDonald (1979) have examined the use of this sidewall correction procedure and found it to be adequately accurate. The procedure is shown in the example that follows.

Wetted perimeter of roughened area only, WP (feet) = 4.1639
Wetted perimeter of non-roughened sidewalls, WWP (feet) = 5.1825
Area of flow, A (ft^2) = 1.3598
Bed slope, S = 0.00061729
Flow rate, Q (cfs) = 1.6013
Open channel flow Reynolds number = 0.27531E+05

Step 1: Find the overall n value using all of the channel walls:

$$Q=\frac{1.486}{n}\frac{A^{\frac{5}{3}}}{P^{\frac{2}{3}}}S^{\frac{1}{2}}$$

If A = 1.3598, Q = 1.6013, P = 5.1825, and S = .00062, then n = 0.0128.

Step 2: Convert this value to a friction factor. This can be done with the following equation (e.g., equation 4 in Yen, 1992a):

$$\sqrt{\frac{8}{f}} = \frac{1.486}{\sqrt{g}} \frac{R^{\frac{1}{6}}}{n}$$

Thus, f = 0.0301, which is the total f for the cross section.

Step 3: Find a friction factor for the smooth wall based on the smooth pipe relationship (Rouse, 1978):

$$f_{wall} = \left(\frac{1}{2\log(R_e\sqrt{f_{wall}}) - 0.80}\right)^2$$

where Re = 4×(0.2753E+05). By trial and error, we find f_{wall} = 0.0176.

Step 4: Using Equation 2.181 of Vanoni (1975), compute an adjusted friction factor:

$$f_b = \left(\frac{WWP}{WP} f\right) - \left(\frac{WWP - WP}{WP}\right) f_{wall}$$

where WWP = 5.1825 and WP = 4.1639. Thus, f_b = 0.0331.

Step 5: Convert back to a Manning n value by using the equation presented in Step 2. Thus, $n_{adjusted}$ = 0.0135. This value is slightly higher than the value computed without adjustment. Hence, the adjustment was done for all the tests. The processed data will be presented later.

The n value thus derived has a dimension of $L^{1/6}$ and the constant k_n has a dimension of $g^{1/2}$ (e.g., Yen 1992b). A dimensionless n, expressed as n_g, would be more appropriate and hence was derived as (Yen, 1992b):

$$n_g = n(g^{0.5}/kn)$$

The more traditional system where kn = 1.486 is used in this report to facilitate comparisons with data of other researchers.

3.7 Error Analysis

Besides the error discussed earlier in not considering roughness height when computing the wetted perimeter and submerged area, two other errors are discussed below.

3.7.1. Error in Determination of Steady Uniform Flow

Under controlled conditions, all measurements should be taken under steady uniform flows. Though the goal was to set the upstream and downstream water depths equal, measurement error made it possible that these values were not exactly equal.

One of the corrections made to the data was to correct for the slight variation of the benchmark elevation along the length of the flume. All of the water surface elevations were measured down from the railing superstructure of the flume. The level tests indicated that this superstructure had minor deflections in the surface and correction values had been determined. There were also several points along the rails where the deviation from perfectly straight was essentially zero and required no correction when conducting the measurement. Therefore these points were used repeatedly during the experiments to determine whether or not steady uniform flow had been achieved. Once steady uniform flow was achieved, additional points along the length of the flume were taken.

When processing the data, the program automatically made corrections to the water surface elevations based on the values determined through level tests. The overall average water surface elevation was then based on these corrected values. In this way, minor imperfections in the benchmark elevation were largely eliminated as a source of error in the experiments.

Occasionally, test results indicated that true steady uniform flow had not been established. Rather than eliminating this dataset, these data were kept for future analyses. In general, questionable data were plotted on the graphs of the experimental data, but not used in evaluating the fit of equations or in developing new equations. The tables in Appendix I give both the used data and the unused data.

3.7.2. Error Due to Reynolds Number Effects

Another possible source of error in the experiment was in using too low Reynolds numbers. Strictly speaking, the Manning equation is applicable only to fully developed turbulent flow, generally at a Reynolds number above 10^5, beyond the point at which friction factor curves on a typical Moody-type diagram have flattened out. Practically speaking, a Reynolds number of 10^5 is difficult to establish in a laboratory setting. Though the availability of an adequate water supply to achieve this Reynolds number was not a

problem, maintaining a wave-free water surface proved difficult. A number of wave damping devices were tried without success. Only additional length of channel proved adequate in reducing the surface waves. The decision was made to use a flow rate high enough to reach that range of the Moody diagram where the friction factor plots have substantially flattened out, while low enough that surface waves were not a problem.

To this end, Moody-type plots of the friction factor diagrams for each material were developed (figures 3.10a, b, and c). As an approximation, the ks value for each material was based on the D_{50} particle diameter, using the form of the Colebrook-White type equation for wide open channels attributed to Rouse by Yen (1992a). This equation, while perhaps not strictly applicable to a composite channel, does give a good estimation of the range of applicable Reynolds number values for a relatively constant friction factor value. Here, it should be mentioned that the graphs are presented with the Manning n value, rather than the friction factor, on the vertical axis, and the standard conversion from the Darcy-Weisbach friction factor to Manning n value published in Yen (1992a) is used. Readers will note that several of the friction factor lines on the graph cross each other. This is due to the form of the equation used.

For the gravel material shown in figure 3.10a, the effect of the Reynolds number on the Manning n value essentially ceases above $Re=2 \times 10^4$. When the Reynolds number increases beyond this point, the Manning n value varies less than 0.0001. No variation of the Manning n value for any combination of ks/R is noted above $Re=7 \times 10^4$. For the gravel material, the cases where the Manning n value is most likely to vary with Reynolds number are those with low ks/R ratios and $Re<2 \times 10^4$.

For the black magnum material in Figure 3.10b, the effect of the Reynolds number on the Manning n value is more pronounced, with an error of 0.0002 until the Reynolds number exceeds 4×10^4. At $Re = 2 \times 10^4$, we would incur an error of no more than 0.0004 with increasing Reynolds number. Here, the most critical cases are those with low ks/R ratios and Reynolds numbers less than 4×10^4. Fortunately, this combination of factors is less likely, as the highest hydraulic radius values tend to coincide with the highest Reynolds number values for this particular channel.

The bed material most likely to produce problems related to Reynolds number effects is sand, shown in figure 3.10c. With sand, errors of 0.0006 are incurred when 2×10^4 is assumed to be the lower cutoff for acceptable tests. It is not until we attain $Re = 7 \times 10^4$ that the error diminishes to less than 0.0002.

One advantage, however, is the fact that the greatest errors in the Manning n value occur at low ks/R ratios and $Re = 2 \times 10^4$. Again, this combination of factors is very rare in this particular channel, since the highest values of hydraulic radius tend to coincide with the highest Reynolds numbers.

From the listings of the experimental data in Appendix I, the reader will note that most of the tests have Reynolds numbers in the range of 2×10^4 to 5×10^4. The maximum variation in Manning n value with Reynolds number over this range is found for the sand

bed roughness material, with an error of about 0.0003. Thus, we can safely say that, except in a very few cases, we incur a maximum error of 0.0003 in the Manning n value due to variations in the Reynolds number.

Considering all of the error factors mentioned in this section to be additive, we might expect a maximum error of about ±0.001 in the composite Manning n values found in this report. This maximum error would occur only in a very few tests, and would require the combination of a high hydraulic radius, a low Reynolds number, and a significant backwater condition. Were any of these three conditions to be removed, the error would drop to a maximum of about ±0.0003. Considering the uncertainties found in choosing a base n value in a design situation, this error in composite n value is quite acceptable.

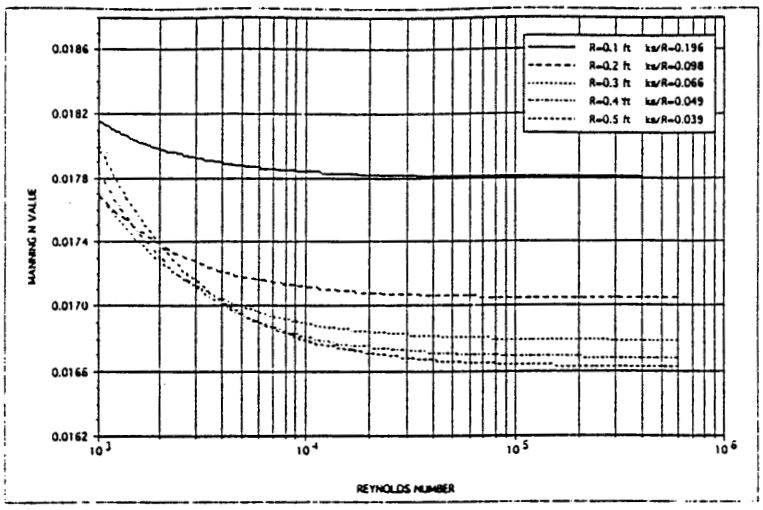

Figure 3.10a Moody-type diagram for gravel material (ks=0.01968 ft)

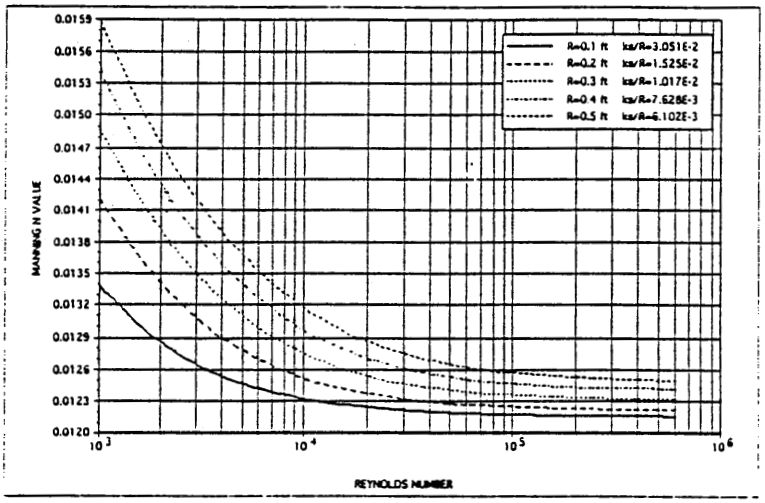

Figure 3.10b Moody-type diagram for black magnum material (ks=3.051E-03 ft)

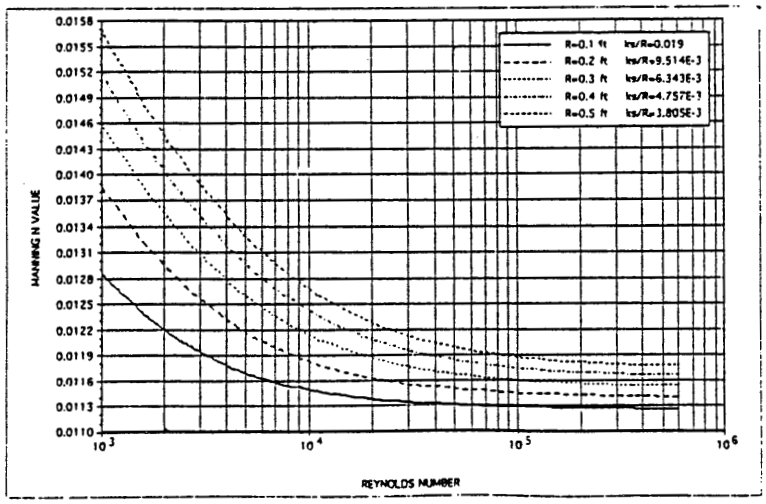

Figure 3.10c Moody-type diagram for sand material (ks=1.902E-03 ft)

4. EXPERIMENTAL RESULTS

The overall n value for each test run was compared in two ways: first, with respect to equations 2.1 to 2.10, and second, with respect to other datasets taken from the present study. These comparisons allowed us to determine which equation(s) best predicted the variations of n over channel depth, and the effects of varying the roughness patterns in the channel.

4.1. Data Presentation Conventions

A uniform alphanumeric coding system is used here to identify the roughness combination in each experimental run. The code consists of five letters, representing the roughness arrangement for each experimental series, and one number, representing each run in the series (at different discharges). The roughness arrangement is read as if looking downstream at the channel, with the first letter indicating the roughness element at the main channel and so on. For example, BBBGG4 indicates the following roughness pattern (the base n value for each roughness is given in parentheses):

Main Channel: black magnum (n=0.0130)
Main Channel Border: black magnum (n=0.0130)
Floodplain 3 (closest to main channel): black magnum (n=0.0130)
Floodplain 2 (center of floodplain): gravel (n=0.0182)
Floodplain 1 (farthest from main channel): gravel (n=0.0182)

The number following the five letters in the code indicates that this is run number 4 of the series. This number is merely for processing purposes. All the actual data are given in Appendix I.

In this chapter each roughness pattern run is presented in a set of three figures, along with experimental data. In the first two figures, part a plots results by equations 2.1 to 2.5, while part b shows the results by equations 2.6 to 2.10. The first figure of each set shows the results of the vertical subdivision method, and the second figure those for the bisectional subdivision method.

In both the vertical and bisection subdivision cases, those portions of the subdivision lines not touching solid boundaries were not considered in the calculation of the wetted perimeter. Moreover, the Plexiglas centerline and plastic sidewall were not considered in wetted perimeter calculations because of the wall correction explained earlier. Figure 4.1 shows the definition of vertical subdivisions in this report, while figure 4.2 shows the definition of bisectional subdivision.

The third figure for each run plots the flow ratio in each of the major subdivisions. Flows in the main channel (MC), main channel border (MCB), and the sum of three

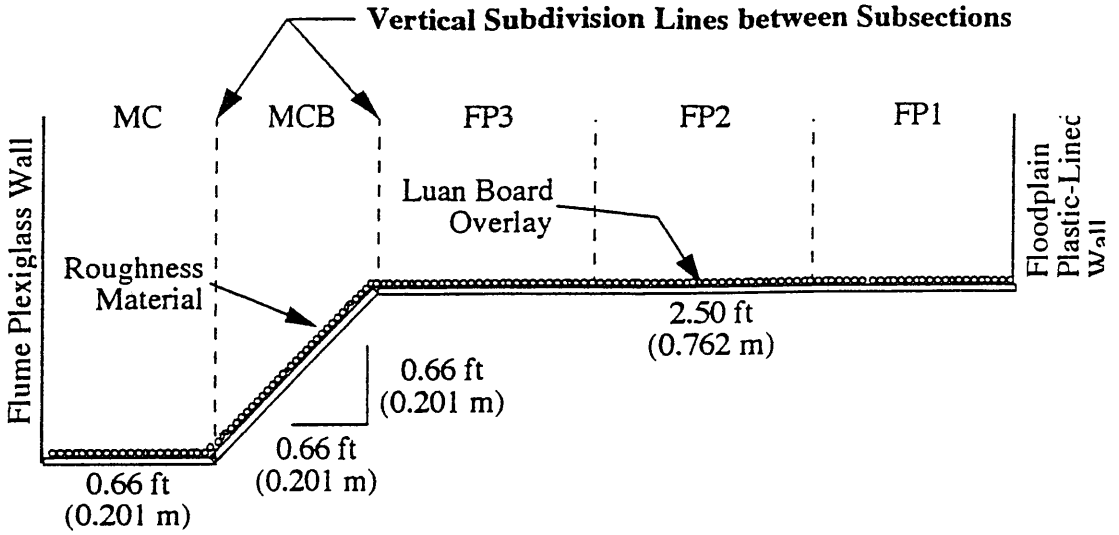

Dimensions are exterior dimensions. Area and Wetted Perimeter Based on interior dimensions measured at luan board surface. Flow direction is into page.

Figure 4.1 Definition of vertical subdivisions used in this report

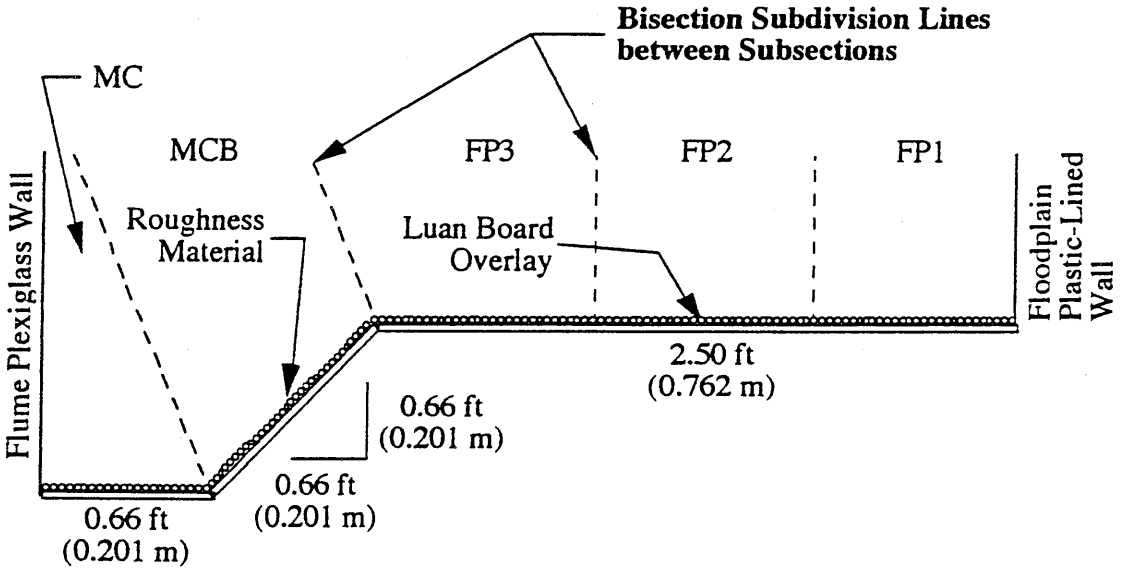

Dimensions are exterior dimensions. Area and Wetted Perimeter Based on interior dimensions measured at luan board surface. Flow direction is into page.

Figure 4.2 Definition of bisectional subdivisions used in this report

floodplain segments, FP3, FP2, and FP1, were measured using the triangular weirs discussed earlier. The measured flow rates were checked to be sure they totaled the measured overall flow rate, and minor corrections were made to the weir flow rates where necessary. The percentage of flow to the total flow found in each subsection was then computed.

In comparisons of experimental data and existing equations, the experimental data are presented as " Data Used" and " Data Not Used". The former includes all data judged to be of good quality based on the absence of backwater or low Reynolds number effects. The later includes all of the data judged to be affected by either or both of these effects. Only the data from the " Used" category were subsequently used in the analyses in this report. However, the " Data Not Used" were sufficient to demonstrate trends in many instances. They also can be used to demonstrate the effects of backwater and low Reynolds numbers. The terms " Data Not Used" and " Unused Data" are interchangeable throughout this report. All of the data are listed in Appendix I.

In all graphic presentations, scale and ranges are kept the same so that comparisons can be made easily. From this point on, the overall n values derived from experiments are denoted as n_o, and those computed from equations 2.1 to 2.10 are denoted as n_c.

4.2. Overall n Value under Uniform Roughness

When roughness is kept uniform throughout a cross section, the effect of geometry on the n versus depth curve can be studied. This study includes two different roughness values, the BBBBB and GGGGG data series. Quite a bit of data on compound channels of a single roughness exist in the literature. Chapter 5 reviews data from other researchers that are useful in this regard.

4.2.1. *GGGGG Data Series*

The base n value for gravel is 0.0182. Thirteen tests numbered GGGGG1 to GGGGG13 were conducted in this series. Four of the tests were taken at depths below bankfull stage, while the remaining tests were taken with the floodplain submerged. Twelve of the 13 tests taken were used in further analysis. The data in this series are considered to be of very good quality.

The general trend in n_o is shown in figure 4.3. In the depth ranges below bankfull, n_o tended to rise from base value to approximately 0.0186 and stayed about constant until bankfull stage (an approximately 4% increase from the base n value). Then n_o decreased to its lowest value at depths slightly above bankfull stage, and gradually increased toward the base n value as the y/D ratio increased (y is the total depth and D is the bankfull

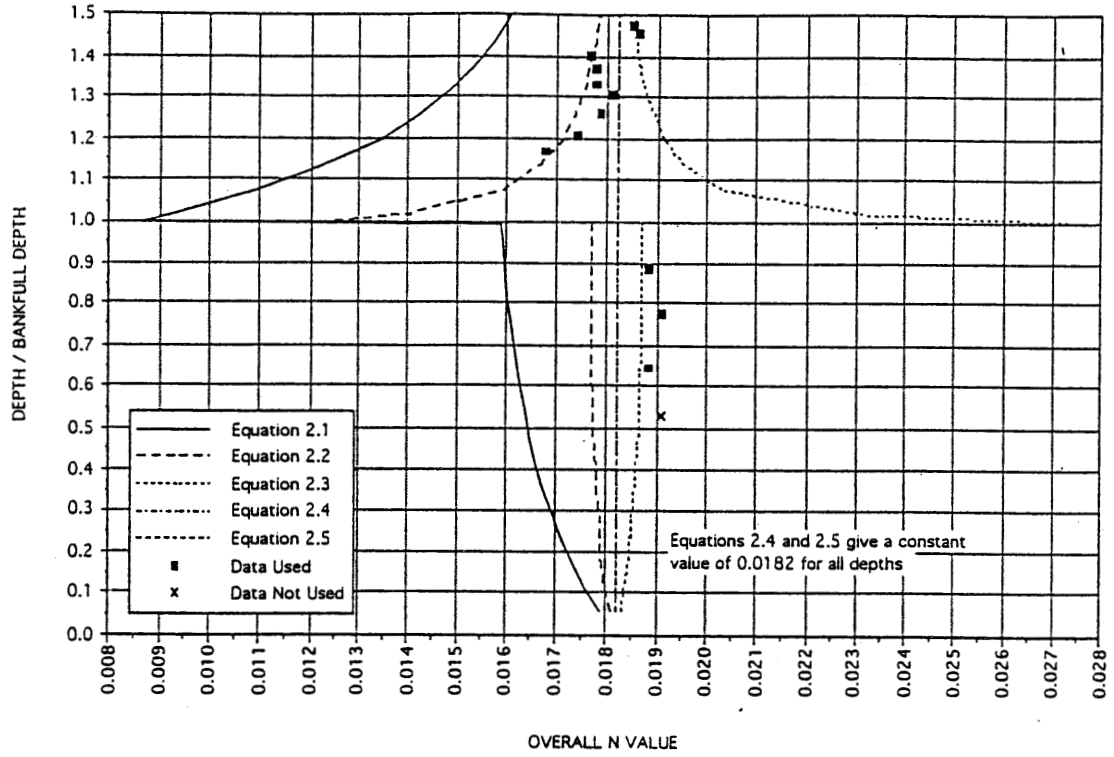

Figure 4.3a Experimental data versus equations 2.1 to 2.5 (vertical subdivisions) for GGGGG data series

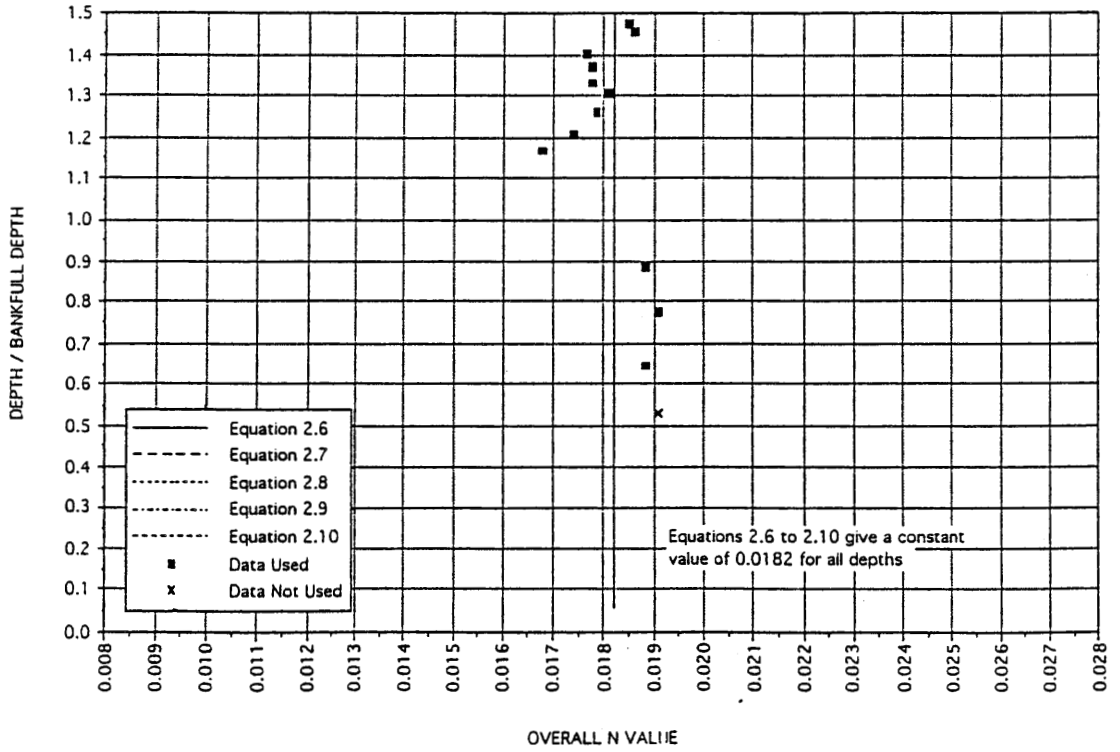

Figure 4.3b Experimental data versus equations 2.6 to 2.10 (vertical subdivisions) for GGGGG data series

depth). Although runs at depths just above bankfull stage were difficult to conduct, the trend is rather clear. As y/D increased, some scatters in data appeared around a depth of 1.35 times bankfull stage, and the final n_o value reached around 0.0185 after a y/D ratio of 1.5. The magnitude did not exceed the base n value by much, but it recessed rather largely at just above bankfull stage.

Vertical Division Method. Figures 4.3a and 4.3b compare the experimental data and the n_c values predicted by equations 2.1 to 2.5 and 2.6 to 2.10 using vertical division lines. Below bankfull stage, equation 2.3 predicted the trend correctly, but with lower magnitudes. Equations 2.1 and 2.2 predicted opposite trends at below bankfull stages, while all other equations predicted a constant n_c value.

The following observations can be made for depths below bankfull stage:

- n_o apparently increased with depth in the simple trapezoidal channel of homogeneous roughness.
- Equations 2.1, 2.2, and 2.3 employ hydraulic radius and area, hence they could demonstrate changes in n_c over depth. For the present test, only equation 2.3 predicted the correct pattern of n_o versus depth.
- Both equations 2.1 and 2.2 predicted decreasing n_c values over depth. The magnitudes of decreases predicted by equation 2.1 were much larger than those predicted by equation 2.2.
- All other equations using either wetted perimeter or submerged areas predicted constant n_c values over depth. This constant n was equal to the base n value.
- Equation 2.3 predicted a slight increase in n_c with increasing depth, leveling off to a value of about 0.0186, or about 2.2% higher than the gravel's base n value of 0.0182.

The following observations can be made for depths above bankfull stage:

- The basic trend in the data was similar to the shape predicted by equations 2.1 and 2.2. Equation 2.2 matched the data better. However, neither of the two equations predicted the variation in the experimental data, in particular for y/D greater than approximately 1.2.
- Equation 2.3 predicts the overall trend incorrectly for above bankfull depths. However, when the y/D ratio exceeded 1.4, it matches the experimental data better than other equations.
- All other equations were unable to predict the variations in n_o over depth.
- The maximum reduction in n predicted by equation 2.1 was approximately 53% and by equation 2.2 about 32% (as compared to the base n value). The maximum increase predicted by equation 2.3 was approximately 49%.

Bisectional Division Method. Results from the bisectional method are presented in figures 4.4a and b. The following observations can be made for below bankfull stages:

- Use of the bisectional method did not change the predictions of equations 2.4 to 2.10. They still predicted the same constant n_c value as for the vertical subdivision method.
- The discrepancies among equations 2.1, 2.2, and 2.3 were reduced. However, the magnitudes predicted by equation 2.3 were also reduced, which increased the error. The trends predicted by these three equations remained the same.

For depths above bankfull stage, the following conclusions can be drawn:

- Equation 2.2 matched the experimental data slightly better for the y/D ratios between 1.2 and 1.4 than the vertical subdivision method.
- Even though equation 2.3 predicted the wrong pattern for above bankfull stages, it gave proper n_o values for y/D ratios greater than 1.5.

Again, no one equation satisfactorily predicted the variations in n_o presented by the experimental data.

Analysis. Equations 2.1, 2.2, and 2.3, which are capable of demonstrating that n varies with depth, employ the hydraulic radius in their computations. As depth passes the bankfull stage, the wetted perimeter increases quickly, causing a reduction in the hydraulic radius in the single channel approach. Assuming a constant n value, this shift incorrectly causes a decrease in the computed discharge. Some investigators contend that this is because the hydraulic radius does not properly represent the effect of channel cross-sectional shape on discharge in such cases (e.g., James and Brown, 1977). Researchers such as Yen and Overton (1973) and James and Brown (1977) also suggest that the main channel and floodplains be treated separately. By doing this, however, one needs to account for the overall energy losses induced by the momentum transfer at the interface. Many researchers have contributed to this area, some whose work was introduced earlier.

Using the n versus depth relationship apparently can provide another way to compute discharge using the cross-sectional approach, which may be simpler than the subarea computations. Since the reduction in hydraulic radius near bankfull stage is suspected to be the main cause of the reduction in discharge, the hydraulic radius versus depth relationship for the current experimental channel was examined as shown in figure 4.5. Note that the hydraulic radius versus depth curve remained the same in all of the following experiments, even though the roughness elements were different.

Comparing the relationship between the hydraulic radius and depth as shown in figure 4.5 and illustrated by the n_c curves predicted by equations 2.1, 2.2, and 2.3, leads to the following observations:

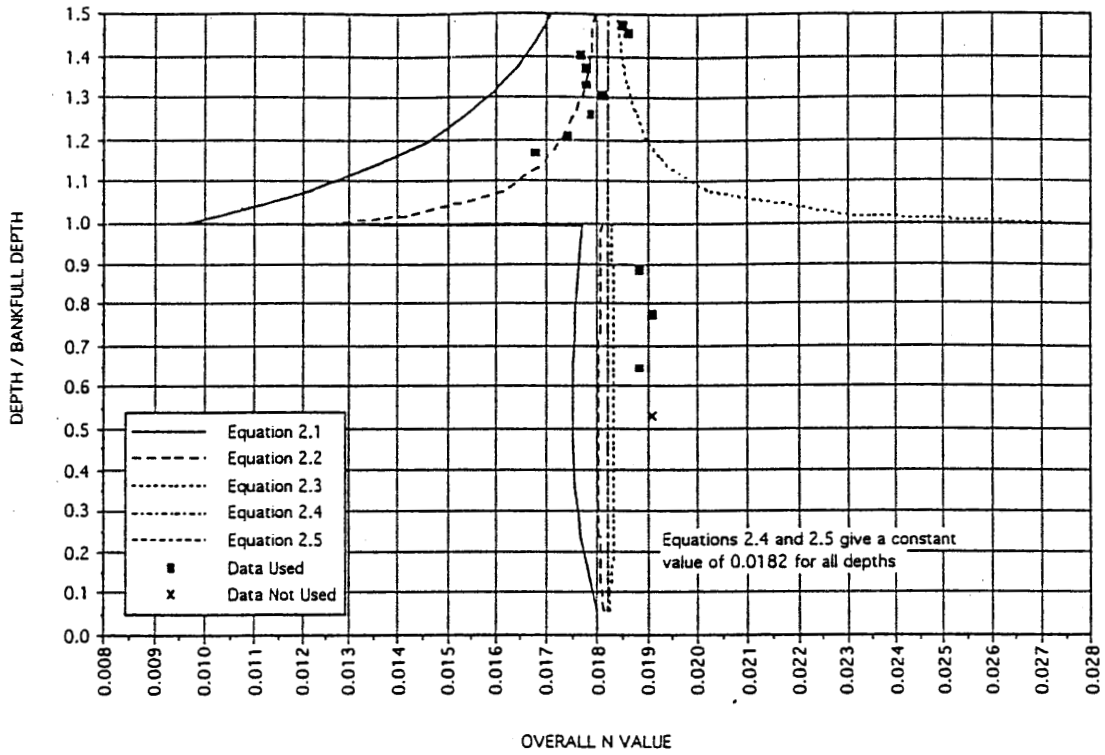

Figure 4.4a **Experimental data versus equations 2.1 to 2.5 (bisectional subdivisions) for GGGGG data series**

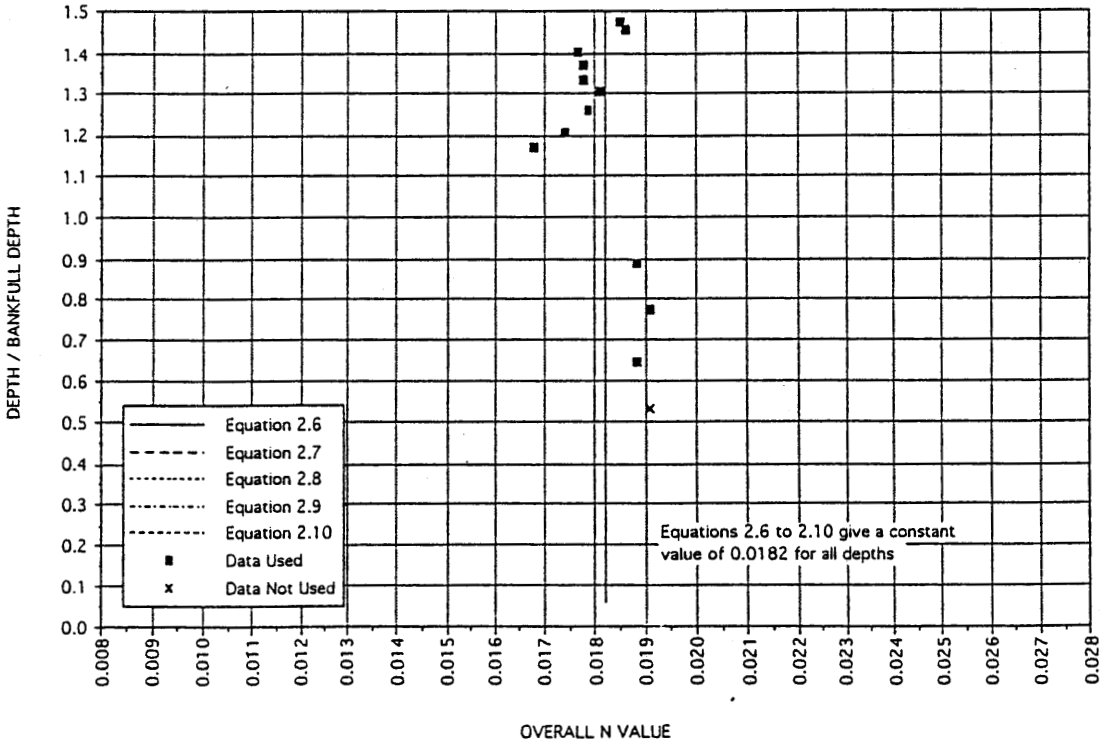

Figure 4.4b **Experimental data versus equations 2.6 to 2.10 (bisectional subdivisions) for GGGGG data series**

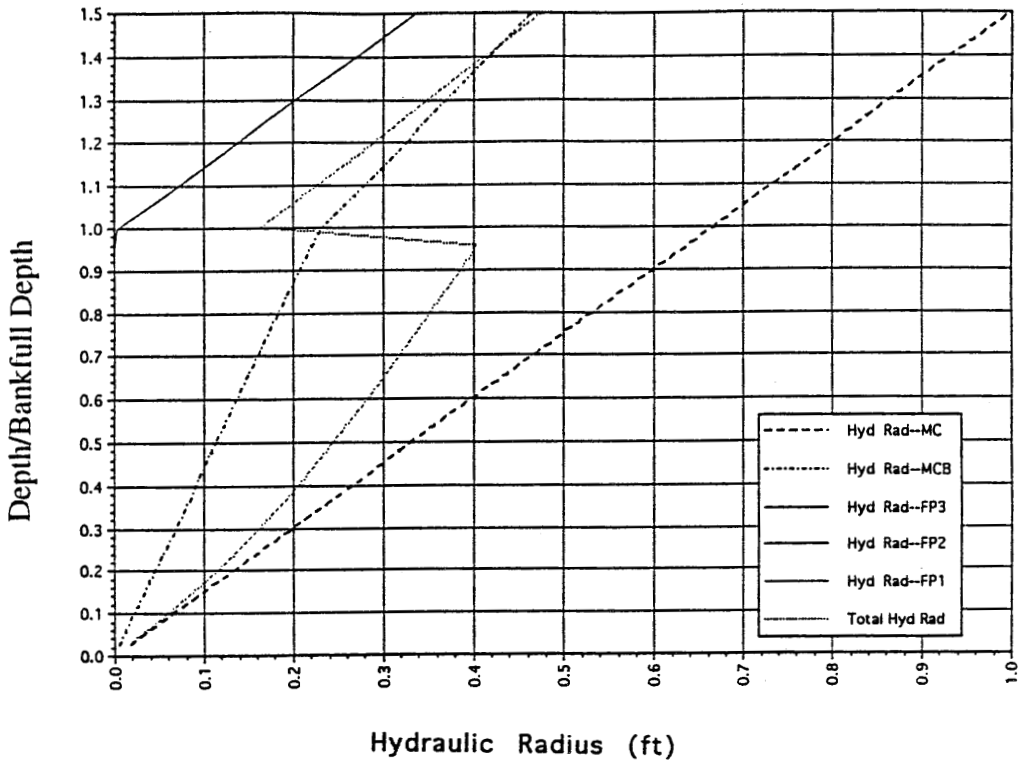

Figure 4.5 Hydraulic radius in subsections versus dimensionless depth

- Below bankfull stage, the hydraulic radius increased from 0 to approximately 0.42 (or a constant for other cases) near bankfull stage. The trend was similar to n_o for the homogeneous roughness channel runs.
- Above bankfull stage, the hydraulic radius decreased to 0.16 (approximately 62% reduction), and regained the before-bankfull value at a y/D ratio of 1.4. After that depth, n_o increased as y/D increased, while n_o approached an asymptotic value as y/D>1.5.

Clearly, although this pattern was very similar to the predictions of equations 2.1 and 2.2, predicted n_c was different. The maximum reduction by equation 2.1 was approximately 53%, and by equation 2.2 approximately 32% at just above bankfull stage.

Figure 4.6 shows the ratio of flow in each of the major channel subdivisions. Remember that the experiment used vertical dividers to separate flows in the three major channel components. Below bankfull stage, the ratio of flow in the MC decreased linearly, while the ratio of flow in the MCB increased linearly. Apparently there was a break in slope for MC and MCB at bankfull depth. Above bankfull stage, the MC curve decreased much faster at a rate similar to the increases in FP, while MCB changed much less rapidly in comparison. The distribution of discharge in each component was directly related to the contribution to the overall n value.

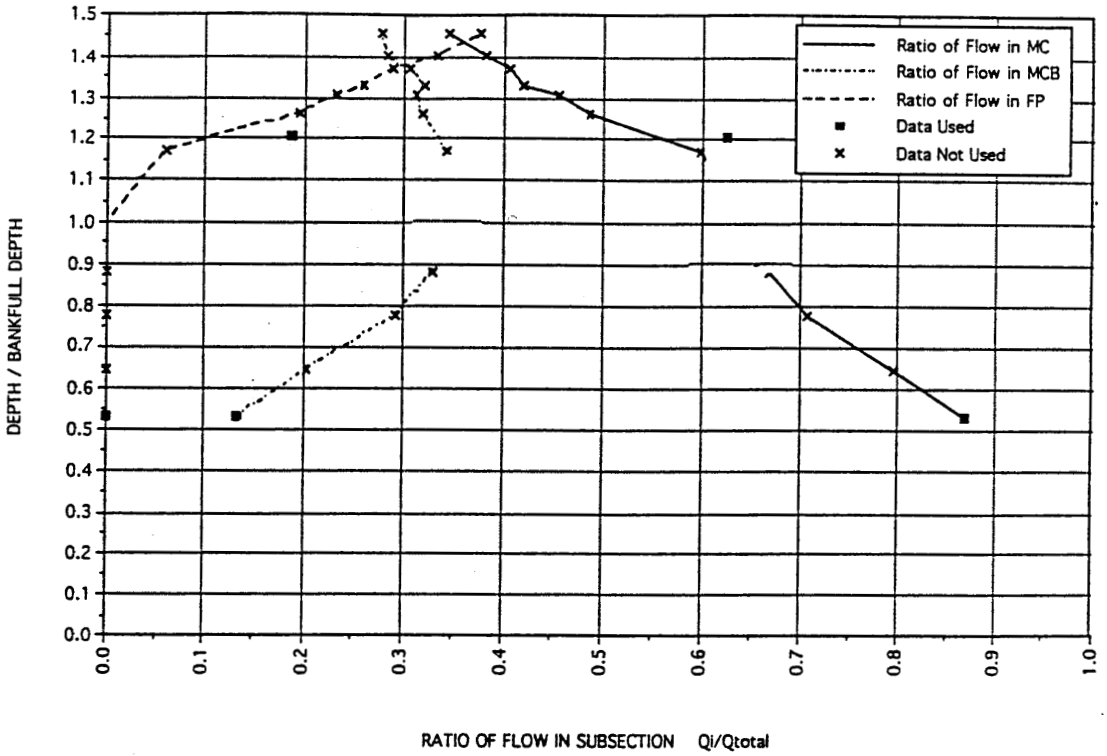

Figure 4.6 Division of flow among subsections for GGGGG data series

To determine the importance of the area and the wetted perimeter for each subsection in the distribution of flow, two additional figures are provided. Figure 4.7 shows the ratio of the area within each subarea to the total area of the channel. Figure 4.8 shows the ratio of wetted perimeters within the various major subareas to the total wetted perimeter. There is a numerical similarity between the ratio of flow area in a subsection and the ratio of flow. Figures 4.6 and 4.8, however, demonstrate that the rate of increase or decrease in the ratio of flow in a subsection is much more closely tied to the ratios of the wetted perimeters. The slope of the line showing the ratio of the wetted perimeter for a given subsection and the slope of the line showing the measured ratio of flow for a subsection are nearly identical. It appears that the area of a subsection does influence how much flow is found in that subsection, but that the rate of increase of the wetted perimeter determines the rate of increase in the flow rate. This is worth noting, especially in examining cases of varying roughness along the wetted perimeter.

Above bankfull stage, however, the ratio of flow area seems to play a more dominant role in determining the rate of increase of flow rate in a subsection. Figures 4.6 and 4.8 show that the slope of the area ratio line and the slope of the measured flow rate ratio are nearly identical above the bankfull stage. This may in part be due to the fact that

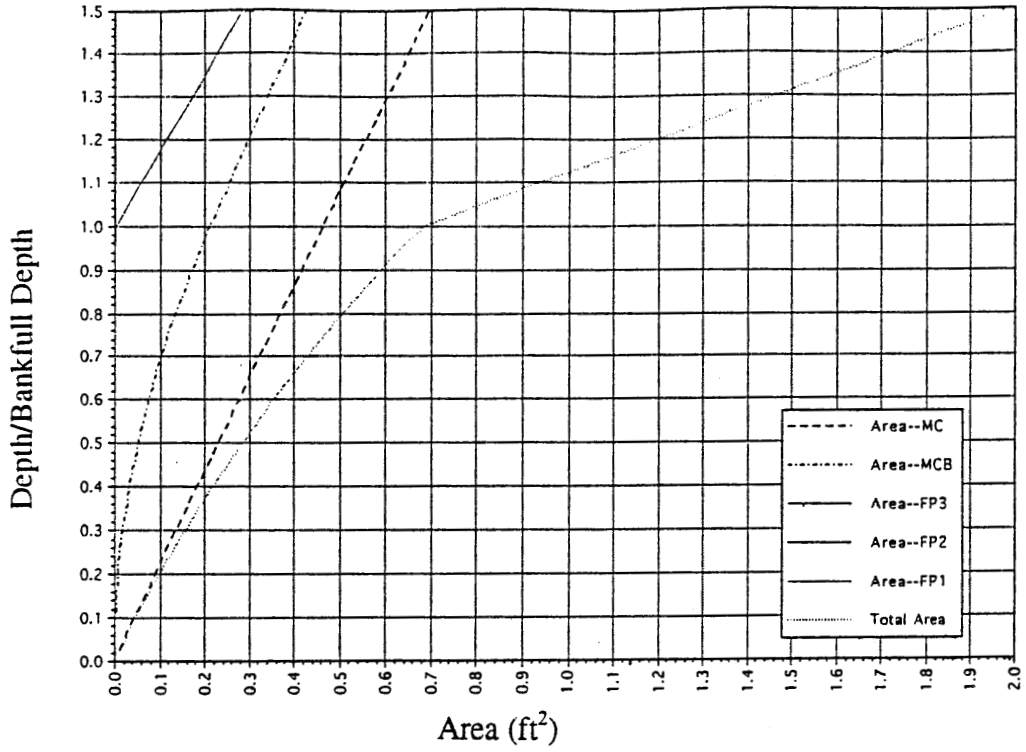

Figure 4.7 **Ratio of areas in subsections to overall area versus dimensionless depth**

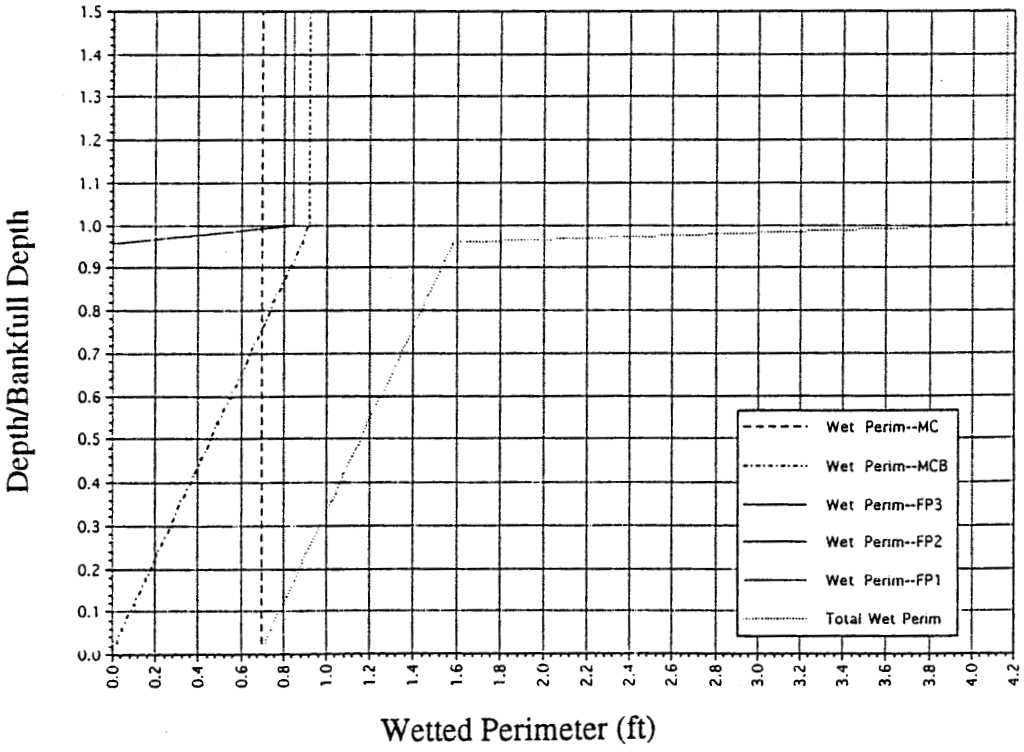

Figure 4.8 **Ratio of wetted perimeters in subsections to overall wetted perimeter versus dimensionless depth**

the ratios of wetted perimeters are constant above bankfull stage due to the wall correction.

Overall, the data from the GGGGG runs indicate the following:

- Equations 2.4 to 2.10 did not reflect the trend of n_o shown in the uniform roughness data. The discrepancies are most obvious above the bankfull depth.
- Equations 2.1 and 2.2 best mirrored the trend of the experimental data in the above bankfull range. The n_o value immediately above bankfull was not derived from the experiment. However at higher depths, equation 2.2 was more accurate in predicting shape and numerical values.
- Equation 2.3, of all other equations, was most accurate in determining n_o below bankfull depths.
- The n_o versus depth curve was similar to the change in the hydraulic radius curve, but did not follow it exactly.
- The rate of increase of the flow ratio in a given subsection was tied most closely to the ratio of the wetted perimeter at below bankfull stages, and to the ratio of areas at the above bankfull stages.

4.2.2. *BBBBB Data Series*

This series included 16 tests (BBBBB2 to BBBBB17). Seven of the tests were conducted at depths below bankfull stage and the remaining tests were conducted above bankfull stage. Of the tests conducted, six are considered to be of high quality.

The experimental results shown in figure 4.9 demonstrate that the n_o versus depth relationship is similar to that of the GGGGG data series but the magnitudes are different. The base n value for black magnum is 0.0130. Although only one dataset was useful in the range of depths below bankfull stage, it can be inferred that the n_o rose from the base value very close to the bed to a constant value near bankfull stage. This constant (around 0.0135) can be described as a percentage of increase from the base n, which for this case was approximately 4%. This increase is very similar to the GGGGG series.

Above bankfull stage, n_o decreased at just above bankfull, then increased as discharge on the floodplain increased. It reached the base value at y/D around 1.2, and reached the maximum value of .0137 at y/D around 1.4, before decreasing somewhat afterward.

Vertical Division Method. Following are observations for depths below bankfull stage:

- Equation 2.3 was the only equation to predict the correct pattern.
- The n_c value predicted by equation 2.3 was farther from experimental n_o than it was in the gravel element tests (figure 4.3a).
- The n_c value predicted by equation 2.3 was approximately 3% higher than the base n value.

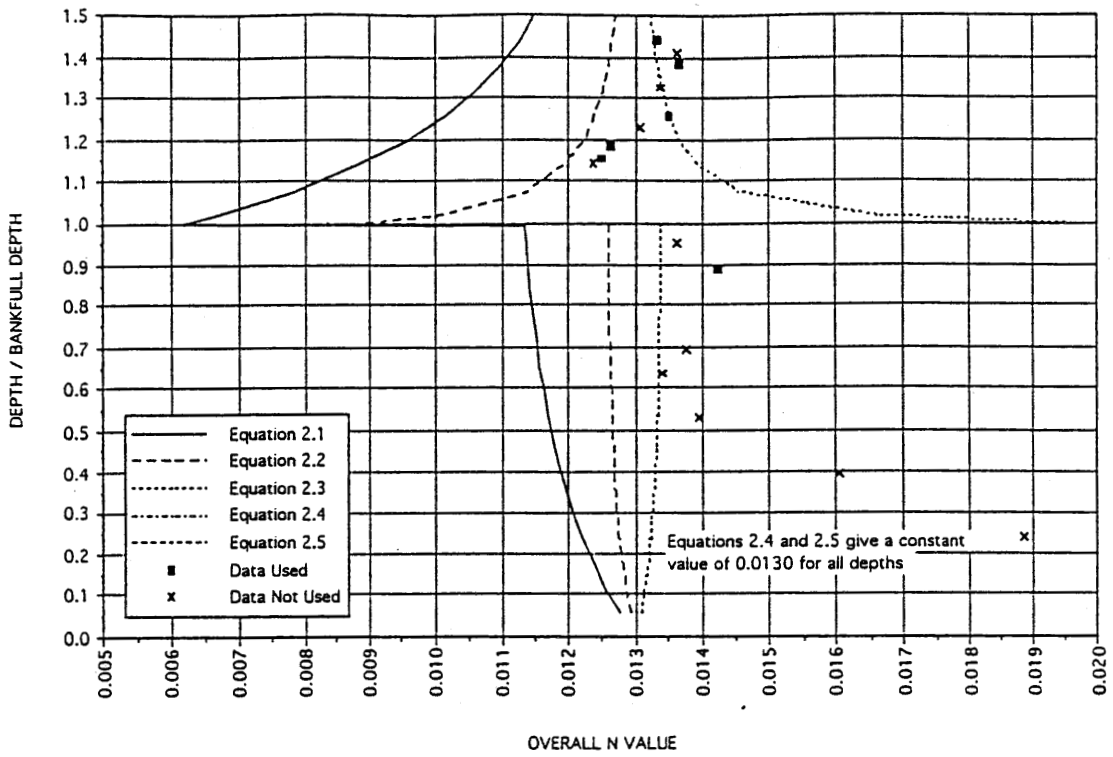

Figure 4.9a **Experimental data versus equations 2.1 to 2.5 (vertical subdivisions) for BBBBB data series**

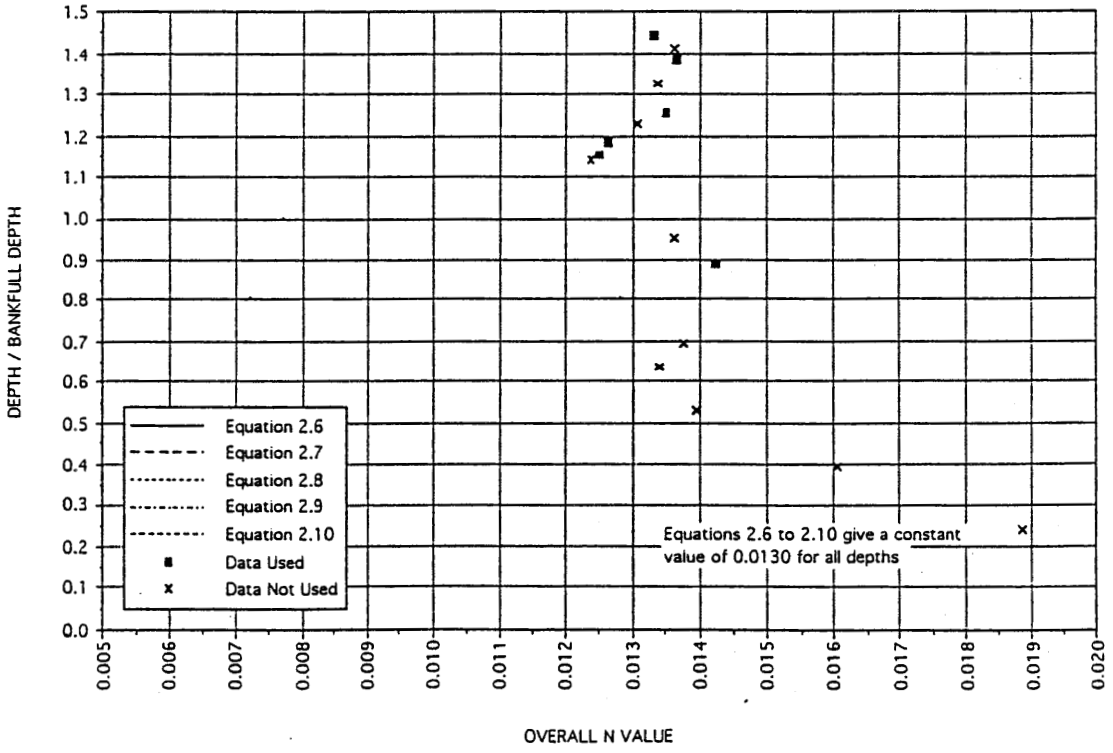

Figure 4.9b **Experimental data versus equations 2.6 to 2.10 (vertical subdivisions) for BBBBB data series**

Following are some observations for depths above bankfull stage:

- Equations 2.1 and 2.2, though correct in predicting the pattern, predicted n values that were much lower than the experimental n_o values.
- The maximum reduction in n_c predicted by equation 2.1 was approximately 52% and by equation 2.2 approximately 31%. On the other hand, the maximum increase predicted by equation 2.3 was approximately 50%. These numbers are similar to those obtained in the GGGGG series. (Flow patterns for the BBBBB and GGGGG series were different.) The similarity in such ratios indicates that these equations may merely reflect the composite roughness.
- Equations 2.2, and 2.3 showed the tendency to approach an asymptotic n_c after y/D > 1.5, with a magnitude closer to that of the base n value. This tendency existed also for the GGGGG series. However, it probably would take larger y/D values because of higher roughness.
- Again, equations 2.4 to 2.10 predicted constant n values equal to the base n value.

Bisectional Division Method. Figures 4.10a and b present the prediction of the equations using the bisectional method, which reduced the discrepancies among equations but also increased the prediction errors in equation 2.3 for depths below bankfull stage. Other observations were similar to those for the GGGGG series.

Flow Distribution: Figure 4.11 shows the ratio of flow in each of the subsections. Comparisons between figures 4.11 and 4.6 show that MCB contained more flow at the same y/D in the BBBBB than in the GGGGG series. At depths above the bankfull stage, especially for y/D > 1.2, flow in the MC was greater in the BBBBB than in the GGGGG series. The increases of flows in the MC were compensated for by reduction of flow in the FPs after y/D > 1.2 and < 1.4, within which range the flow ratio in the MCB did not vary much between the two series. After y/D > 1.4, however, the flow increases in the MC were compensated for solely by the MCB.

4.3. Effect of Changing Floodplain Roughness on Overall n

One of the purposes of this experiment was to quantify the effects of variation in roughness in the floodplain on the n_o value. Unlike studies of the effects of uniform roughness and geometry on the n_o value, sufficient data are not available in the literature to adequately analyze this aspect of channel flow. Thus, this part of the experiment was more heavily emphasized: more datasets were taken and analyzed. This section describes tests on BBSSS, BBSSG, BBSGG, and BBGGG series data, which were conducted under the same slope as that of BBBBB. Note that the base n values for sand, black magnum, and gravel were .0120, 0.0130, and 0.0182, respectively. Incorporating results from the

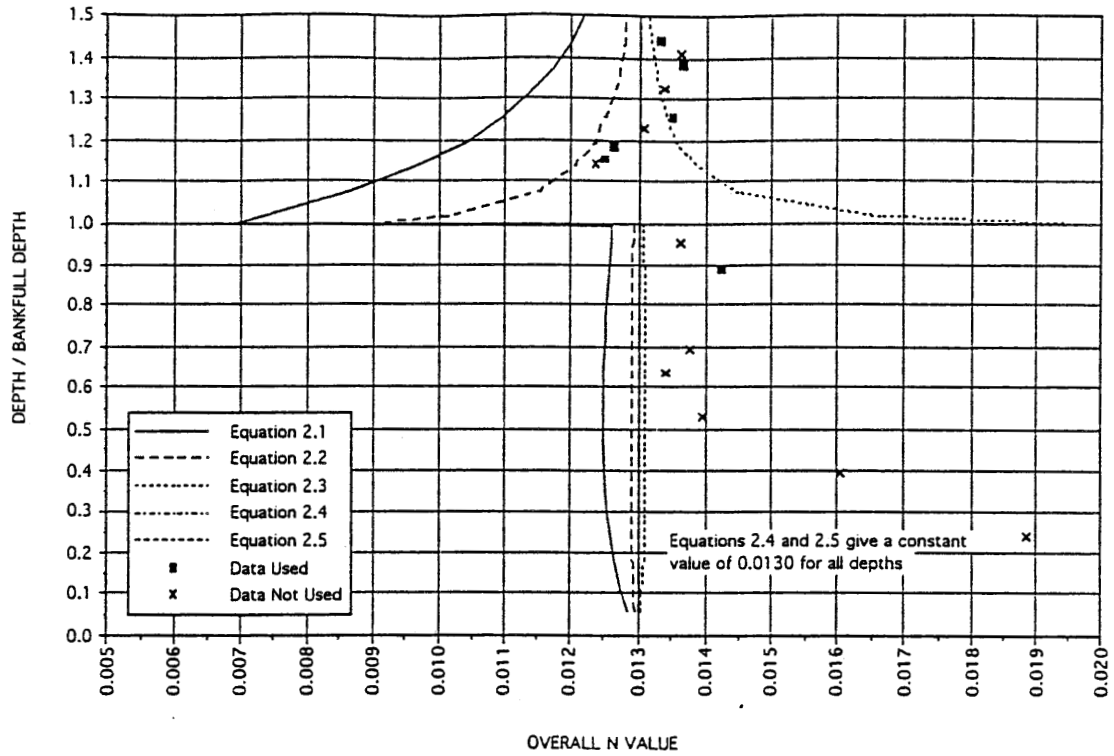

Figure 4.10a Experimental data versus equations 2.1 to 2.5 (bisectional subdivisions) for BBBBB data series

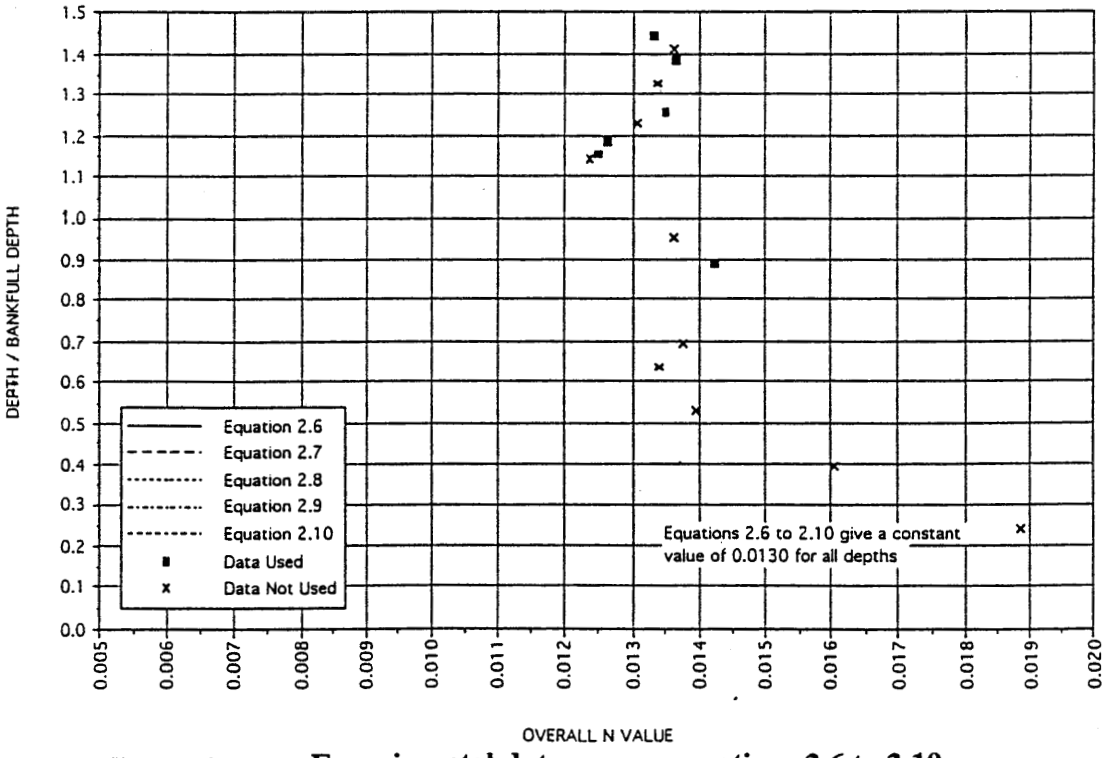

Figure 4.10b Experimental data versus equations 2.6 to 2.10 (bisectional subdivisions) for BBBBB data series

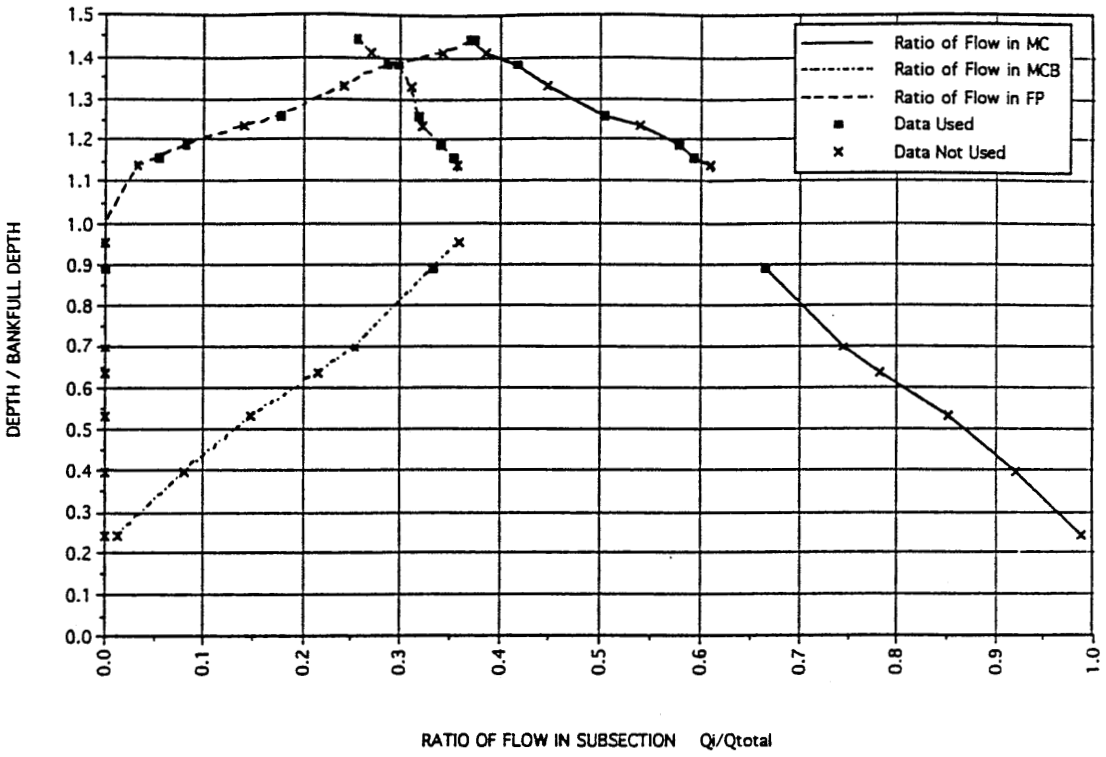

Figure 4.11 Division of flow among subsections for BBBBB data series

BBBBB series provides a good comparison from which we can gain insight to the effects of varying floodplain roughness on n_o at depths above bankfull stage. Comparisons are described below.

4.3.1. *BBSSS Data Series*

The BBSSS data series consisted of eight tests. Of these, six were used in numerical comparisons of the data. Only one of the tests was conducted below bankfull stage, so as not to repeat the below bankfull runs of the BBBBB series. The data in this series of tests are considered to be of moderate quality.

Results are presented in figure 4.12 For the depth range below bankfull stage, the measured n value was similar to the average measured n value for BBBBB runs. In the depth range above bankfull stage, measured n was about .0125 at y/D of 1.3 and reached the maximum value, approximately .0135, at y/D of 1.4, before decreasing at higher y/D. These values were larger than the sand's base n value, which indicates that the influence of MC remained in the above bankfull stages.

Vertical Division Method. Figures 4.12a and b show the comparison of equations 2.1 to 2.10 with the experimental data. It can be seen that the effect of smoother floodplain

roughness (as compared to BBBBB series) on these equations is to shift predicted n_c lower. For equations 2.4 to 2.10, the effect is to shift n_c left toward a value between the two base n values. For the other equations involving the hydraulic radius, the magnitude of such shifts is more obvious for equation 2.3 than equation 2.2 and less so for equation 2.1. These shifts in the predicted n_c reflect the effect of numerical n values on these equations, which were not shown in the experimental data. No data are available for y/D between 1.0 to 1.2, but one can postulate that equations 2.1 and 2.2 generally followed the trend of the data in this range. No equation predicted well for y/D > 1.2. The higher numbered equations predicted mostly constant n_c with the exception of equations 2.8 and 2.10, which predicted the opposite trend from that evidenced by the experimental data.

Bisectional Division Method. Figures 4.13a and b show the variation of equations 2.1 to 2.10 using bisectional subdivision. The use of this method did not seem to improve the accuracy of the various equations.

Flow Distribution. Figure 4.14 shows the ratio of flow in each of the major subdivisions with the data plotted primarily for depths above bankfull stage. As compared to the BBBBB series, flow rates in the FP increased, but decreased in the MC and MCB in the depth range of $1.2 < y/D < 1.4$ (the greatest reduction occurred in the MCB). At depths above $y/D = 1.4$, the differences in the MCB between BBSSS and BBBBB series disappeared and the decreases in the MC for BBSSS were compensated for by increases in the FP. Data were not sufficient to make observations for depth below $y/D = 1.2$. However the trend was flow rate in MC remained about the same for the two data series. Hence the role of MC remained the same in this range of shallow floodplain depth even the floodplain's roughness became less. Beyond this range, the floodplain became more efficient as more mass was transferred to FP from MC as compared to the BBBBB series.

In general, the sand roughness elements were problematic because of difficulty in securing the particles to the boards. That difficulty seems to be reflected in the scatter in the data. The smoothness of the sand section also required much higher discharge for a given depth of flow. This, in turn, led to increased measurement difficulties due to the appearance of wavelets and longer length required to establish flow.

4.3.2. *BBSSG Data Series*

To continue investigating the effect of varying floodplain roughness, the BBSSG data series was tested. The outer edge of the floodplain was the roughest portion of the channel. The BBSSG data series consisted of 12 individual datasets, nine of which were

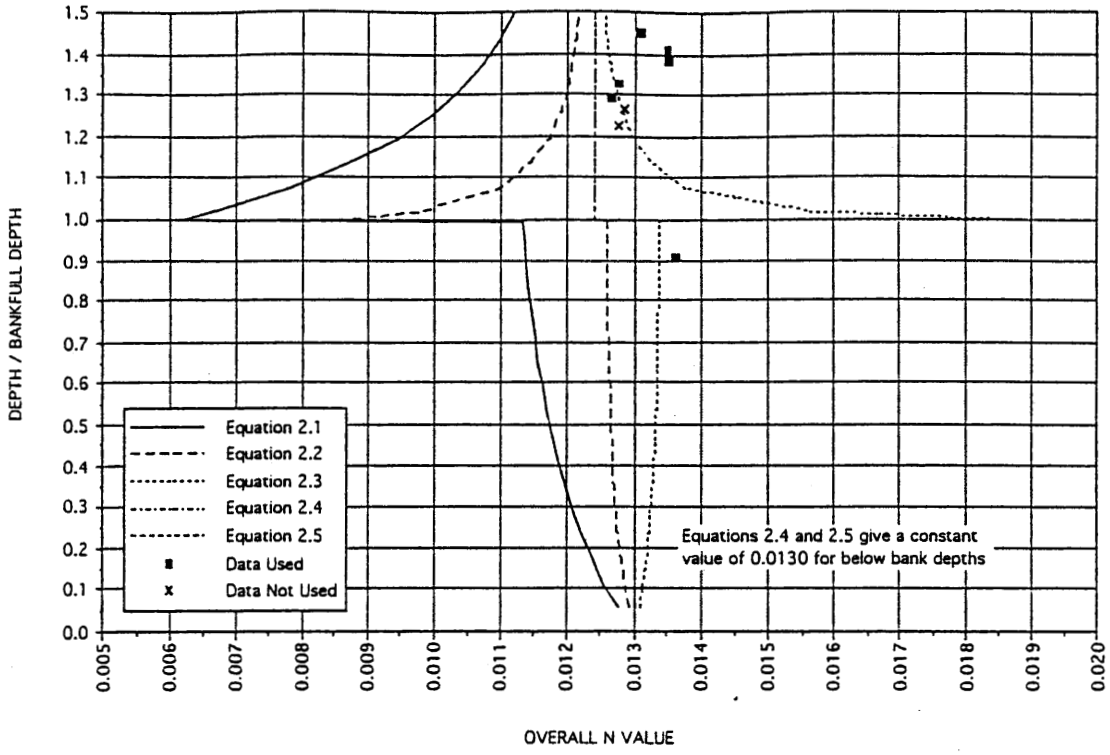

Figure 4.12a **Experimental data versus equations 2.1 to 2.5 (vertical subdivisions) for BBSSS data series**

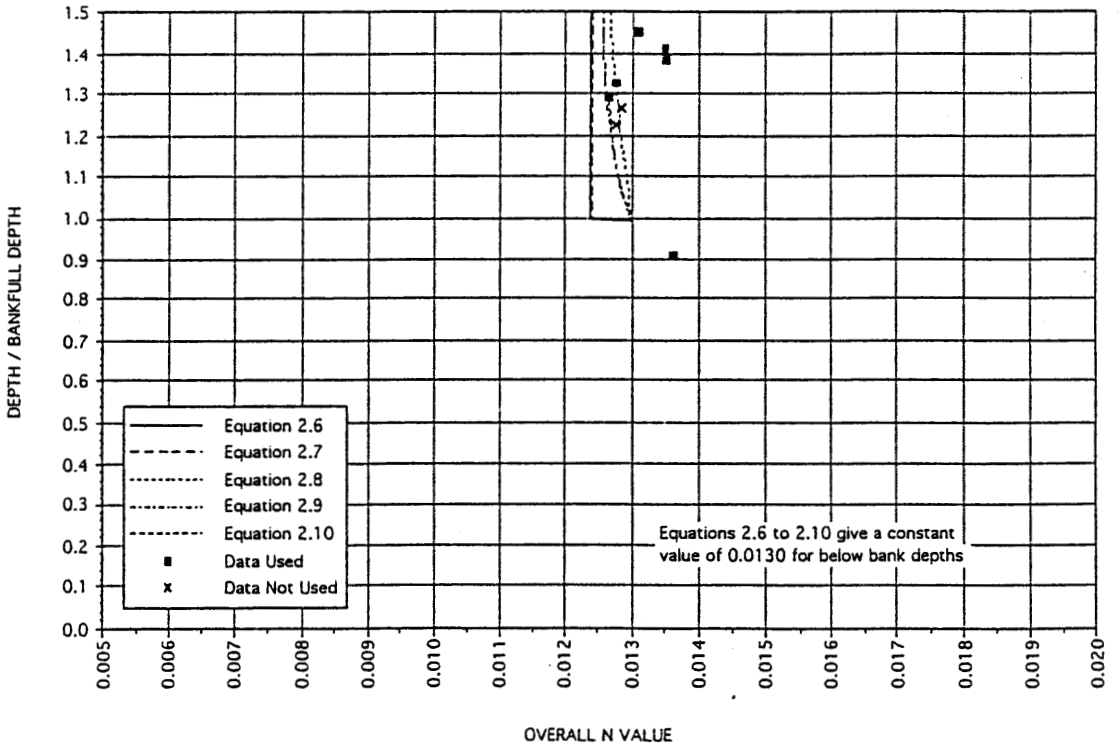

Figure 4.12b **Experimental data versus equations 2.6 to 2.10 (vertical subdivisions) for BBSSS data series**

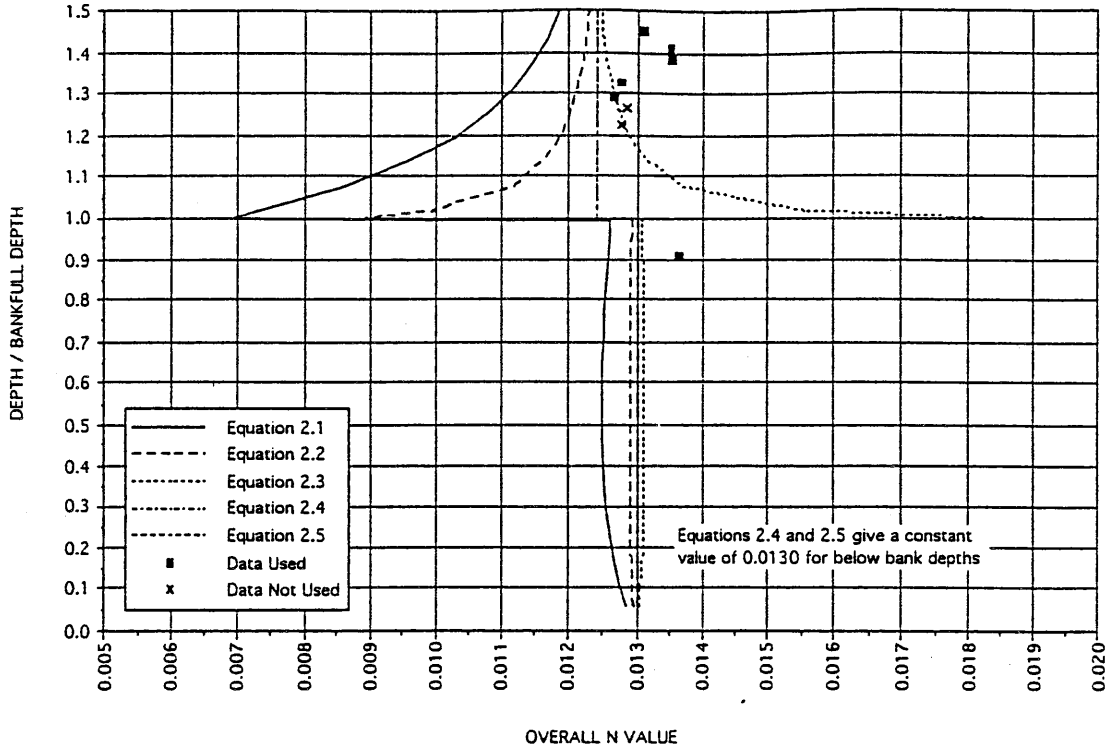

Figure 4.13a **Experimental data versus equations 2.1 to 2.5 (bisectional subdivisions) for BBSSS data series**

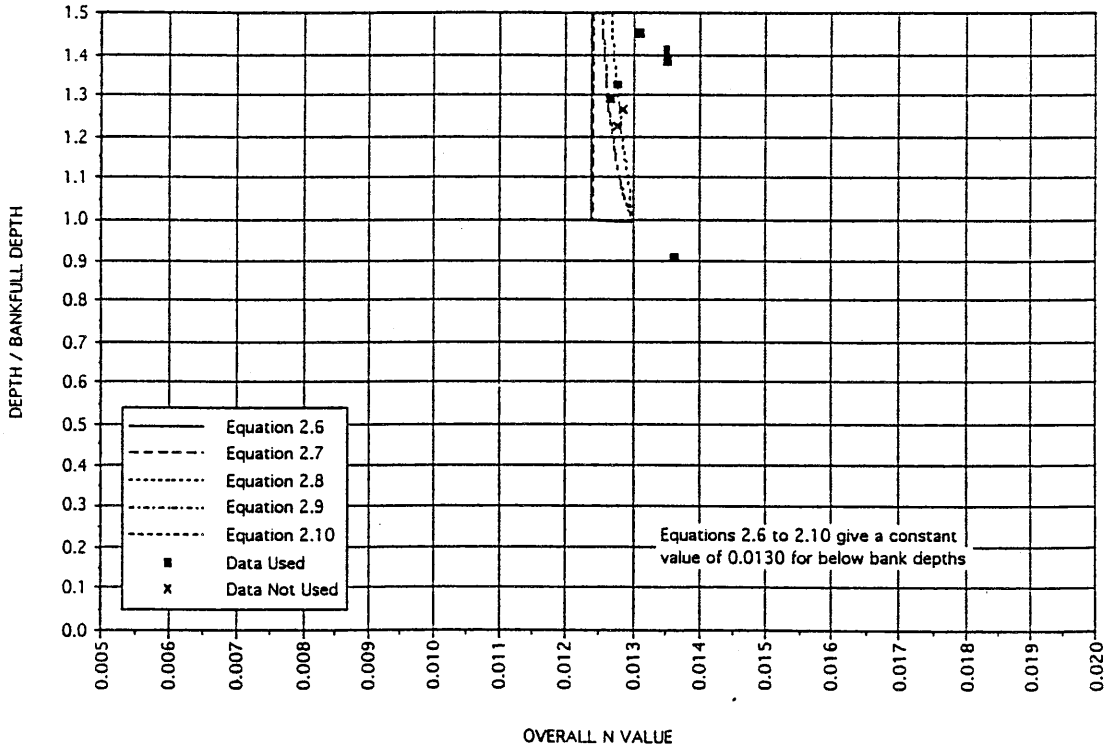

Figure 4.13b **Experimental data versus equations 2.6 to 2.10 (bisectional subdivisions) for BBSSS data series**

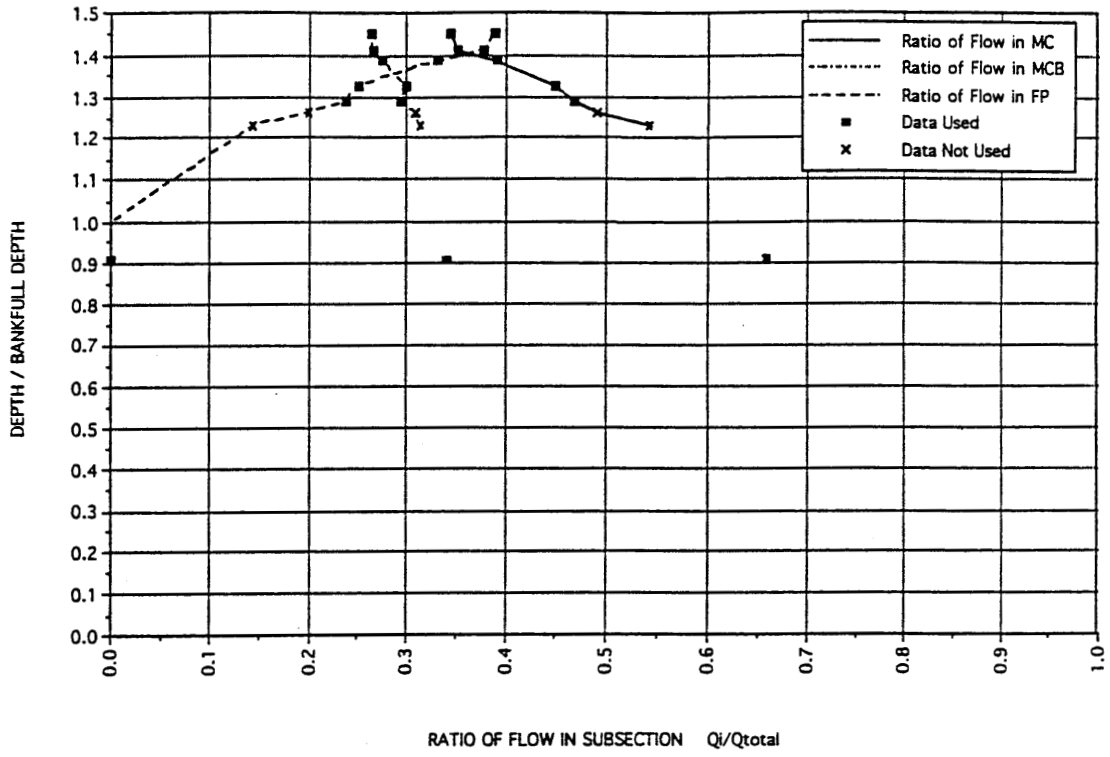

Figure 4.14 Division of flow among subsections for BBSSS data series

acceptable for comparisons. All of the datasets were in the above bankfull stage.

As presented in figure 4.15, the experimental results show an increasing trend. At y/D = 1.2, n_o was approximately 0.127; it reached 0.013 at y/D = 1.3, and approached an asymptotic value of approximately 0.0138 as y/D increased. As compared to the BBSSS series, the effect of a rough element on the floodplain showed after y/D > 1.3. An n_o value of .0145 at y/D = 1.49 was the same as the average of all base n values. However, it seemed to be an outlier to the rest of data. The present experimental setup could not be used to investigate deeper floodplain depth for further verification.

Vertical Division Method. Figures 4.15a and b show the predicted variation in equations 2.1 to 2.10 over depth. Equation 2.2 incidentally closely matched the trend and the numerical values of the experimental data.

When comparing figures 4.12 (BBSSS series) and 4.15 (BBSSG series), note that the n_c values predicted by equations 2.4 to 2.10 shifted substantially to higher values in the above bankfull stage due to a higher roughness on FP1; while n_c predicted by equations 2.1 to 2.3 did not shift as much. Predictions by equation 2.1 shifted only in the high

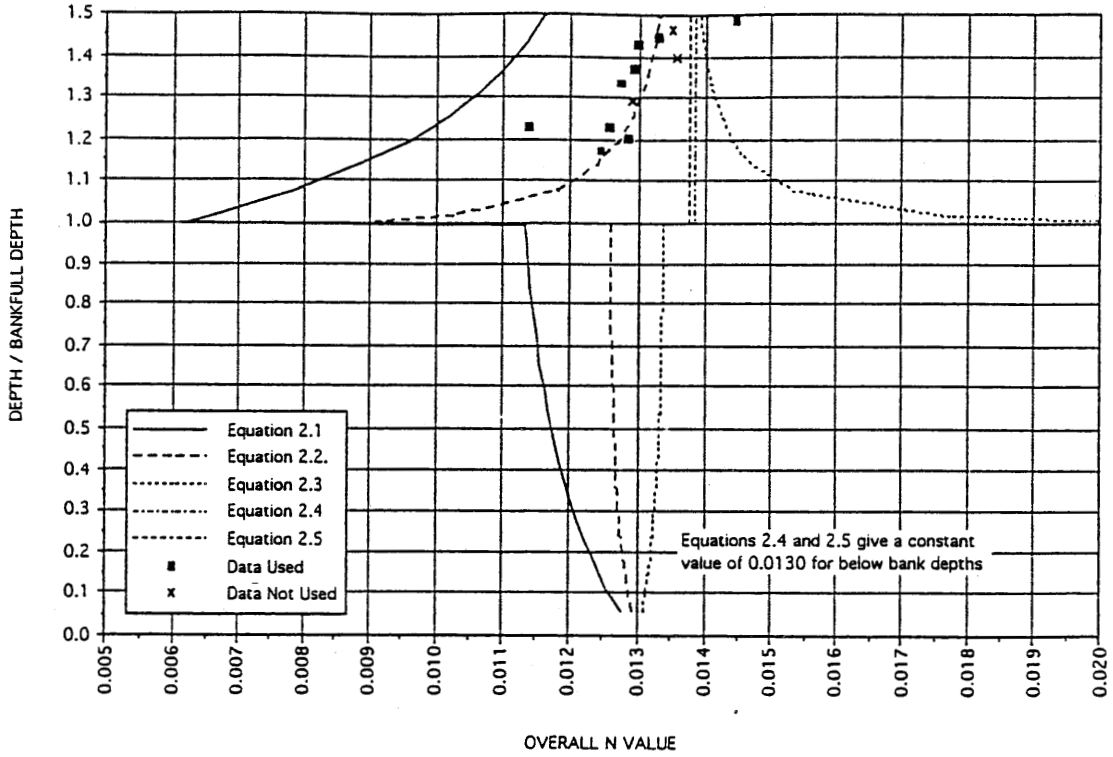

Figure 4.15a Experimental data versus equations 2.1 to 2.5 (vertical subdivisions) for BBSSG data series

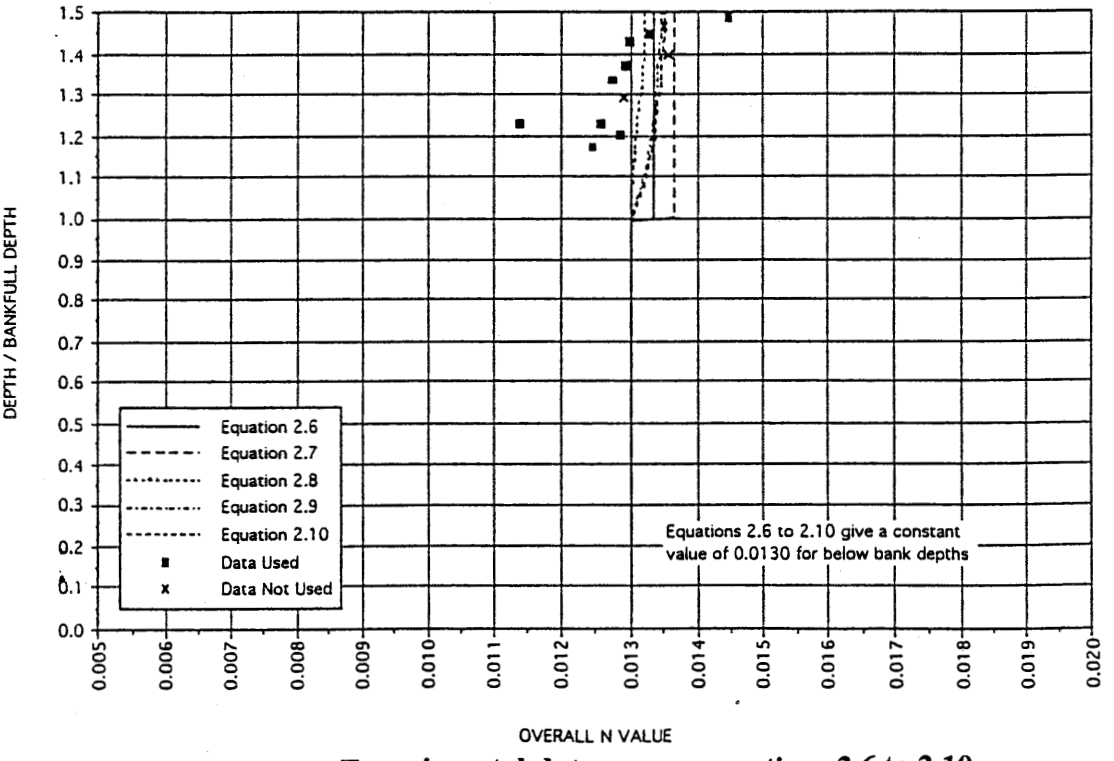

Figure 4.15b Experimental data versus equations 2.6 to 2.10 (vertical subdivisions) for BBSSG data series

floodplain depths by a very small amount (+0.0003 at the highest depth shown); while those by equation 2.2 shifted about +0.001 higher at the deepest depths, and those by equation 2.3 shifted to the right by about +0.002 at the deepest depths.

Notably, the values near bankfull depths were predicted to be identical both for the BBSSS and BBSSG series, because the area and wetted perimeter of the floodplain were not yet strongly introduced into the equations at this depth. Above the bankfull stage, the effect of different n in the floodplain was shown more clearly in equation 2.2. The predicted trends for BBSSS and BBSSG data series began to diverge as soon as the y/D ratio exceeded 1.05. Examining the experimental data, however, indicates that very little change in magnitude occurred in this range. In fact, on average, the trend of the data for the BBSSS and BBSSG series was essentially identical. This seems reasonable because the location of the changed roughness element was on the far edge of the floodplain, which has less effect on the overall flows. A change in the innermost element (i.e., near the MC) would have produced a more noticeable change in the magnitude of the overall n value. Apparently the equations could not differentiate among the differences.

Bisectional Division Method. Figures 4.16a and b show the effect of bisectional subdivisions on the outcome of the equations. Again, the major difference from the vertical division method is that bisectional division narrows the discrepancies among equations. Predicted trends maintain similar patterns.

Flow Distribution. Figure 4.17 shows the ratio of flows in each subsection for this dataset. Examining both figures 4.17 and 4.14, one can find that the difference mostly occurred in the MCB and at $1.3<y/D<1.4$. In this depth range, BBSSG series data had slightly less flow in the MC, and slightly more flow in the MCB than BBSSS series data. Flow in the FP was not affected much. The flow rates for all three subareas became approximately constant as y/D passed beyond 1.4. At this depth, the MC and FP curves intersected. This test series revealed more about flow distribution after the intersection. Apparently the discharge ratios tended to stay constant for higher depths.

4.3.3. *BBSGG Data Series*

This data series consisted of 10 datasets, all with depths above bankfull stage. Nine of these sets were acceptable for use in the numerical comparisons. The experimental results (figure 4.16) showed that a rougher floodplain increased n_o values, which reached 0.0132 at y/D = 1.2 and had a maximum value of .0138 at y/D = 1.4.

Vertical Division Method. Figures 4.18a and b show the variation of equations 2.1 to 2.10 versus the experimental data. It can be seen that the numerical effect of two rough floodplain elements was to shift the predicted values further to the right. As in previous

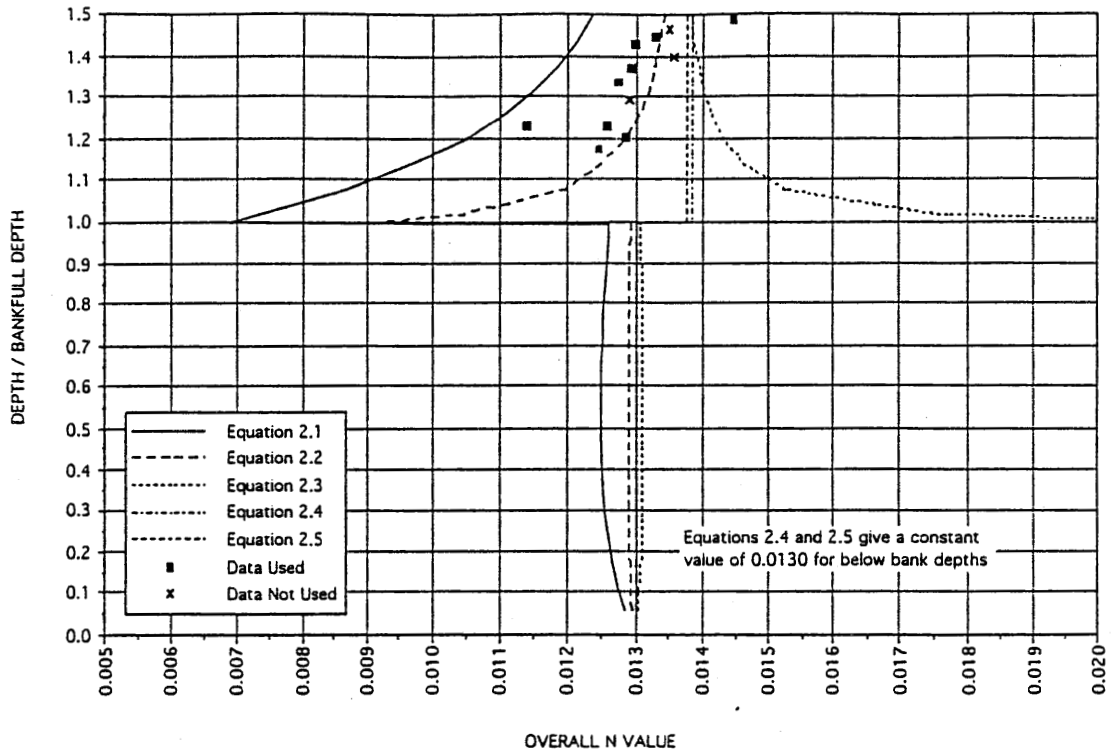

Figure 4.16a **Experimental data versus equations 2.1 to 2.5 (bisectional subdivisions) for BBSSG data series**

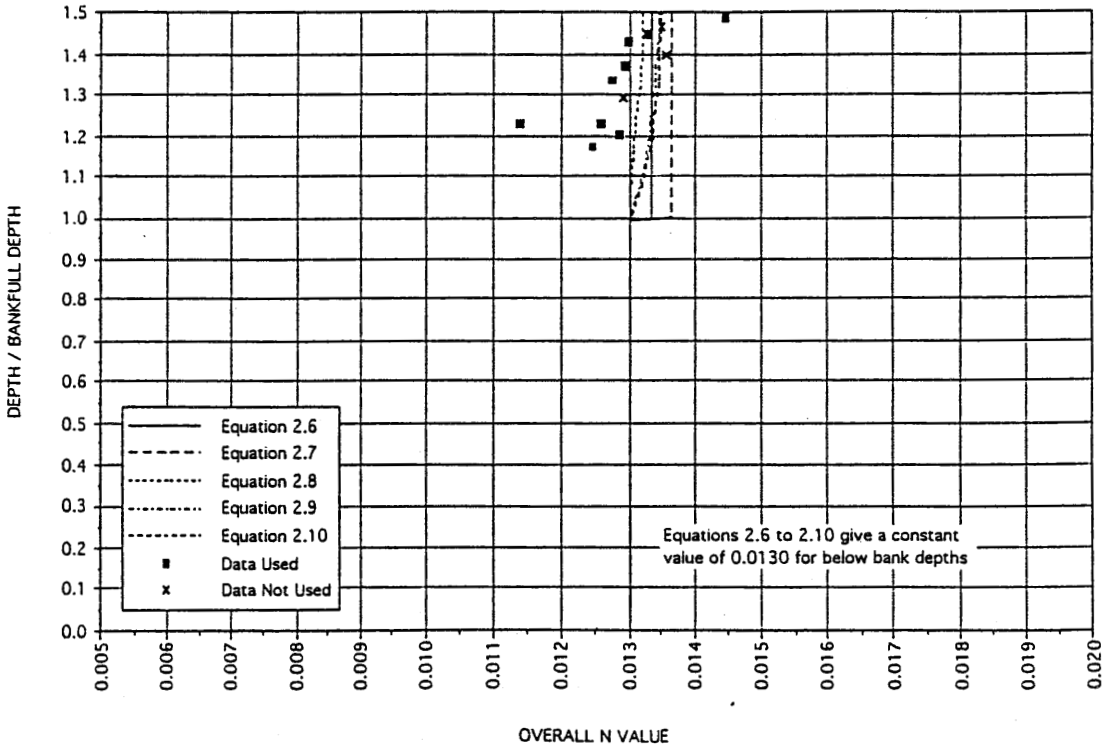

Figure 4.16b **Experimental data versus equations 2.6 to 2.10 (bisectional subdivisions) for BBSSG data series**

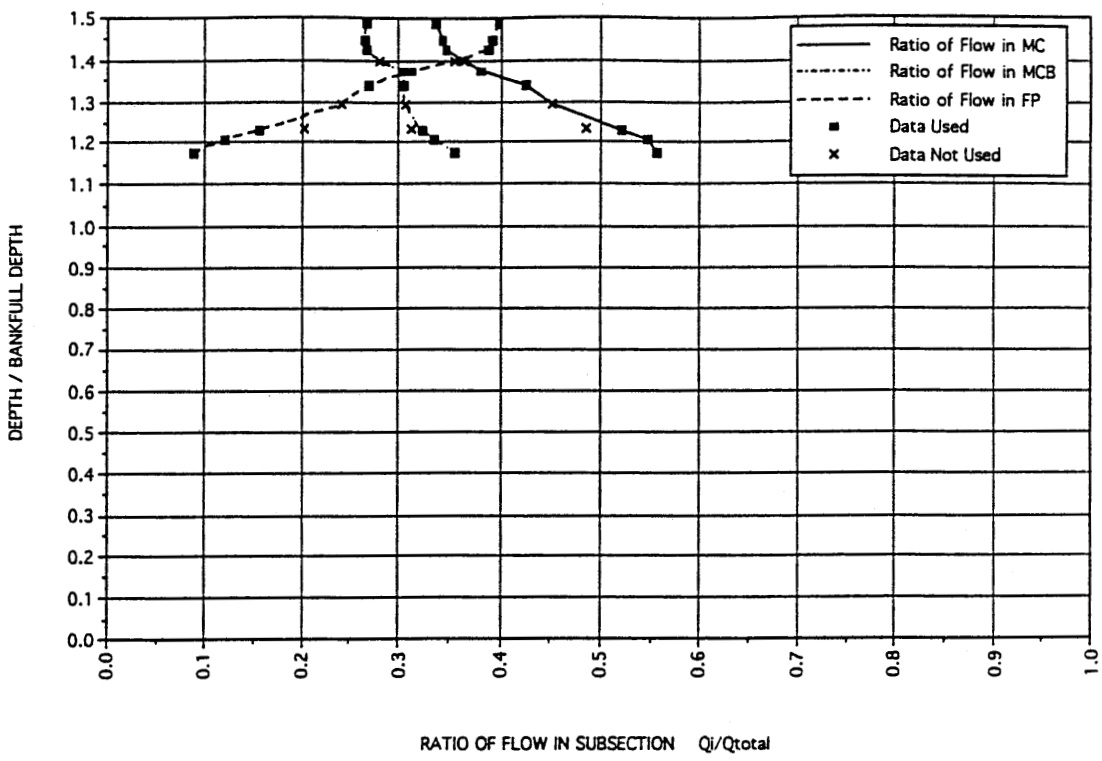

Figure 4.17 Division of flow among subsections for the BBSSG data series

cases, equations 2.1 and 2.2 bracketed the experimental values. Unlike the case for the BBSSG data series, where all higher numbered equations predicted an asymptotic value, equation 2.8 predicted the asymptotic value properly for BBSGG data.

Bisectional Division Method. Figures 4.19a and b show the effect of bisectional subdivisions on the overall n values predicted by the equations. Again, the effect was to narrow the discrepancies among the predictions. Equation 2.1 was affected the most by the use of bisectional subdivisions. Equation 2.8 was the best equation for predicting an asymptotic overall n value.

Flow Distribution. Figure 4.20 shows the flow distribution for the BBSGG series. No significant difference in the flow distribution at 1.0<y/D< 1.2 is evident in comparisons of graphs for the BBSSG and BBSGG data series. At 1.2<y/D<1.35, more flow occurred in the FP for BBSGG data than for GGSSG data. Above y/D = 1.35, more flow appeared in the MC and less in the FP, while the MCB remained about the same as the BBSSG data. The intersection of the MC and FP moved to a higher depth at approximately y/D = 1.42, with a discharge ratio around 0.36. No data are available to show the flow distribution pattern after this y/D ratio.

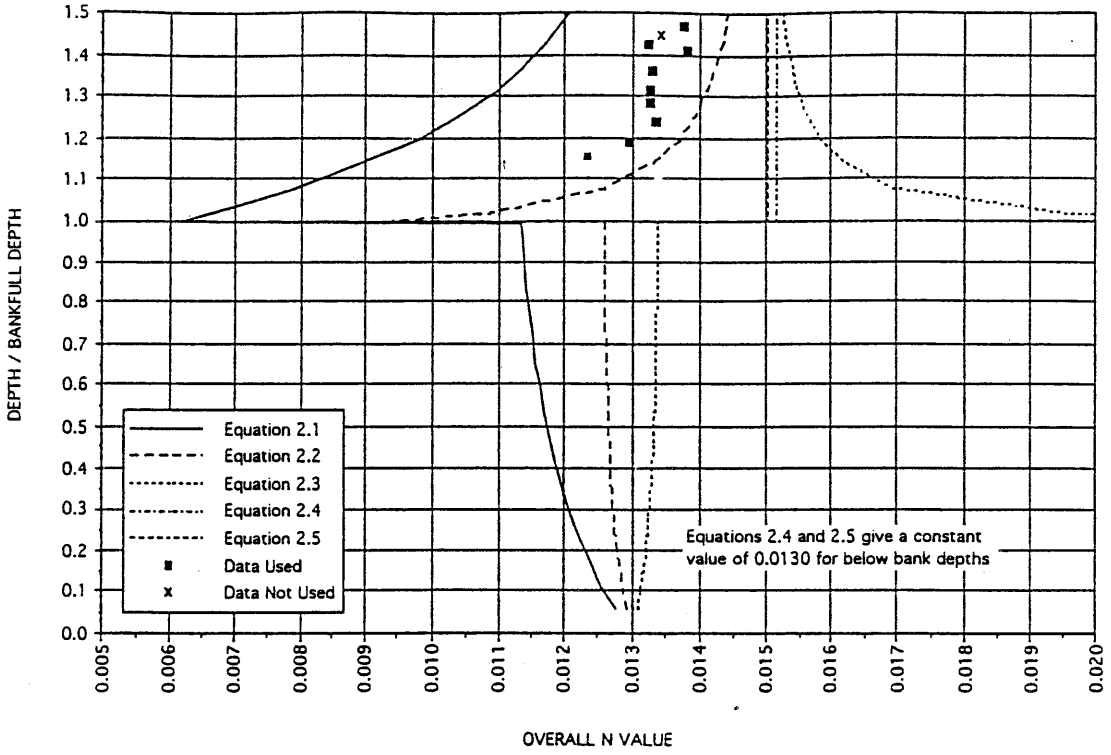

Figure 4.18a Experimental data versus equations 2.1 to 2.5 (vertical subdivisions) for BBSGG data series

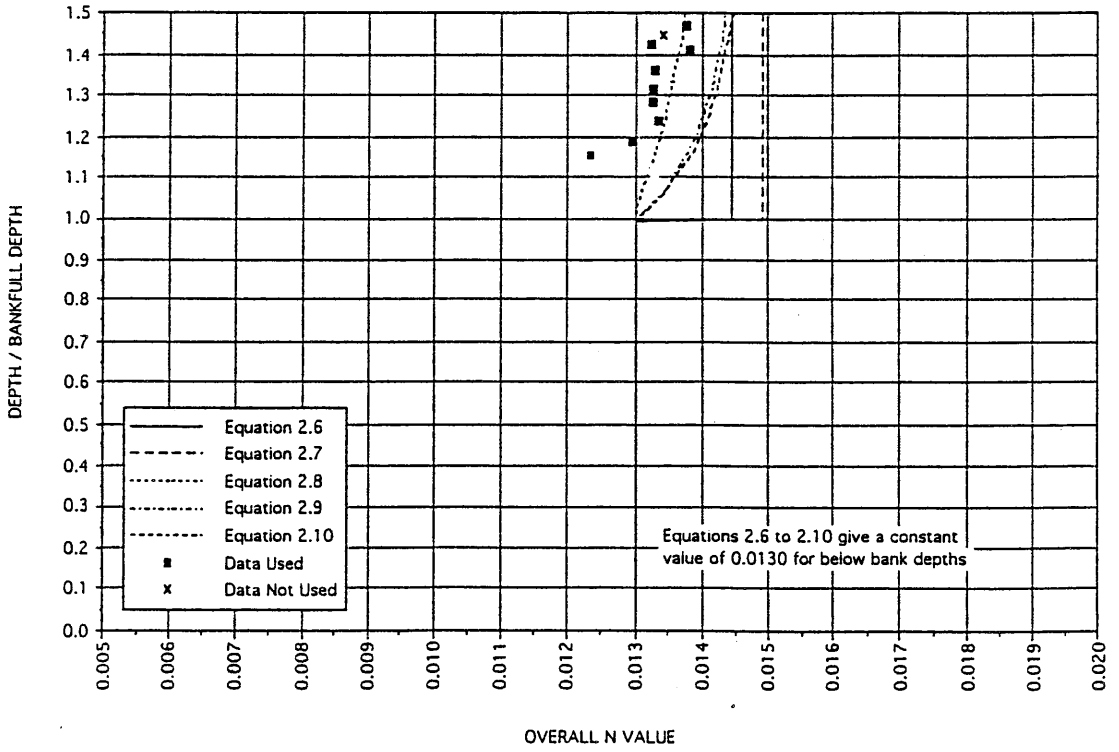

Figure 4.18b Experimental data versus equations 2.6 to 2.10 (vertical subdivisions) for BBSGG data series

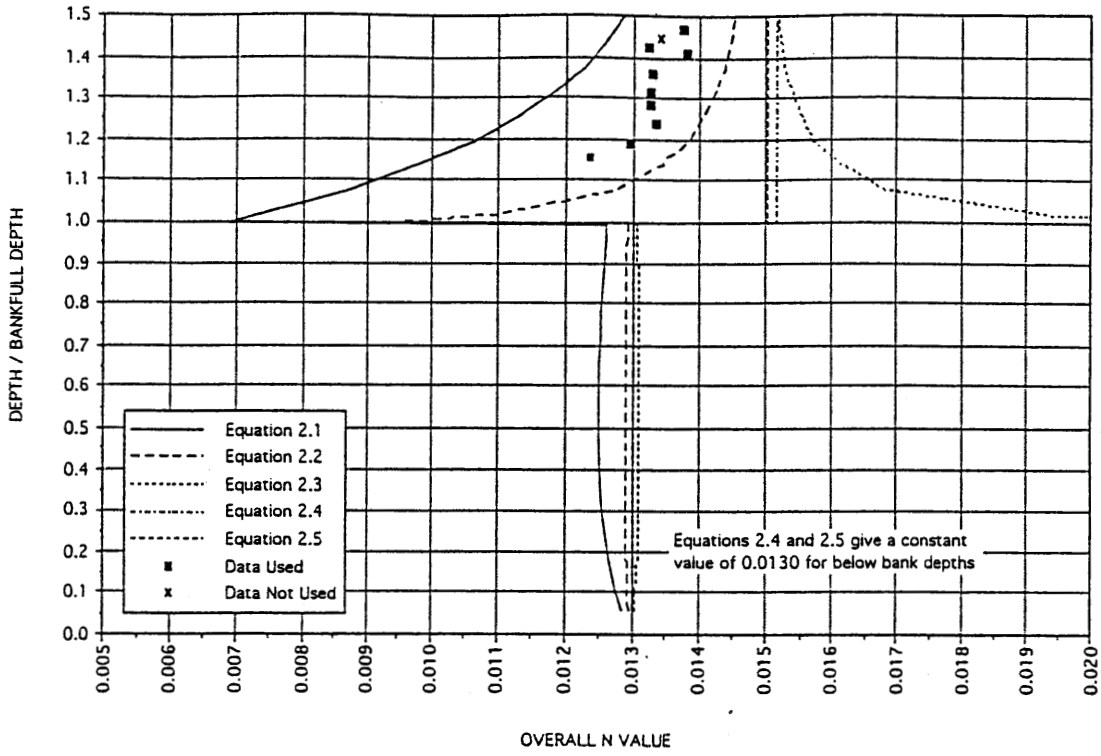

Figure 4.19a **Experimental data versus equations 2.1 to 2.5 (bisectional subdivisions) for BBSGG data series**

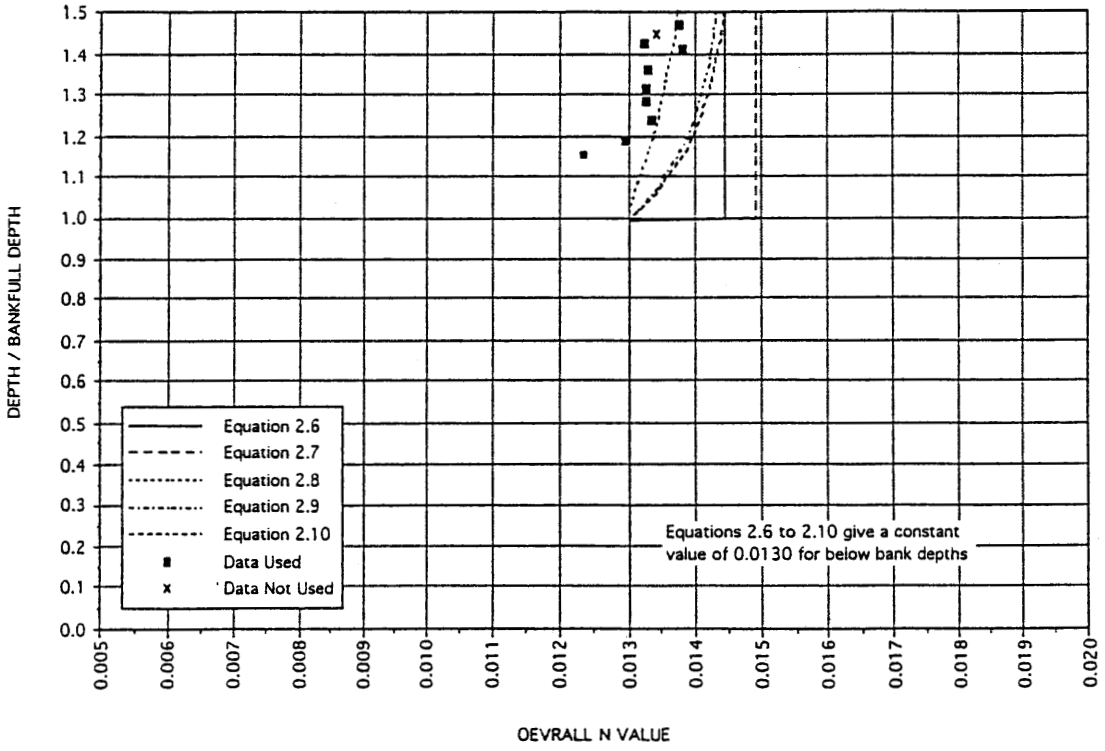

Figure 4.19b **Experimental data versus equations 2.6 to 2.10 (bisectional subdivisions) for BBSGG data series**

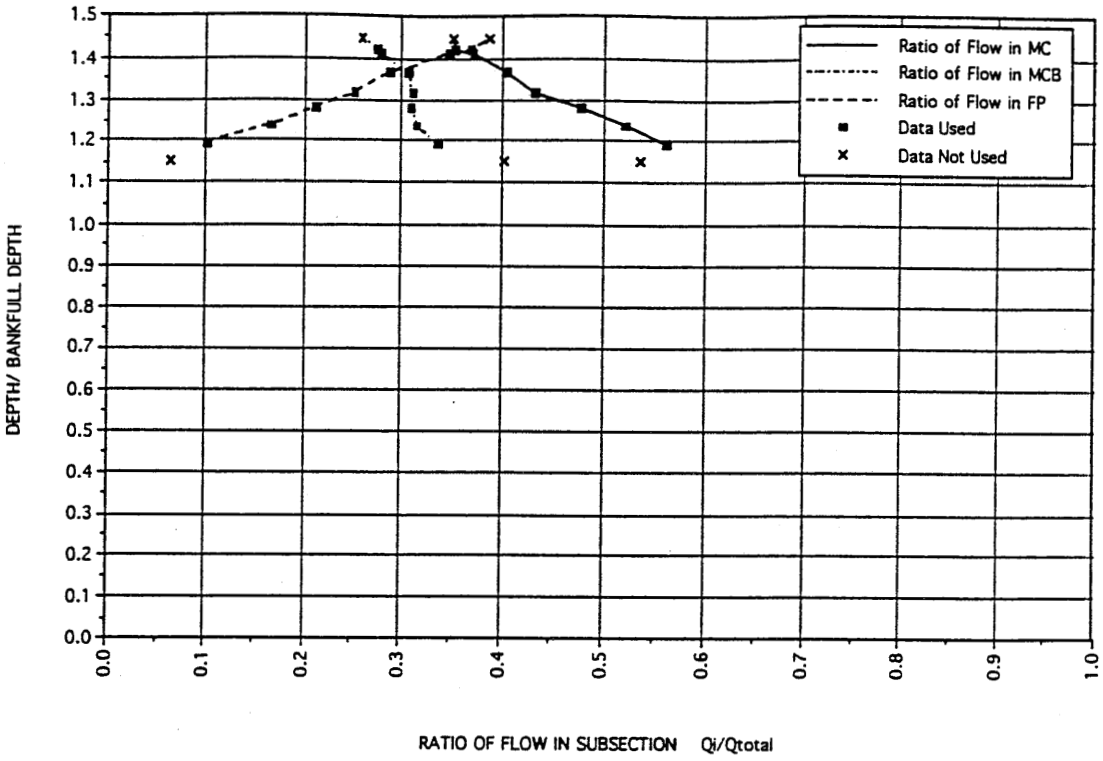

Figure 4.20 Division of flow among subsections for BBSGG data series

4.3.4. *BBGGG Data Series*

The last test of floodplain roughness is the BBGGG series, which consisted of nine datasets, seven of which were acceptable for analysis. All of the datasets were in the above bankfull stage. The data were of moderate quality.

With completely rough floodplains, n_o yielded higher values (compare figures 4.18 and 4.21). The n_o value reached 0.0132 at y/D = 1.2, and 0.014 (approximately the average base n values for gravel and black magnum) at y/D = 1.41. The general tendency of overall n was that at the given y/D the magnitudes increased as compared to the BBSGG series.

Vertical Division Method. Figures 4.21a and b show the n_c values predicted by equations 2.1 to 2.10 and the n_o values derived from the experiment. Most equations predicted higher n_c corresponding to the higher n values on the floodplain, while the experimental data did not show such rapid changes. Equation 2.1 was the only exception, with much slower responses to higher n value along the wetted perimeter due to its higher

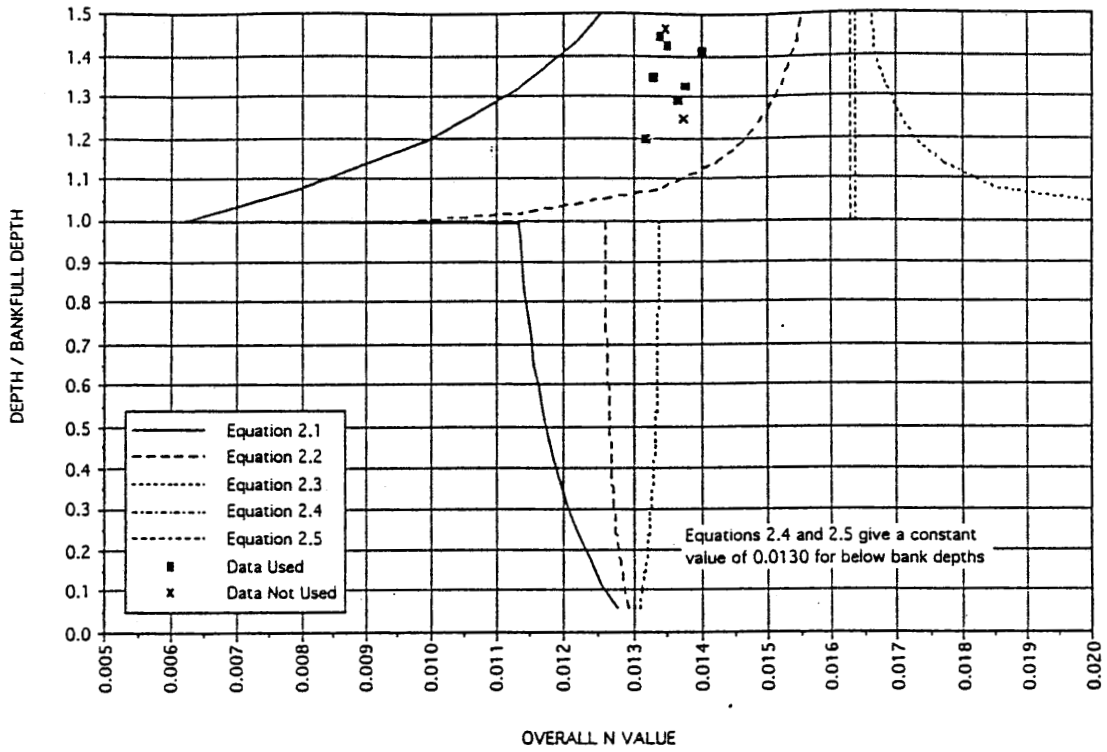

Figure 4.21a Experimental data versus equations 2.1 to 2.5 (vertical subdivisions) for BBGGG data series

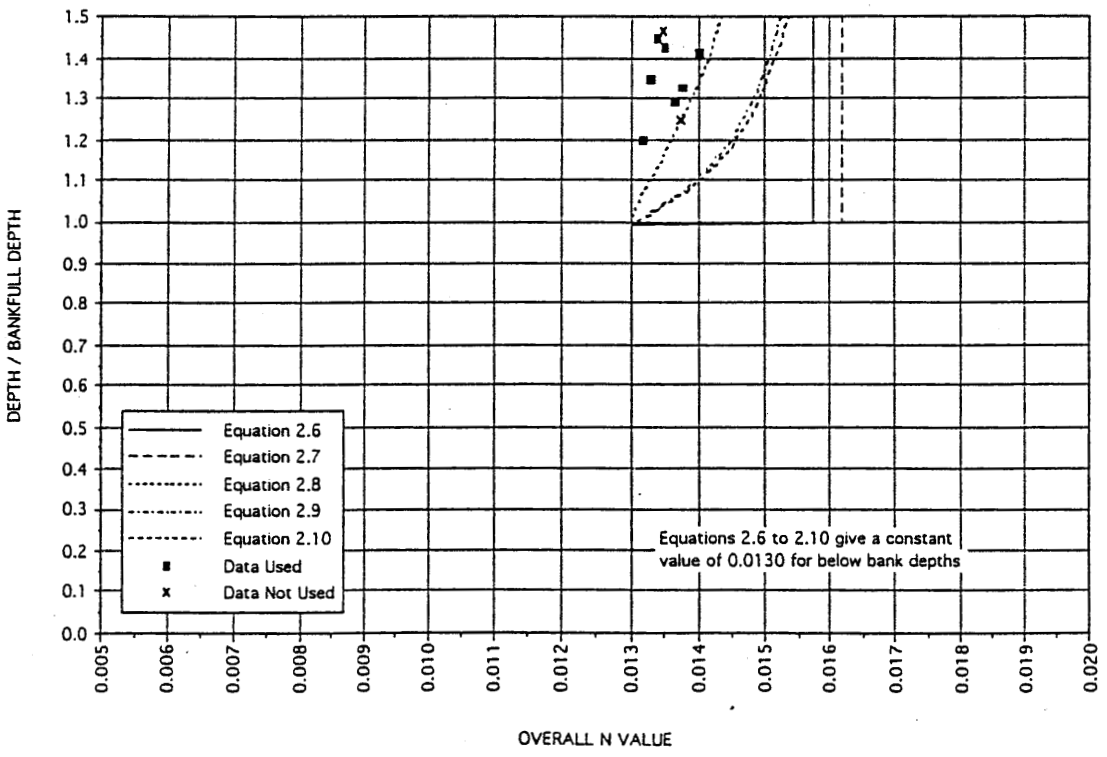

Figure 4.21b Experimental data versus equations 2.6 to 2.10 (vertical subdivisions) for BBGGG data series

exponent on hydraulic radius. As before, equations 2.1 and 2.2 bracketed the data, although the n_c predicted by these equations was quite different from the experimental data. The asymptotic n_o value at higher depths, however, appeared to differ from equation 2.8 for this series.

Bisectional Division Method. Figures 4.22a and b show the variation of equations 2.1 to 2.10 using bisectional subdivision. Again, some improvement in the performance of equation 2.1 with bisectional subdivisions can be observed.

Flow Distribution. Figure 4.23 shows the flow distribution characteristics of the BBGGG channel. The MC and FP curves intersect at y/D = 1.42 where the discharge ratio was about 0.36. The overall differences between this series and BBSGG series were small. However, note that the slope in the MCB curve changed. In the GGSSB and BBSSS series, the MCB curves appeared to have a constant flow rate ratio before intersecting with the FP curve. But this was not the case for the BBGGG and BBSSS series.

Comparing the two data series indicates that for BBGGG, the flow rate decreased on the FP, especially for y/D < 1.3. In the same range, the flow rate increased in the MCB but did not change much on the MC. The MC and FP intersected at higher y/D even at the same flow rate as BBSSS, while in the MCB the intersection remained at about the same y/D but with a higher flow rate.

4.3.5. *Summary*

Five combinations were used to examine the effects of floodplain roughness on n_o values. Despite scatteredness in the experimental data, a general comparison can be made. For such a purpose, the authors used best fitted lines for the experimental data and constructed the following table.

Table 4.1. Fitted n_o Values at Selected y/D for Different Floodplain Roughness

	y/D ratios								
Series	*1.05*	*1.1*	*1.15*	*1.2*	*1.25*	*1.3*	*1.35*	*1.4*	*1.45*
BBBBB	.0111	.0118	.0123	.0127	.0131	.0133	.0135	.0136	.0137
BBSSS	.0111	.0117	.012	.0123	.0126	.0128	.0129	.013	.0131
BBSSG	.0111	.0115	.012	.0123	.0126	.0128	.013	.0132	.0133
BBSGG	--	.0120	.0124	.0128	.0132	.0135	.0137	.0138	.0138
BBGGG	.0118	.0125	.0128	.0132	.0135	.0137	.0138	.014	.0141

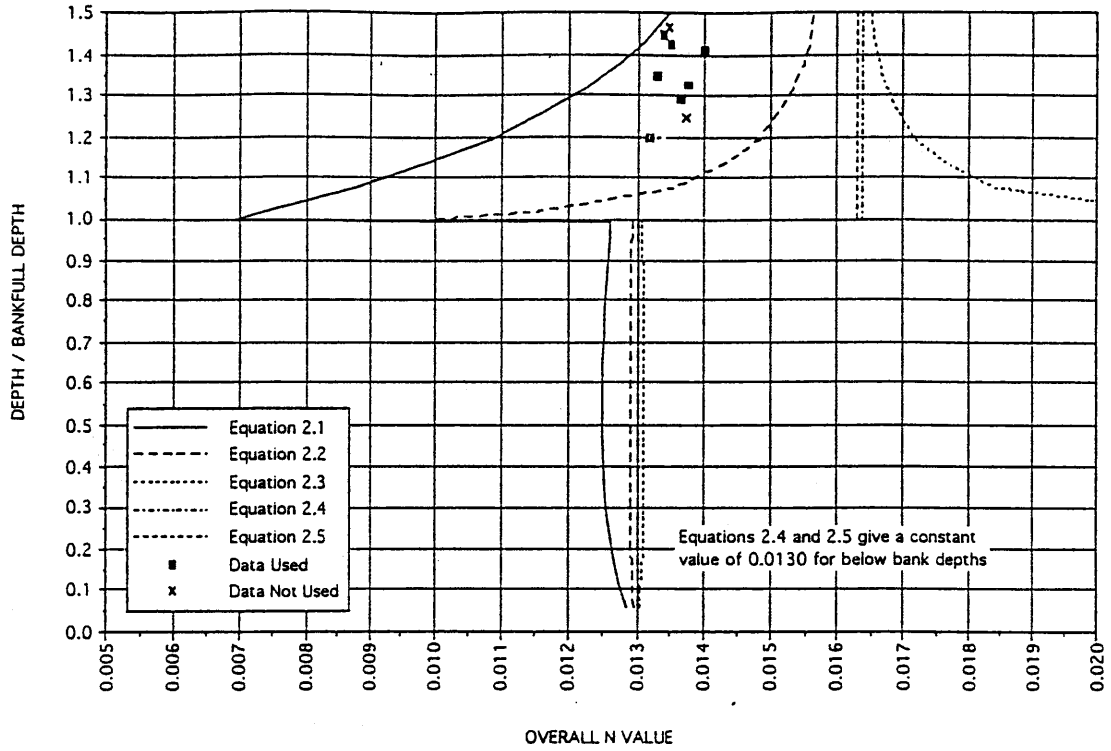

Figure 4.22a **Experimental data versus equations 2.1 to 2.5 (bisectional subdivisions) for BBGGG data series**

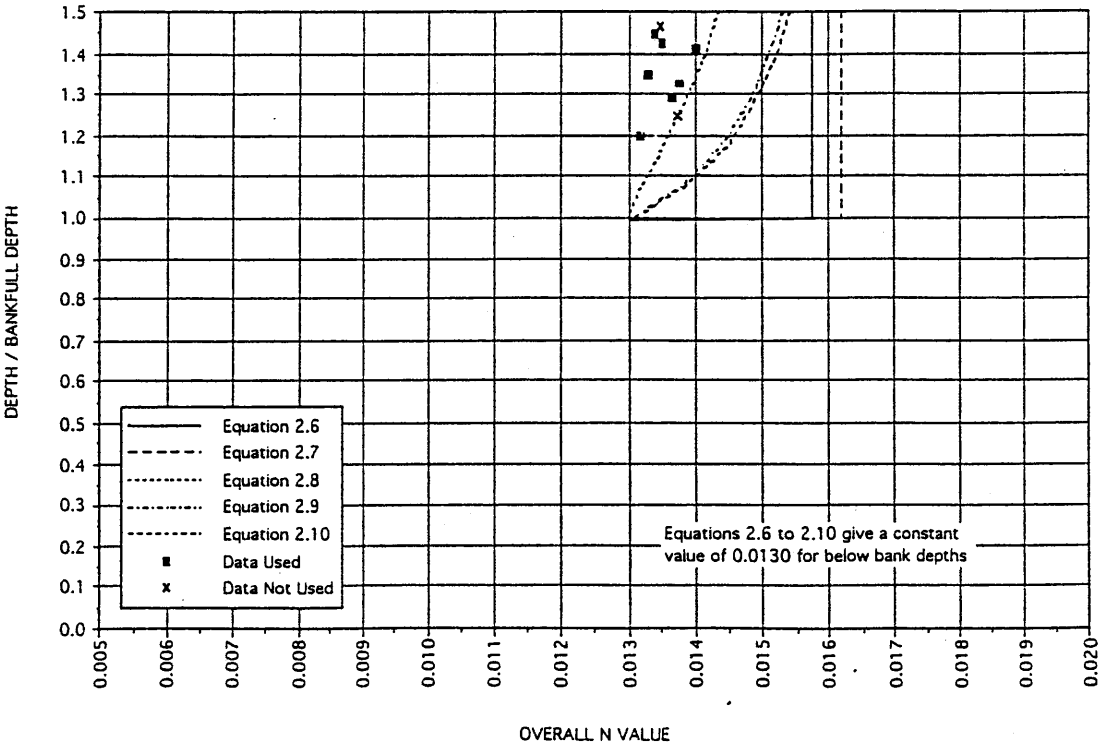

Figure 4.22b **Experimental data versus equations 2.6 to 2.10 (bisectional subdivisions) for BBGGG data series**

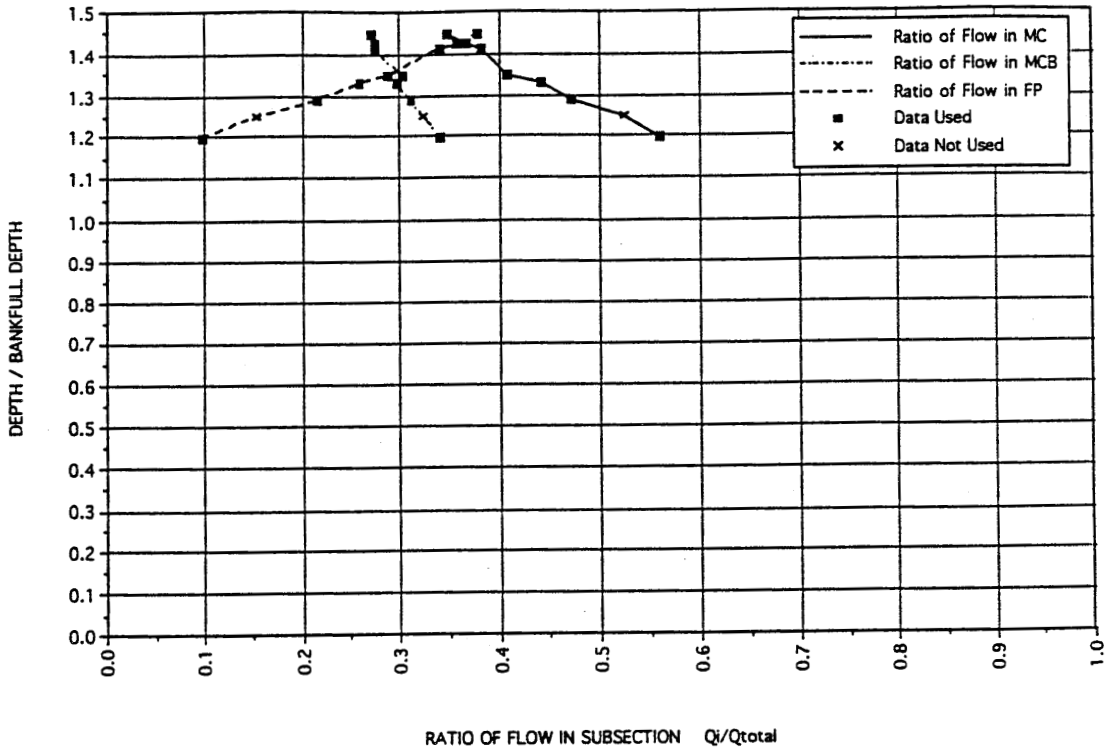

Figure 4.23 Division of flow among subsections for BBGGG data series

Because the base values of sand and black magnum roughness are close, the authors used four decimal numbers to compare their effects. Both roughness magnitudes and their locations alter the overall n_o values. Completely changing the floodplain roughness (BBBBB and BBSSS series) produces differences only at higher floodplain depths.

4.4. Effects of Changing Main Channel Roughness on Overall n_o

The effects of a rough bed or rough sidewalls on n_o were predicted in prismatic channels earlier (Chapter 2). Such effects on n_o are examined here using the BGGGG and GBBBB series, together with the GGGGG set analyzed earlier. All these three sets were conducted at the same slope, 1.045E-03.

4.4.1. BGGGG Data Series

The BGGGG series consisted of 15 datasets, 10 of which were used in the numerical comparison of the data. All five datasets from below bankfull stage were not

used because of the unsteady water surface. These data are still presented in the figures so that the discrepancies can be observed. As discussed at the beginning of this chapter, their values were not used in the numerical evaluation.

Figure 4.24 shows that the experimental data clearly varied from n_o = 0.0156 at y/D = 1.145 to n_o = 0.0178 at y/D = 1.402. After that depth, n_o tended to approach a constant value. The most rapid changes in n_o occurred in the range 1.0 < y/D < 1.2.

Below bankfull stage, n_o mostly fell in a narrow range between 0.018 and 0.019, which was close to the base n value for the gravel element. The influence of a rough sidewall on n_o was very similar to the case shown previously for n_c. If the unused data did not deviate too much from the actual value, then n_o in the MC near bankfull stage was approximately 0.0188. This value is about 3% higher than the base n value for the gravel element. When comparing figure 4.24 to figure 4.3 (GGGGG series), n_o for the BGGGG series is lower but not substantial. At low MC depths, n_o should be closer to the base n of the bed element, providing that the flow regime remains in the turbulence range. The single n_o value (below y/D < 0.5) and those shown in figure 4.9 (BBBBB series) apparently were affected by low Froude numbers. The curvature of n_o for BGGGG in the MC was much larger than that of the GGGGG series

Vertical Division Method. The variations in n_c due to the changes in roughness as predicted by equations 2.1 to 2.10 are presented in figures 4.24a and b. Unlike previous cases (constant roughness in the MC), equations 2.2 to 2.10 predicted correct patterns of n_o below bankfull stage with equation 2.3's prediction being closest to the n_o values. Above bankfull stage, none of the equations properly described the actual n_o variations. But the n_c predicted by equations 2.3 to 2.7 was reasonable for y/D > 1.3 or 1.4.

Bisectional Division Method. Figures 4.25a and b show the variation of equations 2.1 to 2.10 using bisectional subdivision. As before, bisectional subdivisions tended to narrow the discrepancies among equations and to predict higher magnitudes of n_c. Equation 2.1 was the most affected, followed by equation 2.2, and equation 2.3 was the least affected. In general, bisectional subdivision did not substantially improve the predictions of these equations.

Flow Distribution. Figure 4.26 gives the ratio of flow in each of the subsections for the BGGGG data series. Comparing figure 4.26 with figure 4.6 of the GGGGG data series, one can make the following observations:

- Slopes for the MC, MCB, and FP were about the same at y/D > 1.35 for these two series, indicating that the effect of the MC disappeared at higher floodplain depths. Between 1.0 < y/D < 1.35, the flow rate in the MC for BGGGG was higher than GGGGG, but slightly less in the FP and MCB.

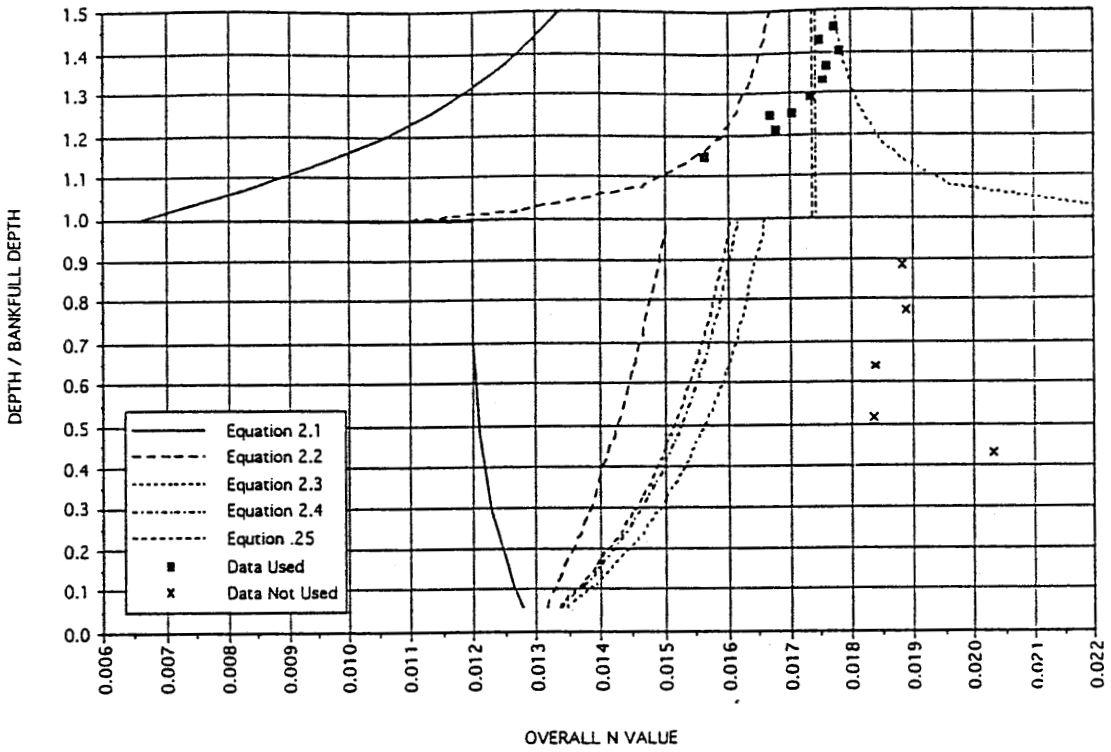

Figure 4.24a Experimental data versus equations 2.1 to 2.5 (vertical subdivisions) for BGGGG data series

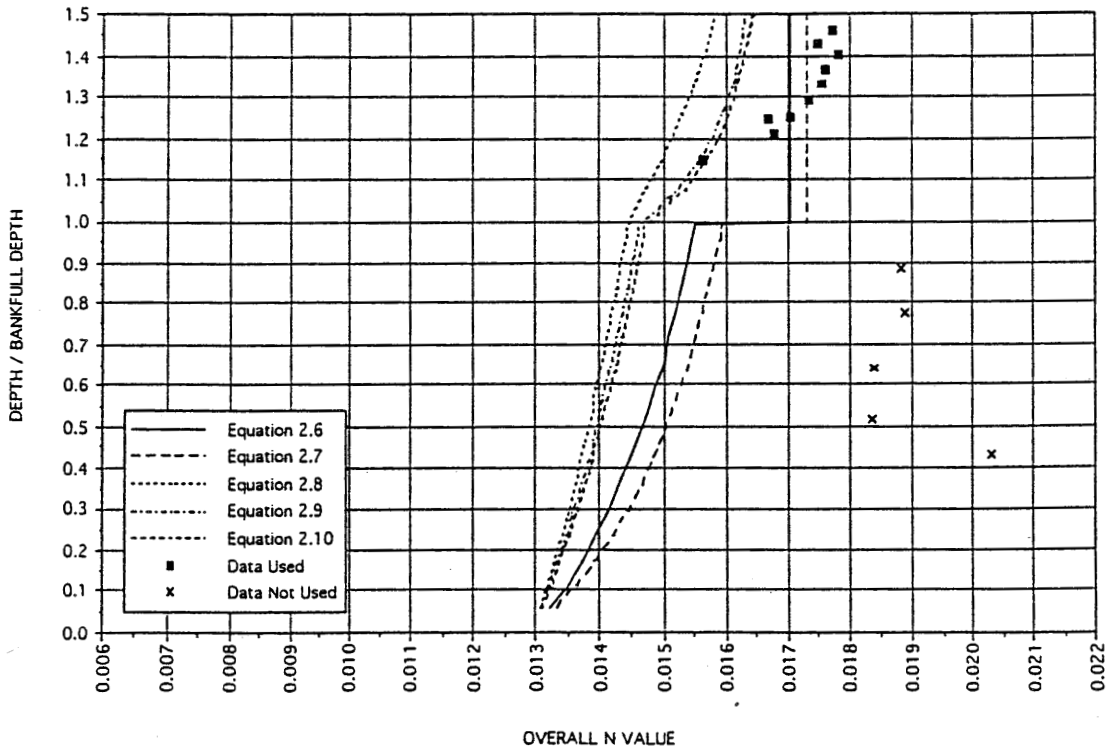

Figure 4.24b Experimental data versus equations 2.6 to 2.10 (vertical subdivisions) for BGGGG data series

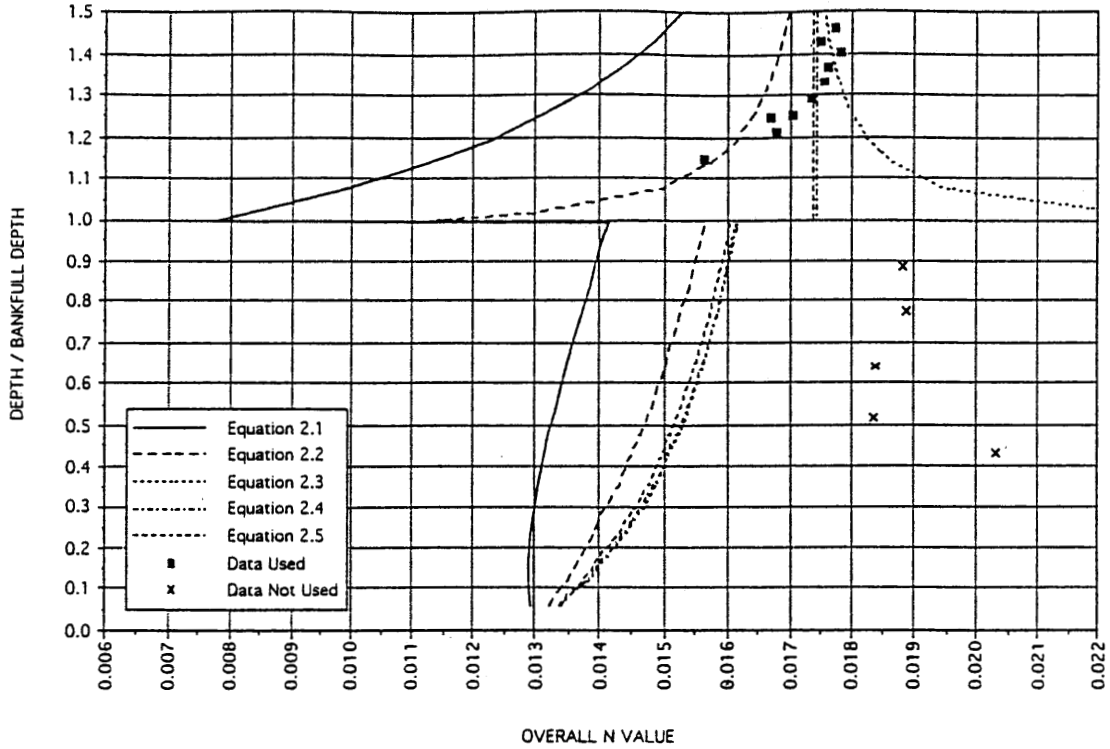

Figure 4.25a Experimental data versus equations 2.1 to 2.5 (bisectional subdivisions) for BGGGG data series

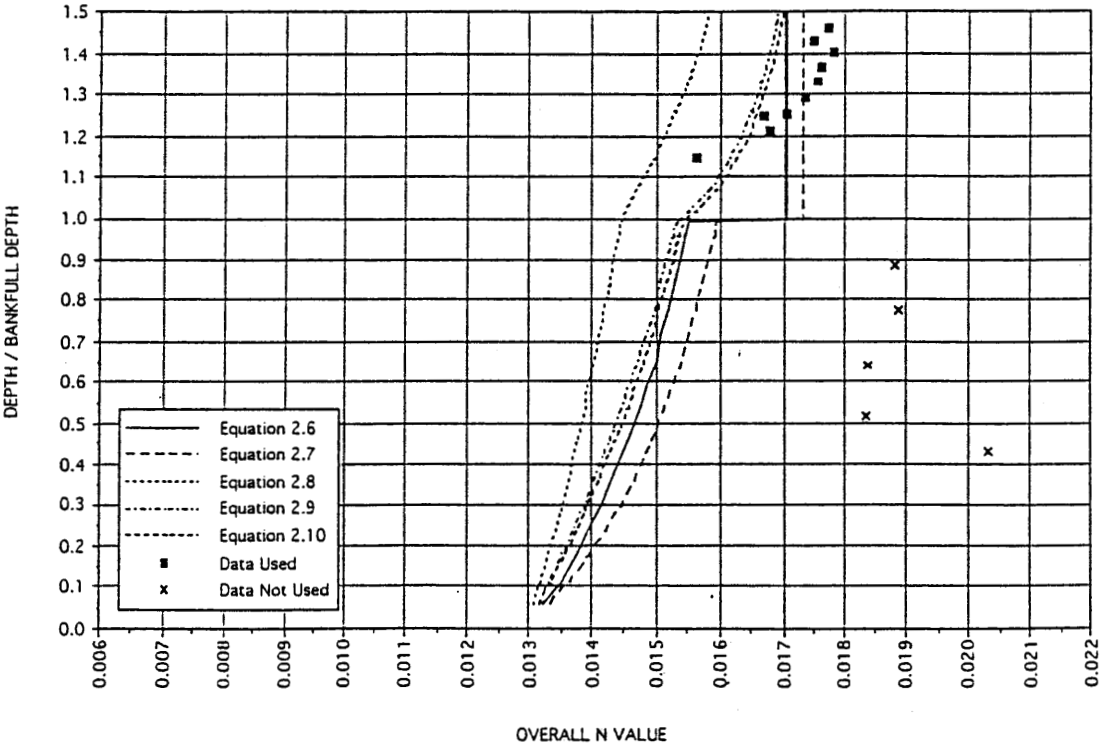

Figure 4.25b Experimental data versus equations 2.6 to 2.10 (bisectional subdivisions) for BGGGG data series

- The slope for the MC above bankfull stage was gentler for the BGGGG series than the GGGGG series. Considering that the intersection of MC and FP were almost at the same location, one can predict that the MC carried more discharge at low y/D ratios above bankfull stage for the BGGGG series.

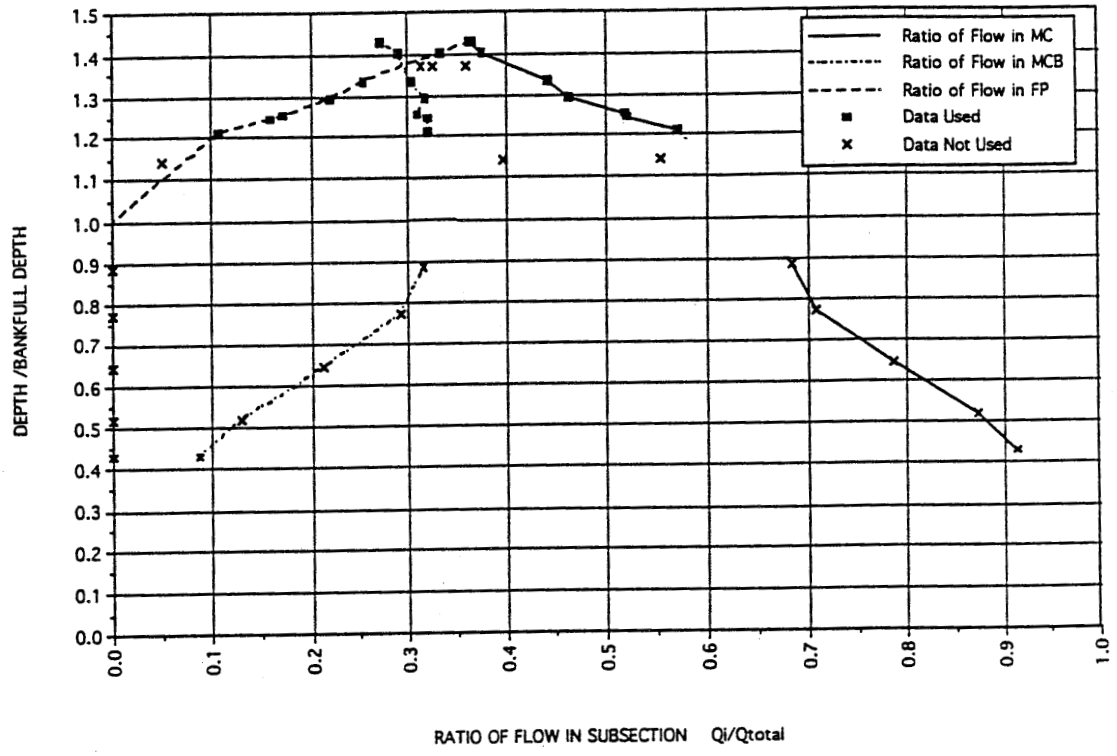

Figure 4.26 Division of flow among subsections for BGGGG data series

Overall, the BGGGG data series indicates that changing the roughness in the MC does have more noticeable effects on the variation of the n_o pattern than similar changes in the FP, due to changes in flow distribution and hence energy losses. The BGGGG series indicates a gentler slope (more rapid changes in n_o) than GGGGG series for depths just above bankfull.

4.4.2. GBBBB Data Series

The GBBBB data series was designed to investigate the effect on n_o due to rough bed and smooth sidewall in the MC. However, only two of the 14 datasets were considered to be good quality. It was extremely difficult to establish steady uniform flow for this roughness combination. More examination will be needed to explain the causes

for the instabilities. The data are presented in figure 4.27. With two good data values and some "unused data" surrounding the y/D axis, one can infer the general magnitudes of n_o.

The n_o value in the MC was about the same magnitude as for the BGGGG series at y/D > 0.6 (figure 4.27). The data point below y/D = 0.6 was affected by a low Reynolds number, similar to the point in the BGGGG series at y/D < 0.5. Above bankfull stages, the maximum n_o value was about 0.017, less than for the BGGGG series.

Vertical Division Method. Figures 4.27a and b show the trend of equations 2.1 to 2.10 with vertical subdivision. The predicted n_c in the MC decreased with increases in y/D, indicating that the equations were affected by the base n values. Equations 2.1 to 2.7 predicted much lower n_c values than equations 2.8 to 2.10, while experimental data showed increasing n_o over y/D. Above bankfull stage, all equations predicted much lower n_c than n_o.

Bisectional Division Method. Figures 4.28a and b show the variation of equations 2.1 to 2.10 with bisectional subdivision. Similar observations can be made as in other cases, with no significant improvement in the data fit.

Flow Distribution. Figure 4.29 shows the flow distribution for the GBBBB data series. Only two data points were considered of good quality. One can infer that the most obvious changes occurred above bankfull stage as compared to the BGGGG series. Between 1.2 < y/D < 1.4, where data were available, GBBBB appeared to have more flow in the FP and less flow in the MC for the same y/D. The FP and MC curves intersected at y/D below 1.4 for this case, but above 1.4 for the BGGGG series.

4.4.3. *Summary*

Table 4.2 presents the best fitted n_o values retrieved from the experimental data series. It can be seen that reducing roughness in the MC (BGGGG) caused an overall reduction in n_o throughout the range of depths tested, as compared to GGGGG data. Complete changes in floodplain roughness, on the other hand, result in different n_o at higher floodplain depths as demonstrated earlier. The effect of using smooth sidewalls is to further reduce the overall n_o.

Table 4.2. Fitted n_o Values at Selected y/D for Different Main Channel Roughness

	y/D ratios								
Series	*1.05*	*1.1*	*1.15*	*1.2*	*1.25*	*1.3*	*1.35*	*1.4*	*1.45*
GGGGG	.0147	.0159	.0167	.0172	.0177	.0180	.0182	.0185	.0186
BGGGG	.0135	.0148	.0159	.0165	.0170	.0173	.0175	.0177	.0178
GBBBB	.0132	.0145	.0153	.0159	.0164	.0167	.0168	.0169	.0170

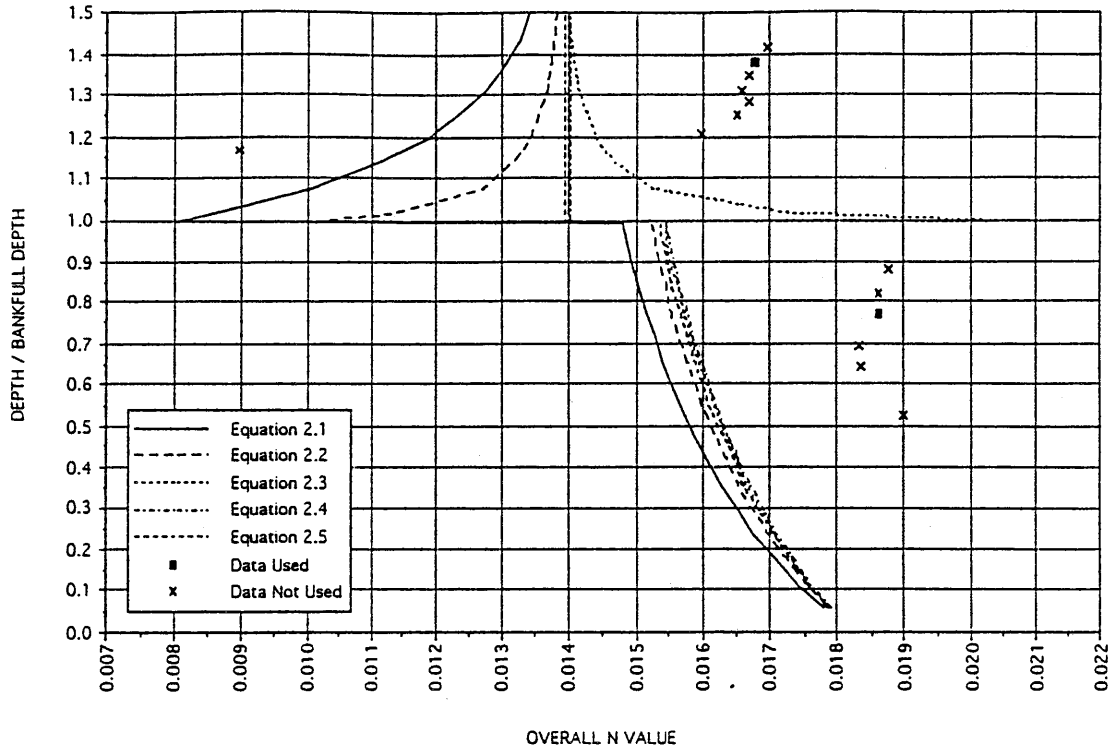

Figure 4.27a Experimental data versus equations 2.1 to 2.5 (vertical subdivisions) for GBBBB data series

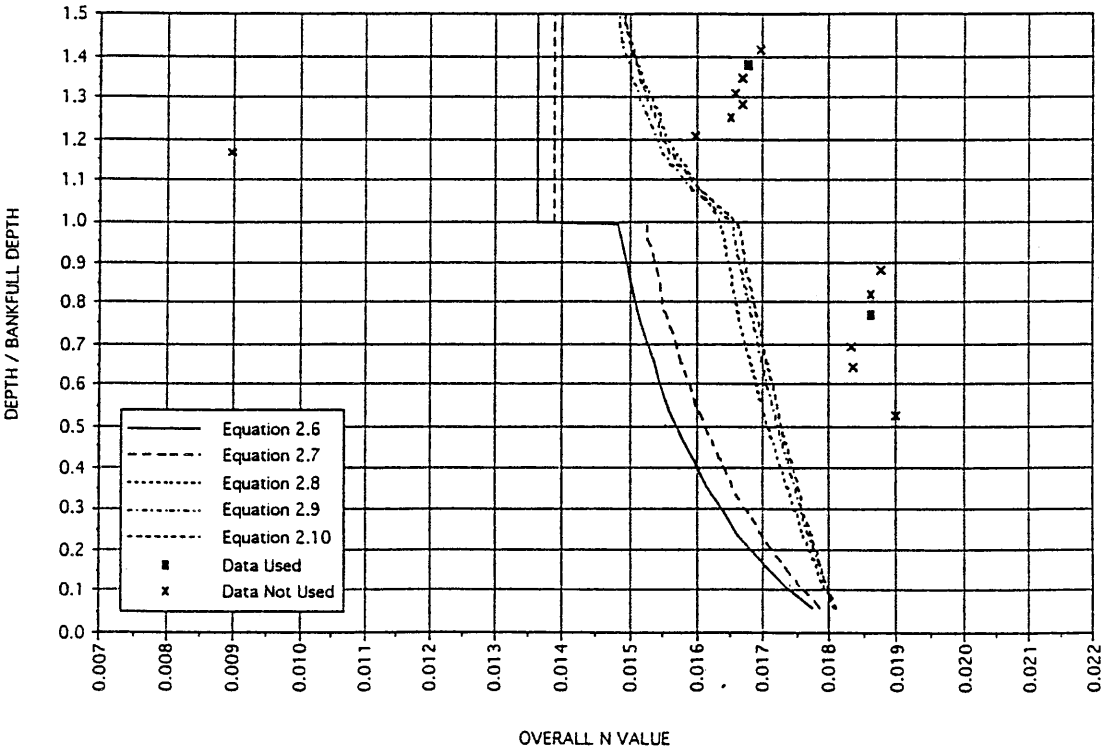

Figure 4.27b Experimental data versus equations 2.6 to 2.10 (vertical subdivisions) for GBBBB data series

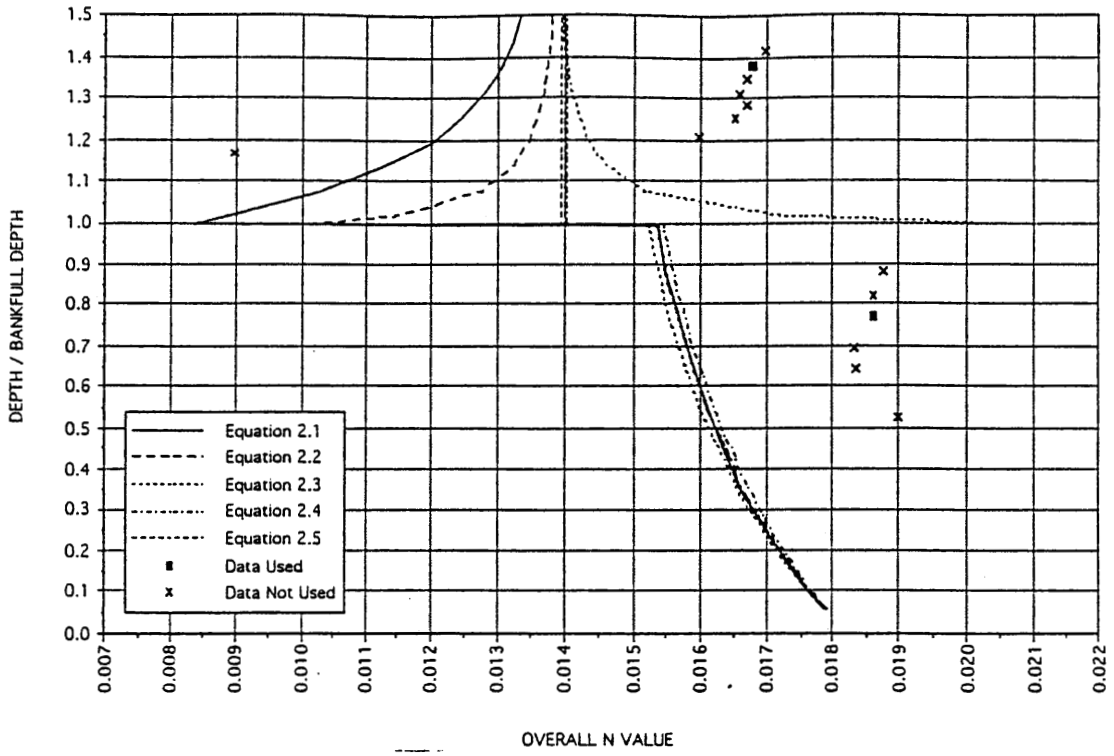

Figure 4.28a Experimental data versus equations 2.1 to 2.5 (bisectional subdivisions) for GBBBB data series

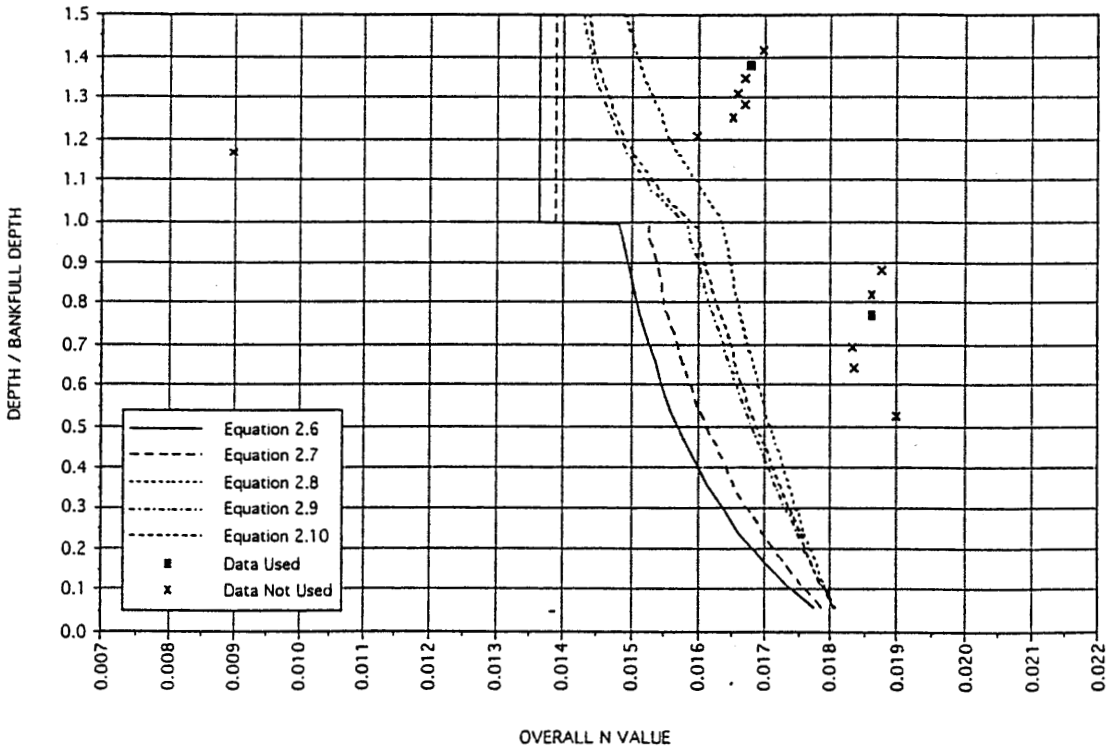

Figure 4.28b Experimental data versus equations 2.6 to 2.10 (bisectional subdivisions) for GBBBB data series

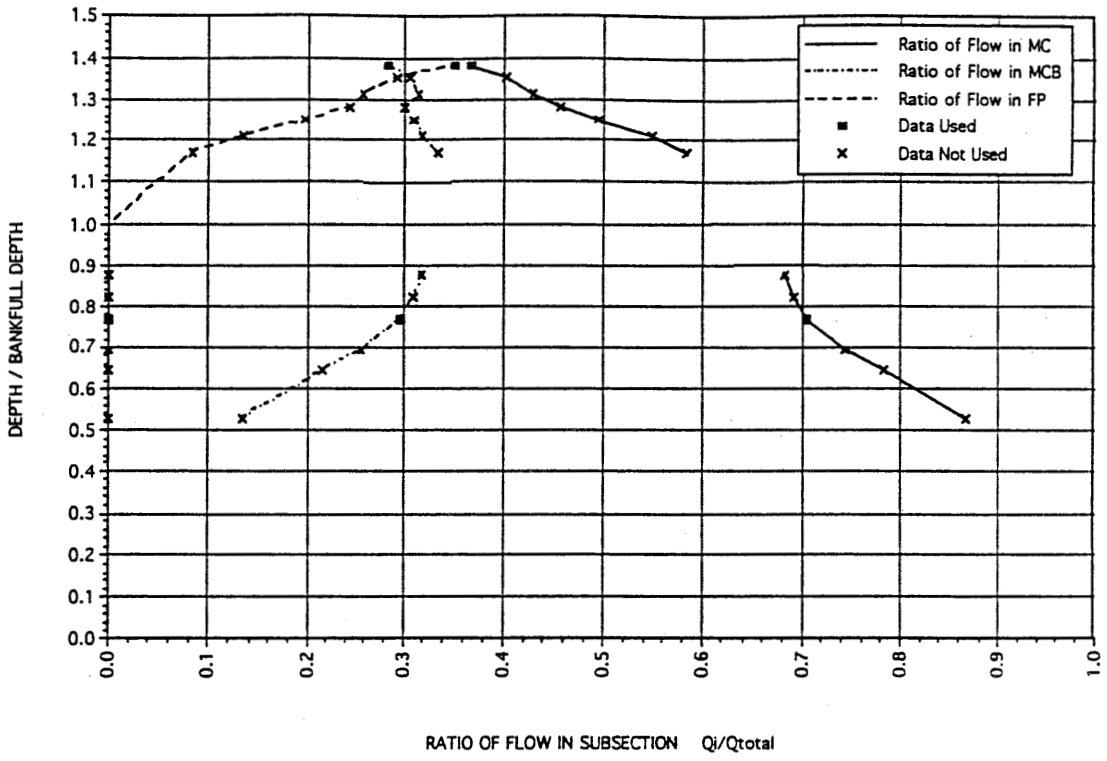

Figure 4.29 Division of flow among subsections for GBBBB data series

4.5. Effects of Floodplain Roughness nearest the Main Channel

Interactions between the MC and FP account for the discrepancies in estimating total discharge, as suggested by many researchers. The effect of roughness in the area next to the MC is examined here. The group of experiments that can be used include the BBSGG and BBGGG series presented before and the BBBGG and BBSBB series presented here. Note that the BBGGG, BBSBB, and BBSGG data series were conducted at the same channel slope, 6.173E-04, while the BBBGG data were conducted under a slope of 7.93E-04.

4.5.1. BBBGG Data Series

The BBBGG data series consisted of 13 datasets. Of these, seven were considered useful and they were all located above bankfull stage. The quality of the data is considered to be moderate. The six samples taken from below bankfull stages were not used, which again reflects the difficulties in establishing steady uniform flow in the MC.

In general, the data series showed that the maximum n_o for stages below bankfull stage (approximately 0.0142, figure 4.30) was higher than the BBBBB and BBSSS series

(approximately 0.0136), as seen previously. The latter two series were conducted at a slope of 6.173E-04. Above the bankfull stage, n_o varied between a y/D of 1.2 and 1.4, and reached a maximum value of around 0.015 at y/D = 1.4. After y/D > 1.42, n_o somehow decreased.

Compared to figure 4.21 of the BBGGG series, the present n_o values actually appeared to be higher than the BBGGG data. The only noted difference was the channel slopes for these two tests. Another possible explanation lies in the fact that the gravel elements were repaired prior to the BBBGG tests. The repair involved some patching-up due mostly to moving elements around the channel. New gravel was added to worn elements until they were visually similar to the unworn elements. The BBBGG data series were the last experimental datasets taken. Since it is not reasonable to expect higher n_o from BBBGG than from BBGGG series, this data group should not be used in comparisons to other datasets.

Vertical Division Method. Figures 4.30a and b show the variation of equations 2.1 to 2.10 with depth. Here one can see that the basic trend and values of the experimental data were predicted relatively well by equation 2.2.

Bisectional Division Method. Figures 4.31a and b show the effect of using bisectional subdivision for the BBBGG series. Equation 2.2 improved its prediction even more in this case.

Flow Distribution. Figure 4.32 shows the flow distribution among the various subdivisions for the BBBGG case. Although this data group will not be used for general comparisons, it still showed that the MC and FP ratios crossed at approximately 1.42 times the floodplain depth.

4.5.2. BBSBB Data Series

The intent of the BBSBB data series was to show the effect of changing a single element nearest the MC, for comparison to the BBBBB series. The BBSBB data series consisted of 10 data points, five of which were used in the later analysis. For depth below bankfull stage, maximum n_o was about 0.0142, which is reasonable. In the MC, the n_o value was very similar to that obtained in the BBBBB series. Above bankfull stage, the data became rather scattered. However, if the point of n_o = 0.0138 at y/D = 1.26 is excluded, then there is a trend of n_o, which rose from a low value at y/D > 1.0 and approached an asymptotic value after y/D > 1.3, with a maximum value of around .0134.

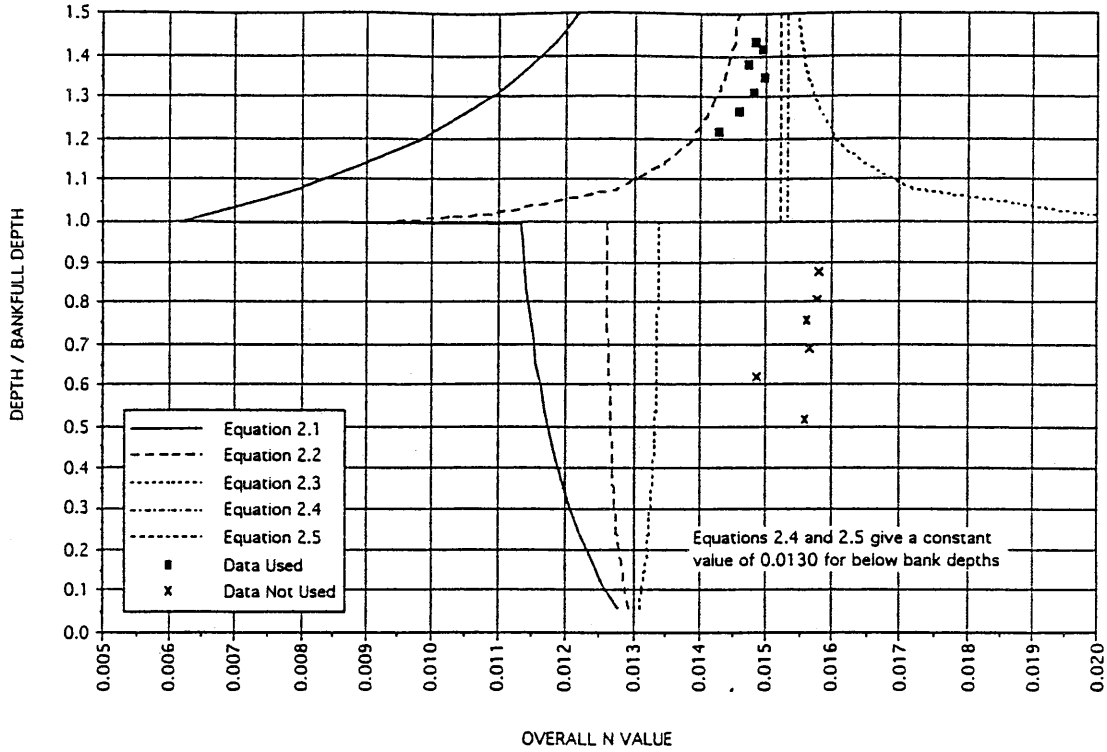

Figure 4.30a Experimental data versus equations 2.1 to 2.5 (vertical subdivisions) for BBBGG data series

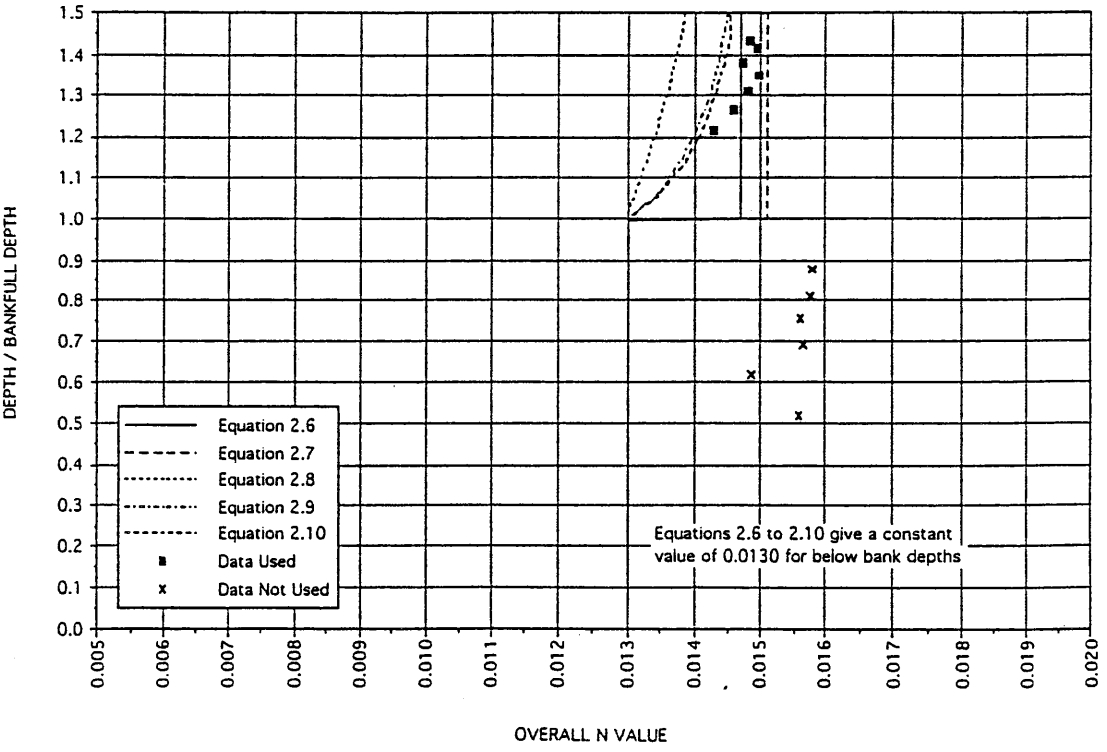

Figure 4.30b Experimental data versus equations 2.6 to 2.10 (vertical subdivisions) for BBBGG data series

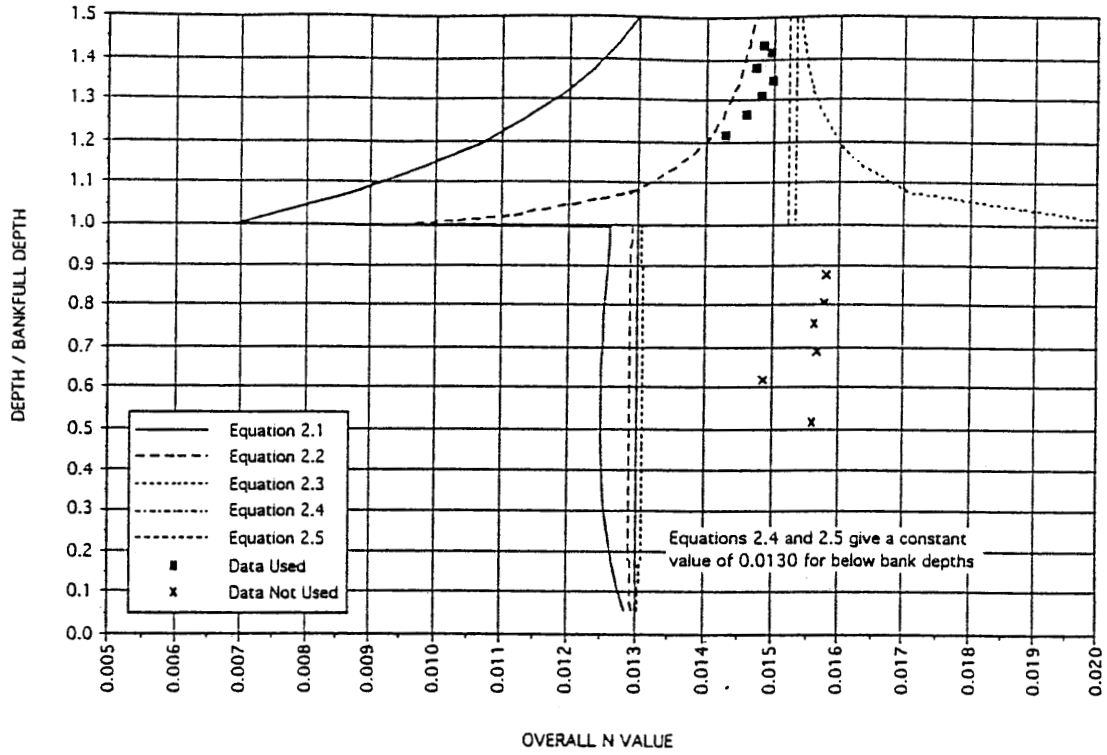

Figure 4.31a Experimental data versus equations 2.1 to 2.5 (bisectional subdivisions) for BBBGG data series

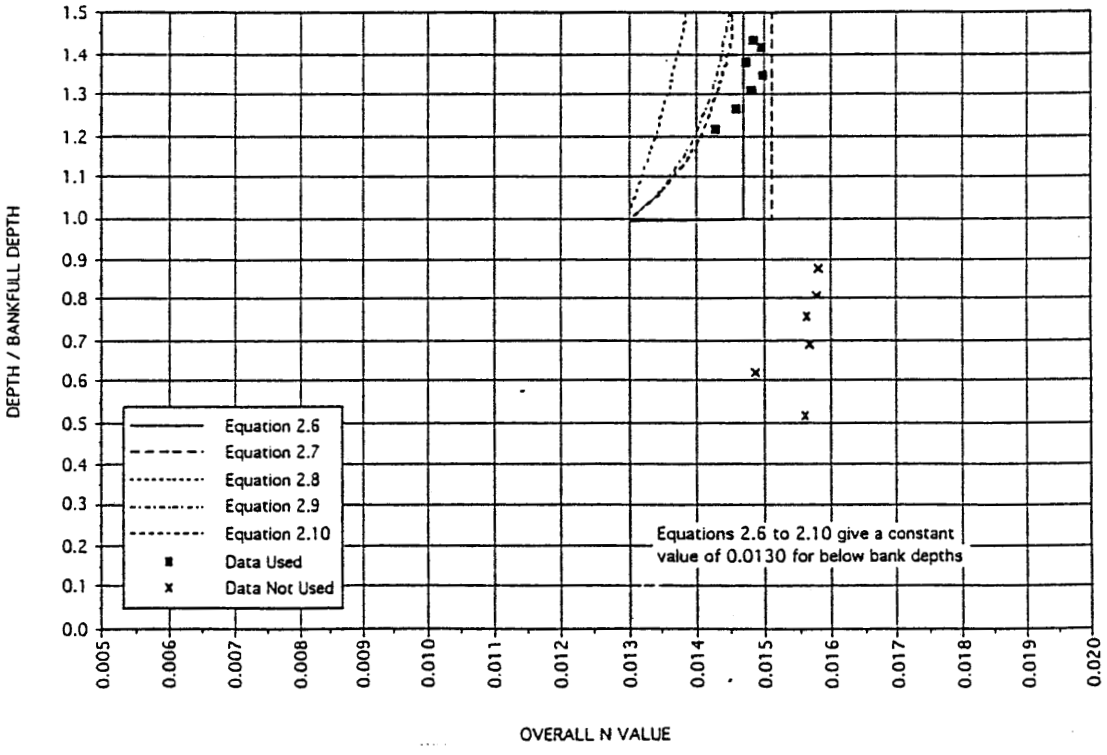

Figure 4.31b Experimental data versus equations 2.6 to 2.10 (bisectional subdivisions) for BBBGG data series

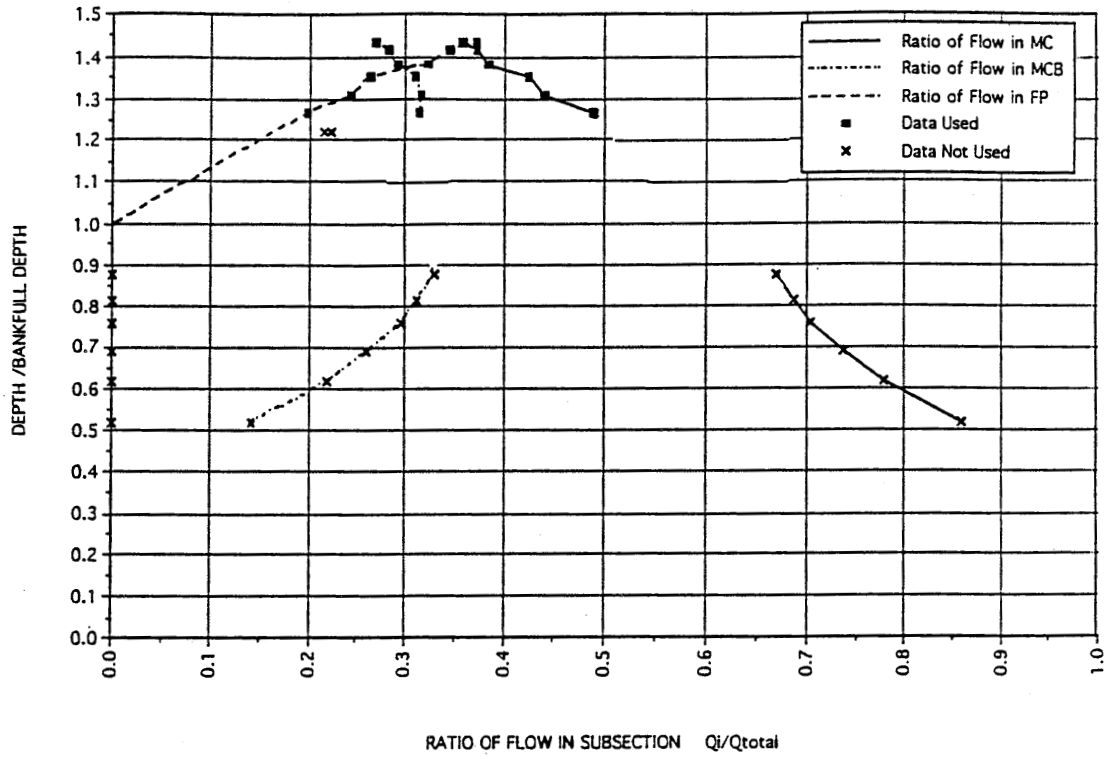

Figure 4.32 Division of flow among subsections for BBBGG data series

Vertical Division Method. Figures 4.33a and b show the variation of equations 2.1 to 2.10 with depth. The effects of different roughness on numerical computation were obvious, but the actual measured differences between BBSBB and BBBBB were not significant.

Bisectional Division Method. Figures 4.34a and b show the effect of bisectional subdivision on the predictions of equations for the BBSBB data series. Again, the predictions of equation 2.2 were more accurate for the BBBBB case than for the BBSBB case.

Flow Distribution. Figure 4.35 shows the variation of the flow distribution for the BBSBB case. When compared with figure 4.11 of the BBBBB series, the distributions in the MC, MCB, and FP above bankfull stage were about the same.

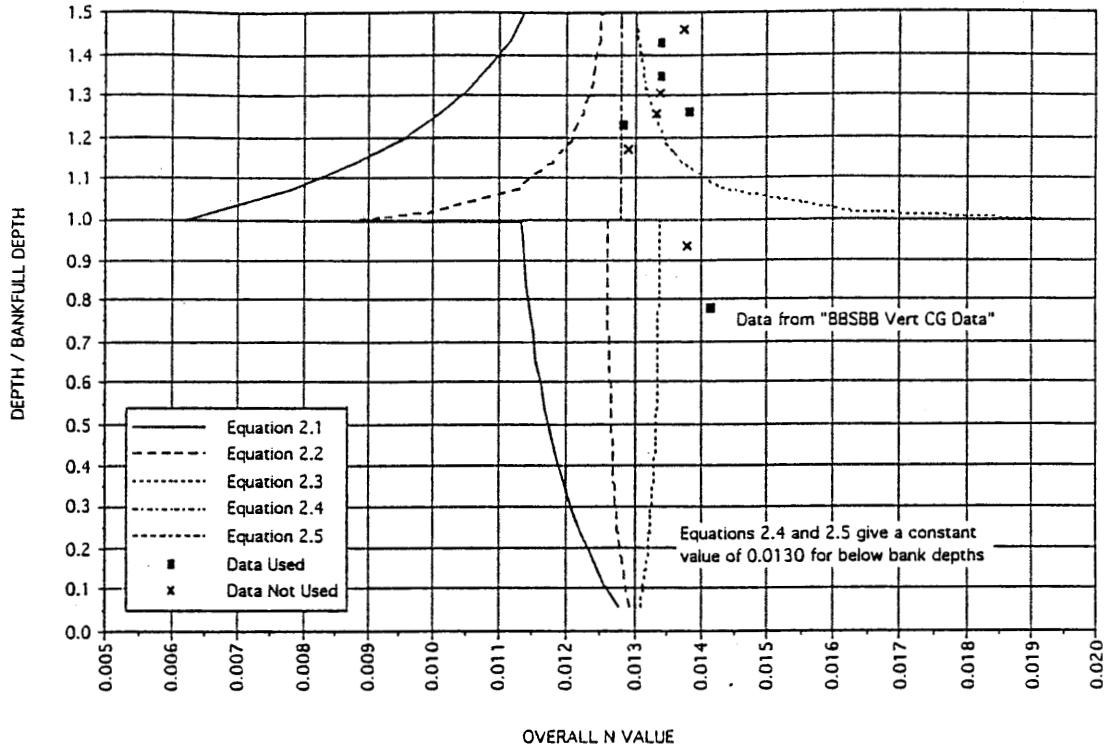

Figure 4.33a Experimental data versus equations 2.1 to 2.5 (vertical subdivisions) for BBSBB data series

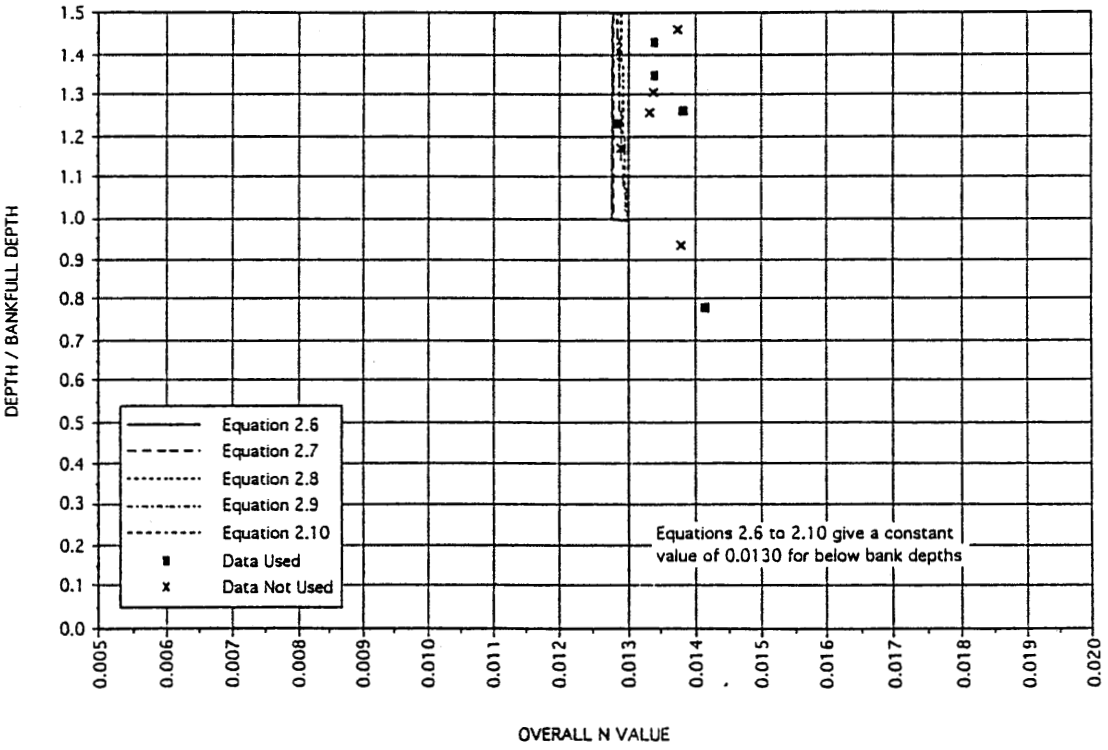

Figure 4.33b Experimental data versus equations 2.6 to 2.10 (vertical subdivisions) for BBSBB data series

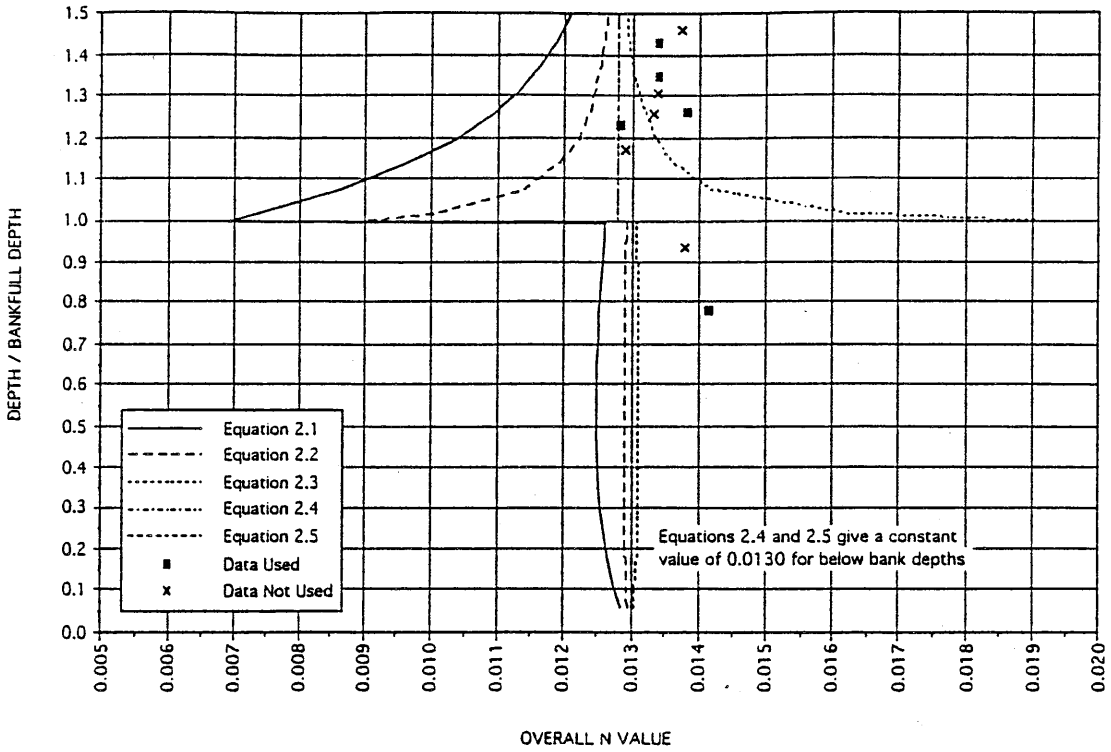

Figure 4.34a Experimental data versus equations 2.1 to 2.5 (bisectional subdivisions) for BBSBB data series

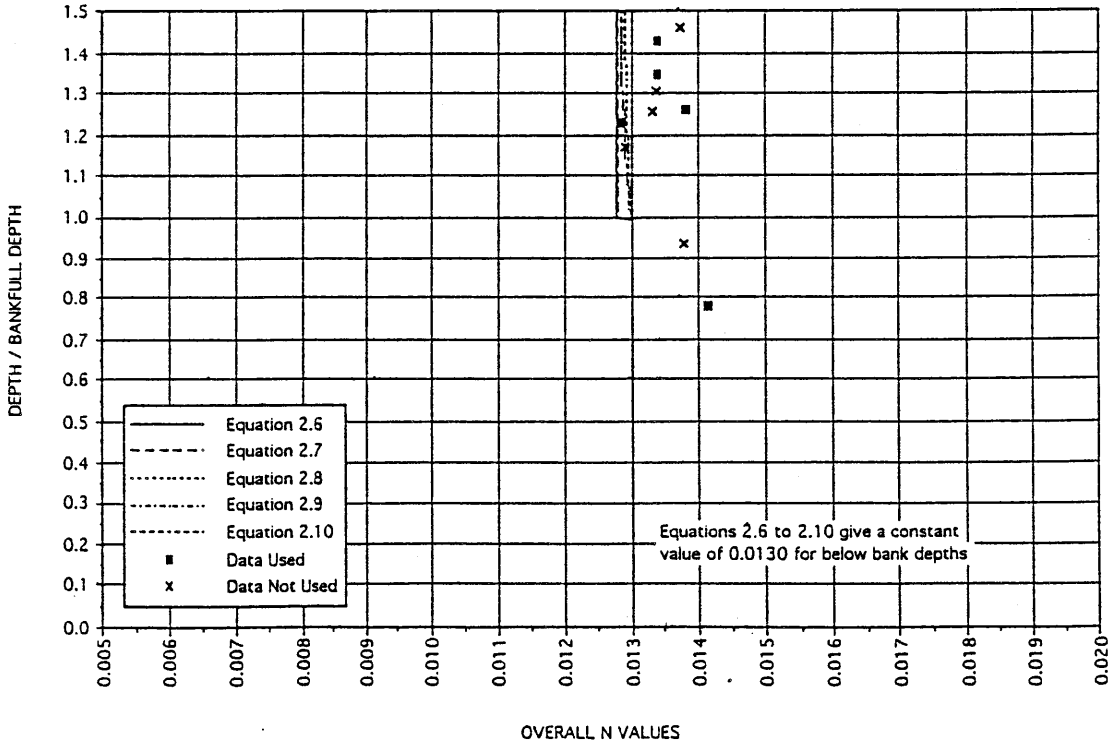

Figure 4.34b Experimental data versus equations 2.6 to 2.10 (bisectional subdivisions) for BBSBB data series

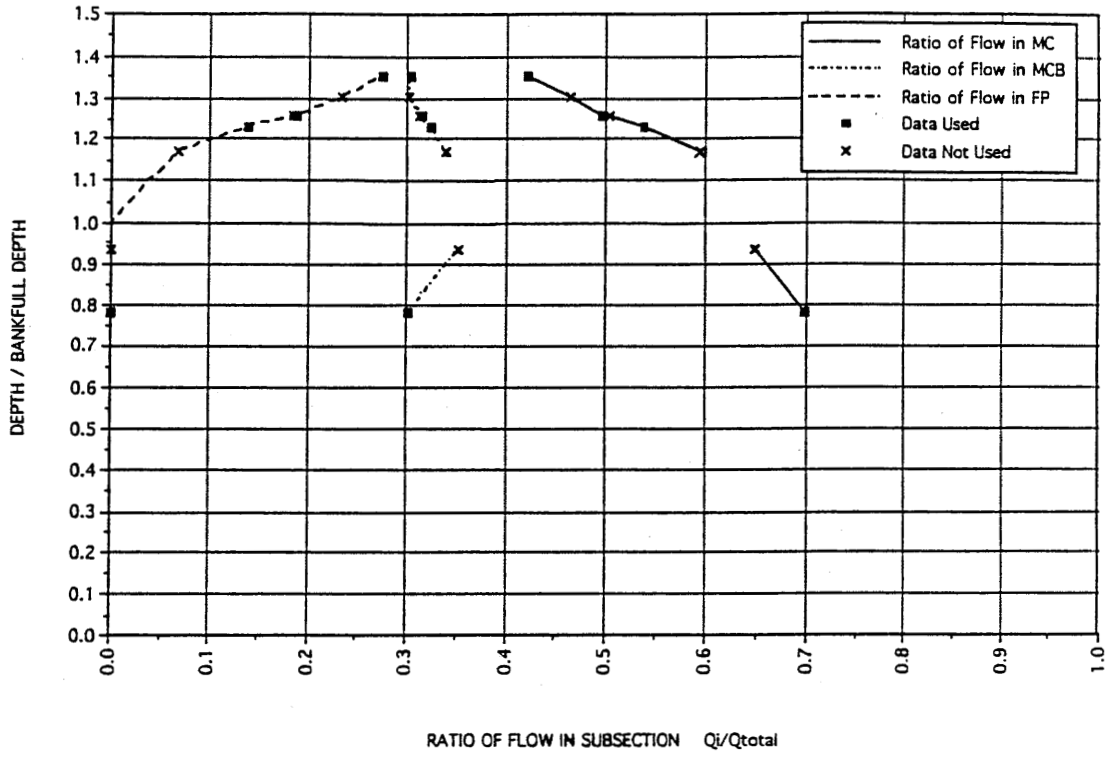

Figure 4.35 Division of flow among subsections for BBSBB data series

5. DATA FROM OTHER STUDIES

The effects of factors such as cross-sectional geometry and bed slopes were investigated using data adapted from other laboratory studies. Some data, such as those from Pillai (1962), were used directly for our purposes; most other data were related to studies on compound channel flows and required some processing for use in this project. All data from other studies are presented in a format identical to the one used for this report.

5.1. Myers and Brennan (1990): Effects of Floodplain Width

The data of Myers and Brennan were selected because their experiments were carried out in a large, realistically sized channel. Although the roughness of the channel boundary was uniform and quite smooth in comparison to the roughness generally found in natural rivers, the data had the advantage of being in a high Reynolds number range (see table 2.2). Another important aspect of their data was that they varied the width of the floodplain. Since the roughness was kept the same for all tests, the geometric effects could be isolated.

On the other hand, the base n value of the tests was not given. Evaluations of all composite roughness equations should begin with a well-judged base n value. Up to now it was understood that adjusting the base n values could artificially fit an equation better to experimental data, which apparently is not correct. The base n values have to be determined on the basis of the composition of boundary roughness. For Myers and Brennans' study, the base n value was derived by averaging all calculated n_o values.

Figure 5.1 shows the geometry of each channel section tested by Myers and Brennan. They referred to the geometry by the ratio of the floodplain half-width (B) to the MC half-width (b). We shall retain their nomenclature here.

5.1.1. Geometry 1.2 - A Trapezoidal Channel

This case serves to verify the variation of the Manning n value in a trapezoidal channel with uniform roughness. Geometry 1.2 had a much wider B/D ratio (D being the MC depth) than the present project, however. The MC depth of Myers and Brennans' experiment was only 0.492 feet while the bottom width was 4.921 feet. Such a ratio can be considered a wide channel. Also note that the total channel depth for geometry 1.2 was twice as high as in other Myers and Brennans' tests (identified as 2D in the analysis).

The recalculated n_o values are presented as shaded squares in figure 5.2, which shows a slight increase in the measured n_o at $y/D < 0.5$, most probably due to the effects

FOR ALL CHANNELS:

Manning n value of all walls:	0.0100
Bed Slope:	1.027E-03
Main Channel Depth:	0.492 feet
Main Channel Bottom Width:	4.921 feet
Sidewall Slopes: (except Geom 6.67)	1:1

Figure 5.1 Channel geometry for Myers and Brennan experimental series (1990)

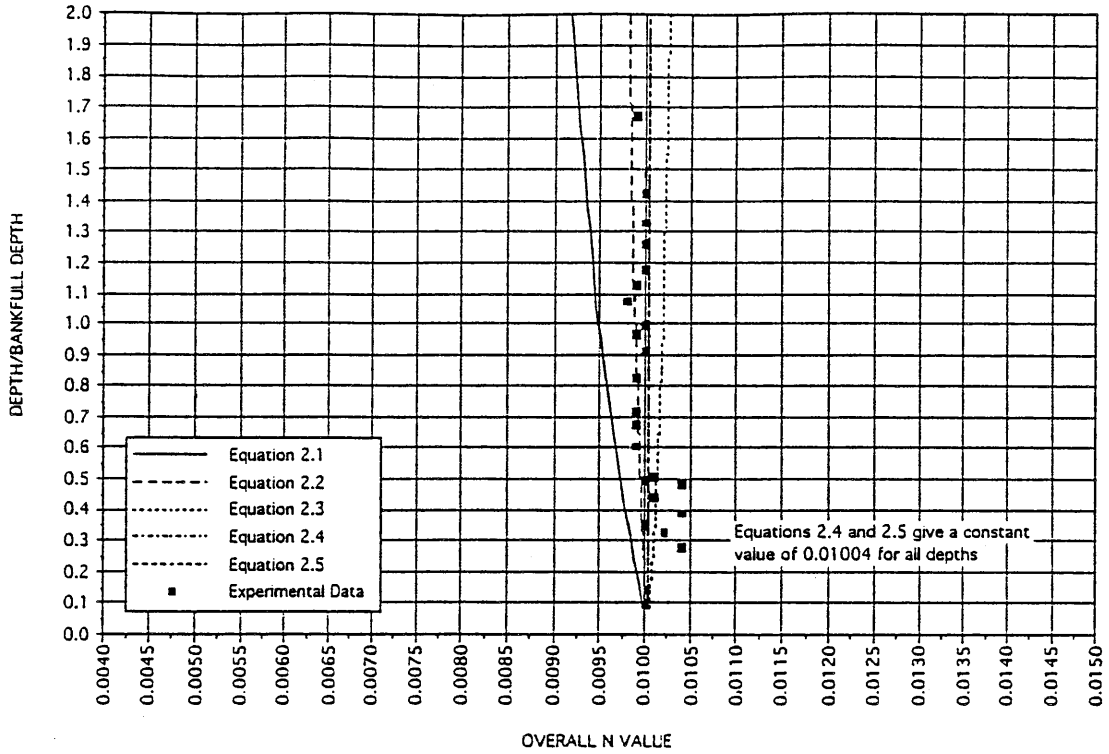

Figure 5.2a Myers and Brennan - Geometry 1.2 data versus equations 2.1 to 2.5

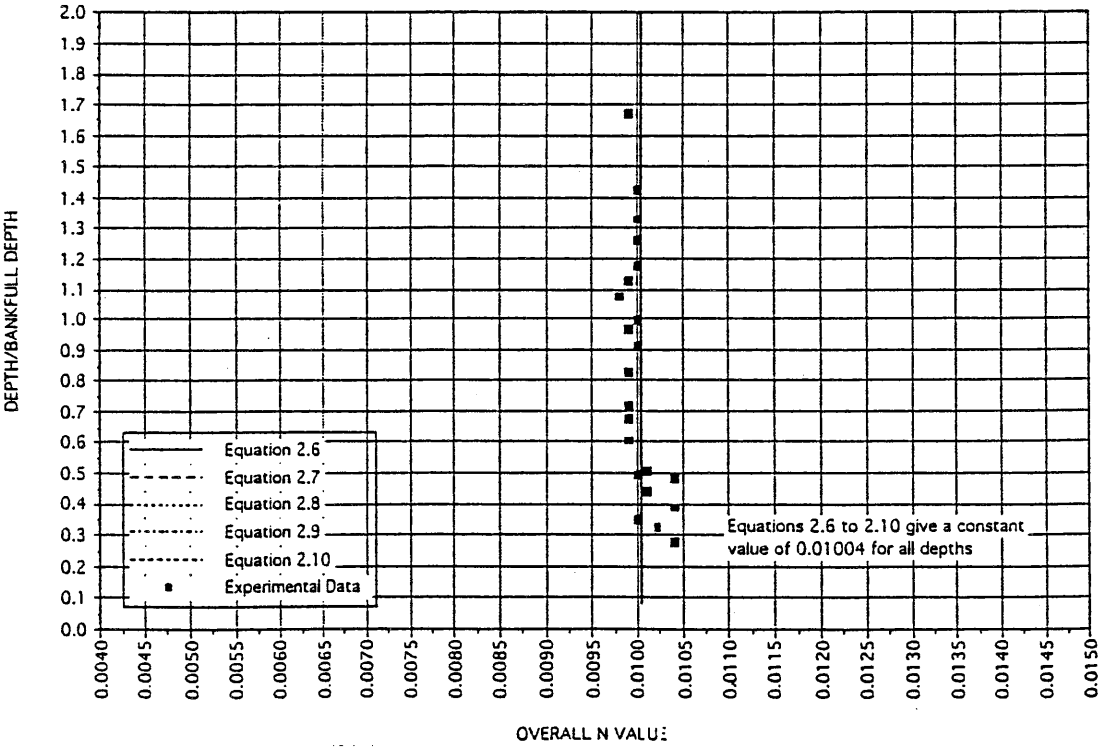

Figure 5.2b Myers and Brennan - Geometry 1.2 data versus equations 2.6 to 2.10

of low Reynolds numbers. Previously we found similar patterns in BBBBB and BGGGG series (see figures 4.9 and 4.24). At $0.5 < y/D < 1.0$, n_o became lower rather than higher than the base n value, contradicting the present findings that higher n_o is expected as y/D increases in the MC. The base n value so determined may also affect such comparisons. The overall variation of n_o was small and should be reasonably considered as constant.

Comparisons of Equations Using Vertical Division. Also shown in figures 5.2a and b are the predicted n_c values from equations 2.1 to 2.10. Equations 2.4 to 2.10 predicted a constant value equal to the determined base n value. As before, equations 2.1 and 2.2 predicted lower n_c and equation 2.3 predicted higher n_c at increasing y/D. Because of the very small base n value, their predictions are also close.

5.1.2. Geometry 2.2 - Symmetrical Compound Channel with B/b = 2

The measured data plotted in figure 5.3 reveal more information for the range of shallow floodplain depths. The data show that n_o reduced to .0072 at just above bankfull stage, a 28% reduction, then rebounded close to the base n at y/D around 1.45. After $y/D > 1.45$, n_o fluctuated slightly but the asymptotic value was that of MC n_o. This is a similar pattern to the BBBBB and GGGGG series.

Comparisons of Equations Using Vertical Division. The variation of equations 2.1 to 2.10 is shown in figures 5.3a. and b. The experimental data matched equation 2.1 at the lowest floodplain depths; the variation of n_o between y/D 1.0 and 1.4 was bracketed by equations 2.1 and 2.2; and equation 2.2 predicted well at higher floodplain depths. For this test, equations 2.4 to 2.7 and 2.9 to 2.10 predicted constant n_c, the asymptotic value at higher depths. Equation 2.8, based on the average depth in the subsections, predicted a decreasing trend of n_c at higher depths for this particular geometry.

5.1.3. Geometry 4.2 - Symmetrical Compound Channel with B/b = 4

With wider floodplain widths, the effect on n_o became more evident as shown in figure 5.4. The n_o value decreased to 0.0055 at a depth just above bankfull, about a 45% reduction from n_o before bankfull stage. The n_o value did not return to the original n_o for the MC as y/D increased.

Comparisons of Equations Using Vertical Division. Figures 5.4a and b relate equations 2.1 to 2.10 to the experimental data. Again equation 2.1 predicted well at very low floodplain depths, equations 2.1 and 2.2 bracketed the experimental data for the y/D range from 1.0 to 1.6, and equations 2.4 to 2.7 and 2.9 to 2.10 predicted constant n_o through the whole depth.

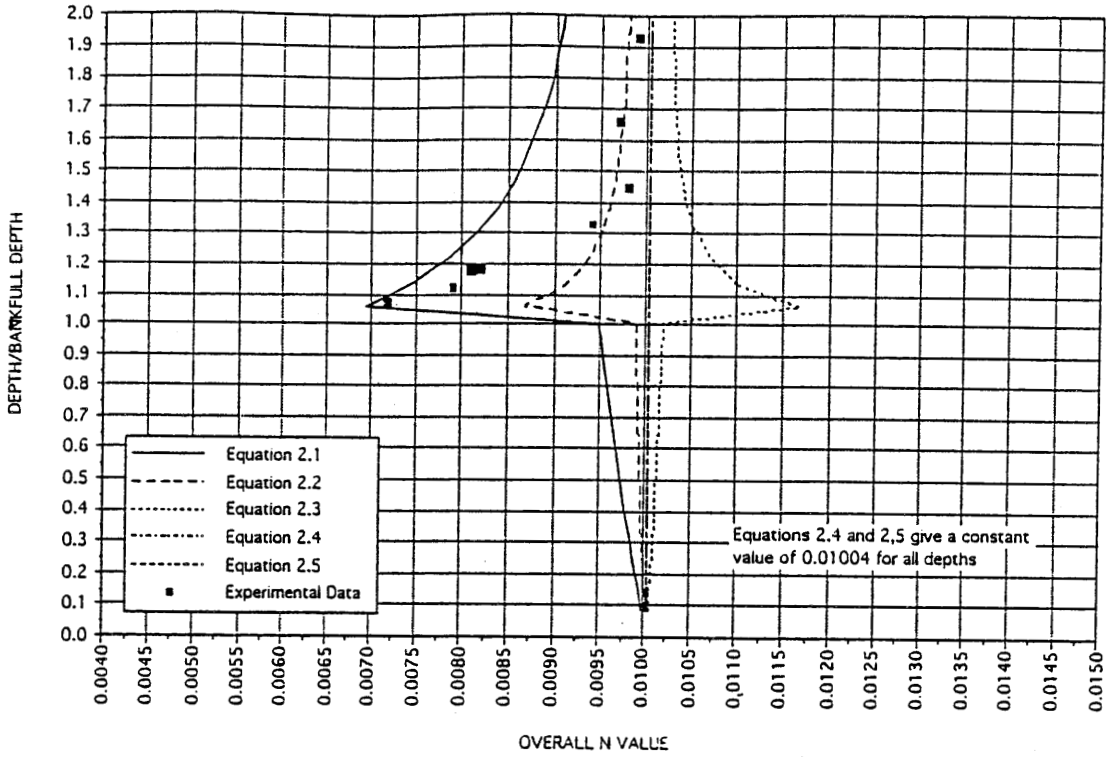

Figure 5.3a **Myers and Brennan - Geometry 2.2 data versus equations 2.1 to 2.5**

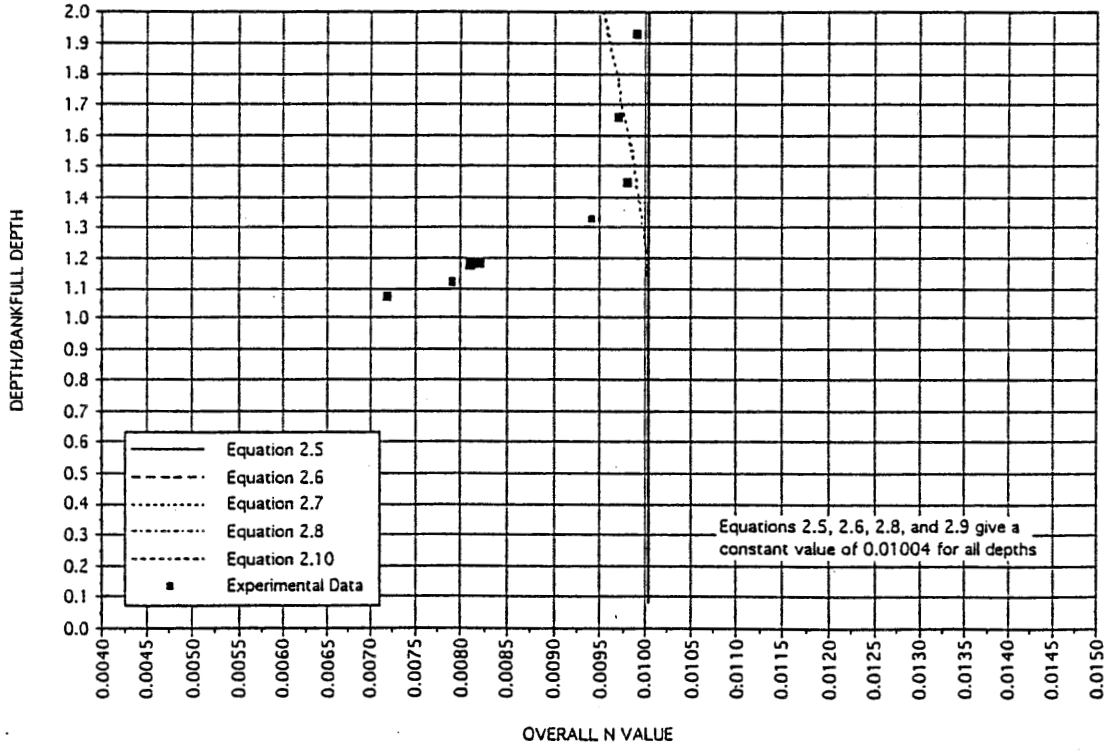

Figure 5.3b **Myers and Brennan - Geometry 2.2 data versus equations 2.6 to 2.10**

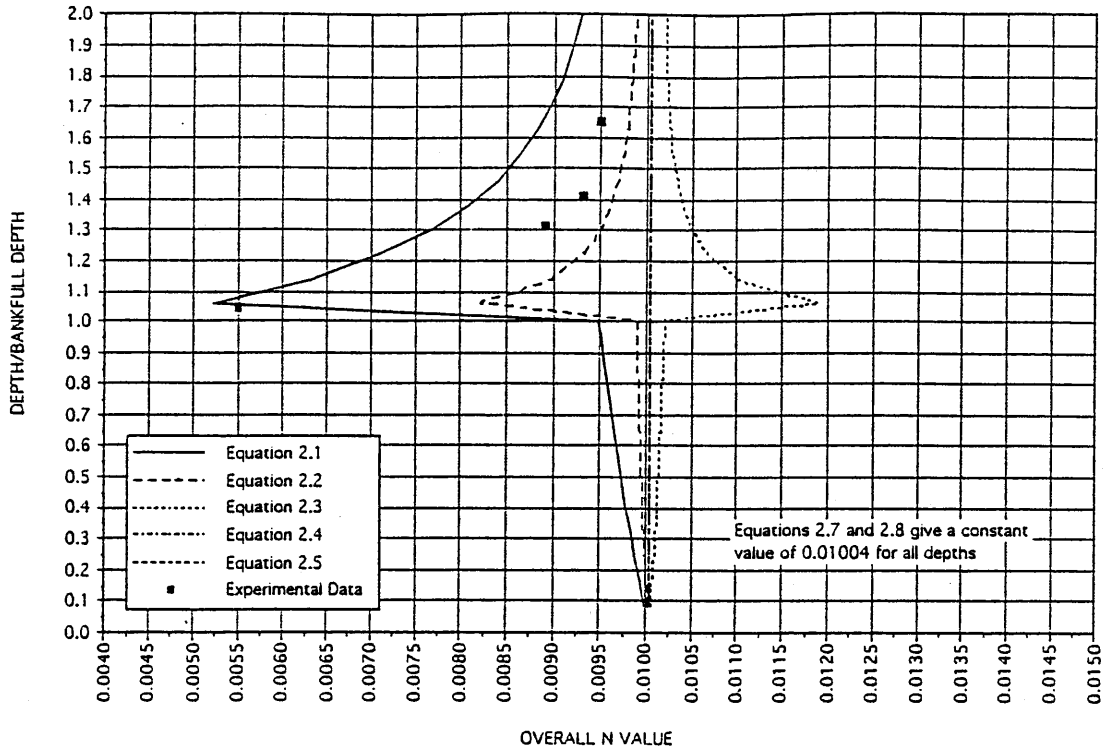

Figure 5.4a **Myers and Brennan - Geometry 4.2 data versus equations 2.1 to 2.5**

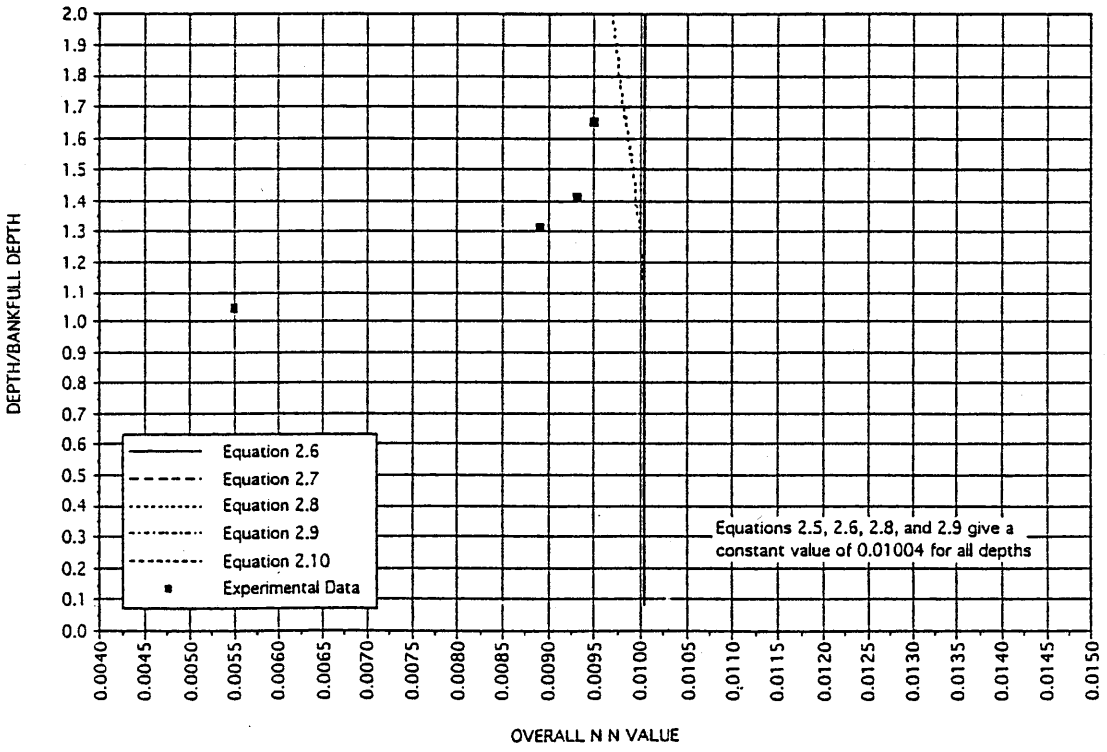

Figure 5.4b **Myers and Brennan - Geometry 4.2 data versus equations 2.6 to 2.10**

5.1.4. Geometry 6.67 - Symmetrical Compound Channel with B/b ≅ 6.4

This dataset contained a fairly large number of experimental runs that allowed a good comparison of the equations. The large wetted perimeter of the section also allowed the channel to be divided into many subareas to test the effect of the number of subdivisions used on the overall n value.

As shown in figure 5.5, the experimental n_o value at just above the bankfull stage was 0.0054, about a 46% reduction from n_o just before bankfull stage. This is very similar to the case for geometry 4.2. At shallow floodplain depths, most of the floodplain area is considered storage that does not contribute to total flows. Therefore, the MC and MCB area experienced higher velocity to pass through higher flows. As the y/D increased, n_o gradually increased. With more data points available, one can now see the tendency of n_o at higher y/D to approach the n_o before bankfull stage. This is similar to the authors' uniform roughness results, but Myers and Brennans' results extended to higher y/D.

Comparisons of Equations Using Vertical Division. Figures 5.5a and b show the variation of equations 2.1 to 2.10 versus the experimental data. As in previous comparisons, equation 2.1 fit the experimental data well at low floodplain depths, and equation 2.2 fit data well at high floodplain depths (y/D > 1.7). Considering the assumptions behind equations 2.1 (i.e., total discharge is the sum of discharge for each subarea) and 2.2 (total shear force is the sum of subarea shear forces), and their fitness to the experimental data at different floodplain depths, one can postulate that a single fit equation may have to be formed by the combination of these equations. Equations 2.4 to 2.10 predicted constant n_o over depth.

Comparisons of Equations Using Bisectional Division. Using the bisectional division method reduced the discrepancies between equations 2.1 and 2.2 as shown in the project's experimental data. The general result is that a slight improvement in equation 2.1 sometimes led to overestimation by equation 2.2 in n_o values. This method was tested here for the wide floodplain channel, and the results are shown in figure 5.6. Comparing figures 5.5a and 5.6a, one can see that the effect of using bisection subdivisions was similar to the previous observations. Equation 2.1 fit the data slightly better than equation 2.2. Equation 2.3 was not correct, and the performances of other equations were unchanged.

For the trapezoidal channel, the consequence of bisecting the channel was to reduce the area in the MC and increase that in the MCB. The wetted perimeter did not change because the imaginary division lines were not considered part of the wetted perimeter. Hence, the hydraulic radius for MC and MCB was the only parameter that changed, which led to different predictions in equations 2.1 to 2.3, as compared to the vertical division method.

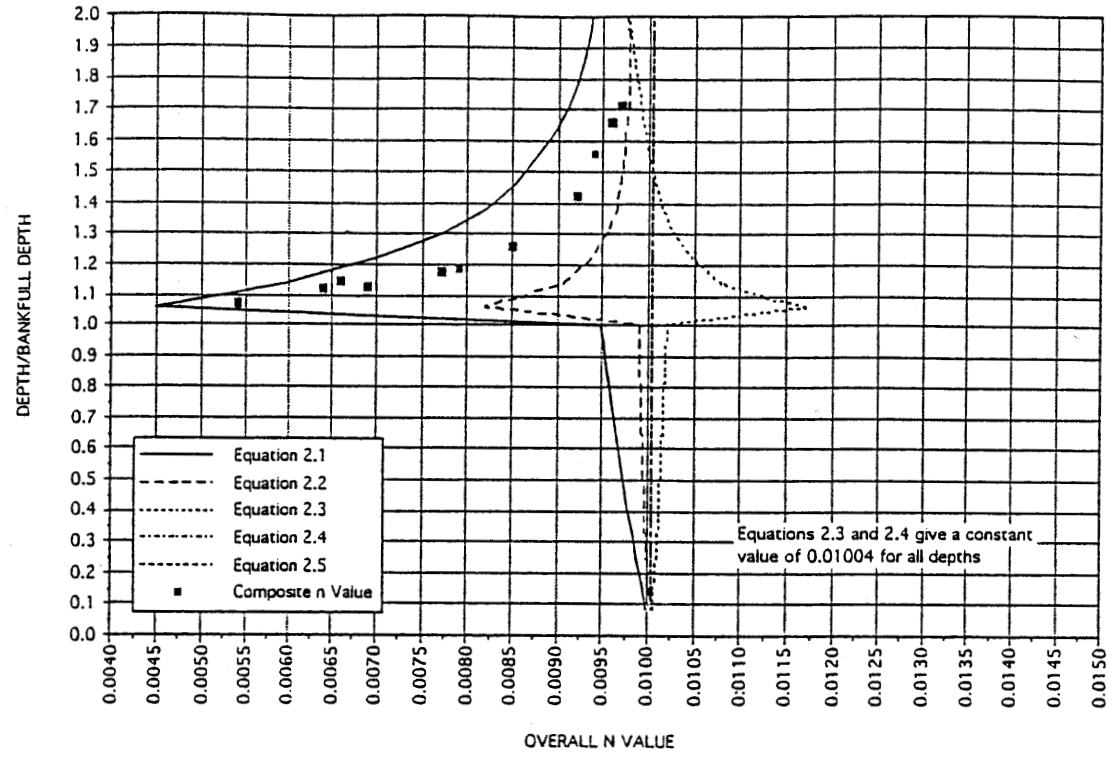

Figure 5.5a Myers and Brennan - Geometry 6.67 data versus equations 2.1 to 2.5

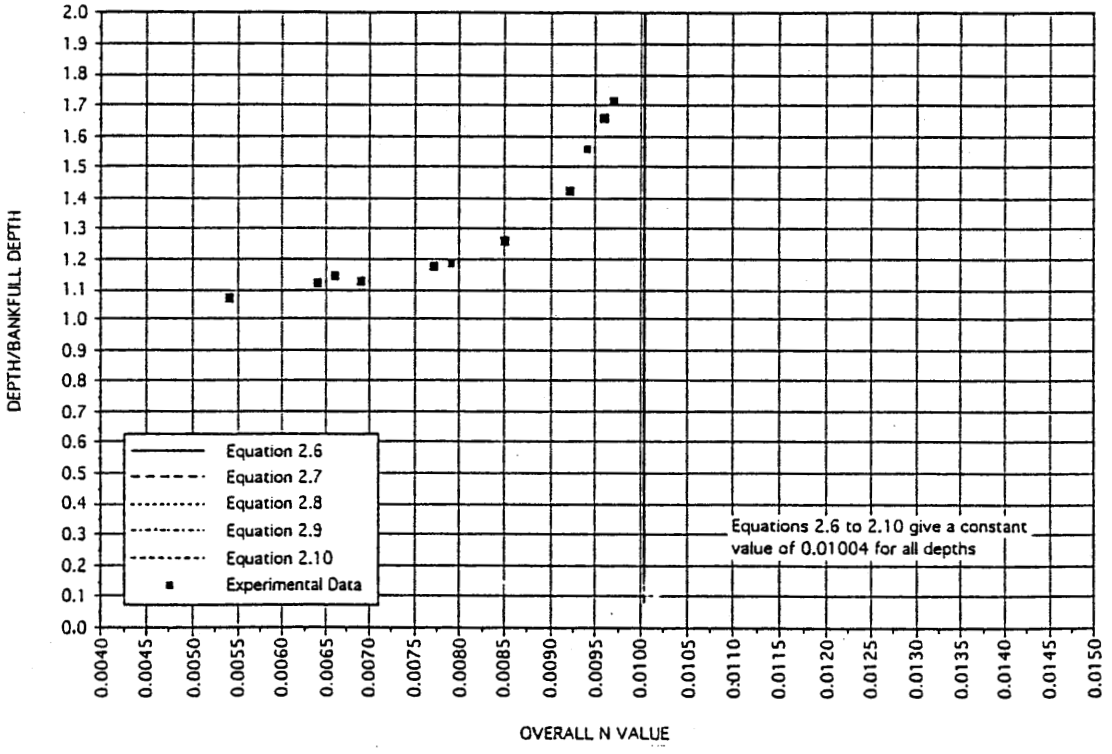

Figure 5.5b Myers and Brennan - Geometry 6.67 data versus Equations 2.6 to 2.10

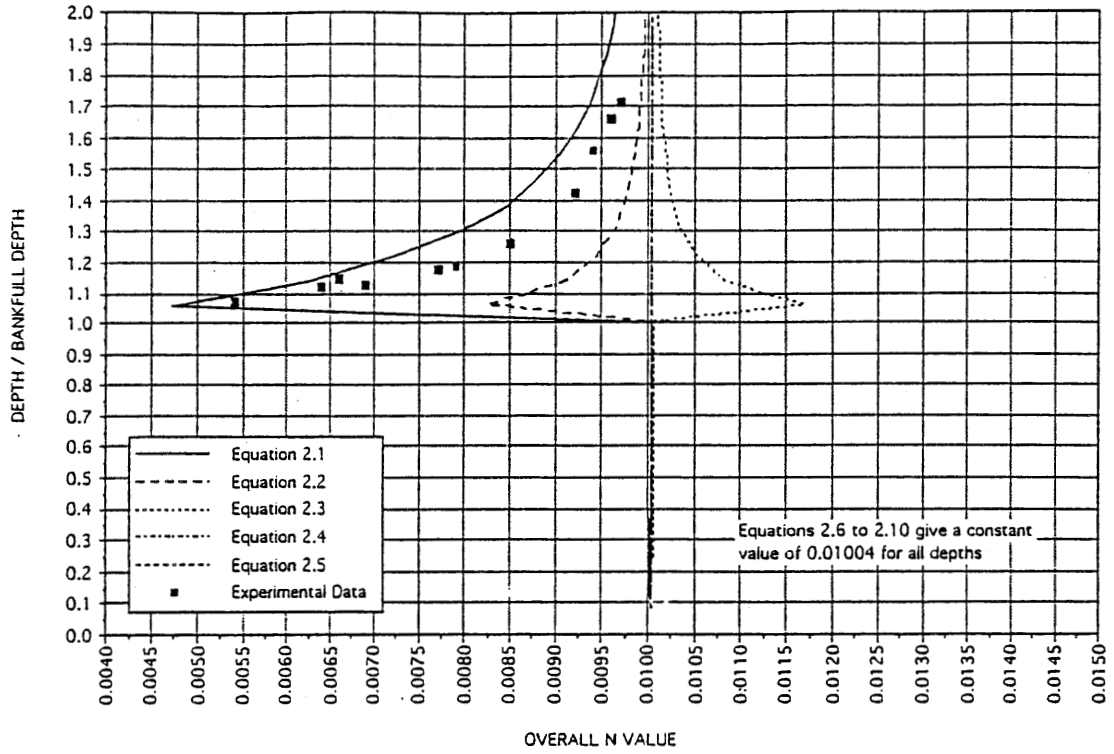

Figure 5.6a Myers and Brennan -- Geometry 6.67 data versus equations 2.1 to 2.5. Bisectional subdivision used in this plot

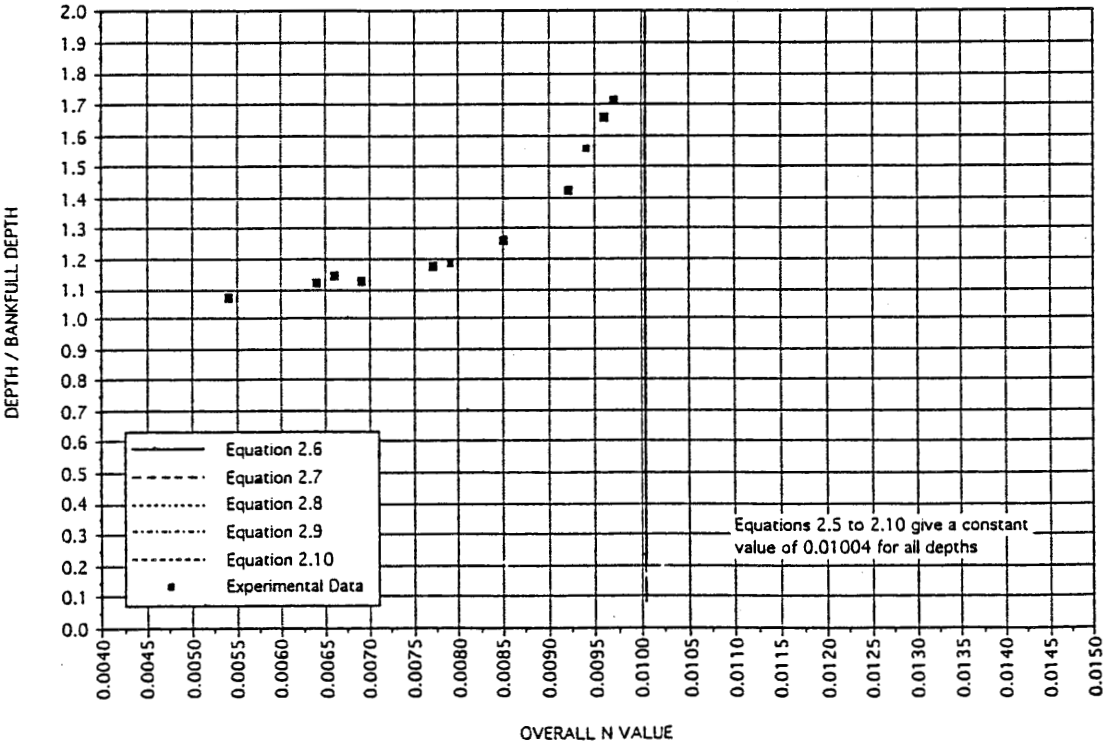

Figure 5.6b Myers and Brennan -- Geometry 6.67 data versus equations 2.6 to 2.10. Bisectional subdivisions used in this plot

5.1.5. Asymmetrical Geometry

Asymmetrical geometry is of particular interest not only for its effect on n_o values but also for comparison to the project's results, which are derived from a half-channel model. Using the same base roughness values as before, Myers and Brennan built a channel with a single floodplain next to the MC with a B/b ratio of 1.5 (see figure 5.1). The authors' experimental geometry had a B/b ratio of approximately 3.8; the MC depth to width ratios were quite different, however.

The retrieved n_o values are shown in figure 5.7. It can be seen that the general trend of n_o versus depth was preserved, but some differences (as compared to geometry 2.2) can be observed:

- Minimum n_o at a depth just above bankfull stage was 0.0066, approximately a 34% reduction from n_o just before bankfull stage.
- The n_o value tended to exceed the n_o of the MC and reach an asymptotic value. It reached the base n value in the y/D range of 1.4 ~ 1.5.
- Asymptotic n_o tended to exceed the base n value at higher y/D ratios.

Comparisons of Equations Using Vertical Division. Figures 5.7a and b show the results of equations 2.1 to 2.10 versus the experimental data. The asymmetrical geometry did not alter the prediction much except at lower floodplain depths. Equation 2.1 overestimated the n_o value at such depths in this case. Equations 2.4 to 2.10 all predicted a constant n_o value over depth.

5.1.6. Effect of the Number of Subsections

One untouched question is whether the number of subsections used will affect the results of these equations. A test was performed with the Myers and Brennan data on uniform roughness. Tests using between 5 and 66 subsections for the geometry 6.67 data series were prepared. Only vertical subdivisions are shown here. The bisectional subdivisions were evaluated for the 7 and 66 subdivision cases, and the results did not show significant variation from those for vertical subdivisions.

Figure 5.8 shows the effects of the number of subsections on computational accuracy. Clearly the number of subsections did not make a significant difference in the value obtained from equations 2.1 and 2.2. Slight variations in the values obtained for different numbers of subsections may have come from rounding errors.

Results indicate that as long as the major change points in channel geometry are used as subarea dividing lines, the results obtained from equations 2.1 and 2.2 should be consistent. While an excessive number of subdivisions is not necessary, neither are too few subdivisions.

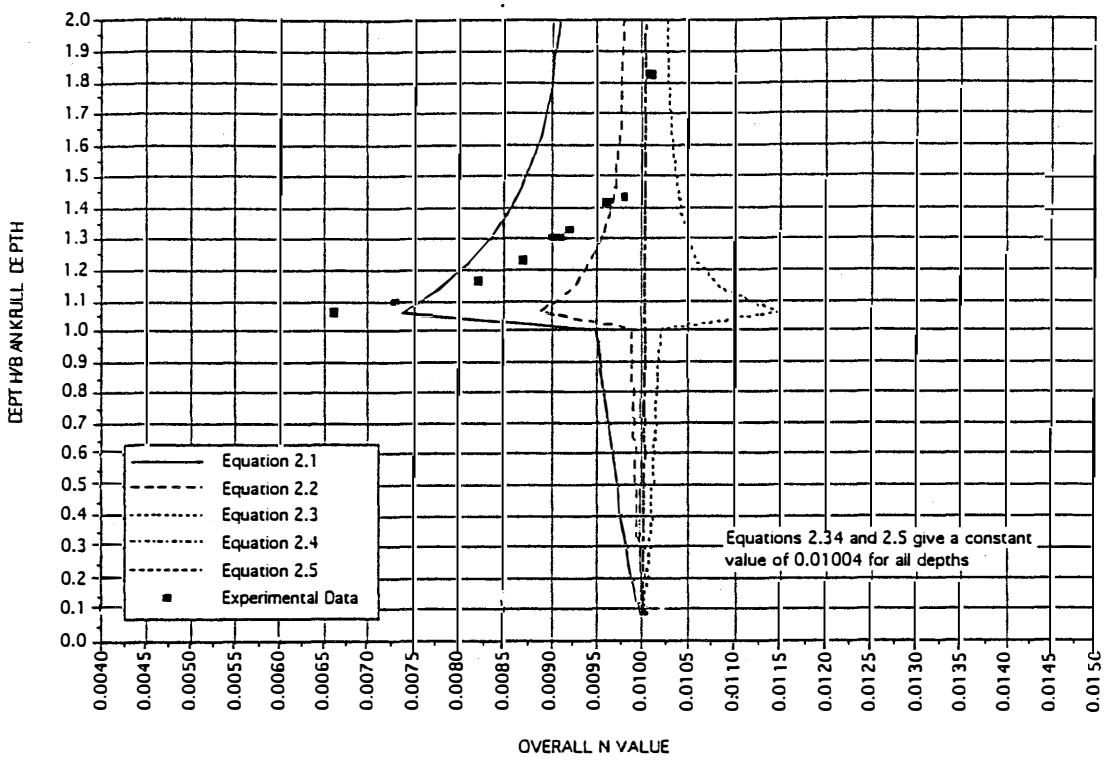

Figure 5.7a **Myers and Brennan - asymmetric geometry data versus equations 2.1 to 2.5**

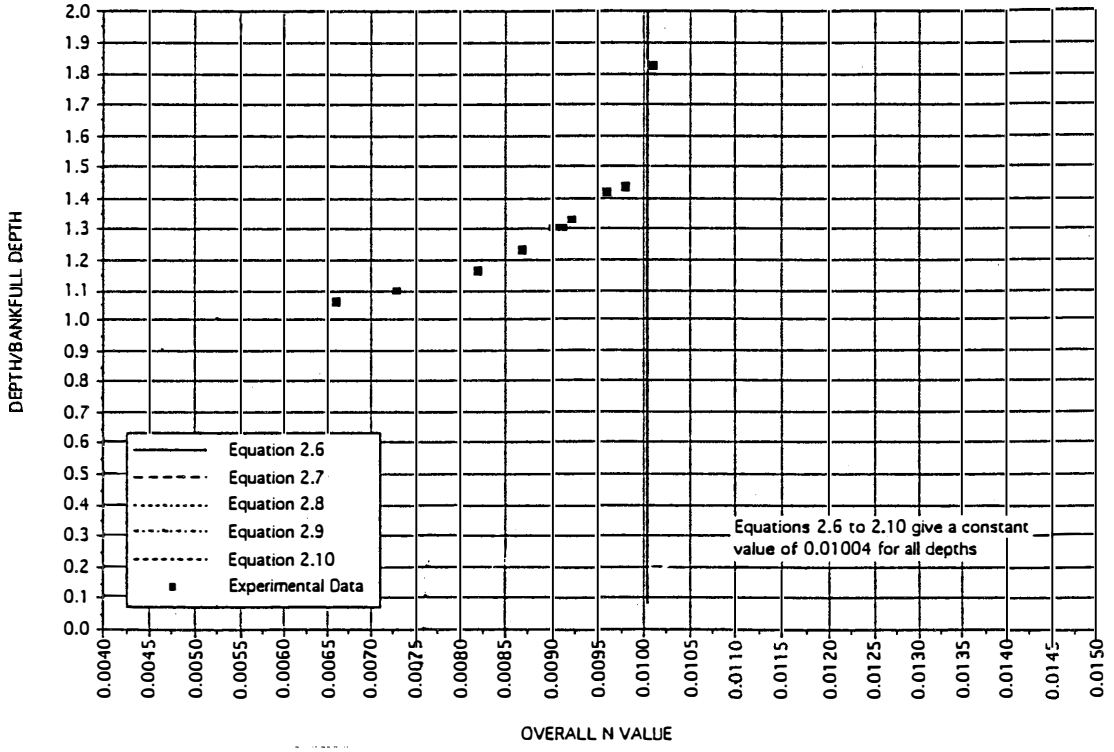

Figure 5.7b **Myers and Brennan - asymmetric geometry data versus equations 2.6 to 2.10**

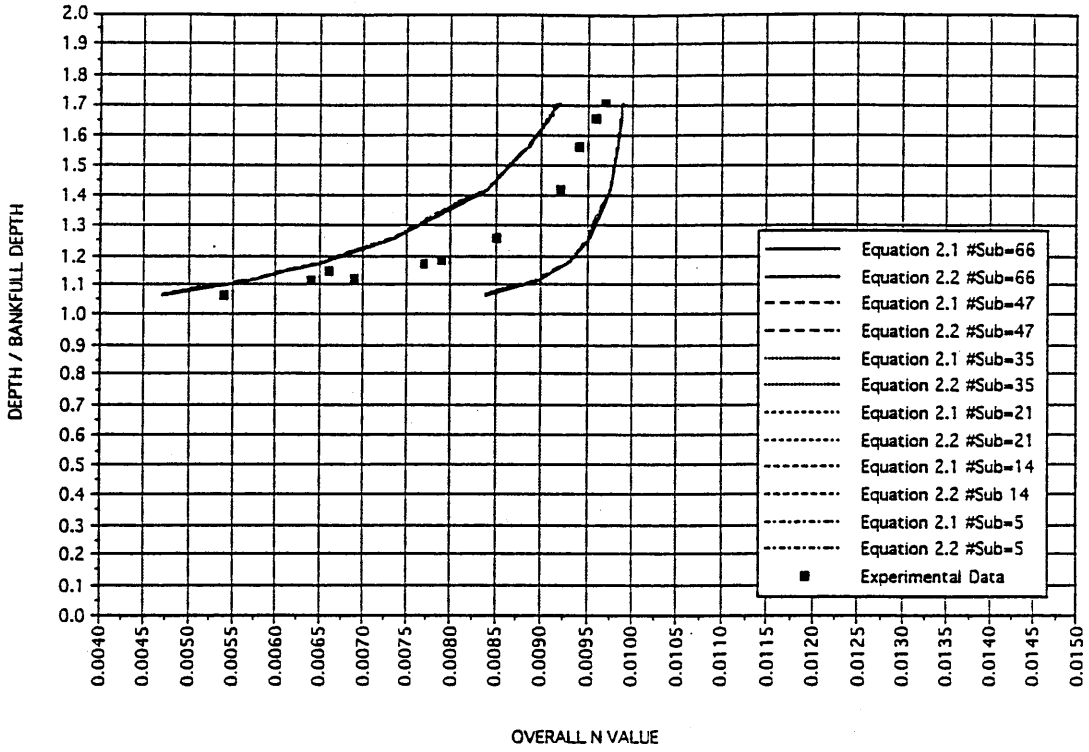

Figure 5.8 Effect of number of subdivisions on equations 2.1 and 2.2 for Myers and Brennan - Geometry 6.67

General conclusions regarding the data of Myers and Brennan (1990) can be summarized as follows:

- Geometry effects cause the overall manning n value to vary with depth.
- Widening the floodplain while holding the size of the MC steady causes n_o to decrease further at above bankfull depths. However, the reduction seems to approach a maximum value around 45% after B/b ~ 4.0.
- At higher depths, the overall n values tend to approach the MC n_o just before bankfull stage.
- At depths above bankfull stage, equation 2.1 predicts better results at lower y/D ($1.0 < y/D < 1.2$) and equation 2.2 predicts better results at y/D ~ 1.4.

5.2. James and Brown (1977): Effects of Asymmetrical Floodplains

The next set of experiments studied was performed by James and Brown (1977) on both symmetrical and asymmetrical compound channels. Only the asymmetrical cases were examined. These test configurations are shown in figure 5.9, and the base roughness remained the same for both the MC and the FP.

James and Brown used rather shallow depths in their study -- the full MC depth was 2 inches, plus another 2 inches for the full FP depth. Therefore, even though the base roughness was similar to other studies cited here, the relative roughness was different. Their studies investigated three slopes for each channel setting. Thus, their data are useful for examining the effect of floodplain width in an asymmetrical channel as well as the effect of channel slope on the overall n value.

As shown in figure 5.9, the three cases studied had an MC 7 inches wide. The FP was 7 inches wider in each case. Thus, following the parameters convention that we have been using, the half-channel width to half-MC width ratios (B/b) are 3.2, 5.2, and 7.4 respectively, and the B/D ratio 3.5. In all cases, the base n value for all subareas of the channel is estimated to be 0.0117. At this point, it is necessary to repeat that determining the base n is a critical step in evaluating the overall n value. The base n value determines the starting point of all equations. From what we have observed up to now, one can deduce the base n at very low MC depths. When such data were lacking, such as in this dataset, the base n value was determined by averaging the n values from different runs.

5.2.1. Test 5 - B/b =3.2

Figure 5.10 shows the n_o values retrieved from James and Brown's data for the Test 5 series. At depths below bankfull stage, n_o differed for different channel slopes, i.e., higher n_o at higher slope. No clear pattern of n_o versus depth could be found except for the S = 0.003 case, which showed some consistency that n_o stayed closer to the base n value. The pattern for S = 0.003 is similar to that of geometry 1.2 from Myers and Brennan (1990), in which the base n was 0.010 and slope was 0.00103, but channel depth was 6 inches. One possible explanation is that the depths were much shallower in James and Browns' experiment, which led to lower Reynolds numbers. These results -- higher overall friction at higher Reynolds numbers -- contradict what is generally believed. They are examined in Moody type diagrams in figures 3.5 to 3.7.

At above bankfull depths, the trend of n_o is clear but at least two curves exist. The n_o value for S = 0.01 was lower while n_o values for S = 0.002 and S = 0.003 were higher and remained closer. They stayed close until the y/D ratio reached approximately 1.3. The curvature for S = 0.003 case was smoother after that depth.

The data for above bankfull depths were well grouped and did not have the scatteredness presented in the below bankfull range. The tendency of n_o for S = 0.001 was

FOR ALL CHANNELS:

Manning n value of all walls:	0.0117
Bed Slopes:	0.001 0.002 0.003
Main Channel Depth:	2 inches
Main Channel Bottom Width:	7 inches
Sidewall Slopes:	1:1

Figure 5.9 Channel geometry for USACOE Tests 5, 6 and 7 experimental series. (After James and Brown 1977)

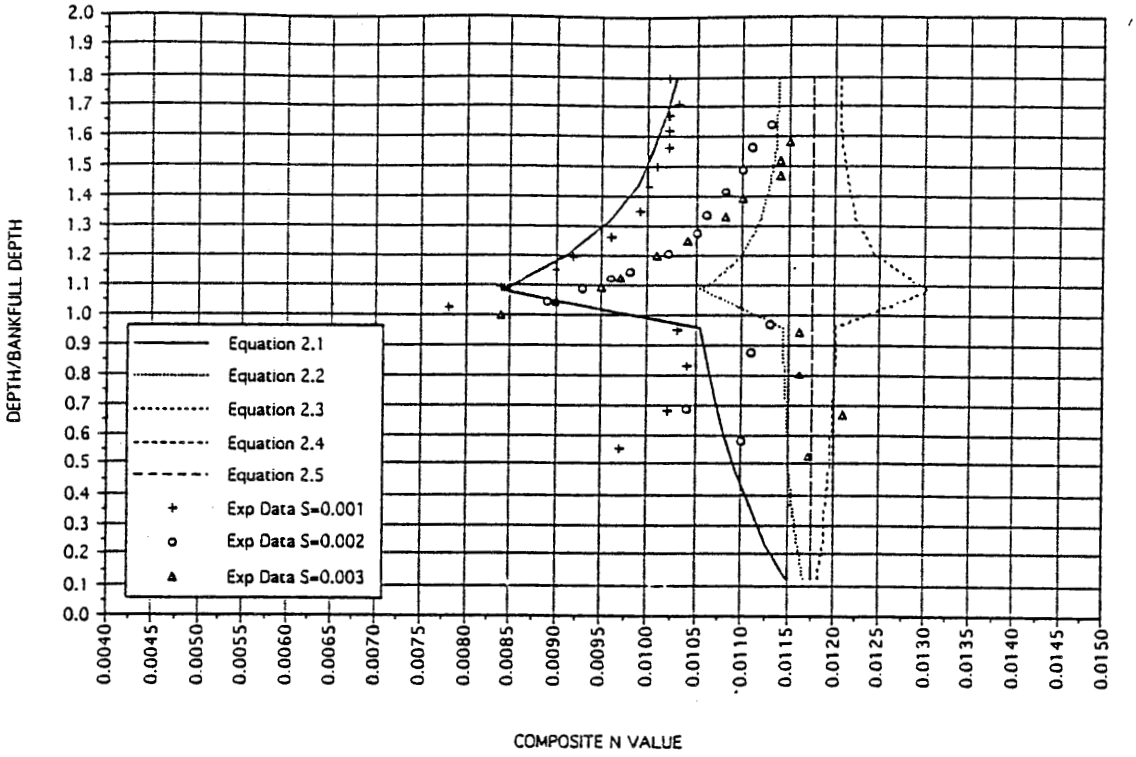

Figure 5.10a USACOE -- Test 5 experimental data versus equations 2.1 to 2.5

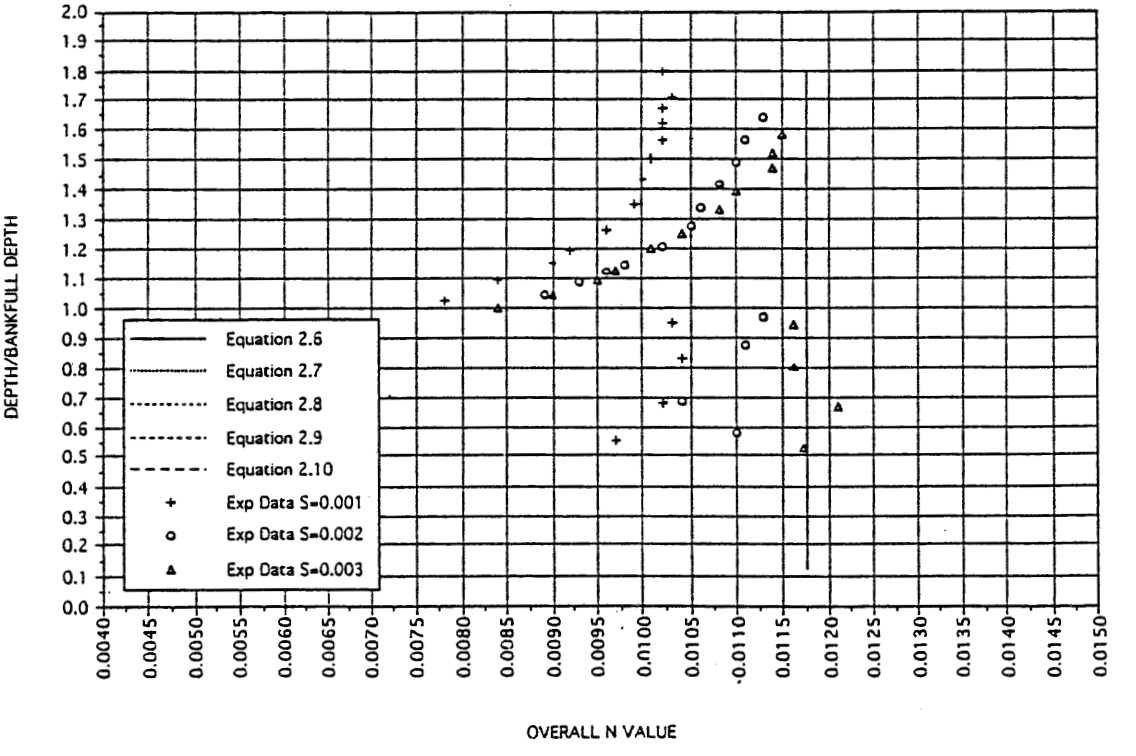

Figure 5.10b USACOE -- Test 5 experimental data versus equations 2.6 to 2.10

to approach a much lower n_o than the base n value as y/D increased, while the tendency of n_o for the other two slopes was to gradually regain the base n value; the S = 0.003 case attained the base n value faster (at lower y/D). This is similar to what has been observed until now. Also, comparing the n_o values from Myers and Brennans' asymmetrical channel case, in which the base n and channel slope (approximately 0.001) were similar but the floodplain narrower and deeper, the n_o pattern is rather similar to the S= 0.003 case presented here. Overall, the minimum n_o just above bankfull depth was approximately 34% lower than the base n value.

Figure 5.10 also shows that equations 2.1 and 2.2 bracketed the data above bankfull stage. For the low slope (S = 0.001), equation 2.1 performed quite well, matching the trend and the numerical values of n_o at most depths above bankfull stage. The depth increment around bankfull stages should be reduced further in the numerical evaluation to show the predictions compared to the experimental data.

On the other hand, equations 2.4 and 2.5 and 2.6 to 2.10 (figure 5.10) all predicted constant n_o for the uniform roughness channel.

5.2.2. Test 6 - B/b ~ 5.2

The experimental results for the Test 6 series are shown in figure 5.11. The effect of a wider floodplain in this asymmetrical case was to reduce the n_o value above bankfull stage. At depths just above bankfull stage, the n_o for S = 0.002 and S = 0.003 decreased further than in the B/b ~ 3.2 case. The overall reduction at this depth was also approximately 34%. As the depth increased, n_o for the two higher slope cases tended to regain the base n value. The locations at which n_o reached the base n value were approximately at the same y/D ratios as shown in figure 5.10. The gap between S = 0.002 and S = 0.003 increased starting at y/D of approximately 1.2.

For S = 0.001 n_o reduced to similar values as in Test 5. As the depth increased, n_o also tended to recover the n_o value for S = 0.001 in the previous case. In the depth range below bankfull stage, the data were less scattered. The added floodplain width should not have had any effects at depths below bankfull stage. The data showed more constancy in the high slope case. Overall, it is still unclear if any pattern is presented in these data.

Comparing the predictions from each equation with the experimental data, one can see very similar results as in Test 5; that the S=0.001 data were well matched by equation 2.1, and that equations 2.1 and 2.2 bracketed the remaining data. Overall, equation 2.1 also predicted better in shallow floodplain depths.

Comparing figures 5.11 and 5.10, one can see that widening the floodplain affected equation 2.1 the most. Equations 2.4 to 2.10, on the other hand, predicted constant n_o as before (see figure 5.11).

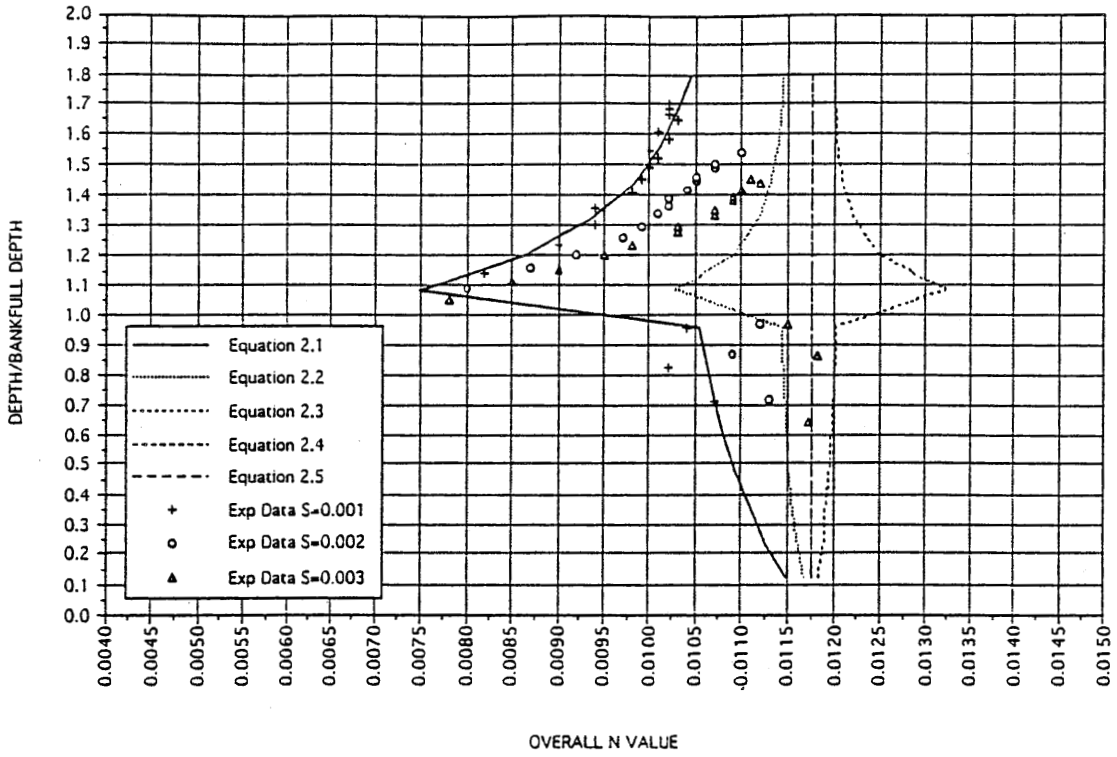

Figure 5.11a USACOE -- Test 6 experimental data versus equations 2.1 to 2.5

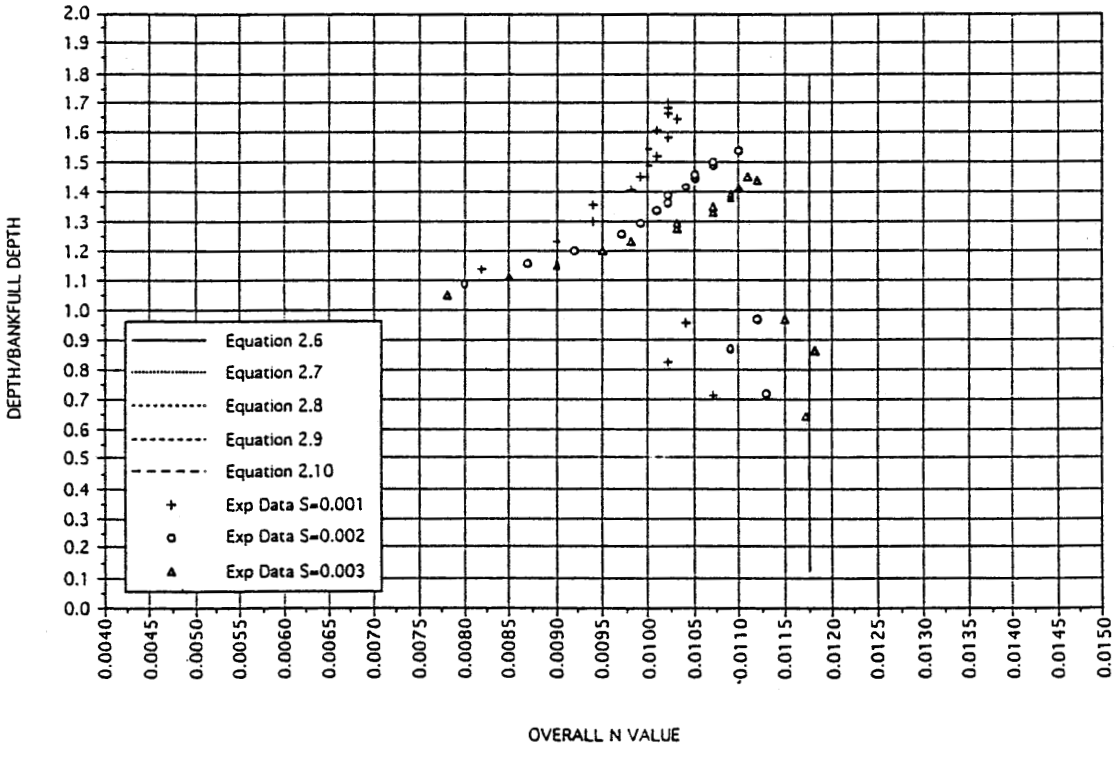

Figure 5.11b USACOE -- Test 6 experimental data versus equations 2.6 to 2.10

5.2.3. Test 7 - B/b ~ 7.4

Figure 5.12 shows the experimental n_o series for this wide floodplain, asymmetrical compound channel case. It can be seen that below bankfull stage the n_o values were smaller than the base n value for all three slopes. The effect of an even wider floodplain was to further reduce the n_o value just above bankfull stage, by approximately 51%. As depths increased, n_o increased. However, the pattern shows that series for S = 0.002 were closer to S = 0.001 than to S = 0.003 cases.

Figure 5.12a also shows the variation of equations 2.1 to 2.5 for Test 7. The effect of a wider floodplain is most pronounced on equation 2.1, as demonstrated in the previous case. In this case, equation 2.1 did very well in predicting the values and trends of n_o for both the 0.001 and 0.002 slope cases. Equations 2.1 and 2.2, as well as equations 2.6 to 2.10 (figure 5.12b) predicted no variation in the overall n value.

5.3. Pillai (1962): Prismatic Channels with Changing Roughness

Pillai's study (extracted in Cox, 1973) has the characteristics of simple channels with varying roughness along the walls. Two channel geometries, rectangular and trapezoidal, and two roughnesses, one for the bed and one for the sidewalls (figure 5.13), were examined in this study. Because of the nature of the setting, the bisection method had to be used for the rectangular channel in this case. For simplicity, the bisectional division method was also used for the trapezoidal channel. The effect of these two division methods on the ten selected composite roughness equations was shown to be minor and predictable.

5.3.1. Series C - Rectangular Channel with Rough Bed

Pillai's Series C channel was rectangular with the bed significantly rougher than the walls. The channel width (figure 5.13) varied around 3 feet and the depth was less than 1 foot. The n_o values retrieved from experimental data are shown in figure 5.14. From the available data it can be seen that n_o did vary with depth in the prismatic channel having different roughness on the bed and walls. If a best-fit line was applied, then n_o could have started at a point close to the base n value for the bed, and decreased gradually for higher depths. The effect of smooth sidewalls was to reduce n_o, which would have been at least a constant for the uniform roughness case. The tendency of n_o at higher depths could not be determined.

The predictions by all equations are shown in figures 5.14a and b. All equations predicted the decreasing trend but only equation 2.6 provided a reasonable estimate of the

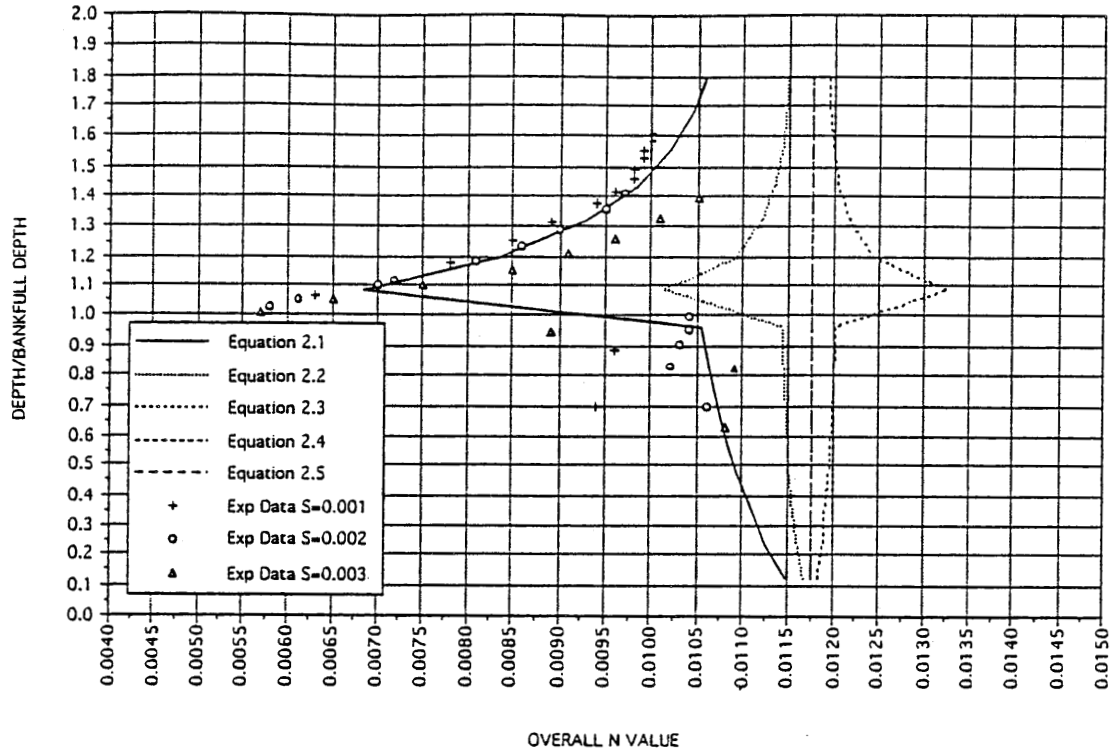

Figure 5.12a USACOE -- Test 7 experimental data versus equations 2.1 to 2.5

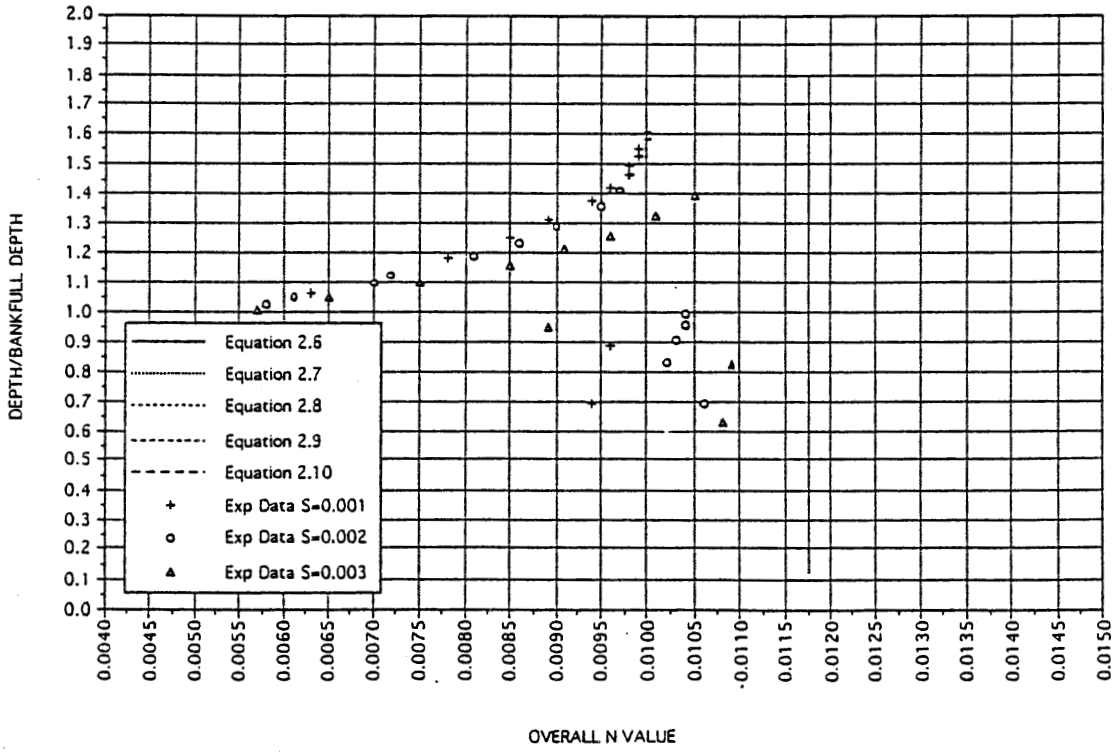

Figure 5.12b USACOE -- Test 7 experimental data versus equations 2.6 to 2.10

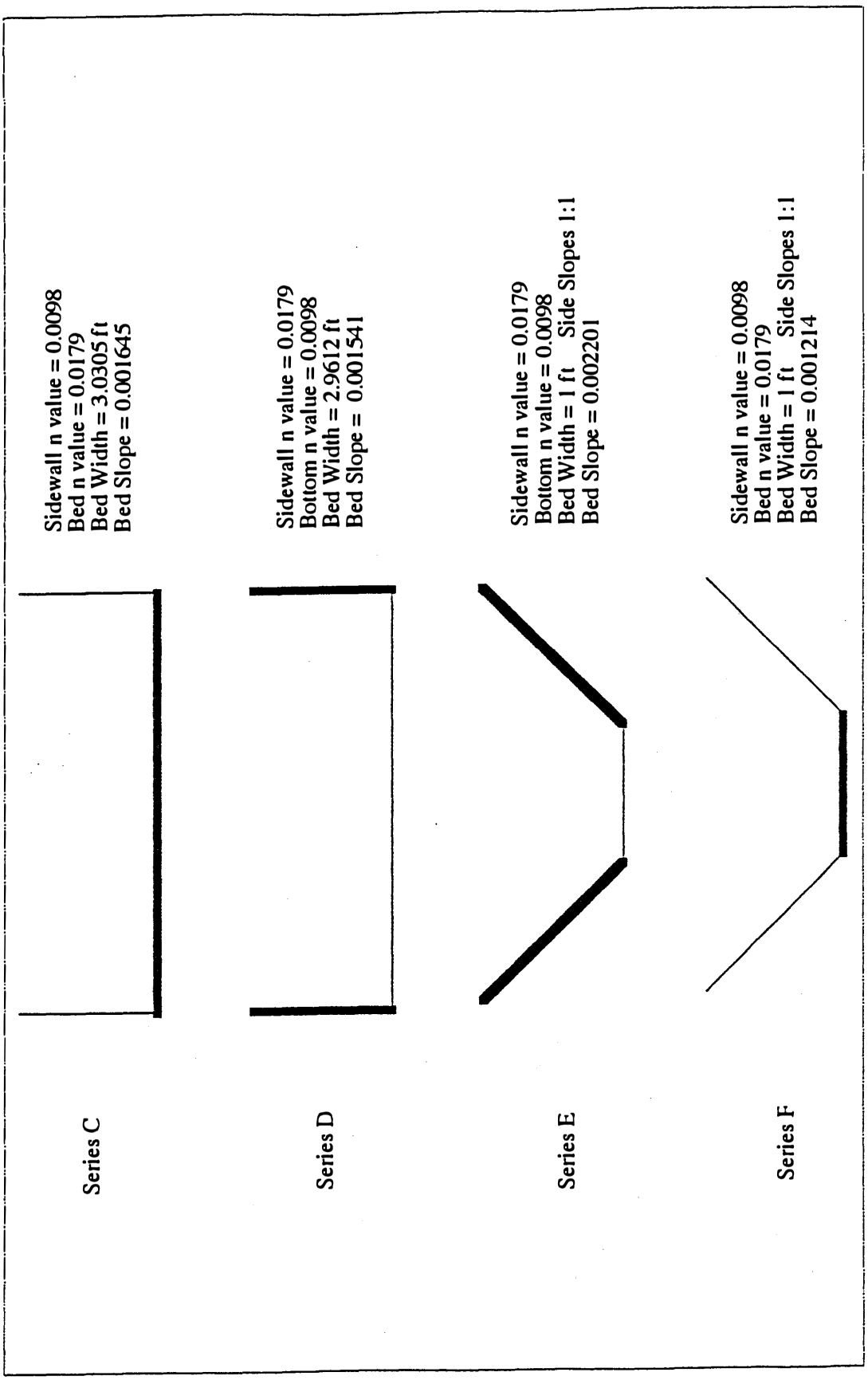

Figure 5.13 **Channel geometry for Pillai Series C, D, E, and F experimental tests (after Cox 1973)**

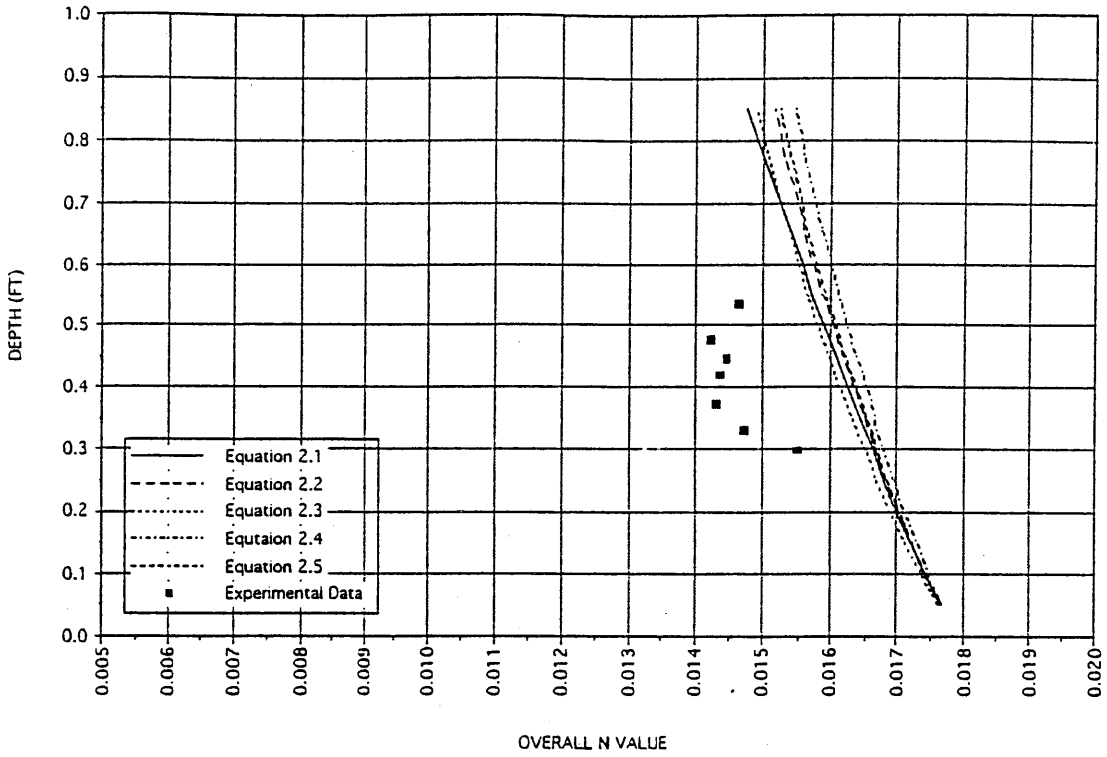

Figure 5.14a Pillai -- Series C experimental data versus equations 2.1 to 2.5

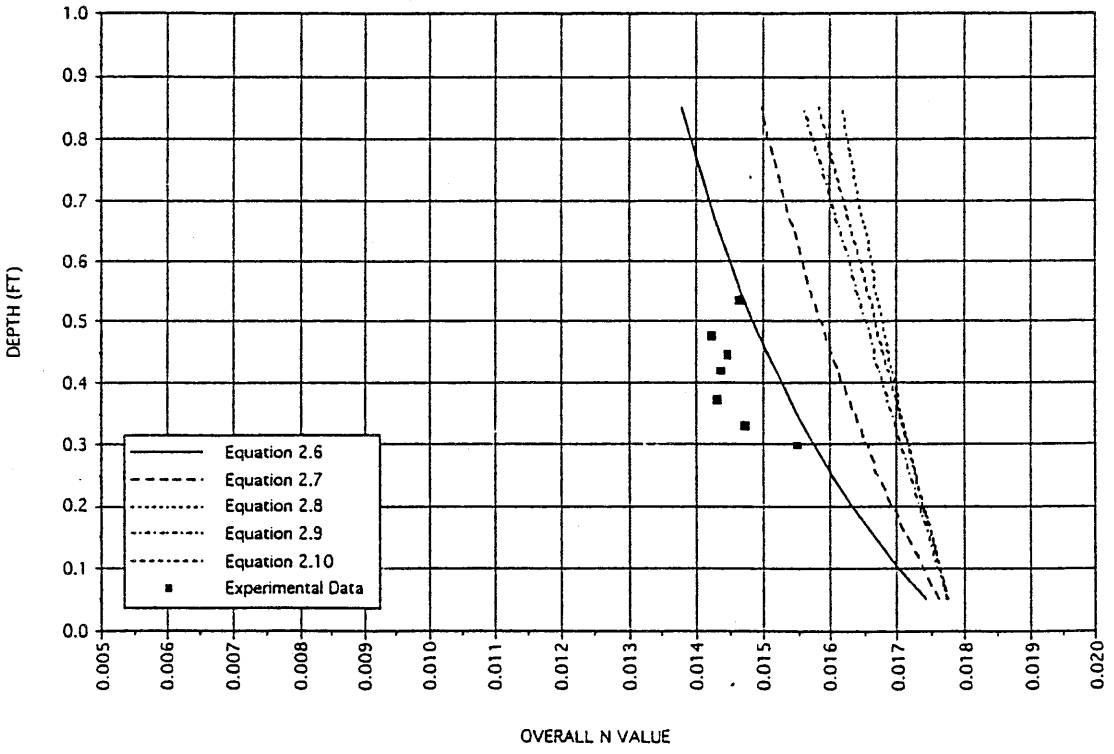

Figure 5.14b Pillai -- Series C experimental data versus equations 2.6 to 2.10

numerical values. The trend of n_c was opposite the pattern of hydraulic radius, which increased with depth for this case.

5.3.2. Series D - Rectangular Channel with Rough Sidewalls

The Series D channel was also rectangular, but the roughnesses for the bed and sidewalls were reversed. The effect of having sidewalls rougher than the bed was that n_o began from a lower n (similar to the base n of the bed) and increased as depth increased. The increase due to the rough walls was also significant as compared with the uniform roughness (trapezoidal, geometry 1.2) channel case; in that case it was about 5% and here approximately 20% from the base n value. The n_o at higher depths was not available, but the tendency seemed to be approaching a constant value.

Figures 5.15a and b show the results from all equations. The closest estimation was achieved by equation 2.4. Hence, the performance of the equations was not consistent with different settings. However, the bed slope in Series D was slightly smaller than in Series C.

5.3.3. Series E - Trapezoidal Channel with Rough Sidewalls

The Series E channel differed from the Series D channel in that the geometry was trapezoidal instead of rectangular, and the bed slope was steeper. On the other hand, the roughness in the wall and bed remained the same as Series D. The inclination of the sidewalls was 45°, the same as the project's experiment and the ideal case illustrated in Chapter 2 of this report.

Experimental results are shown in figure 5.16. The effect of rougher sidewalls appeared more significant than for the rectangular channel: n_o increased more rapidly with depth and approached a higher value than the rectangular case. Conceptually, the trapezoidal channel is considered to be more efficient than the rectangular channel. The distribution of the roughness pattern, however, can alter the result dramatically.

Figures 5.16a and b illustrate the results from the ten equations. The equations' predicted n_c matched the n_o reasonably well, especially equations 2.2 and 2.7. In general, results of equations 2.1 to 2.5 were fairly close to the experimental data. An existing concept is that all equations will perform similarly in simple channels. This research, as a matter of fact, has demonstrated the equations' differences under different channel geometry and roughness settings. In simple channels, changes in roughness pattern, rather than geometry, affected n_o more.

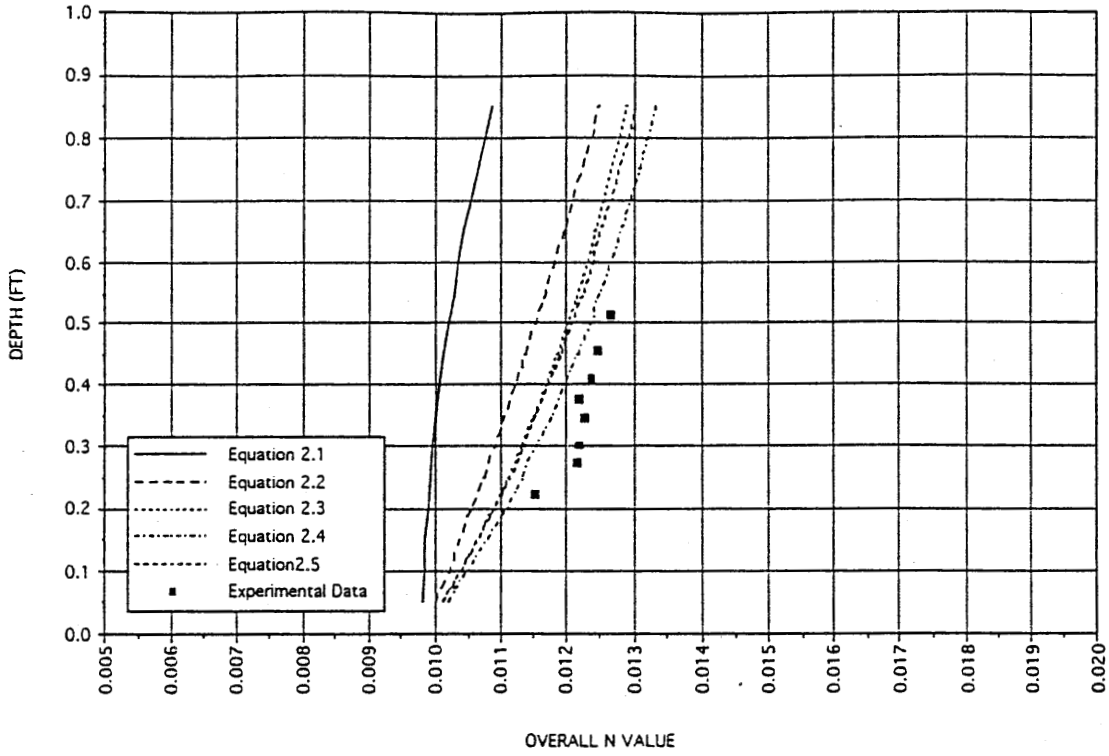

Figure 5.15a Pillai -- Series D experimental data versus equations 2.1 to 2.5

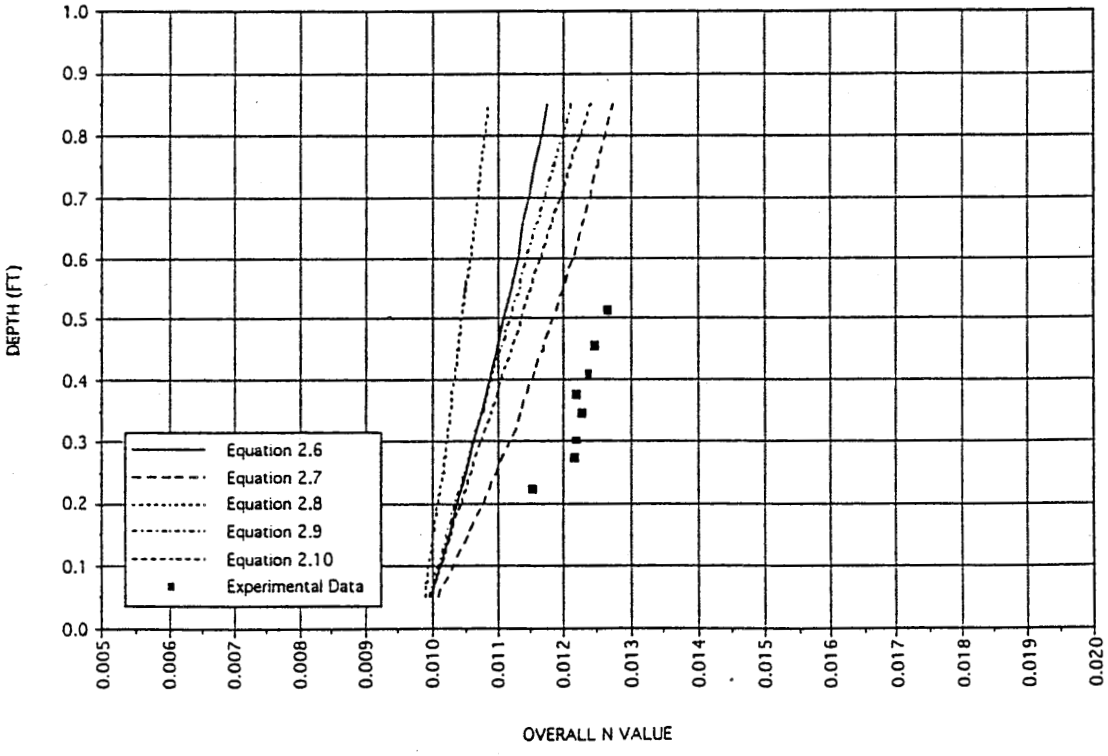

Figure 5.15b Pillai -- Series D experimental data versus equations 2.6 to 2.10

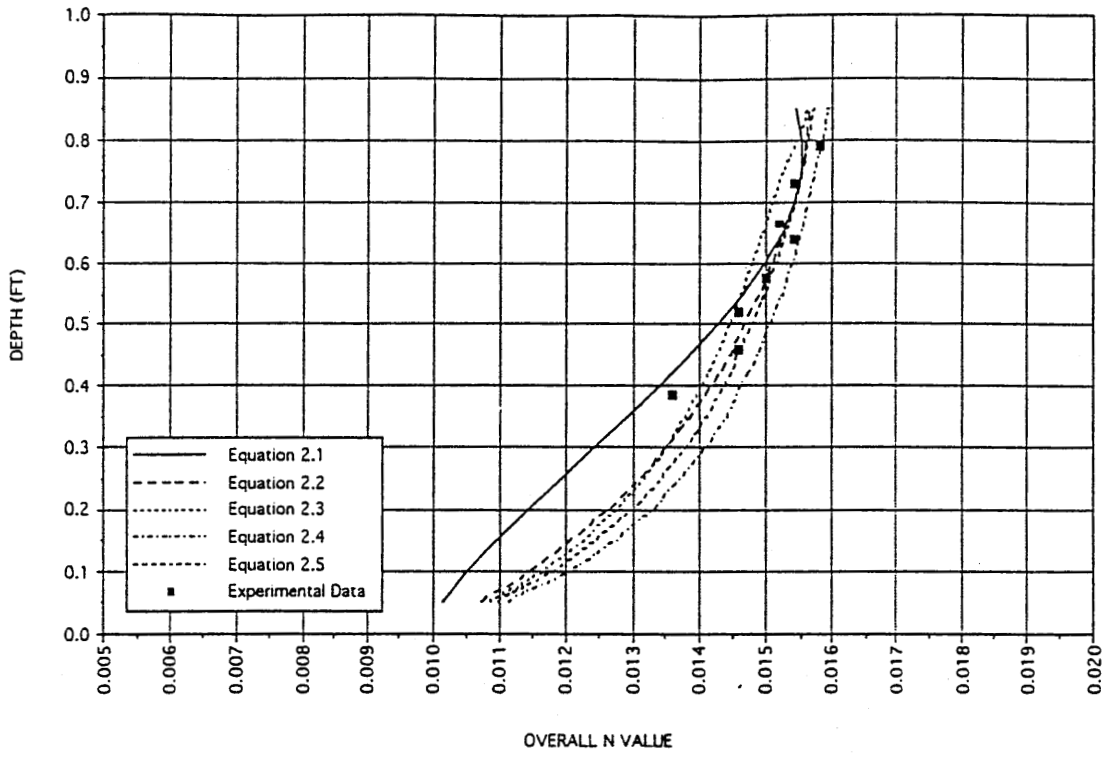

Figure 5.16a Pillai -- Series E experimental data versus equations 2.1 to 2.5

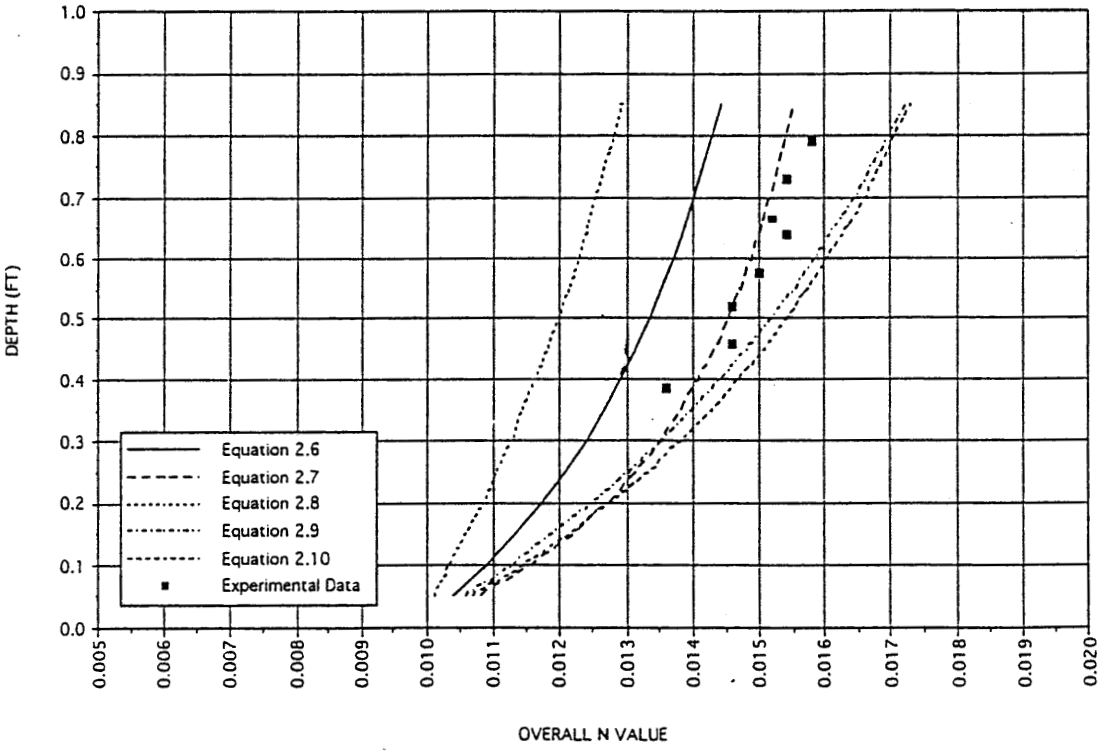

Figure 5.16b Pillai -- Series E experimental data versus equation 2.6 to 2.10

5.3.4. Series F - Trapezoidal Channel with Rough Bed

The Series F channel, a trapezoidal channel with smooth sidewalls and rough bed, was used here to confirm several observations made above. The experimental results for Series F are shown in figure 5.17. It is not surprising to see that n_o decreased with depth, reflecting the effect of smooth sidewalls, and that the reduction was more than in the rectangular channels. One can observe that n_o tended to approach a constant value at higher depths, and this constant value was lower than the rectangular case (Series C).

In terms of numerical predictions, equations 2.6 and 2.7 demonstrated a better fit with the data than other equations (figures 5.17a and b). Equation 2.2 also prescribed the data reasonably well. Since secondary circulation is less in trapezoidal channels than in rectangular channels, equations such as 2.6 and 2.7, which depend solely on the proportions of the wetted perimeter, should have performed well here. In general, equations based on the assumption of the balance of shear forces would be best for the purpose. The reasonable performance of equation 2.2 was expected. However, neither equation 2.2 nor 2.7 predicted n_o correctly in the full depth range in the trapezoidal channel The discrepancies clearly indicate that some adjustments will be needed for obtaining a more general application.

Overall, the data by Pillai (1962) serve to explain the n_o pattern in prismatic channels with varying roughness. These data were very useful for the present study.

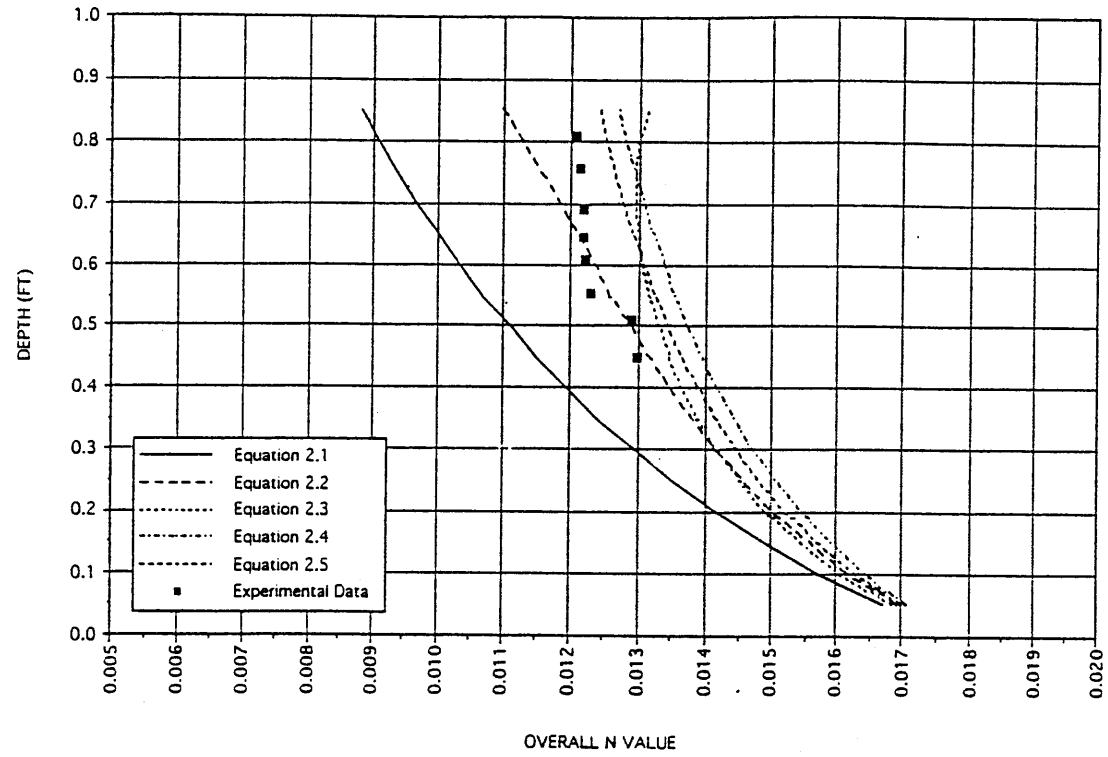

Figure 5.17a Pillai -- Series F experimental data versus equations 2.1 to 2.5

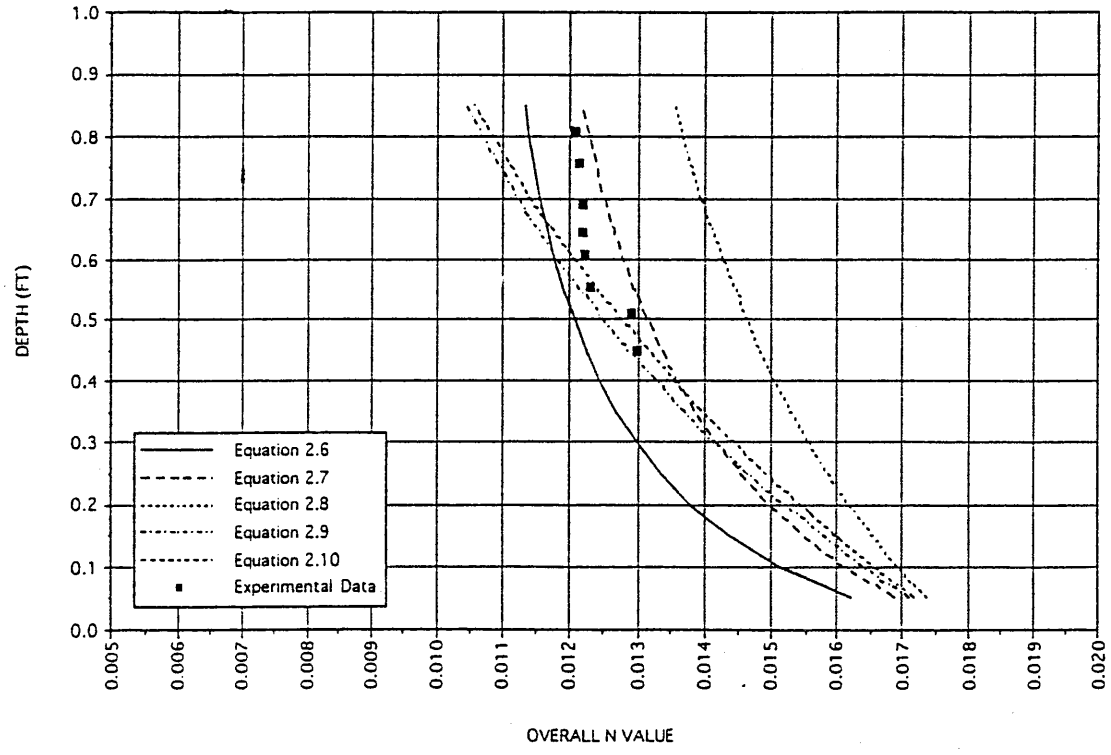

Figure 5.17b Pillai -- Series F experimental data versus equations 2.6 to 2.10

6. SUMMARY AND CONCLUSIONS

This report summarizes a laboratory research project conducted by the authors to investigate how the Manning coefficient varies with depth in a cross section of rivers and channels. The experimental results, in conjunction with data adapted from other research, clearly showed a general trend of such variation for compound channels. Different roughness patterns on the wetted perimeter affected the magnitude of overall roughness at given depths but not the general pattern of variation. For prismatic channels, on the other hand, such trends also existed but they varied with the cross-sectional geometry and were affected more significantly by the distribution of roughness in the cross section.

The impetus for this study was the current lack of a realistic method for determining the Manning's coefficient. Common calibration procedures used by practitioners are generally hampered by limited data. In many cases, n_o (overall Manning coefficient) is treated as a constant for a cross section without regard to depth fluctuations. Evidence from field data, however, has shown that such assumptions may not be valid. Examples (see Chapter 2) illustrate that the changes in n_o are significant and warrant our attention. If a generalized n_o pattern can be established at a cross section using its basic hydraulic properties, then practitioners can apply the limited observations to the generalized form and determine the appropriate n_o at other depths.

In addition to this application, an n_o curve may also provide an alternative way to calculate discharge in compound channels while still using the Manning's equation for the whole cross section. The goals of this project were to enhance the use of Manning's equation and improve its practical applications. This research provides initial results for a larger scope of investigation.

6.1. Experiment Scope and Limitations

Many factors can affect the n_o value. This research started from a composite roughness concept; that changes in n_o with depth are mainly due to the addition or deletion of roughness elements to the cross-sectional area. Currently there are ten equations capable of computing the composite roughness in simple prismatic channels. However, their assumptions vary and they have not been tested systematically; further, their applications to compound channels, which are more common in natural rivers, have not been examined.

The authors conducted a controlled experiment to study the effects of different roughness patterns along the wetted perimeter on the overall roughness coefficient n_o. The channel design allowed higher Froude number tests, but flow regimes remained in steady uniform and the boundary was rigid. See Chapter 3 for details on the experimental setup and its limitations.

Three types of roughness elements, gravel, black magnum, and sand, were applied to the main channel, main channel border, and three floodplain areas. A coding system was designed, using the abbreviation of one roughness material at one location starting from the main channel to the far end of the floodplain, to identify the combination of roughness elements. Throughout the experiment the bed slope varied three times: 6.2E-04, 1.1E-03, and 7.9E-04. Experimental data are included in Appendix I.

The experiment studied the effects of roughness patterns on n_o in the following combinations:

Uniform Roughness
4.2.1. GGGGG Series
4.2.2. BBBBB Series

Changing Roughness in Main Channel
4.4.1. BGGGG Series
4.4.2. GBBBB Series

Changing Roughness in Floodplain
4.3.1. BBSSS Series
4.3.2. BBSSG Series
4.3.3. BBSGG Series
4.3.4. BBGGG Series

Roughness in Floodplain nearest the Main Channel
4.5.1. BBBGG Series
4.5.2. BBSBB Series

The performance of the ten equations was compared with results derived from each experimental series. In addition, data from other research were also sought to investigate factors not covered in this study. The literature data include:

Myers and Brennan (1990): Effects of Floodplains (Uniform Roughness)
5.1.1. A Trapezoidal Channel
5.1.2. Symmetrical Compound Channel with B/b = 2
5.1.3. Symmetrical Compound Channel with B/b = 4
5.1.4. Symmetrical Compound Channel with B/b ≅ 6.4
5.1.5. Compound Channel of Asymmetrical Geometry

James and Brown (1977): Asymmetrical Compound Channels (Uniform Roughness)
5.2.1. Asymmetrical Compound Channel with B/b =3.2
5.2.2. Asymmetrical Compound Channel with B/b ≅ 5.2
5.2.3. Asymmetrical Compound Channel with B/b ≅ 7.4

Pillai (1962): Prismatic Channels with Changing Roughness
5.3.1. Rectangular Channel with Rough Bed
5.3.2. Rectangular Channel with Rough Walls
5.3.3. Trapezoidal Channel with Rough Walls
5.3.4. Trapezoidal Channel with Rough Bed

The variation of n_o versus depth differs with cross-sectional geometry and roughness distribution. The influences of these two factors on n_o differ in prismatic channels and compound channels. The following conclusions are related to general observations, prismatic channels, and compound channels, respectively.

6.2. General

The base n of roughness materials must be determined properly when using the composite equations. Errors resulting from an improperly estimated base n value may be more significant than those from one of the composite equations. This study verified that Strickler's (1923) and to a large degree Henderson's (1966) equations are capable of predicting the base n value for fairly uniformly sized materials. The base n values were reproduced at shallow flow depths in the prismatic channel. Further verification is needed to test these equations on other materials, especially those in which the granular composition is not uniform. If these tests proven successful, then n values in natural rivers can be determined more easily by using the base n for roughness materials and results from this investigation.

In terms of the equations' predictions, bisectional subdivisions slightly narrowed the discrepancies among equations, but sometimes yielded a worse outcome than the vertical subdivisions. The slight improvement does not justify the greater effort required to use them. Overall, vertical subdivisions are easier to use and their performance was acceptable.

Whether the equations' performances improve with increases in the number of subareas was tested with the wide compound channel data of Myers and Brennan (1990) for a uniform roughness case. The test showed that, as long as all of the major breaks in channel geometry were denoted by a division line, the equations would produce acceptable results. It is reasonable to assume that such a conclusion would be valid for heterogeneous roughness cases in compound channels. On the other hand, the effects of the number of subdivisions in a prismatic channel with heterogeneous roughness have not been tested. Our ability to assess variation of n_o for such cases is limited.

6.3. Prismatic Channels

For prismatic channels with similar cross-sectional areas, cross-sectional shapes affect the corresponding magnitudes of n_o. This study further verified that for the same cross section, arrangements of roughness elements significantly alter the n_o versus depth relationship. This is rather crucial because current knowledge expects little variation of n_o

with depth for prismatic channels, even if the channel has varying roughness along its wetted perimeters.

For trapezoidal channels of uniform roughness, those with smaller aspect ratios (approximately 4 in our experiments) showed a higher percentage of increase in n_o than those with larger ratios (approximately 10 in Myers and Brennans' tests). Aspect ratio is defined as width divided by depth. Nezu (1994) defined " narrow open-channels" as those with aspect ratios less than 5, while those with ratios above 5 are " wide open-channels." For wide channels n_o practically can be assumed constant over depth, but for narrow channels an increasing trend exists. Secondary circulation, although not discussed in the one-dimensional flow context, would be the main mechanism for energy losses and increased n_o values. Data from our experiments, the GGGGG and BBBBB series (see Chapter 4), had similar percentages of increases, and we found that equation 2.3 predicted the n_o trend satisfactorily. Data were limited for comparisons with other cross-sectional shapes. However, following Chow's (1959) postulation (see Chapter 2), it is reasonable to assume that n_o would decrease from rectangular, trapezoidal, triangular, to circular channels.

The authors used Pillai's data (1962) to investigate the case of prismatic channels with varying roughness. These data showed that the n_o versus depth relationship is a function of the patterns of roughness distribution, and that these variations of n_o are not predicted well by existing equations. For the given rectangular and trapezoidal channels (figure 5-13), one finds the following:

1. When both channels had a rough bed and smooth sidewalls, n_o decreased approximately 20% from bed roughness in the rectangular channel at 0.5 feet of depth, and approximately 29% in the trapezoidal channel.
2. When both channels had a smooth bed and rough sidewalls, n_o increased about 25% from bed roughness in the rectangular channel at 0.5 feet of depth, and about 45% in the trapezoidal channel.

Our experimental data were not conclusive enough to verify such observations. When the ten equations were compared, equation 2.7 performed well for trapezoidal channels of varying roughness. For rectangular channels with varying roughness, the case was less conclusive, but the results from equation 2.7 were acceptable. The equation was based on the assumption that contribution of component roughness is linearly proportional to the wetted perimeter. Natural channels have several roughness materials over different portions of the wetted perimeter. There is a need for further study in this fundamental area.

6.4. Compound Channels

For compound channels, geometric changes at depths near bankfull stage cause significant changes in hydraulic properties, and overall n_o follows. The general trend of n_o in compound channels is to decrease significantly from just before bankfull depth, and then gradually recover as the depth increases. The trend of n_o when flow is restricted in the main channel is equivalent to that for a prismatic channel. The general trend of n_o for the floodplain is preserved even when roughness arrangements change, but the magnitude of n_o changes.

Changes in related hydraulic properties, including submerged area, wetted perimeter, and hydraulic radius, were studied. When discharge is estimated by applying Manning's equation for the whole cross section, errors occurred at near bankfull stage. Many researchers would consider such errors to be due to the fact that the hydraulic radius was not properly represented in this region by the conventional definition. However, the representative hydraulic radius was not developed. Hence different division methods were introduced, assuming uniform n_o. The present approach apparently can resolve the estimation errors in Manning's equation near bankfull stage while still keeping the simple whole cross-sectional approach.

Through thorough comparisons of experimental data and predictive equations, the authors concluded that equations 2.1 and 2.2 were suitable for use on the floodplain. In several instances, the n_o pattern was bracketed by equations 2.1 and 2.2, with equation 2.1 fitting better in a range between $1.0 < y/D < 1.2$, and equation 2.2 fitting better at higher depths. For most cases, equation 2.2 fit better overall. DePue (1996) has further developed weighting percentages for compound channels with homogeneous roughness. The weighting factor, w, shown in figure 6.1, seems to produce reasonable results for the data of Myers and Brennan (1990). The form of the equation would be:

$$\textit{Suggested } n_o = w*(n_o \textit{ by eqn. 2.1}) + (1 - w)*(n_o \textit{ by eqn 2.2}) \qquad (6.1)$$

Furthermore, the variation of n_o above bankfull stage due to different roughness arrangements also demonstrated certain trends. By comparing n_o values at given depth intervals, it was found that changes could be described in at least two regions: shallow floodplain and deep floodplain depths. Although the experimental data contained some degree of scatteredness, it is feasible to draw best fit lines to describe the trend and for use in comparisons. Conclusions are summarized as follows.

6.4.1. *Effect on n_o of Changing Floodplain Roughness*

Data for five different roughness arrangements (see table 4.1) are plotted in figure 6.2, which shows a general trend of increases over y/D. Table 4.1 uses for decimal

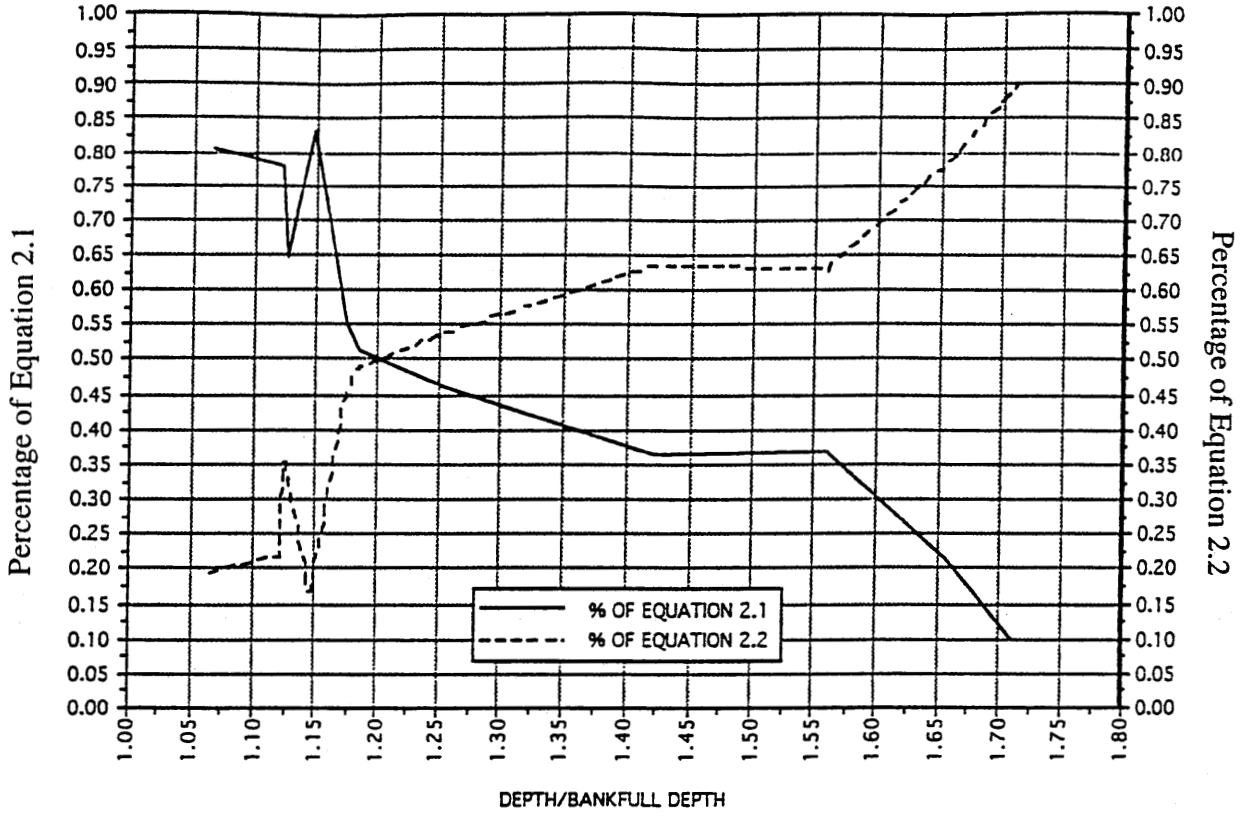

Figure 6.1. Suggested weighting factors for compound channels of homogeneous roughness

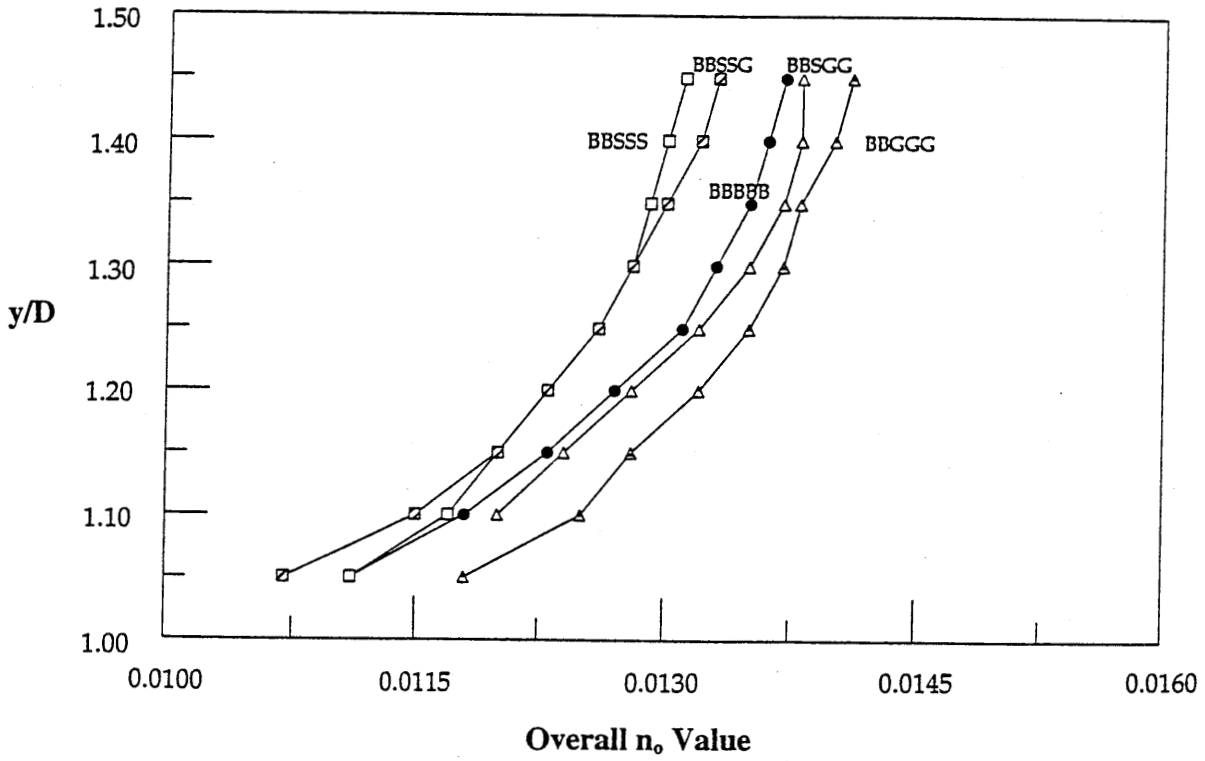

Figure 6.2. Fitted n_o for various roughness combinations on the floodplain

numbers because the base n values for three roughness elements fall in a small range between 0.012 and 0.018. In general, the magnitudes of n_o increased as rougher elements were used. The BBSSS, BBSSG, BBBBB, and BBSGG series all started with similar n_o values at shallow floodplain depths. This indicates that flows in the main channel still dominate. As the depth increased beyond y/D = 1.3, effects of floodplain roughness were reflected in the n_o value for each arrangement. The floodplain generally carried approximately 20~25 percent of flow at this depth (see flow ratios in Chapter 4).

All these experimental tests were conducted under the same slope, 6.173E-04. Since all derived data showed a similar trend, and because the only difference among these tests was the arrangement of roughness elements, it is feasible to derive a general function for such variations. An attempt was made to derive such an equation using these best fit data. This equation has the form:

$$n_o = \frac{PR^{1.116}}{\sum \frac{P_i R_i^{1.116}}{n_i}} \qquad (6.2)$$

which is the form of equation 2.1 but with a different exponent.

6.4.2. *Effect on n_o of Changing Main Channel Roughness*

Figures 4.24 and 4.27 demonstrated that both the raw data and the predictions responded more readily to changes in main channel roughness. Data derived in table 4.2 are plotted in figure 6.3. It can be seen that changing roughness in the main channel affected the n_o values more than it did on the floodplain. Even though these three experiments were conducted at a slope of 1.045E-03, the magnitudes of n_o for GBBBB were much larger than for the BBBBB data series (figure 6.2). The effect of changing roughness in the main channel can further be demonstrated with the BGGGG and GGGGG data series, which had larger differences at shallow floodplain depths, although decreases in n_o also remained throughout the range of depths.

In the uniform roughness channel described in Chapter 5, we see that the influence of the main channel decreased roughly linearly from above bankfull to about 1.4 times bankfull depth. This depth corresponded to the intersection of flow distribution between the floodplain and main channel presented in our experiments. At this intersection, the floodplain began to carry more flow than the main channel, and could thus be assumed to become the dominant flow subsection.

On the basis of data presented in table 4.2, a similar attempt to derive a best fit equation was made. We found that although further improvement could be made by fine-tuning the exponent, equation 6.2 fit sufficiently well for data in both tables.

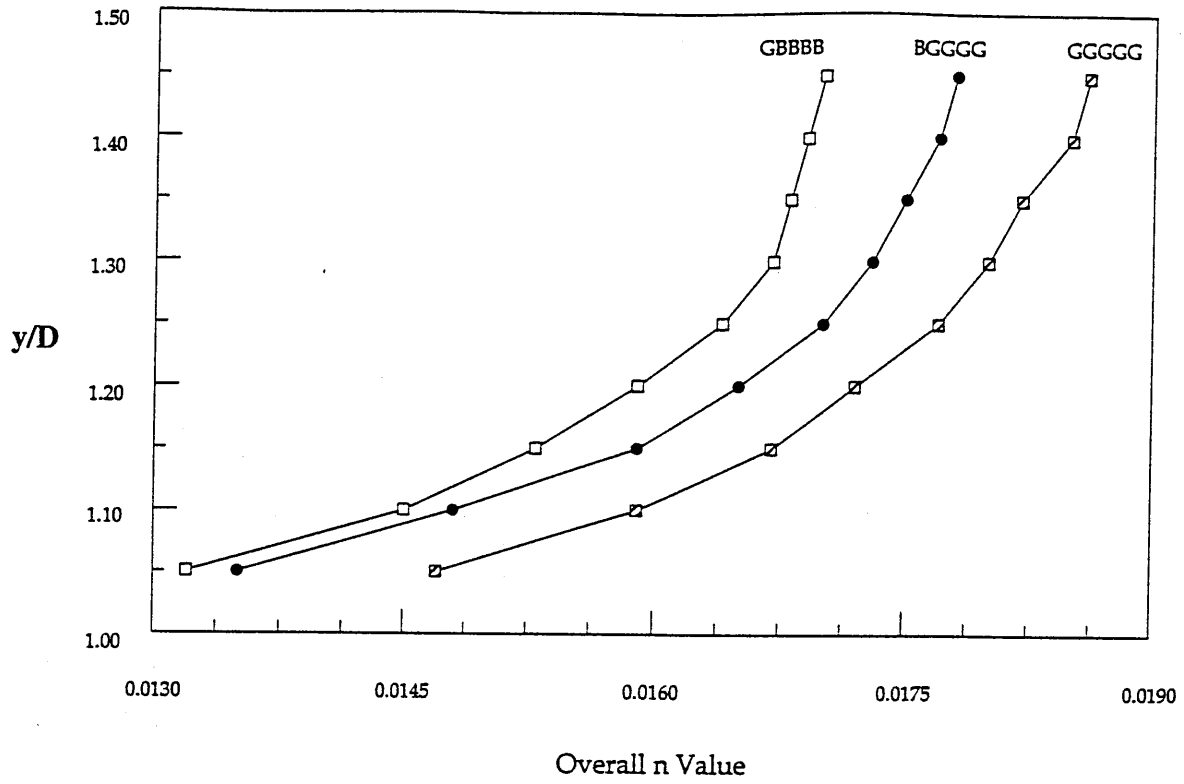

Figure 6.3. Fitted n_o for various roughness combinations in the main channel

6.4.3. *Effect on n_o of Changing Floodplain Roughness nearest the Main Channel*

Experimental data series BBSGG, BBGGG, BBSBB, and BBBBB were used for examining the effects of changing floodplain roughness nearest the main channel. These tests were conducted at a slope of 6.173E-04. In figure 6.4, one can observe that changing the roughness on this floodplain element from gravel to sand reduced n_o most greatly in the range of $y/D < 1.3$, while changing from black magnum to sand materials did not significantly affect n_o values. The base n values for sand and black magnum in this study are rather close. Since the n_o curves have similar trends, equation 6.2 can be reasonably assumed to perform well.

6.4.4. *Effect on n_o of Asymmetrical Floodplains*

The effect of asymmetrical floodplains was illustrated using data from Myers and Brennan (1990). Comparisons of the best fitted n_o values from Geometry 2.2 and Asymmetrical Channel (figure 6.5) show that there was no significant difference in n_o values at above bankfull stages. Myers and Brennans' experiments were of uniform roughness, fixed bed

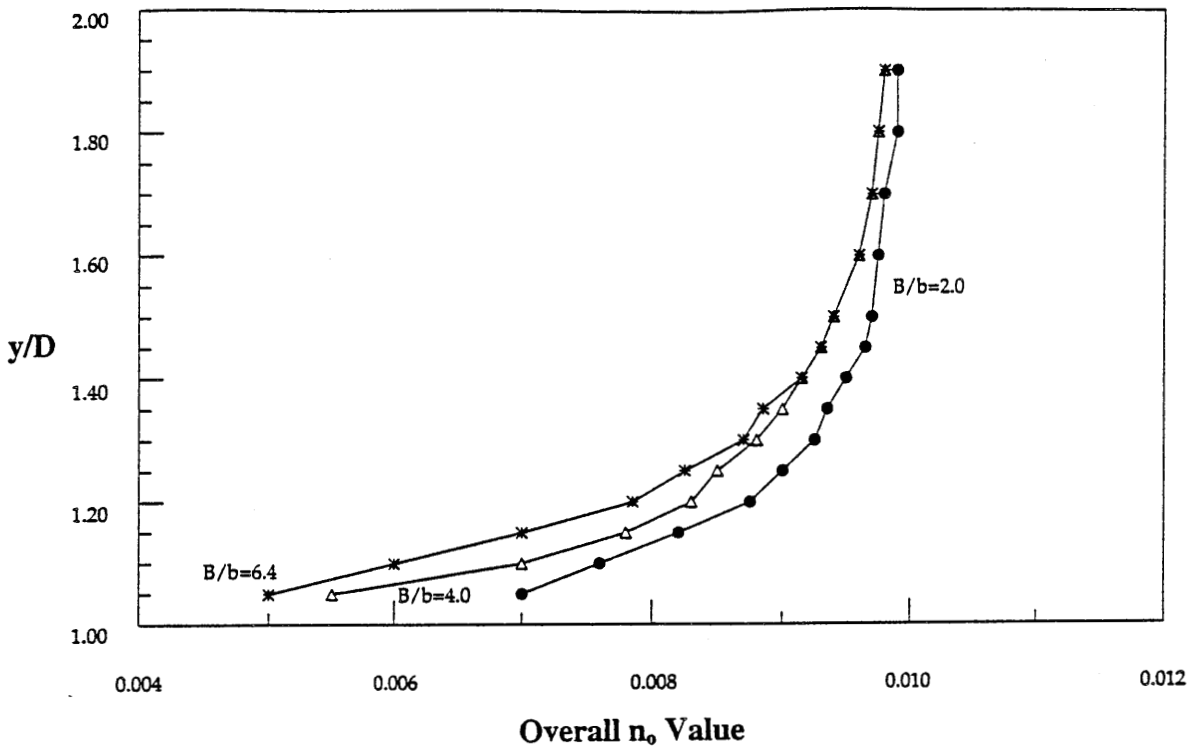

Figure 6.6. Fitted n_o from Geometries 2.2, 4.2, and 6.67 (Myers and Brennan, 1990)

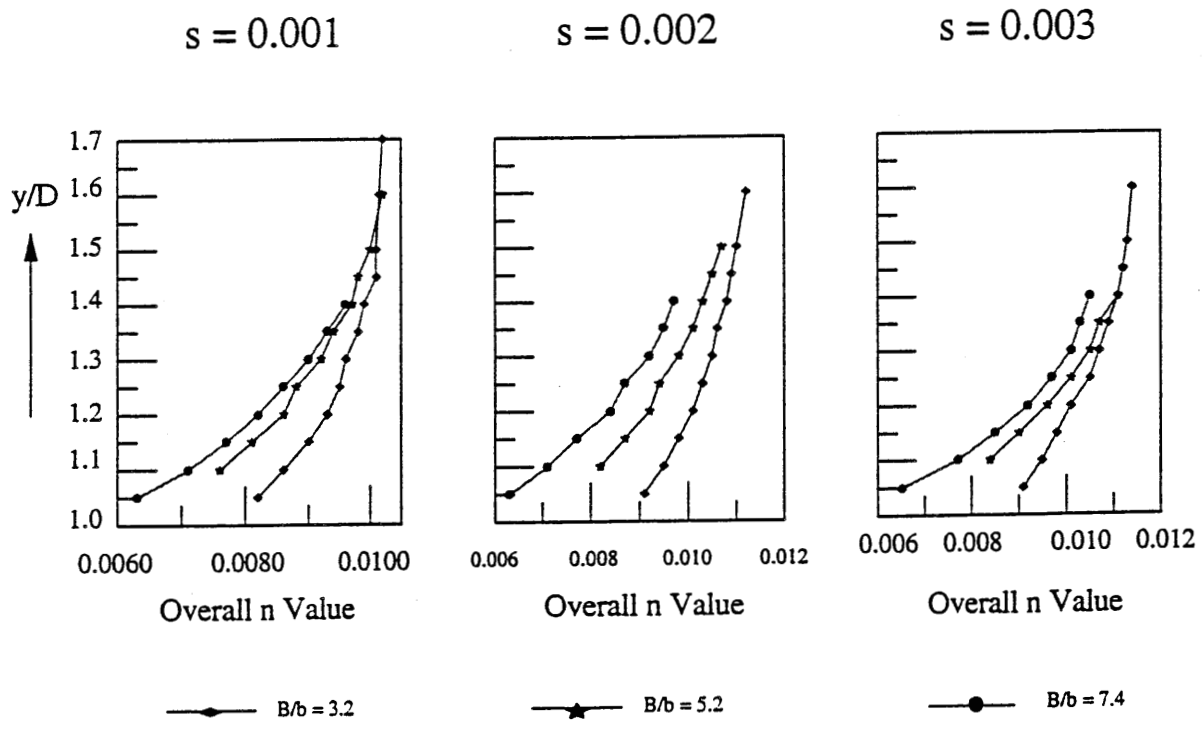

Figure 6.7. Fitted n_o from Tests 5, 6, and 7 to show effects of floodplain width (James and Brown, 1977)

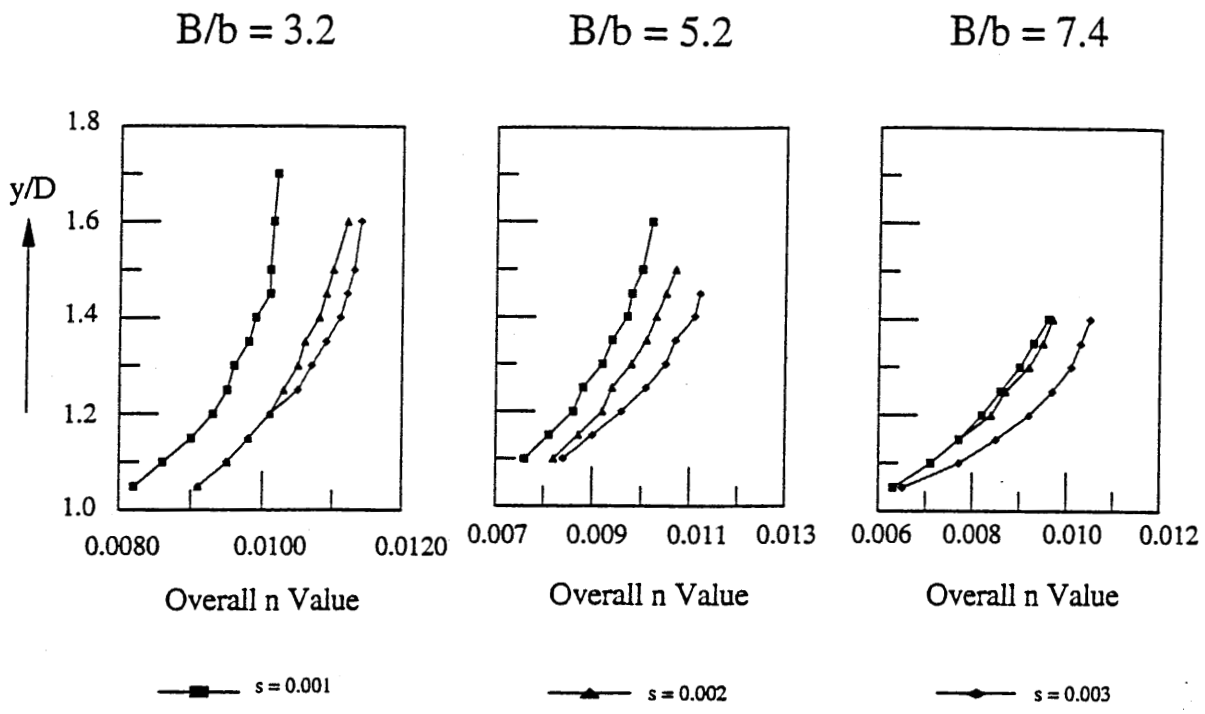

Figure 6.8. Fitted n_o from Tests 5, 6, and 7 to show effects of channel slopes (James and Brown, 1977)

narrow floodplain channels (B/b = 3.2), the n_o values for two higher slopes (S = 0.002 and 0.003) were similar in shallower depths until about y/D = 1.3; for wide floodplain channels (B/b=7.4), similar n_o was found in two gentler slopes until y/D = 1.4. Changes in geometry, namely increasing the width of the floodplain, were combined with the effects of varying slopes on n_o patterns.

Equations 2.1 and 2.2 perform well for James and Browns' data. Apparently floodplain width and channel slope both affect the discharge and shear force distributions. As shown earlier in Chapter 5, equation 2.2, which is based on the sum of shear forces, performed better for higher slopes. Among the variations a higher slope with faster flow tended more towards the values of equation 2.2, while a slower flow tended more towards the values of equation 2.1.

6.5. Summary

This study has verified that n_o varies with depth in both prismatic and compound channels. The magnitude of variation is considerable in compound channels regardless of whether the channel has uniform or heterogeneous roughness along the wetted perimeter. For compound channels, changing the magnitudes of roughness does affect the overall n_o patterns, especially in the main channel. For prismatic channels, changing the roughness arrangement alone significantly affects n_o patterns. The authors postulated that these changes could be reasonably predicted by equations using the basic hydraulic properties of the section.

It is clear that results from this experiment explain only part of the complex channel hydraulics. For example, in using the predictive equations, it is important to determine the base n value properly for the materials present along the wetted perimeter, especially material with for non-uniform granular compositions. Overall n_o also varies with channel slope, which apparently affects n_o in conjunction with floodplain width. Further efforts to quantify the relationship among the variables in simple channels of heterogeneous roughness are required. While some of the issues regarding Manning's n value have been clarified in this report, more information is required for the proper application of this simple and widely used equation.

REFERENCES

Arcement, G.J., Jr., and V.R. Schneider. 1989. *Guide for Selecting Manning's Roughness Coefficients for Natural Channels and Flood Plains.* U.S. Geological Survey Water Supply paper no. 2339, U.S. Government Printing Office, Washington, D.C.

Anderson, D.N. *Evaluation of the Manning Roughness Coefficient for Compound River Channels.* Deaprtment of Theoretical and Applied Mechanics, TAM 293/294 bResearch and Design Project. University of Illinois Urbana, Illinois, 1994

Azmon, B. 1992 *Manning coefficient of roughness — a case study along Soreq Stream, 1971-1981.* Journal of Hydrology. No. 132. Elsevire Science Publishers, B.V., Amsterdam, Holland, pp.. 361-377.

Baird, J.I., and D.A. Ervine. 1984. *Resistance to flow in channels with overbank flood plain flow.* Proceedings 1st International Conference on Channels and Channel Control Structures, Computational Mechanics Center, Southampton, United Kingdom, pp.. 4137-4150.

Barnes, H.H., Jr. 1967. *Roughness characteristics of natural streams.* U.S. Geological Survey, Water Supply Paper No. 1849, U.S. Government Printing Office, Washington, D.C.

Blalock, M.E, and T.W. Sturm. 1981 *"Minimum Specific Energy in Compound Open Channel."* Journal of the Hydraulics Division, Proceedings of the American Society of Civil Engineers 107:HY6 (1981): 699-717.

Bray, D.I. 1979. *Estimating Average Velocity in Gravel-Bed Rivers.* Journal of the Hydraulics Division, Proceedings of the American Society of Civil Engineers 105:HY9 (1979): 1103-1122.

Chow, V.T. 1959. *Open channel hydraulics.* McGraw-Hill, New York, NY, 680p.

Christensen, B.A. 1992. Discussion on *Calculation of Total Conveyance in Natural Channels.* Journal of the Hydraulics Division, American Society of Civil Engineers Vol. 118, No.8, pp. 1196-1197.

Cokljat, D., and B.A. Younis 1995. *Compound Channel Flows: A Parametric Study Using a Reynolds Stress Transport Closure.* Journal of Hydraulic Research. Vol.33, No.3, 1995. pp. 307-320.

Colebatch, G.T. 1941. *Model Tests on the Lawrence Canal Roughness Coefficients.* Journal, Institute of Civil Engineers (Australia). No. 13 (2): 27-32.

Cox, R.G. 1973. *Effective hydraulic roughness for channels having bed roughness different from bank roughness.* Army Engineer Waterways Experiment Station, Vicksburg, Mississippi. Miscellaneous Papers H-73-2. 52p.

Cruff, R.W. 1965. *Cross Channel Transfer of Linear Momentum in Smooth Rectangular Channels.* U.S. Geological Survey, Water Supply Paper 1592-B.

Daugherty, R.L., and J.B. Franzini. 1977. Fluid Mechanics with Engineering Applications. McGraw-Hill Book Co. New York.

DePue, P.M. 1996. *Variation of Manning's Roughness Coefficient with Changes in Channel Geometry and Roughness Pattern.* M.S. Thesis. Department of Civil Engineering, University of Illinois at Urbana-Champaign.

Einstein, H.A. 1934. *Der hydraulische oder profile-radius (The hydraulic or cross section radius),* Schweizerische Bauzeitung, Zurich, Switzerland, Vol. 103, No. 8, pp. 89-91.

Einstein, H.A., and R.B. Banks. 1950. *Fluid resistance of composite roughness.* Transactions, American Geophysical Union, Vol. 31, No. 4, pp. 603-610.

Felkel, K. 1960. *Gemessene Abflusse in Gerinnen mit Weidenbewuchs.* Mitteilungen der BAW, Heft 15, Karlsruhe, Germany. (Cited from Yen, 1992b)

Fread, D.L. 1989. *Flood routing models and Manning's n.* In Channel Flow and Catchment Runoff, Proceedings, International Conference for Centennial of Manning's Formula and Kuichling's Rational Formula (B.C. Yen, editor), University of Virginia, Charlottesville, Virginia, pp. 699-708.

Garbrecht, J., and G.O. Brown. 1991. *Calculation of Total Conveyance in Natural Channels.* Journal of Hydraulic Engineering. ASCE. Vol.117, No.6. pp. 788-798.

Ghosh, S.N., and P.J. Mehta. 1974. *Boundary Shear Distribution in a Compound Channel with Varying Roughness Distribution.* Proceedings, Institute of Civil Engineers, Vol.57, March.

Greenhill, R.K. and R.H.J. Sellin. 1993. *Development of a Simple Method to Predict Discharges in Compound Meandering Channels.* Proceedings of the Institution of Civil Engineers, Water Maritime and Energy. Vol 101, No 1. Mar. 1993, pp. 37-44.

Hadzipanos, P. 1980. *Flow in Compound Channels with Varying Roughness.* Ph.D. Thesis. London: University of London.

Henderson, H. 1966. Open Channel Flow. The Macmillan Company, New York, NY.

Hollinrake, P.G. 1989 *The Structure of Flow in Open Channels--a Literature Search.* Vol. 3, Research Report SR209, Wallingford, England: Hydraulics Research Ltd.

Hollinrake, P.G. 1988. *The Structure of Flow in Open Channels--a Literature Search.* Vol. 2, Research Report SR153, Wallingford, England: Hydraulics Research Ltd.

Hollinrake, P.G. 1987. *The Structure of Flow in Open Channels--a Literature Search.* Vol. 1, Research Report SR96, Wallingford, England: Hydraulics Research Ltd.

Horton, R.E. 1933. *Separate roughness coefficient for channel bottom and sides.* Engineering News-Record, Vol. 111, No. 22, pp. 652-653.

James, M., and B.J. Brown. 1977. *Geometric Parameters that Influence Floodplain Flow.* Research Report H-77-1. Hydraulics Laboratory U.S. Army Engineer Waterways Experiment Station, Vicksburg, Mississippi.

Knight, D.W., and J.D. Demetriou. 1983. *Floodplain and main channel flow interaction.* Journal of Hydraulic Engineering, American Society of Civil Engineers, Vol. 109, No. HY8, pp. 1073-1092.

Knight, D.W., and J.A. MacDonald. 1979. *Open Channel Flow with Varying Bed Roughness*. Journal of the Hydraulics Division, Proceedings of the American Society of Civil Engineers Vol. 105: HY9 (1979): 1167-1183.

Krishnamurthy, M., and B.A. Christensen. 1972. *Equivalent roughness for shallow channels*. Journal of the Hydraulics Division, Proceedings of the American Society of Civil Engineers, Vol. 98, No. HY12, pp. 2257-2263.

Lane, E.W. 1951. *Discussions on Slope Discharge Formulae of Alluvial Streams and Rivers* (E.C. Schnackenberg, editor). Proceedings, New Zealand Institution of Engineers, Vol. 37, Wellington, pp. 435-438.

Lotter, G.K. 1933. *Considerations on hydraulic design of channels with different roughness of walls.* Transactions, All-Union Scientific Research Institute of Hydraulic Engineering, Vol. 9, Leningrad, Russia, pp. 238-241.

Maxwell, W.H.C. 1972. *Hydrosystems Lab Tour Information.* Internal documentation. Hydrosystems Lab. University of Illinois at Urbana-Champaign. 11p.

Motayed A.K., and M. Krishnamurthy. 1979. *Composite roughness of natural channels.* Journal of Hydraulic Engineering, ASCE, Vol. 106, No. 6, 1979. pp.. 1111-1116.

Muhlhofer, L. 1933. *Roughness investigations in a shaft with concrete bottom and unlined walls.* Wasserkraft und Wasserwirtschaft, Munich, Germany, Vol. 28, No. 8, pp. 85-88.

Myers, W.R.C. 1991. *Influence of Geometry on Discharge Capacity of Open Channels.* Journal of Hydraulic Engineering 117.5 (1991): 676-680.

Myers, W.R.C. 1987. *Velocity and Discharges in Compound Channels.* Journal of Hydraulic Engineering Vol. 113. No.6: pp. 753-766.

Myers, W.R.C. 1978. *Momentum Transfer in a Compound Channel.* Journal of Hydraulic Research. V.16.2 (1978): 139-150.

Myers, W.R.C., and E.K. Brennan. 1990. *Flow resistance in compound channels.* Journal of Hydraulic Research, Vol. 28, No. 2, pp.. 141-155.

Nalluri, C., and N.D. Judy. 1985. *Interaction between main channel and flood plain flows.* Proceedings, 21st Congress International Association for Hydraulic Research, Melbourne, Australia.

Nezu, I. 1994. *Compound Open-Channel Turbulence and Its Role in River Environment --Significance of Secondary Currents.* Ninth Congress of the Asian and Pacific Division of the Interantional Association for Hydraulic Research, Aug 24-26, Singapore, 1994.

Nikuradse, J. 1932. Gesetzmassigkeiten der turbulenten Stromung in glatten Rohren (Laws of turbulent flow in smooth pipes), *Forschungsheft des Vereins deutscher Ingenieure, No. 356*, Berlin.

Pavlovskii, N.N. 1931. *On a design formula for uniform movement in channels with nonhomogeneous walls.* Transactions, All-Union Scientific Research Institute of Hydraulic Engineering, Vol. 4, Leningrad, Russia, pp.. 157-164.

Pillai, C.R.S. 1962. *Composite Roughness Coefficient in Open Channel Flow.* Irrigation and Power: Journal of Central Board of Irrigation and Power 19.3 (1962): 174-189.

Posey, C.J.F. 1967. *Shape Effects on Resistance in Floodplain Channels.* Civil Engineering, ASCE, No.CE4, Vol. 37, April.

Rouse, H. 1978. Elementary Mechanics of Fluids. New York: Dover Publications, Inc.

Rouse, H. 1965. *Critical analysis of open-channel resistance.* Journal of Hydraulic Division. Proceedings of the American Society of Civil Engineers, Vol. 91, No. HY4, pp. 1-25.

Sellin, R.H.J. 1964. *A Laboratory Investigation Into the Interaction Between the Flow in the Channel of a River and That Over Its Flood Plain.* La Houille Blanche 7 (1964): 793-802.

Shen, H.W. (ed). 1979. Modeling of Rivers. New York: John Wiley and Sons.

Strickler, A. 1923. *Beiträge zur Frage der Geschwindigkeits-formel und der Rauhigkeitszahlen für Ströme, Kanäle und geschlossene Leitungen [Some Contributions to the Problems of the Velocity Formula and Roughness Factor for Rivers, Canals, and Closed Conduits.* Mitteilungen des Eidgenössischer Amtes für Wasserwirtschaft, nr. 16.

U.S. Army Corps of Engineers. 1981. *Guidelines for the Calibration and Application of Computer Program HEC-6.* The Hydrologic Engineering Center, U.S. Army Corps of Engineers, Davis, California. 39p.

U.S. Army Corps of Engineers. 1968. "Hydraulic Design Criteria". Chart 631-4, *Open Channel Flow; Composite Roughness Effective Manning's n* and Chart 631-4/1. *Open Channel Flow; Composite Roughness Wetted Perimeter Relation.*

Vanoni, V. (ed). 1975. Sedimentation Engineering. New York: ASCE Task Committee for the Preparation of the Manual on Sedimentation of the Sedimentation Committee of the Hydraulic Division.

Wormleaton, P.R., and P. Hadjipanos. 1985. *Flow Distribution in Compound Channels.* Journal of Hydraulic Engineering, ASCE. Vol.111, No.2, pp 357-360.

Wormleaton, P.R., Allen, J. and P. Hadjipanos. 1981. *Discharge Assessment in Compound Channel Flow.* Journal of Hydraulic Engineering, ASCE. Vol.108, No.9, pp.975-994.

Wright, R.R. and M.R. Carstens. 1970. *Linear Momentum Flux to Overbank Sections.* Journal of Hydraulic Engineering, ASCE. Vol. 96, HY9.

Yen, B.C. 1992a. *Hydraulic resistance in open channels.* In Channel Flow: Centennial of Manning's Formula (B.C. Yen, editor), Water Resources Publications, Littleton, CO. pp. 1-135.

Yen, B.C. 1992b. *Dimensionally Homogeneous Manning's Formula.* Journal of the Hydraulics Engineering, Vol. 118, No. 9, September, 1992. American Society of Civil Engineers: pp. 1326-1332.

Yen, B.C., R. Camacho, and R. Kohane. 1985. *Significance of Floodplains in Backwater Computation.* International Association for Hydraulic Research, 21st Congress, Vol. 3, August 1985, Melbourne, Australia, pp. 439-445.

Yen, C.L. and D.E. Overton. 1973. *Shape Effects on Resistance in Flood-Plain Channels.* Journal of the Hydraulics Division, Proceedings of the American Society of Civil Engineers 99:HY1 (1973): 219-238.

Appendix I

Processed Experimental Data

Appendix I Notes:

- The elevation of the bottom of the MC is, on average, at elevation 1.363. To find the total depth, subtract this value from the overall water surface elevation.
- The bankfull elevation is 2.030. Thus, the bankfull depth is 0.667 ft.
- The MC weir measures the flow from the MC subarea only.
- The MCB weir measures the flow from the MCB subarea only.
- The FP weir measures the flow from the FP1, FP2, and FP3 subareas.
- WP refers to the wetted perimeter of the roughened area of the channel bed only.
- WWP refers to the wetted perimeter of the smooth channel side walls only.

The information for each data series is split into two tables. As an example, the first page of data contains the first table, and the second page of data contains the second table. The third page of data contains the first table for the next group of data. This is repeated until all of the Used Data has been presented. The Unused data is then presented in a similar fashion.

The first table contains:

Test name
Base n values for all subareas
Overall water surface elevation
Depth / Bankfull depth
Overall area
Overall WP
Overall WP+WWP
Overall Bed Slope

The second table contains

Overall Flowrate
Overall Reynolds number
Floodplain Reynolds number
Overall Froude number
Overall adjusted n value
Ratio of flow in MC, MCB, and FP subsections

Please note that a subsection may be composed of as many as three subareas. The FP subsection is composed of the FP1, FP2, and FP3 subareas. The MC subsection is composed of the MC subarea only. The MCB subsection is composed of the MC subarea only.

Used Data

Test Name	MC Subarea Base n value	MCB Subarea Base n value	FP3 Subarea Base n value	FP2 Subarea Base n value	FP1 Subarea Base n value	Overall Water Surface Elevation (ft)	Depth/ Bankfull Depth	Overall Area (sf)	Overall WP (ft)	Overall WP+WWP (ft)	Overall Bed Slope (ft/ft)
BBBBB 4	0.0130	0.0130	0.0130	0.0130	0.0130	1.956	0.890	0.585	1.524	2.122	6.173E-04
BBBBB 5	0.0130	0.0130	0.0130	0.0130	0.0130	2.134	1.157	1.096	4.164	5.047	6.173E-04
BBBBB 6	0.0130	0.0130	0.0130	0.0130	0.0130	2.154	1.187	1.175	4.164	5.087	6.173E-04
BBBBB 7	0.0130	0.0130	0.0130	0.0130	0.0130	2.202	1.258	1.360	4.164	5.182	6.173E-04
BBBBB 15	0.0130	0.0130	0.0130	0.0130	0.0130	2.285	1.384	1.684	4.164	5.349	6.173E-04
BBBBB 17	0.0130	0.0130	0.0130	0.0130	0.0130	2.324	1.442	1.835	4.164	5.427	6.173E-04
BBSBB 1	0.0130	0.0130	0.0120	0.0130	0.0130	2.316	1.429	1.803	4.164	5.411	6.173E-04
BBSBB 3	0.0130	0.0130	0.0120	0.0130	0.0130	2.262	1.349	1.594	4.164	5.303	6.173E-04
BBSBB 4	0.0130	0.0130	0.0120	0.0130	0.0130	2.203	1.260	1.365	4.164	5.185	6.173E-04
BBSBB 6	0.0130	0.0130	0.0120	0.0130	0.0130	2.182	1.229	1.283	4.164	5.143	6.173E-04
BBSBB 9	0.0130	0.0130	0.0120	0.0130	0.0130	1.882	0.779	0.493	1.420	1.943	6.173E-04
BBSSS 1	0.0130	0.0130	0.0120	0.0120	0.0120	2.224	1.292	1.446	4.164	5.227	6.173E-04
BBSSS 2	0.0130	0.0130	0.0120	0.0120	0.0120	2.286	1.385	1.688	4.164	5.351	6.173E-04
BBSSS 3	0.0130	0.0130	0.0120	0.0120	0.0120	2.304	1.411	1.756	4.164	5.386	6.173E-04
BBSSS 4	0.0130	0.0130	0.0120	0.0120	0.0120	2.330	1.450	1.857	4.164	5.438	6.173E-04
BBSSS 5	0.0130	0.0130	0.0120	0.0120	0.0120	2.247	1.326	1.535	4.164	5.273	6.173E-04
BBSSS 8	0.0130	0.0130	0.0120	0.0120	0.0120	1.967	0.906	0.599	1.539	2.147	6.173E-04
BBSSG 1	0.0130	0.0130	0.0120	0.0120	0.0182	2.145	1.173	1.139	4.164	5.069	6.173E-04
BBSSG 2	0.0130	0.0130	0.0120	0.0120	0.0182	2.183	1.230	1.286	4.164	5.144	6.173E-04
BBSSG 6	0.0130	0.0130	0.0120	0.0120	0.0182	2.355	1.488	1.954	4.164	5.489	6.173E-04
BBSSG 7	0.0130	0.0130	0.0120	0.0120	0.0182	2.166	1.205	1.222	4.164	5.112	6.173E-04
BBSSG 8	0.0130	0.0130	0.0120	0.0120	0.0182	2.183	1.231	1.288	4.164	5.145	6.173E-04

Used Data

Test Name	Overall Flowrate (cfs)	Overall Reynolds Number	Floodplain Reynolds Number	Overall Froude Number	Overall Adjusted n value	Ratio of Flow in MC	Ratio of Flow in MCB	Ratio of Flow in FP
BBBBB 4	0.697	2.921E+04	0.000E+00	0.310	0.0142	0.666	0.334	0.000
BBBBB 5	1.212	2.139E+04	2.196E+03	0.367	0.0125	0.592	0.354	0.054
BBBBB 6	1.342	2.345E+04	3.661E+03	0.366	0.0126	0.578	0.340	0.082
BBBBB 7	1.601	2.753E+04	9.240E+03	0.351	0.0135	0.504	0.320	0.176
BBBBB 15	2.231	3.734E+04	2.041E+04	0.355	0.0137	0.416	0.298	0.286
BBBBB 17	2.612	4.289E+04	3.075E+04	0.365	0.0133	0.369	0.256	0.375
BBSBB 1	2.528	4.196E+04	0.000E+00	0.363	0.0134	0.000	0.000	0.000
BBSBB 3	2.078	3.536E+04	1.863E+04	0.359	0.0134	0.421	0.303	0.276
BBSBB 4	1.576	2.735E+04	9.798E+03	0.343	0.0138	0.497	0.315	0.188
BBSBB 6	1.524	2.668E+04	6.959E+03	0.365	0.0128	0.537	0.326	0.137
BBSBB 9	0.555	2.580E+04	0.000E+00	0.310	0.0142	0.699	0.301	0.000
BBSSS 1	1.870	3.360E+04	1.530E+04	0.374	0.0127	0.467	0.294	0.239
BBSSS 2	2.258	3.962E+04	2.509E+04	0.358	0.0135	0.392	0.276	0.332
BBSSS 3	2.409	4.201E+04	3.047E+04	0.360	0.0135	0.352	0.268	0.380
BBSSS 4	2.704	4.669E+04	3.481E+04	0.371	0.0131	0.345	0.265	0.390
BBSSS 5	2.039	3.613E+04	1.726E+04	0.373	0.0128	0.450	0.300	0.250
BBSSS 8	0.746	3.264E+04	0.000E+00	0.322	0.0136	0.659	0.341	0.000
BBSSG 1	1.295	2.380E+04	3.997E+03	0.370	0.0125	0.555	0.356	0.088
BBSSG 2	1.558	2.814E+04	8.329E+03	0.371	0.0126	0.522	0.322	0.155
BBSSG 6	2.687	4.548E+04	3.464E+04	0.342	0.0145	0.335	0.266	0.398
BBSSG 7	1.409	2.571E+04	5.876E+03	0.362	0.0129	0.546	0.334	0.120
BBSSG 8	1.703	3.092E+04	1.194E+04	0.405	0.0114	0.486	0.311	0.203

Used Data Continued

Test Name	MC Subarea Base n value	MCB Subarea Base n value	FP3 Subarea Base n value	FP2 Subarea Base n value	FP1 Subarea Base n value	Overall Water Surface Elevation (ft)	Depth/ Bankfull Depth	Overall Area (sf)	Overall WP (ft)	Overall WP+WWP (ft)	Overall Bed Slope (ft/ft)
BBSSG 9	0.0130	0.0130	0.0120	0.0120	0.0182	2.255	1.338	1.565	4.164	5.288	6.173E-04
BBSSG 10	0.0130	0.0130	0.0120	0.0120	0.0182	2.278	1.372	1.656	4.164	5.335	6.173E-04
BBSSG 11	0.0130	0.0130	0.0120	0.0120	0.0182	2.314	1.427	1.797	4.164	5.408	6.173E-04
BBSSG 12	0.0130	0.0130	0.0120	0.0120	0.0182	2.328	1.447	1.849	4.164	5.434	6.173E-04
BBSGG 1	0.0130	0.0130	0.0120	0.0182	0.0182	2.132	1.153	1.088	4.164	5.042	6.173E-04
BBSGG 2	0.0130	0.0130	0.0120	0.0182	0.0182	2.157	1.191	1.186	4.164	5.093	6.173E-04
BBSGG 3	0.0130	0.0130	0.0120	0.0182	0.0182	2.188	1.238	1.308	4.164	5.156	6.173E-04
BBSGG 4	0.0130	0.0130	0.0120	0.0182	0.0182	2.217	1.282	1.420	4.164	5.214	6.173E-04
BBSGG 5	0.0130	0.0130	0.0120	0.0182	0.0182	2.239	1.314	1.504	4.164	5.256	6.173E-04
BBSGG 6	0.0130	0.0130	0.0120	0.0182	0.0182	2.271	1.362	1.628	4.164	5.321	6.173E-04
BBSGG 7	0.0130	0.0130	0.0120	0.0182	0.0182	2.305	1.413	1.760	4.164	5.388	6.173E-04
BBSGG 8	0.0130	0.0130	0.0120	0.0182	0.0182	2.312	1.423	1.786	4.164	5.402	6.173E-04
BBSGG 10	0.0130	0.0130	0.0120	0.0182	0.0182	2.342	1.468	1.904	4.164	5.463	6.173E-04
BBGGG 1	0.0130	0.0130	0.0182	0.0182	0.0182	2.162	1.198	1.204	4.164	5.102	6.173E-04
BBGGG 3	0.0130	0.0130	0.0182	0.0182	0.0182	2.224	1.291	1.444	4.164	5.226	6.173E-04
BBGGG 4	0.0130	0.0130	0.0182	0.0182	0.0182	2.249	1.329	1.543	4.164	5.277	6.173E-04
BBGGG 5	0.0130	0.0130	0.0182	0.0182	0.0182	2.262	1.348	1.593	4.164	5.303	6.173E-04
BBGGG 6	0.0130	0.0130	0.0182	0.0182	0.0182	2.304	1.411	1.757	4.164	5.387	6.173E-04
BBGGG 7	0.0130	0.0130	0.0182	0.0182	0.0182	2.312	1.424	1.789	4.164	5.403	6.173E-04
BBGGG 8	0.0130	0.0130	0.0182	0.0182	0.0182	2.327	1.445	1.845	4.164	5.432	6.173E-04
BGGGG 6	0.0130	0.0182	0.0182	0.0182	0.0182	2.126	1.145	1.065	4.164	5.031	1.045E-03
BGGGG 7	0.0130	0.0182	0.0182	0.0182	0.0182	2.171	1.212	1.240	4.164	5.121	1.045E-03

Used Data Continued

Test Name	Overall Flowrate (cfs)	Overall Reynolds Number	Floodplain Reynolds Number	Overall Froude Number	Overall Adjusted n value	Ratio of Flow in MC	Ratio of Flow in MCB	Ratio of Flow in FP
BBSSG 9	2.110	3.726E+04	1.909E+04	0.374	0.0127	0.427	0.305	0.268
BBSSG 10	2.276	3.980E+04	2.376E+04	0.371	0.0129	0.382	0.306	0.313
BBSSG 11	2.586	4.479E+04	3.315E+04	0.373	0.0130	0.346	0.267	0.387
BBSSG 12	2.650	4.562E+04	3.419E+04	0.366	0.0133	0.342	0.265	0.392
BBSGG 1	1.212	2.270E+04	2.703E+03	0.371	0.0123	0.534	0.403	0.063
BBSGG 2	1.334	2.486E+04	4.762E+03	0.359	0.0130	0.562	0.338	0.101
BBSGG 3	1.521	2.801E+04	8.841E+03	0.353	0.0133	0.519	0.315	0.166
BBSGG 4	1.745	3.186E+04	1.295E+04	0.358	0.0133	0.476	0.311	0.213
BBSGG 5	1.913	3.464E+04	1.675E+04	0.361	0.0132	0.434	0.313	0.253
BBSGG 6	2.167	3.877E+04	2.134E+04	0.362	0.0133	0.405	0.307	0.288
BBSGG 7	2.370	4.285E+04	2.854E+04	0.353	0.0138	0.371	0.280	0.349
BBSGG 8	2.520	4.544E+04	3.213E+04	0.367	0.0132	0.353	0.276	0.370
BBSGG 10	2.697	4.819E+04	0.000E+00	0.357	0.0138	0.000	0.000	0.000
BBGGG 1	1.344	2.540E+04	4.750E+03	0.354	0.0132	0.560	0.342	0.098
BBGGG 3	1.746	3.220E+04	1.330E+04	0.349	0.0137	0.472	0.312	0.216
BBGGG 4	1.929	3.524E+04	1.751E+04	0.350	0.0138	0.442	0.298	0.260
BBGGG 5	2.093	3.806E+04	2.094E+04	0.362	0.0133	0.408	0.304	0.288
BBGGG 6	2.333	4.193E+04	2.731E+04	0.348	0.0140	0.382	0.277	0.341
BBGGG 7	2.482	4.475E+04	3.049E+04	0.361	0.0135	0.366	0.277	0.357
BBGGG 8	2.626	4.709E+04	3.418E+04	0.364	0.0134	0.348	0.272	0.380
BGGGG 6	1.231	2.429E+04	2.296E+03	0.389	0.0156	0.553	0.397	0.050
BGGGG 7	1.475	2.847E+04	5.809E+03	0.371	0.0168	0.571	0.322	0.107

Used Data Continued

Test Name	MC Subarea Base n value	MCB Subarea Base n value	FP3 Subarea Base n value	FP2 Subarea Base n value	FP1 Subarea Base n value	Overall Water Surface Elevation (ft)	Depth/ Bankfull Depth	Overall Area (sf)	Overall WP (ft)	Overall WP+WWP (ft)	Overall Bed Slope (ft/ft)
BGGGG 8	0.0130	0.0182	0.0182	0.0182	0.0182	2.194	1.246	1.328	4.164	5.166	1.045E-03
BGGGG 9	0.0130	0.0182	0.0182	0.0182	0.0182	2.198	1.253	1.345	4.164	5.175	1.045E-03
BGGGG 10	0.0130	0.0182	0.0182	0.0182	0.0182	2.225	1.293	1.451	4.164	5.229	1.045E-03
BGGGG 11	0.0130	0.0182	0.0182	0.0182	0.0182	2.251	1.332	1.551	4.164	5.281	1.045E-03
BGGGG 12	0.0130	0.0182	0.0182	0.0182	0.0182	2.276	1.369	1.646	4.164	5.330	1.045E-03
BGGGG 13	0.0130	0.0182	0.0182	0.0182	0.0182	2.297	1.402	1.731	4.164	5.374	1.045E-03
BGGGG 14	0.0130	0.0182	0.0182	0.0182	0.0182	2.317	1.431	1.806	4.164	5.412	1.045E-03
BGGGG 15	0.0130	0.0182	0.0182	0.0182	0.0182	2.335	1.459	1.879	4.164	5.450	1.045E-03
GGGGG 2	0.0182	0.0182	0.0182	0.0182	0.0182	1.792	0.644	0.389	1.295	1.728	1.045E-03
GGGGG 3	0.0182	0.0182	0.0182	0.0182	0.0182	1.879	0.775	0.490	1.417	1.937	1.045E-03
GGGGG 4	0.0182	0.0182	0.0182	0.0182	0.0182	1.951	0.883	0.579	1.518	2.110	1.045E-03
GGGGG 5	0.0182	0.0182	0.0182	0.0182	0.0182	2.143	1.170	1.131	4.164	5.065	1.045E-03
GGGGG 6	0.0182	0.0182	0.0182	0.0182	0.0182	2.168	1.208	1.228	4.164	5.115	1.045E-03
GGGGG 7	0.0182	0.0182	0.0182	0.0182	0.0182	2.204	1.262	1.369	4.164	5.187	1.045E-03
GGGGG 8	0.0182	0.0182	0.0182	0.0182	0.0182	2.234	1.307	1.485	4.164	5.247	1.045E-03
GGGGG 9	0.0182	0.0182	0.0182	0.0182	0.0182	2.250	1.330	1.545	4.164	5.278	1.045E-03
GGGGG 10	0.0182	0.0182	0.0182	0.0182	0.0182	2.277	1.370	1.650	4.164	5.332	1.045E-03
GGGGG 11	0.0182	0.0182	0.0182	0.0182	0.0182	2.298	1.403	1.735	4.164	5.375	1.045E-03
GGGGG 12	0.0182	0.0182	0.0182	0.0182	0.0182	2.334	1.457	1.875	4.164	5.448	1.045E-03
GGGGG 13	0.0182	0.0182	0.0182	0.0182	0.0182	2.346	1.475	1.922	4.164	5.472	1.045E-03
GBBBB 4	0.0182	0.0130	0.0130	0.0130	0.0130	1.876	0.770	0.486	1.412	1.929	1.045E-03
GBBBB 13	0.0182	0.0130	0.0130	0.0130	0.0130	2.283	1.381	1.677	4.164	5.346	1.045E-03

Used Data Continued

Test Name	Overall Flowrate (cfs)	Overall Reynolds Number	Floodplain Reynolds Number	Overall Froude Number	Overall Adjusted n value	Ratio of Flow in MC	Ratio of Flow in MCB	Ratio of Flow in FP
BGGGG 8	1.655	3.215E+04	9.784E+03	0.376	0.0167	0.519	0.321	0.160
BGGGG 9	1.658	3.189E+04	1.046E+04	0.370	0.0170	0.518	0.310	0.172
BGGGG 10	1.842	3.535E+04	1.484E+04	0.366	0.0174	0.462	0.318	0.220
BGGGG 11	2.028	3.855E+04	1.871E+04	0.365	0.0176	0.442	0.304	0.254
BGGGG 12	2.229	4.197E+04	2.619E+04	0.367	0.0176	0.313	0.360	0.327
BGGGG 13	2.391	4.491E+04	2.870E+04	0.365	0.0178	0.375	0.291	0.335
BGGGG 14	2.604	4.882E+04	3.400E+04	0.373	0.0175	0.364	0.272	0.364
BGGGG 15	2.740	5.103E+04	0.000E+00	0.370	0.0177	0.000	0.000	0.000
GGGGG 2	0.406	2.385E+04	0.000E+00	0.312	0.0188	0.797	0.203	0.000
GGGGG 3	0.551	2.893E+04	0.000E+00	0.310	0.0191	0.708	0.292	0.000
GGGGG 4	0.701	3.377E+04	0.000E+00	0.316	0.0188	0.669	0.331	0.000
GGGGG 5	1.269	2.543E+04	2.904E+03	0.367	0.0168	0.598	0.342	0.060
GGGGG 6	1.405	2.805E+04	9.960E+03	0.359	0.0174	0.188	0.625	0.186
GGGGG 7	1.634	3.203E+04	1.187E+04	0.354	0.0178	0.486	0.319	0.194
GGGGG 8	1.837	3.576E+04	1.589E+04	0.353	0.0181	0.454	0.313	0.233
GGGGG 9	1.999	3.878E+04	1.917E+04	0.362	0.0177	0.420	0.321	0.259
GGGGG 10	2.221	4.274E+04	2.351E+04	0.364	0.0178	0.407	0.305	0.288
GGGGG 11	2.422	4.634E+04	2.948E+04	0.368	0.0176	0.383	0.284	0.333
GGGGG 12	2.611	4.935E+04	3.555E+04	0.353	0.0186	0.345	0.278	0.377
GGGGG 13	2.730	5.130E+04	0.000E+00	0.356	0.0185	0.000	0.000	0.000
GBBBB 4	0.558	2.980E+04	0.000E+00	0.318	0.0186	0.704	0.296	0.000
GBBBB 13	2.400	4.607E+04	3.075E+04	0.384	0.0168	0.367	0.284	0.350

Used Data Continued

Test Name	MC Subarea Base n value	MCB Subarea Base n value	FP3 Subarea Base n value	FP2 Subarea Base n value	FP1 Subarea Base n value	Overall Water Surface Elevation (ft)	Depth/ Bankfull Depth	Overall Area (sf)	Overall WP (ft)	Overall WP+WWP (ft)	Overall Bed Slope (ft/ft)
BBBGG 7	0.0130	0.0130	0.0130	0.0182	0.0182	2.175	1.219	1.257	4.164	5.129	7.932E-04
BBBGG 9	0.0130	0.0130	0.0130	0.0182	0.0182	2.208	1.267	1.383	4.164	5.194	7.932E-04
BBBGG 10	0.0130	0.0130	0.0130	0.0182	0.0182	2.235	1.309	1.490	4.164	5.250	7.932E-04
BBBGG 11	0.0130	0.0130	0.0130	0.0182	0.0182	2.263	1.349	1.596	4.164	5.304	7.932E-04
BBBGG 12	0.0130	0.0130	0.0130	0.0182	0.0182	2.284	1.382	1.681	4.164	5.348	7.932E-04
BBBGG 13	0.0130	0.0130	0.0130	0.0182	0.0182	2.307	1.416	1.770	4.164	5.393	7.932E-04
BBBGG 14	0.0130	0.0130	0.0130	0.0182	0.0182	2.319	1.433	1.814	4.164	5.416	7.932E-04

Used Data Continued

Test Name	Overall Flowrate (cfs)	Overall Reynolds Number	Floodplain Reynolds Number	Overall Froude Number	Overall Adjusted n value	Ratio of Flow in MC	Ratio of Flow in MCB	Ratio of Flow in FP
BBBGG 7	1.523	3.053E+04	1.302E+04	0.376	0.0143	0.216	0.560	0.224
BBBGG 9	1.742	3.425E+04	1.302E+04	0.372	0.0146	0.486	0.314	0.199
BBBGG 10	1.939	3.798E+04	1.764E+04	0.370	0.0148	0.441	0.315	0.243
BBBGG 11	2.143	4.154E+04	2.103E+04	0.369	0.0150	0.424	0.311	0.265
BBBGG 12	2.363	4.596E+04	2.828E+04	0.377	0.0147	0.385	0.293	0.322
BBBGG 13	2.532	4.882E+04	3.215E+04	0.374	0.0149	0.372	0.283	0.345
BBBGG 14	2.649	5.062E+04	3.591E+04	0.377	0.0148	0.357	0.272	0.371

Unused Data

Test Name	Overall Flowrate (cfs)	Overall Reynolds Number	Floodplain Reynolds Number	Overall Froude Number	Overall Adjusted n value	Ratio of Flow in MC	Ratio of Flow in MCB	Ratio of Flow in FP
BBBBB 8	0.061	5.040E+03	0.000E+00	0.226	0.0189	0.987	0.013	0.000
BBBBB 2	0.158	1.058E+04	0.000E+00	0.271	0.0160	0.920	0.080	0.000
BBBBB 3	0.293	1.685E+04	0.000E+00	0.311	0.0140	0.853	0.147	0.000
BBBBB 9	0.415	2.174E+04	0.000E+00	0.324	0.0134	0.783	0.217	0.000
BBBBB 10	0.469	2.326E+04	0.000E+00	0.317	0.0138	0.746	0.254	0.000
BBBBB 11	0.813	3.287E+04	0.000E+00	0.322	0.0136	0.640	0.360	0.000
BBBBB 12	1.149	2.053E+04	1.264E+03	0.369	0.0124	0.610	0.357	0.032
BBBBB 13	1.513	2.639E+04	6.981E+03	0.359	0.0131	0.538	0.323	0.139
BBBBB 14	1.969	3.351E+04	1.545E+04	0.358	0.0134	0.448	0.310	0.242
BBBBB 16	2.394	3.979E+04	2.611E+04	0.356	0.0136	0.386	0.271	0.344
BBSBB 10	0.776	3.206E+04	0.000E+00	0.318	0.0138	0.648	0.352	0.000
BBSBB 7	1.249	2.232E+04	2.833E+03	0.358	0.0129	0.594	0.340	0.067
BBSBB 8	1.619	2.835E+04	9.947E+03	0.355	0.0133	0.504	0.312	0.184
BBSBB 5	1.843	3.173E+04	1.419E+04	0.357	0.0134	0.464	0.301	0.234
BBSBB 2	2.649	4.362E+04	0.000E+00	0.356	0.0137	0.000	0.000	0.000
BBSSS 6	1.521	2.772E+04	7.581E+03	0.366	0.0128	0.542	0.315	0.143
BBSSS 7	1.706	3.087E+04	1.178E+04	0.367	0.0128	0.491	0.309	0.200
BBSSG 3	1.848	3.297E+04	1.521E+04	0.368	0.0129	0.450	0.308	0.242
BBSSG 4	2.331	4.054E+04	2.758E+04	0.357	0.0136	0.364	0.279	0.356
BBSSG 5	2.715	4.641E+04	0.000E+00	0.362	0.0135	0.000	0.000	0.000
BBSGG 9	2.627	4.719E+04	3.501E+04	0.364	0.0134	0.352	0.260	0.388

Unused Data Continued

Test Name	MC Subarea Base n value	MCB Subarea Base n value	FP3 Subarea Base n value	FP2 Subarea Base n value	FP1 Subarea Base n value	Overall Water Surface Elevation (ft)	Depth/ Bankfull Depth	Overall Area (sf)	Overall WP (ft)	Overall WP+WWP (ft)	Overall Bed Slope (ft/ft)
BBGGG 2	0.0130	0.0130	0.0182	0.0182	0.0182	2.195	1.248	1.334	4.164	5.169	6.173E-04
BBGGG 9	0.0130	0.0130	0.0182	0.0182	0.0182	2.338	1.463	1.890	4.164	5.455	6.173E-04
BGGGG 1	0.0130	0.0182	0.0182	0.0182	0.0182	1.648	0.429	0.239	1.094	1.383	1.045E-03
BGGGG 2	0.0130	0.0182	0.0182	0.0182	0.0182	1.706	0.516	0.297	1.175	1.522	1.045E-03
BGGGG 3	0.0130	0.0182	0.0182	0.0182	0.0182	1.791	0.643	0.388	1.294	1.726	1.045E-03
BGGGG 4	0.0130	0.0182	0.0182	0.0182	0.0182	1.878	0.773	0.489	1.416	1.935	1.045E-03
BGGGG 5	0.0130	0.0182	0.0182	0.0182	0.0182	1.953	0.885	0.581	1.519	2.113	1.045E-03
GGGGG 1	0.0182	0.0182	0.0182	0.0182	0.0182	1.717	0.531	0.308	1.190	1.547	1.045E-03
GBBBB 1	0.0182	0.0130	0.0130	0.0130	0.0130	1.714	0.526	0.304	1.185	1.540	1.045E-03
GBBBB 2	0.0182	0.0130	0.0130	0.0130	0.0130	1.792	0.644	0.389	1.295	1.729	1.045E-03
GBBBB 3	0.0182	0.0130	0.0130	0.0130	0.0130	1.825	0.693	0.426	1.341	1.806	1.045E-03
GBBBB 5	0.0182	0.0130	0.0130	0.0130	0.0130	1.911	0.822	0.528	1.460	2.012	1.045E-03
GBBBB 6	0.0182	0.0130	0.0130	0.0130	0.0130	1.949	0.879	0.576	1.514	2.104	1.045E-03
GBBBB 7	0.0182	0.0130	0.0130	0.0130	0.0130	2.143	1.170	1.131	4.164	5.065	1.045E-03
GBBBB 8	0.0182	0.0130	0.0130	0.0130	0.0130	2.169	1.210	1.234	4.164	5.118	1.045E-03
GBBBB 9	0.0182	0.0130	0.0130	0.0130	0.0130	2.197	1.251	1.340	4.164	5.172	1.045E-03
GBBBB 10	0.0182	0.0130	0.0130	0.0130	0.0130	2.217	1.282	1.420	4.164	5.213	1.045E-03
GBBBB 11	0.0182	0.0130	0.0130	0.0130	0.0130	2.236	1.309	1.492	4.164	5.251	1.045E-03
GBBBB 12	0.0182	0.0130	0.0130	0.0130	0.0130	2.264	1.351	1.600	4.164	5.306	1.045E-03
GBBBB 14	0.0182	0.0130	0.0130	0.0130	0.0130	2.308	1.418	1.773	4.164	5.395	1.045E-03

Unused Data Continued

Test Name	Overall Flowrate (cfs)	Overall Reynolds Number	Floodplain Reynolds Number	Overall Froude Number	Overall Adjusted n value	Ratio of Flow in MC	Ratio of Flow in MCB	Ratio of Flow in FP
BBGGG 2	1.527	2.837E+04	8.254E+03	0.345	0.0137	0.523	0.324	0.153
BBGGG 9	2.711	4.832E+04	0.000E+00	0.363	0.0135	0.000	0.000	0.000
BGGGG 1	0.191	1.402E+04	0.000E+00	0.285	0.0203	0.914	0.086	0.000
BGGGG 2	0.286	1.907E+04	0.000E+00	0.317	0.0183	0.872	0.128	0.000
BGGGG 3	0.415	2.443E+04	0.000E+00	0.319	0.0184	0.786	0.214	0.000
BGGGG 4	0.555	2.924E+04	0.000E+00	0.314	0.0189	0.708	0.292	0.000
BGGGG 5	0.703	3.390E+04	0.000E+00	0.316	0.0188	0.684	0.316	0.000
GGGGG 1	0.290	1.903E+04	0.000E+00	0.306	0.0191	0.869	0.131	0.000
GBBBB 1	0.287	1.916E+04	0.000E+00	0.307	0.0190	0.867	0.133	0.000
GBBBB 2	0.417	2.484E+04	0.000E+00	0.320	0.0183	0.783	0.217	0.000
GBBBB 3	0.473	2.696E+04	0.000E+00	0.321	0.0183	0.744	0.256	0.000
GBBBB 5	0.624	3.206E+04	0.000E+00	0.318	0.0186	0.691	0.309	0.000
GBBBB 6	0.697	3.415E+04	0.000E+00	0.317	0.0188	0.683	0.317	0.000
GBBBB 7	1.221	4.480E+04	7.090E+03	0.642	0.0090	0.583	0.334	0.083
GBBBB 8	1.531	3.063E+04	7.779E+03	0.388	0.0160	0.550	0.317	0.133
GBBBB 9	1.696	3.363E+04	1.261E+04	0.380	0.0165	0.495	0.308	0.197
GBBBB 10	1.843	3.627E+04	1.691E+04	0.379	0.0167	0.456	0.300	0.244
GBBBB 11	2.009	3.926E+04	1.932E+04	0.383	0.0166	0.429	0.313	0.258
GBBBB 12	2.237	4.335E+04	2.418E+04	0.384	0.0167	0.403	0.305	0.292
GBBBB 14	2.598	4.963E+04	0.000E+00	0.382	0.0170	0.000	0.000	0.000

Unused Data Continued

Test Name	MC Subarea Base n value	MCB Subarea Base n value	FP3 Subarea Base n value	FP2 Subarea Base n value	FP1 Subarea Base n value	Overall Water Surface Elevation (ft)	Depth/ Bankfull Depth	Overall Area (sf)	Overall WP (ft)	Overall WP+WWP (ft)	Overall Bed Slope (ft/ft)
BBBGG 1	0.0130	0.0130	0.0130	0.0182	0.0182	1.708	0.518	0.299	1.177	1.526	7.932E-04
BBBGG 2	0.0130	0.0130	0.0130	0.0182	0.0182	1.776	0.619	0.371	1.272	1.688	7.932E-04
BBBGG 3	0.0130	0.0130	0.0130	0.0182	0.0182	1.823	0.690	0.424	1.338	1.802	7.932E-04
BBBGG 4	0.0130	0.0130	0.0130	0.0182	0.0182	1.869	0.759	0.477	1.402	1.911	7.932E-04
BBBGG 5	0.0130	0.0130	0.0130	0.0182	0.0182	1.903	0.810	0.519	1.450	1.994	7.932E-04
BBBGG 6	0.0130	0.0130	0.0130	0.0182	0.0182	1.948	0.877	0.574	1.512	2.101	7.932E-04

Unused Data Continued

Test Name	Overall Flowrate (cfs)	Overall Reynolds Number	Floodplain Reynolds Number	Overall Froude Number	Overall Adjusted n value	Ratio of Flow in MC	Ratio of Flow in MCB	Ratio of Flow in FP
BBBGG 1	0.291	1.984E+04	0.000E+00	0.320	0.0156	0.859	0.141	0.000
BBBGG 2	0.410	2.522E+04	0.000E+00	0.336	0.0149	0.780	0.220	0.000
BBBGG 3	0.470	2.714E+04	0.000E+00	0.322	0.0157	0.738	0.262	0.000
BBBGG 4	0.555	3.018E+04	0.000E+00	0.324	0.0156	0.703	0.297	0.000
BBBGG 5	0.616	3.211E+04	0.000E+00	0.321	0.0158	0.688	0.312	0.000
BBBGG 6	0.705	3.489E+04	0.000E+00	0.322	0.0158	0.669	0.331	0.000